SEISMIC RESPONSE OF LATERALLY LOADED PILE FOUNDATION CONSIDERING NON-LINEAR SOIL-STRUCTURE INTERACTION

Thesis submitted by

MONIRUL MALLICK

DOCTOR OF PHILOSOPHY IN ENGINEERING

CIVIL ENGINEERING DEPARTMENT
FACULTY COUNCIL OF ENGINEERING & TECHNOLOGY
JADAVPUR UNIVERSITY
KOLKATA-700032, INDIA

2023

INDEX NO.: 187/19/E

1. Title of the Thesis:

SEISMIC RESPONSE OF LATERALLY LOADED PILE FOUNDATION CONSIDERING NON-LINEAR SOIL-STRUCTURE INTERACTION

2. Name, Designation and Institution of the Supervisors:

(1) Prof. (Dr.) Kalyan Kumar Mandal,
Associate Professor,
Department of Civil Engineering,
Jadavpur University,
Kolkata-700032, India.

(2) Prof. (Dr.) Ramendu Bikas Sahu,
Professor,
Department of Civil Engineering,
Jadavpur University,
Kolkata-700032, India.

3. List of Publications:

(i) Mallick M, Mandal KK, Sahu RB (2022) Seismic Response of Laterally Loaded Single Piles in Liquefiable Multi-Layered Sloping Ground Using Pseudo-Static Approach. Indian Geotechnical Journal. https://doi.org/10.1007/s40098-022-00653-9

(ii) Mallick M, Mandal KK, Sahu RB (2022) Effects of axial loading on dynamic response of laterally loaded single piles in liquefiable layered soil of Kolkata city considering nonlinearity of soil. SN Applied Sciences Journal 4:297. https://doi.org/10.1007/s42452-022-05184-9

(iii) Mallick M, Mandal KK, Sahu RB (2021) Failure Mechanisms of Pile-Supported Port Building in Liquefiable Sloping Ground during Earthquake. In: Kasinathan Muthukkumaran, R. Ayothiraman, Sreevalsa Kolathayar (eds.) Soil Dynamics, Earthquake and Computational Geotechnical Engineering. Lecture Notes in Civil Engineering, Volume 5, Springer, Singapore, 539-550. https://doi.org/10.1007/978-981-19-6998-0

(iv) Mallick M, Mandal KK, Sahu RB (2020) A Case Study of Liquefaction-induced Damages to A Port Building Supported on Pile Foundation. In: C.N.V. Satyanarayana Reddy,

A. Murali Krishna, Neelima Satyam (eds.) Dynamics of Soil and Modelling of Geotechnical Problems. Lecture Notes in Civil Engineering, Volume 5, Springer, Singapore,319-330. https://doi.org/10.1007/978-981-16-5605-7

(v) Mallick M, Mandal KK, Sahu RB (2020) Analysis of Laterally Loaded Single Pile in Cohesionless Soil Considering Nonlinear Soil-Structure Interaction Effects. In: C.N.V. Satyanarayana Reddy, A. Murali Krishna, Neelima Satyam (eds.) Dynamics of Soil and Modelling of Geotechnical Problems. Lecture Notes in Civil Engineering, Volume 5. Springer, Singapore, 341-350. https://doi.org/10.1007/978-981-16-5605-7

(vi) Mallick M, Raychowdhury P (2015) Seismic analysis of highway skew bridges with nonlinear soil–pile interaction. Transportation Geotechnics Journal 3: 36–47. http://dx.doi.org/10.1016/j.trgeo.2015.03.002

4. List of Presentations in National/International Conferences/Workshops:

(i) Mallick M, Mandal KK, Sahu RB (2021) Failure Mechanisms of Pile-Supported Port Building in Liquefiable Sloping Ground during Earthquake. Presented in Indian Geotechnical Conference, NIT Tiruchirappalli, Paper No. TH 06-011, Dec 16-18,2021.

(ii) Mallick M, Mandal KK, Sahu RB (2020) A Case Study of Liquefaction-induced Damages to A Port Building Supported on Pile Foundation. Presented in Indian Geotechnical Conference, Andhra University, Visakhapatnam, Paper No. TH-11-007, Dec 17-19, 2020.

(iii) Mallick M, Mandal KK, Sahu RB (2020) Analysis of Laterally Loaded Single Pile in Cohesionless Soil Considering Nonlinear Soil-Structure Interaction Effects. Presented in Indian Geotechnical Conference, Andhra University, Visakhapatnam, Paper No. TH-11-10, Dec 17-19, 2020.

(iv) Mallick M, Raychowdhury P (2014) Seismic Response of Skew Bridges under Bi-directional Ground Motions. International conference on Sustainable Civil Infrastructure, Organised by ASCE India Section and Department of Civil Engineering, IIT Hyderabad, Oct 17-18, 2014.

STATEMENT OF ORIGINALITY

I, Monirul Mallick, registered on 26.06.2019 do hereby declare that the thesis entitled "**Seismic Response of Laterally Loaded Pile Foundation Considering Non-linear Soil-structure Interaction**" contains literature survey and original research work done by the undersigned candidate as part of Doctorial studies.

All information in this thesis have been obtained and presented in accordance with existing academic rules and ethical conduct. I declare that, as required by these rules and conduct, I have fully cited and referred all materials and results that are not original to this work.

I also declare that I have checked this thesis as per the "Policy on Anti Plagiarism, Jadavpur University, 2019", and the level of similarity as checked by iThenticate software is 9.0 %.

Monirul Mallick

Signature of Candidate

Date: 05/04/2023

Certified by Supervisor(s):

(Signature with date, seal)

1. Kalyan Kr. Mandal 05/04/2023
   Associate Professor
   Department of Civil Engineering
   Jadavpur University
   Kolkata-700 032

2. 05/04/2023
   DR. R. B. SAHU
   Professor of Civil Engineering
   JADAVPUR UNIVERSITY
   Kolkata – 700 032

CERTIFICATE FROM THE SUPERVISOR(S)

This is to certify that the thesis entitled **"Seismic Response of Laterally Loaded Pile Foundation Considering Non-linear Soil-structure Interaction"** submitted by Monirul Mallick, who got his name registered on 26.06.2019 for the award of Ph.D (Engineering) degree of Jadavpur University is absolutely based upon his own work under the supervision of **Prof. (Dr.) Kalyan Kumar Mandal**, Associate Professor, Department of Civil Engineering, Jadavpur University & **Prof. (Dr.) Ramendu Bikas Sahu**, Professor, Department of Civil Engineering, Jadavpur University and that neither his thesis nor any part of the thesis has been submitted for any degree/diploma or any other academic award anywhere before.

1. Kalyan Kr. Mandal 05/04/2023

Signature of the Supervisor and date with Official Seal

Associate Professor
Department of Civil Engineering
Jadavpur University
Kolkata-700 032

2. 05/04/2023

Signature of the Supervisor and date with Official Seal

DR. R. B. SAHU
Professor of Civil Engineering
JADAVPUR UNIVERSITY
Kolkata – 700 032

ACKNOWLEDGEMENTS

I feel honoured to express my deepest gratitude and appreciation to my thesis advisors, Dr. Kalyan Kumar Mandal and Dr. Ramendu Bikas Sahu for their involvement, inspiring guidance, motivation, constant encouragement and immeasurable support throughout my time at Jadavpur University which lead to the successful completion of my thesis work. Their novel ideas and knowledge guided me to the right direction of scientific pursuit and help to complete my thesis on right time. I would like to render special thanks towards external member of my PhD Research Advisory Committee, Prof. Jagat Jyoti Mandal, Civil Engineering Department, NITTTR, Kolkata for giving me useful suggestions and encouragement at every point of my study.

I express my sincere thanks to Professor Dr. Partha Bhattacharya (present HOD, Civil Engineering department), Dr. Sibapriya Mukherjee, Dr. Depankar Chakravorty, Dr. Shibnath Chakraborty for their friendly nature, excellent guidance and for enhancing my knowledge in Civil Engineering. I would also like to thank the entire Civil engineering faculties and staff for their help and friendly cooperation whom I spent three and half years of my stay and learned many things.

I am grateful to my all friends especially Md. Niamot Ali, Nikhil Das, Siddhartha Sen Gupta who have contributed immensely to my personal and professional life at Jadavpur University. They have made my days here cherished and immensely enjoyable.

I would like to offer heartiest acknowledgement towards my department Public Works Department, Govt. of West Bengal for giving me no objection certificate for pursuing PhD. and help me all through these days from my starting day of service life.

Finally, I would like to express my cordial homage to my parents from whom I have been constantly away. Special thanks to my lovely wife, son, daughter, brothers, sister for their unconditional patience, sacrifice, support and encouragement during the past years, and for bringing me to this stage of my life.

Last but not least, I thank to almighty Allah for showering all blessings throughout my life.

Monirul Mallick

ABSTRACT

The seismic response of pile foundations is a complicated soil-structure interaction (SSI) problem. The problem of soil-pile interaction during earthquake in liquefiable soil gets further intricate than non-liquefiable soil because of degradation of strength and stiffness of soil over time, soil nonlinearity and development of excess pore water pressure. A significant number of damages and/or collapses of pile foundations and pile-supported structures are reported in liquefiable soil after past major earthquakes such as San Francisco (1906), Niigata (1964), Northridge (1994), Kobe (1995), Chi-Chi (1999), Bhuj (2001), Sumatra (2004), Tohoku (2011) and Sikkim (2011). So, it is challenging job for geotechnical earthquake engineers to ensure safe and economical design of pile foundation and pile-supported high-rise structures in liquefiable soil. As the soil behaves nonlinearly during strong seismic event, nonlinear SSI is extremely necessary for the analysis of soil-pile interaction in liquefiable soil.

In the present study, 1D effective stress-based nonlinear ground response analysis (GRA) has been conducted using the finite element program Cyclic1D for Kolkata metropolitan city in India, where population and infrastructure are growing rapidly. Two different sites of Kolkata city having two distinct soil formations as Normal Kolkata Deposit (NKD) and River Channel Deposit (RCD) are selected for ground response analysis. The input motions considered for present analysis are 1940 Imperial Valley, 2001 Bhuj and 2011 Sikkim earthquakes whose PGA are well within the reported range of Kolkata city. The validation of the present model is performed by comparing the results of peak ground acceleration (PGA) and its magnification factor profile with that predicted using SHAKE 2000 computer program. Further, liquefaction potential of Kolkata soil has been assessed using the results obtained from the present analysis. Then a well-documented case study on liquefaction-induced damages of Kandla port building (Gujarat) during 2001 Bhuj earthquake has been analysed and presented in this paper. The results of the present analysis are compared with the post-earthquake observations as well as the analyses reported in the literature. It has been observed from nonlinear GRA that PGA at surface ranges from 0.109g to 0.119g for NKD soil and 0.072g to 0.091g for RCD soil. The range of variation of peak spectral acceleration for 5% damping ratio is 0.51g to 0.67g for NKD soil and 0.33g to 0.46g for RCD soil of Kolkata. It is also found that top 12 m of RCD soil is susceptible to liquefaction if these considered input earthquake motions are experienced at bedrock.

Next, beam on nonlinear Winkler foundation (BNWF) model is developed using open-source finite element-based code OpenSees for pseudo-static analysis of nonlinear soil-structure interaction in non-liquefiable homogenous cohesionless soil and liquefiable multi-layered sloping ground using results obtained from nonlinear GRA. Pile and soil are simulated by displacement-based beam element and nonlinear spring element respectively. The present numerical model has been validated with the established theoretical solution and past case study. The effects of relative density of cohesionless soil, length to diameter (L/d) ratio of pile and fixity of pile head on pile and soil responses are investigated. The simplified BNWF numerical model is then used to investigate the seismic response of single piles in liquefiable multi-layered sloping ground taking into account of both kinematic and inertial interaction effects. The parametric studies have been performed for evaluating the influence of various parameters on seismic response of layered soil-pile system. The results from pseudo-static analysis show that the peak lateral displacement and bending moment of piles are significantly influenced by ground slope, L/d ratio of pile, pile head fixity condition, depth of liquefiable layer and pile embedment depth. The peak bending moment occurs near the interface between liquefiable and non-liquefiable layer when the depth of liquefiable layer is almost 22% and embedment depth is almost 45% of total length of pile. It is also observed that peak lateral displacement of pile reduces and peak kinematic pile bending increases in liquefiable sloping ground with increasing of embedment depth of pile.

Then, an advanced nonlinear finite-element based 3D numerical study has been carried out to investigate the effects of axial loading on dynamic response of soil-pile system in liquefiable layered level and sloping ground of Kolkata city. An advanced soil constitutive law based on multi-yield surface plasticity model implemented in fully-coupled u-p formulation is adopted for soil-fluid interaction and pore water pressure development reasonably. The present model is validated with the past experimental results. Then, a detailed systematic parametric study is performed for numerical simulation of pile failures in layered level and sloping ground under axial loading by taking into account various soil conditions, pile and ground motion parameters. Parametric studies of dynamic analysis reveal that the bending moment response of pile under axial loading can be higher in non-liquefiable condition, with reference to the liquefiable condition. The peak lateral displacement and bending moment decreases in both non-liquefiable and liquefiable condition due to decrease of axial load. So, the designer should consider both extreme scenarios for safe and economical design. Also, it is noticed that the buckling capacity of pile is improved significantly by using larger diameter pile and the

bending capacity is increased by selecting higher grade of concrete. The amplification factors of bending moment for sloping ground with respect to level ground due kinematic and combined loading increases significantly with an increase of ground slopes. The combined peak lateral displacement and bending moment co-efficient decreases when L/d ratio decreases. Also, the peak combined lateral displacement decreases by 48.7% and combined bending moment co-efficient increases by 14.3% when soil condition changes from liquefiable state to dry condition. So, it is recognised from the present study that the bending and buckling failure mode may be avoided in liquefiable level and sloping ground under combined loading condition by selecting a suitable combination of material strength and pile geometry.

Keywords: Cyclic1D; Nonlinear; Liquefaction; Laterally Loaded Pile; BNWF; OpenSees; Finite element; Soil-Structure Interaction; Sloping ground; Pseudo-static; Bending-buckling interaction

CONTENTS

LIST OF FIGURES

LIST OF TABLES

LIST OF ABBREVIATIONS

$[M]$	Mass matrix
$[C]$	Damping matrix
$[K]$	Stiffness matrix
u	Nodal relative displacement
$\dot{u}$	Nodal relative velocity
ü	Nodal relative acceleration
$\ddot{u}_{ff}(t)$	Free-filed acceleration
τ	Shear stress
σ_v	Overburden pressure
u	Excess pore water pressure
C_u	Undrained shear strength
φ	Soil friction angle
N	SPT number
V_s	Shear wave velocity
M_w	Earthquake moment magnitude
g	Acceleration due to gravity
I	Unit vector
K_0	Lateral earth pressure co-efficient at rest
y_{max}	Maximum shear strain percentage
NYS	Number of yield surfaces
μ	Poisson's ratio of soil
V_{sr}	Reference shear wave velocity
p_{ref}	Reference effective mean confinement
n	Co-efficient of confinement dependence
φ_{PT}	Dilation or phase transformation (PT) angle
c_1 and c_2	Contraction co-efficient
d_1 and d_2	Dilation co-efficient
Liq	Liquefaction co-efficient
k	Co-efficient of permeability
p	Confinement

p_a	Atmospheric pressure
γ_d	Cumulative octahedral plastic strain
S	Ground slope
R_d	Shear stress reduction co-efficient
Ts	Initial time period of ground
p	Soil resistance per unit length of pile
y	Lateral relative soil-pile displacement
t	Skin friction along pile length
z	Vertical relative soil-pile displacement
Q	End bearing at pile base
L	Length of pile
d	Diameter of pile
E	Young's Modulus of Pile
μ_p	Poisson's ratio of pile
I	Moment of inertia of pile
γ_s	Unit weight of soil
E_s	Young's Modulus of soil
P_s	Static axial load
α	Dynamic axial load factor
P_d	Maximum axial load
m_1	Peak ground acceleration
H	Lateral inertial load
α	Inclination angle with ground surface
P_{ult}	Ultimate lateral resistance of p-y material
y_{50}	Displacement at 50% of P_{ult}
γ'	Effective unit weight
z	Depth below ground
J	Factor determined experimentally by Matlock
K_{qD}	Earth pressure coefficient for overburden pressure
K_{cD}	Earth pressure coefficient for cohesion
ε_{50}	Strain corresponding to one-half the maximum principal stress difference
k_{API}	API recommended initial modulus of subgrade reaction
k^*	Corrected modulus of subgrade reaction

C_σ	Overburden stress correction factor
σ_{ref}'	Reference effective overburden stress
σ_v'	Effective overburden stress
A	Loading type coefficient
$p_{u,liq}$	Ultimate soil resistance of liquefiable soil
S_u	Mobilized shear resistance of the liquefied soil
R	Degradation factor for soil stiffness due to liquefaction
R_o	Degradation factor at the top of liquefiable crust
L_{Liq}	Depth of liquefiable crust
T	Relative stiffness factor
n_h	Coefficient of subgrade reaction
γ_p	Unit weight of pile
f_{ck}	Characteristic compressive strength of concrete
h	Building height from GL
M	Bending moment
F	Shear force
Mp	Plastic moment capacity
F_p	Plastic shear capacity
Z_p	Plastic section modulus
σ_y	Yield stress
F_{sy}	Shear capacity of transverse reinforcement
F_c	Shear capacity of concrete
f_y	Yield strength of steel
T_b	Fundamental period of RCC building
b	Base dimension of the building at plinth level
S_a	Spectral acceleration
V_b	Base shear
A_h	Seismic coefficient
W	Total seismic weight of the building
Z	Zone factor
I	Importance factor
R	Response reduction factor
M_R	Rocking moment

P_{ext}	Extra axial compressive load
r_i	Distance from C.G of pile group to centre of each pile
L_f	Fixity level from ground surface
k_s	Stiffness at liquefied condition
$T_{b,liq}$	Time period at liquefied condition
P_{cr}	Euler's buckling load
L_e	Effective length
H_{30}	Thickness of top 30 m soil layer
E_{NL}	Depth of embedment at bottom stiff non-liquefiable layer
f	Yield function
s	Deviatoric stress tensor
p'	Mean effective stress
p_0'	Positive constant for finite size of yield surface
α	Second order kinematic deviatoric tensor
m	Size of yield surface
$P"$	Shear-induced dilation or contraction
η	Stress ratio
η_{PT}	Stress ratio along PT surface
c_3 & d_3	Parameters of PDMY02 material to account K_σ effect
ρ	Mass density
G	Low-strain shear modulus
B	Low-strain bulk modulus
τ	Shear stress
γ	Shear strain
B	Strain-displacement matrix
Q	Coupling matrix
S	Compressibility matrix
H	Permeability matrix
$f^{(s)}$	Body and surface forces in soil
$f^{(p)}$	Body and surface forces in fluid
β	Factor which depends on end conditions of pile
L_0	Length of pile in buckling zone
D_F	Depth of fixity

D_L	Depth of liquefiable layer
λ	Slenderness ratio
r_{min}	Minimum radius of gyration
A_{cs}	Cross-sectional area
P_{cb}	Critical buckling load
σ_{cb}	Elastic critical buckling stress
σ_f	Rankine's failure stress considering both crushing and buckling criteria,
σ_y	Yield stress of material
P	Axial load
P_y	Squash load without bending
σ_c	Compressive strength of concrete
D_r	Relative density of soil
R_u	Excess pore water pressure ratio
σ	Axial stress on pile
f_n	Natural frequency
M_s	Lumped mass
L_1	Free head length
D_{NL}	Depth of non-liquefiable layer
P_{all}	Allowable axial load

Chapter 1

Introduction

1.1 General

Piles are structurally slender members primarily used to carry and transfer superstructural load through weak soil layer onto deep strong soil layer or rock of comparatively higher bearing capacity. Pile foundations are widely used to support multi-storied buildings, bridge piers and abutments, transmission towers, retaining wall and offshore structures. These structures are subjected to the high degree of lateral load in addition to the axial load due to wind action, earth pressure, water pressure, traffic movement and most importantly seismic action. The seismic analysis of pile foundations is a complicated soil-structure interaction (SSI) problem. The problem of soil-pile interaction during earthquake in liquefiable soil gets further intricate than non-liquefiable soil because of degradation of strength and stiffness of soil over time, soil nonlinearity and development of excess pore water pressure (EPWP). A significant number of damages and/or collapses of pile foundations and pile-supported structures are reported in liquefiable soil after past major earthquakes such as San Francisco (1906), Niigata (1964), Northridge (1994), Kobe (1995), Chi-Chi (1999), Bhuj (2001), Sumatra (2004), Tohoku (2011) and Sikkim (2011) (Bhattacharya 2003). So, it is challenging job for geotechnical earthquake engineers to ensure safe and economical design of pile foundation and pile-supported high-rise structures in liquefiable soil of metropolitan city like Kolkata, where rapid growing of population and infrastructure makes it essential. As the soil behaves nonlinearly during strong seismic event, nonlinear SSI is extremely necessary for the analysis of soil-pile interaction in liquefiable soil.

The following section presents an overview to Pile foundation, Soil Structure Interaction (SSI) and soil liquefaction briefly.

1.1.1 Pile Foundation

Piles are deep foundation. A foundation is described as ‘piled’ when its depth is more than three times its breadth. Piles are long, columnar element normally made of steel, reinforced concrete or timber. Piles transfer load to the soil partly by shaft resistance and partly by base resistance. Piles may be classified as end-bearing or friction piles based on their functional mechanisms. Base resistance dominated piles are described as end-bearing piles while shaft resistance dominated piles are described as friction piles. The performance of end-bearing piles is better than friction piles in high seismic zone. Pile foundations are also extensively used as foundation in potentially liquefiable soil. However, there are case histories of failure of pile foundation in liquefiable soil because of additional loads imparted by liquefaction and the associated loss of support.

1.1.2 Soil-Structure Interaction (SSI)

Soil-structure interaction (SSI) analysis is the study on the influence of the behaviour of soil in the response of structure and vice versa. SSI analysis is necessary for the heavy structure resting on relatively weak soil stratum. Over the years, the research in the field of Geotechnical Earthquake Engineering has been developed considerably. But the effect of SSI on the seismic response of structures is still not fully recognised. Conventional design methods neglect the SSI effects due to the difficulties encountered in modelling SSI. Advanced model for soil nonlinearity, soil-pile interface mechanism and variation of soil profile is still scarce.

SSI effects for linear soil-structure system have been evaluated over the times analytically by various researchers. These techniques are used to complement the conventional design methods based on fixed-based approach. In addition, the effects of SSI have been evaluated using many full-scale or small-scale tests. However, the analytical and experimental studies are not able to capture the nonlinear SSI effects during strong seismic events. Advanced numerical techniques using high-speed computer are facilitating to incorporate the 3D nonlinear SSI effects for high-rise structures.

In general, there are two numerical approaches to consider effects of SSI on soil-foundation-structure system such as direct approach and equivalent substructure approach (Kramer 2005).

1.1.2.1 Direct Approach

In the direct approach, the soil, pile foundation and superstructure are modelled and analysed in a single step as shown in Fig. 1.1 using following equation (Kramer 2005):

$$[M]\{\ddot{u}\} + [K]\{u\} = -[M]\{\ddot{u}_{ff}(t)\} \quad (1.1)$$

where $[M], [K]$ are mass and stiffness matrix; *u*, ü are displacement and acceleration of the system; $\{\ddot{u}_{ff}(t)\}$ is far-field input motion at the boundary node points.

The material and geometric nonlinearities of both the structure and the supporting soil can be captured within same model using direct approach. Therefore, seismic response of structure using this approach is considered to be more accurate (Elgamal et al. 2008; Bao et al. 2012). However, modeling and analysing structure using this approach is computationally quite pricey.

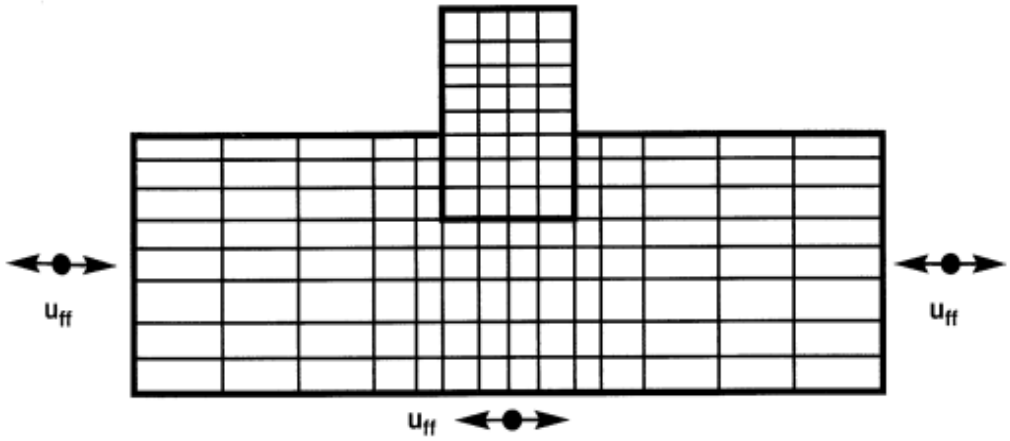

Fig.1.1 Direct approach of SSI analysis (Kramer 2005)

1.1.2.2 Substructure Approach

On the other hand, in the equivalent substructure approach, SSI effects are evaluated by three individual steps (Mylonakis et al. 1997). First step is to evaluate the foundation kinematic response. Second step is to determine the spring/dashpot constants based on the inertial mechanism. Third step is the seismic analysis of the structure resting on compliant base. The major convenience of this approach is that each step is independent to each other and the most important aspects of the problem can be focused by designer (Stewart and Fenves 1998).

An earthquake causes horizontal and vertical deformations of soil in the free-field condition. However, the same soil can't follow the free-field motion when the foundation is embedded

in it. So, the base of super-structure does not follow the free-field motion. This difference in response of soil-pile system from the free-field motion is termed as kinematic interaction. Different modes of vibration is induced in a structure due to kinematic interaction. The kinematic response can be evaluated using following equation supposing foundation has stiffness but no mass (Kramer 2005):

$$[M_{soil}]\{\ddot{u}_{KI}\} + [K]\{u_{KI}\} = -[M_{soil}]\{\ddot{u}_b(t)\} \quad (1.2)$$

where $[M_{soil}]$ *is the* mass matrix supposing massless structure and foundation; $\{u_{KI}\}$ is the foundation input motion.

On the other hand, inertial interaction is due to the mass of foundation and structure which causes them for responding dynamically. Foundation movement is occurred due to the force transmitted to soil by foundation when the supporting soil is compliant. This effect would not happen for fixed-base structure. The influence of soil compliance on the resulting response is because of inertial interaction. The inertial interaction is dependent on both the base motion and the foundation input motion. The inertial response can be evaluated using following equation supposing foundation and structure do have mass (Kramer 2005):

$$[M]\{\ddot{u}_{II}\} + [K]\{u_{II}\} = -[M_{str}]\{\ddot{u}_{KI}(t)+\ddot{u}_b(t)\} \quad (1.3)$$

where $[M_{str}]$ *is the* mass matrix supposing massless soil.

Kinematic and inertial interaction analysis is illustrated in Fig.1.2 (a) and (b) respectively.

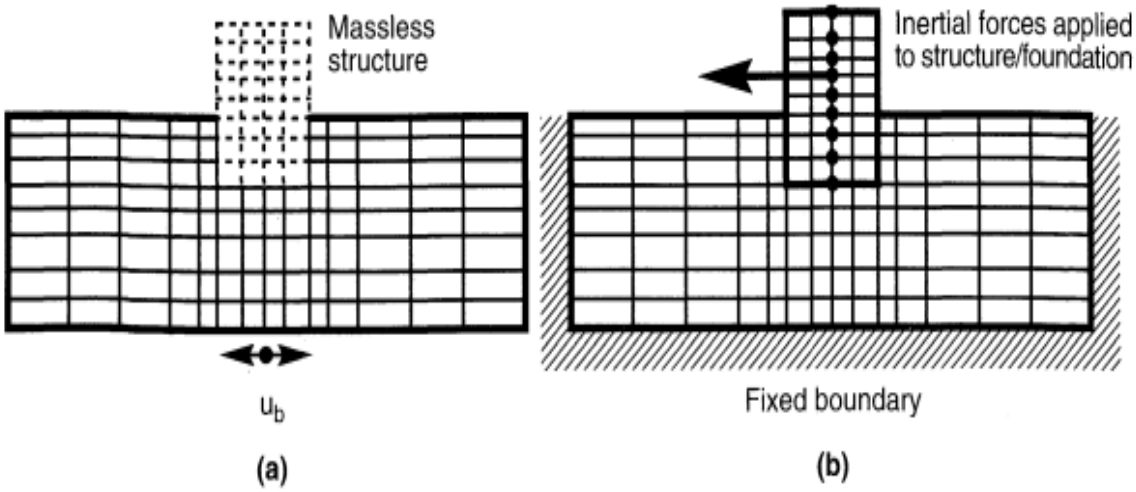

Fig.1.2 Substructure approach of SSI analysis **a** Kinematic and **b** Inertial interaction (Kramer 2005)

1.1.3 Soil Liquefaction

Liquefaction is one of the most significant, complicated and controversial subjects in geotechnical earthquake engineering. Hazen has first used the word "liquefies" in 1920 after failure of the Calaveras dam in California (Kramer 2005). Shear stress induced in cohesionless soil during earthquake is given by the following equation:

$$\tau = (\sigma_v - u)\tan\varphi \quad (1.4)$$

where τ=shear stress, σ_v =overburden pressure, u=excess pore water pressure (EPWP) and φ =soil friction angle.

During earthquake event, *u* will increase over time and when u will equal to σ_v, soil will behave like a fluid losing its shear strength. This phenomenon of sudden loss of strength for saturated cohesionless soil under cyclic loading due to zero effective stress is known as liquefaction. The destructive effects of liquefaction drew great attention to the geotechnical engineers after the 1964 Good Friday earthquake (Alaska) followed by the Niigata earthquake (Japan). Large numbers of liquefaction-induced failures of slope, dam, bridge and building foundation and flotation of buried structures were noticed after earthquake. After 55 years of these earthquakes, several researchers around the world have been studying the effects of liquefaction widely. Different approaches and methods have been proposed for liquefaction analysis yet much more has been learned.

1.2 Research Motivation

After 1964 Niigata and Alaska earthquakes, it was understood that the seismic damage to the structure is dependent on both the response of superstructure and supporting soil medium. From then onwards, several efforts have been made by various researchers to understand the dynamic response of soil during earthquake. However, this research was intensified using experimental, analytical and numerical procedures after widespread damages of various pile-supported structures during the 1995 Kobe earthquake. Although nonlinear soil response has been investigated up to some extent, yet the seismic response of soil-pile system considering soil nonlinearity is very few. It is understood from the comprehensive literature review that the three-dimensional nonlinear SSI is extremely necessary for the analysis of soil-pile system under earthquake loading.

Moreover, there are limited studies of dynamic response of soil-pile system in liquefiable multi-layered soil deposit, and there are even fewer studies on dynamic response of pile foundations in liquefiable multi-layered slopping ground considering the effects of kinematic and inertial interaction. Full-scale field tests are best reliable way to understand the behaviour of laterally loaded pile foundations. But due to high-cost involvement and technical difficulties, it is not always feasible to perform field tests. Numerical approaches enable investigators to consider various parameters together in a detailed way.

The present study is motivated towards the seismic nonlinear soil-structure interaction analysis of laterally loaded pile foundation in liquefiable and non-liquefiable multi-layered soil considering kinematic and inertial effects using finite element-based numerical model. The above facts are the major motivations of this research.

1.3 Failure Case Studies

Past earthquakes have pointed out the vulnerability of structures in liquefiable soil during earthquakes. This section reviews some important case histories of damages of pile-supported structures in liquefiable soil around the world during past earthquakes.

1.3.1 Niigata Earthquake (Japan) in 1964

Figs. 1.3(a) & (b) shows the damage of NHK building during 1964 Niigata earthquake in Japan. The RC pile-supported four-storied building was tilted after the earthquake. Fig. 1.3(c) shows the 10 to 15 degree rotation of pile base. Soil liquefaction and lateral spreading were noticed at this site. The amplified response of piles due to liquefaction, P-delta effects and lateral spreading were the reported plausible causes of damages of building and pile foundation.

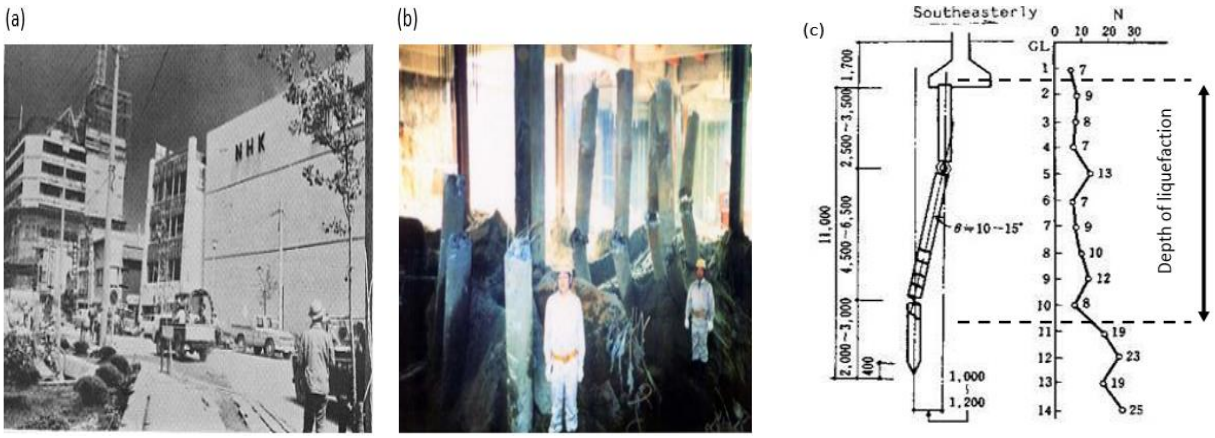

(a) **(b)** **(c)**

Fig. 1.3 a Tilting of NHK building **b** Observed damages of piles after excavation and **c** Failure pattern of pile of the building following the 1964 Niigata Earthquake (Dash and Bhattacharya, 2012)

Figure 1.4(a) shows the shallow foundation failure of Kawagishi – cho apartment during 1964 Niigata earthquake. No damages of superstructure are observed. The foundation was failed due to combined action of inertial force from superstructure and lateral spreading due to soil liquefaction during the earthquake. The Showa Bridge over the Shinano River was collapsed as shown in Fig. 1.4(b) during the Niigata earthquake in 1964. Lateral spreading was noticed at the Showa Bridge riverbanks. It is widely believed that bending failure of piles due to liquefaction-induced lateral spreading is the main cause of collapse Showa Bridge.

(a) **(b)**

Fig. 1.4 Failures of **a** Kawagishi-cho apartment and **b** Showa bridge following the 1964 Nigaata Earthquake due to liquefaction (Choudhury et al. 2014)

1.3.2 Kobe Earthquake (Japan) in 1995

The four-storied firehouse building was leaned unto sea side during 1995 Kobe earthquake in Japan as shown in Fig. 1.5(a). The building is located near the foot of the Kobe O-Hashi Bridge on Port Island. The schematic diagram of failure pattern of foundation is shown in Fig. 1.5(b). The wharf wall was moved by 2 m and building was leaned by 3 degree after the earthquake. The failure of pile foundation was due to buckling and bending of piles at complete liquefaction of soil during earthquake as reported by Bhattacharya (2003).

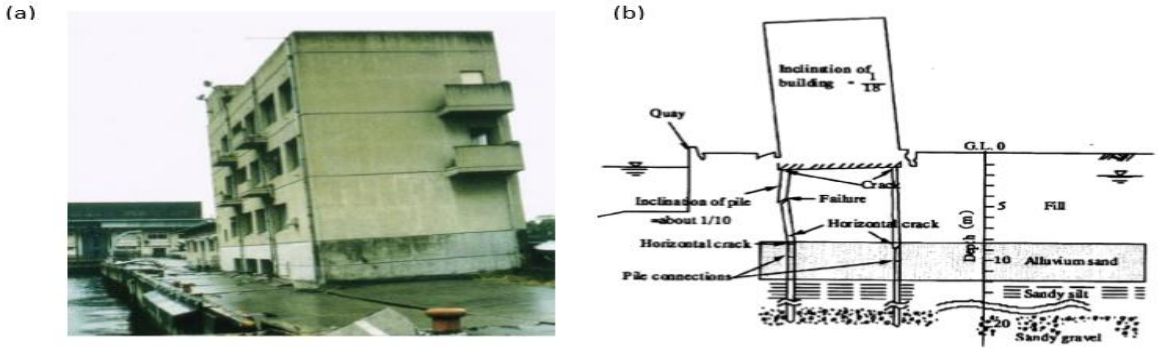

(a) **(b)**

Fig. 1.5 a Tilting of Firehouse building and **b** Failure of the piles of the building following the 1995 Kobe earthquake (Dash and Bhattacharya, 2012)

1.3.3 Bhuj Earthquake (India) in 2001

The 22.0 m high six-storied Kandla Port tower building supported on combined pile-raft foundation was tilted about 0.3 m towards sea side during 2001 Bhuj earthquake in India. There was very little damage of superstructure and significant damages observed in the foundation. Figs. 1.6(a) and (b) show the tilted building, schematic drawing of its damages respectively. The building was located in laterally spreading ground. Dash et al. (2009) performed case study of Kandla Port building and analysed the pile foundation with combined action of axial load and lateral spreading. They conclude that building was damaged due to axial load induced ground settlement during soil liquefaction and bending failure of piles due to lateral spreading.

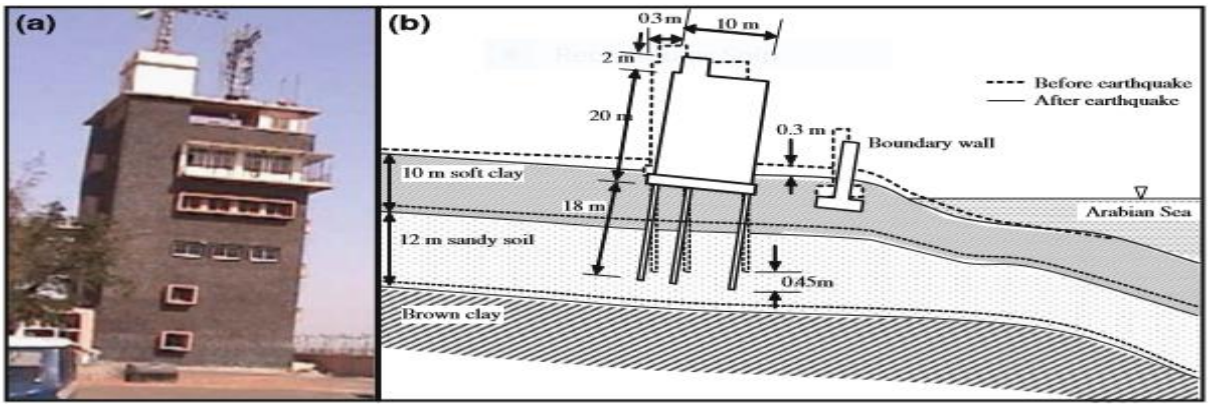

(a) **(b)**

Fig. 1.6 a Tilting of Kandla Port tower building and **b** probable settlement mechanism of failure following the 2001 Bhuj earthquake (Dash and Bhattacharya, 2012)

1.3.4 Sumatra Earthquake (Indonesia) in 2004

Large numbers of pile-supported buildings, coastal and harbour structures were damaged in Andaman and Nicobar Islands during the 2004 Sumatra earthquake. Most of the structures were constructed in sloping ground. The damages were occurred predominantly due to the tsunami, liquefaction and liquefaction-induced lateral spreading. Damage of a government residential building in middle Andaman due to high ground motion and liquefaction is shown in Fig. 1.7(a). Also, Fig. 1.7(b) shows the failure of Passenger terminal building due to liquefaction-induced settlement of pile foundation and heavy damage at the junction of pile & pile cap of a RC storage building storage at Haddo Wharf is shown in Fig 1.7(c).

(a) **(b)** **(c)**

Fig. 1.7 a Damage of residential building in middle Andaman Island **b** failure of Passenger terminal building due to settlement of pile foundation and **c** dislocation of a pile cap in an RC storage building at Haddo Wharf (Murty et al. 2006)

1.3.5 Wenchuan Earthquake (China) in 2008

Large numbers of bridges were collapsed during 2008 Wenchuan earthquake in China. The failure of one span of the MPZ (Miaoziping bridge in Chengdu) bridge is shown in Figure 1.8. The bridge site was located near the epicenter of the earthquake. The reported reasons of failure are: i) high horizontal (1g) and vertical PGA (0.95g) near bridge site, ii) soil liquefaction, iii) structural deficiency such as inadequate stiffness of beam column, unsymmetrical shape of bridge(curved).

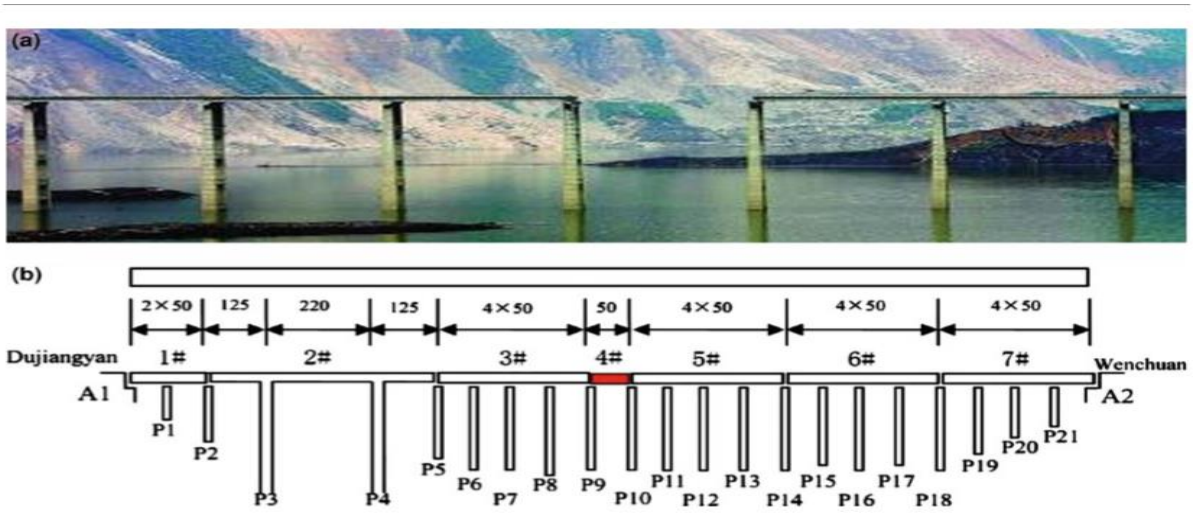

Fig. 1.8 a Failure of the MPZ bridge and **b** Schematic drawing of the bridge during the 2008 Wenchuan earthquake (Bhattacharya et al. 2012)

1.3.6 Chile Earthquake (Maule) in 2010

Three bridges constructed over the river Bio-Bio in Concepcion city were collapsed during 2010 Chile earthquake. The magnitude of earthquake (Mw) was 8.8. The bridge site is located at 105 km from the earthquake source. The collapse of several spans of Bio–Bio Bridge is shown in Fig. 1.9(a). Degraded strength and bending failure due to liquefaction-induced lateral spreading was reported as main cause of collapse of bridge span. However, the failure of middle span is not understood with this explanation. The failure of Llacolen bridge during the same earthquake is shown Figure 1.9(b).

(a) **(b)**

Fig. 1.9 Failure of **a** Bio– Bio bridge and **b** Llacolen bridge following the 2010 Chile earthquake (Bhattacharya et al. 2012)

1.3.7 Tohoku Earthquake (Japan) in 2011

The far-reaching destruction of a coastal town after 2011 Tohoku earthquake in Japan is shown in Fig. 1.10(a). The earthquake occurred in the north-western Pacific Ocean with epicenter 72 km from Tohoku,Japan and the duration of earthquake was almost 6 minutes. The earthquake caused high up-thrust on seabed resulting serious tsunami. Severe liquefaction was also observed. The long duration of the earthquake played a vital role in soil liquefaction. Fig. 1.10(b) shows the collapse of the pile-supported building in Onagawa. The superstructures remain intact and the piles of the building were fully uprooted. It is widely accepted the structures were failed due to tsunami and soil liquefaction (Bhattacharya et al. 2012).

(a) **(b)**

Fig. 1.10 a Destruction of a Coastal City and **b** eradication of pile-supported building in Onagawa following the 2011 Japan earthquake (Bhattacharya et al. 2012)

1.3.8 Sikkim Earthquake (India) in 2011

Many government and private RC multi-storied buildings were severely damaged in Gangtok during 2011 Sikkim earthquake (Fig. 1.11 a&b). The buildings were damaged due to noncompliance of earthquake resistance design features of structures. As a result, shear and flexure failure of column, shear failure of beam-column junctions, in-plane failure of weak infills causes damages of the structures (Fig. 1.11c). The infill walls were failed due to its inferior quality and imperfect connection with RC frame structure.

(a) **(b)** **(c)**

Fig. 1.11 a Structural failure of two intermediate storeys of 9-storied building **b** failure pattern of column and **c** failure of infirm masonry wall at Gangtok during 2011 Sikkim earthquake (Rai et al. 2012)

So, the failure of pile-supported structures may be due to structural failure, geotechnical failure or combination of both. The major causes of geotechnical failure are the response of soil supporting the piles. It was observed that the tendency of damage increases significantly for piles in liquefiable soil.

1.4 Objectives of the Present Study

In view of the above-mentioned issues and present state-of-the-art, the main objectives of this research work are as follows:

1. To study the effect of soil nonlinearity in seismic ground response analysis and liquefaction assessment.
2. To investigate the static lateral response of single piles in liquefiable and non-liquefiable multi-layered sloping ground taking into account of both kinematic and inertial interaction effects.

3. To evaluate the effects of axial loading on dynamic response of laterally loaded single piles in liquefiable and non-liquefiable layered soil considering nonlinearity of soil.
4. To investigate the nonlinear dynamic response of laterally loaded single piles in liquefiable multi-layered sloping ground under the influence of axial load.

1.5 Scope of the Present Work

The scopes of this research works are:

- Performing nonlinear ground response analysis and liquefaction assessment of level layered soil deposit of Kolkata city (NKD and RCD soil) and sloping layered soil deposit of Kandla Port site using nonlinear finite element-based software Cyclic1D.
- Development of Beam on nonlinear Winkler foundation (BNWF) model for soil-pile system using open-source finite element-based code, OpenSees and evaluation of the effects of various parameters on soil and pile response in homogenous cohesionless soil using pseudo-static analysis.
- Performing pseudo-static analysis of pile foundation using developed BNWF model considering both kinematic and inertial interaction in Kandla Port site using the results obtained from nonlinear GRA.
- Development of 3D finite-element based model using OpenSeesPL user-interface and performing dynamic analysis of pile foundations in Kolkata city (NKD&RCD soil).
- Evaluation of the effects of axial load on dynamic response of laterally loaded single piles in NKD and RCD layered soil of Kolkata city under three different input motions.
- Performing nonlinear dynamic analysis of laterally loaded single piles in NKD and RCD layered soil considering various ground slopes under the influence of axial load.

1.6 Organization of the Thesis

The thesis consists of seven chapters. The brief description of each chapter is as follow:

Chapter 1 deals with the general introduction, research motivation, failure case studies of pile foundations. It also describes objectives & scope of the present study and organization of the thesis.

Chapter 2 comprises comprehensive literature review of ground response analysis & seismic site characterization for Indian subcontinent, past research on laterally loaded pile foundation in non-liquefiable soil, seismic design guidelines for piles in liquefiable soil according to various codes of practice and finally past studies of piles in liquefiable level & sloping ground.

Chapter 3 provides the effect of soil nonlinearity in seismic ground response analysis and liquefaction assessment of Kolkata soil in India. Details of study area Kolkata, geotechnical data, input ground motions, methodology, validation of the model and important results & discussions are presented in this chapter.

Chapter 4 presents the seismic response of laterally loaded single piles in liquefiable multi-layered sloping ground using pseudo-static approach. Various design approaches for kinematic pile response, methodology for kinematic & inertial interaction effects, validation and present study are discussed. The effects of different parameters such as ground slope, slenderness ratio of pile, pile head fixity condition, existence of liquefiable layer, depth of liquefiable soil layer and embedment depth of pile on kinematic pile response are evaluated. Comparisons of present numerical methodology with the simplified formulations available in the literature are also done.

Chapter 5 describes the effects of axial loading on dynamic response of laterally loaded single piles in liquefiable layered soil of Kolkata city considering nonlinearity of soil. The details of numerical modelling, methodology adopted and validation have been given. The following responses of soil and pile are focused on: liquefaction potential assessment, near and far field soil response, lateral pile displacement, pile bending moment and bending-buckling interaction analysis for various soil and pile properties.

Chapter 6 presents the extension of the above work for piles in liquefiable multi-layered sloping ground. The effects of soil type, ground slope, ground motions, ground water table location, pile head fixity conditions and slenderness ratio are also evaluated using the validated numerical model.

Chapter 7 provides the summary with major conclusions derived from the present study. The scope for future research work is also suggested.

Chapter 2

Literature Review

From the significant number of cases of failure and/or damages of piles and pile-supported structures during recent past earthquakes, it has been evidenced that response of soil to earthquake load plays major role in the damages. It was noticed that the extent of damage of piles is more in liquefiable soil. In this chapter, literature review part is divided into different categories for better understanding. First, past studies of ground response analysis (GRA) and site characterization for Indian subcontinent are presented briefly. Then various approaches and past research on laterally loaded pile foundation in non-liquefiable soil are discussed. Finally, seismic design guidelines for piles in liquefiable soil according to various codes of practice are reviewed and past studies of piles in liquefiable level and sloping ground scenario are presented.

2.1 Seismic Ground Response Analysis and Site Characterization for Indian Subcontinent

The effect of local soil condition was first observed in India during the Bhuj earthquake in 2001 (Govindaraju et al. 2004). The linear and equivalent linear method are extensively used for seismic ground response analysis (GRA). Several researchers in the past attempted to study the seismic GRA at various important cities in India.

Hanumantharao and Ramana (2008) carried out 1D GRA using equivalent linear method (EL) at four different locations of Delhi to compare the response with Indian standard code of practices. The shear wave velocity profiles of those site were determined using spectral analysis of surface wave (SASW) method. It was showed that the free-filed ground acceleration response matches with the standard code for long distance input motions only.

Seismic GRA using EL method of Bangalore city has been carried out by Anbazhagan and Sitharam (2008) to evaluate the effect of local soil condition and micro zonation of the city. Both SPT and shear wave velocity database obtained from multi-channel analysis of surface

waves (MASW) technique were used for GRA. The results showed that the magnification factor varies from 1 to 4.7 in the city.

Boominathan et al. (2008) performed GRA by the EL method using SHAKE computer program to evaluate the seismic hazard of Chennai city. The velocity of shear wave (V_s) was determined using both the empirical correlation and MASW method. It was observed that the high frequency structures are more susceptible to amplification due to local soil conditions in the city.

Mohanty and Walling (2008) performed GRA for Kolkata City using probabilistic seismic hazard assessment with 10% probability of exceedance in 50 years. The PGA at ground surface obtained for the city varies from 0.1g to 0.34g.

Phanikanth et al. (2011) performed EL GRA at three typical sites of Mumbai city using correlation between shear modulus and SPT-N values for evaluating the effect of local soil conditions in seismic ground response for wide varieties of ground motions. It was observed that the peak amplitude, frequency content and bracketed duration of input motions have profound influence on ground response magnification. The magnification factor of acceleration was obtained in the range of 2.5 to 3.45 at various locations of the city.

Akhila et al. (2012) carried out linear GRA at the Park hotel in Kolkata city using DEEPSOIL. SPT and dynamic CPT tests were conducted for determination of V_s and soil parameters. They reported the maximum bedrock level acceleration for Kolkata city from 0.1g to 0.34g and magnification factor from 1.5 to 3.8.

Govindaraju and Bhattacharya (2012) performed GRA adopting EL method using SHAKE at four different locations. Five different spectrum-compatible synthetic earthquake motions were used in their analysis. The variation of magnification factor from 4.46 to 4.82 and maximum spectral acceleration from 0.78g to 0.95g were obtained.

Roy and Sahu (2012) conducted EL GRA using SHAKE considering two types of typical soil deposit, Normal Kolkata deposit (NKD) and River Channel Deposit (RCD) in Kolkata city. Synthetic ground motion model was used to generate bedrock level acceleration for GRA. Eocene Hinge Zone was identified as main concern for future earthquake and maximum magnification of acceleration from 2.2 to 3.0 was reported for the city.

Shukla and Choudhury (2012) performed site-specific GRA of four typical port sites in Gujarat using probabilistic approach. Different PGA values were recommended at various cities in the state for the use of seismic design of structures.

1D and 2D GRA of Kanpur city has been carried out by Jishnu et al. (2013) using both EL and nonlinear (NL) approach conducting SPT and seismic downhole tests at four different locations. Three Himalayan earthquakes were considered as input motions. Liquefaction assessment and post-liquefaction settlement was evaluated using the average PGA obtained from 1D and 2D GRA. It was shown that the Kanpur soil is prone to liquefaction under strong earthquakes.

Kumar and Krishna (2013) carried out EL GRA at six locations of Guwahati city using seven different input motions. The effect of local soil condition and characteristics of input motions were highlighted on ground response.

Kumar et al. (2014) performed GRA adopting EL and NL method for two typical sites of Guwahati City using DEEPSOIL software. It was reported that both the methods provide similar results for stiffer soil.

Desai and Choudhury (2014) presented spatial variableness of probabilistic seismic hazard for Mumbai region. Seven different ground motions prediction equations were considered for seismic hazard assessment (SHA). The study covered Mumbai city, Thane district and Navi Mumbai region as these regions are seismically active. The predicted results underestimate the seismic hazard in comparison with the Indian standard seismic code.

Naik and Choudhury (2014) performed site-specific EL GRA of Panjim City, GOA using DEEPSOIL software. V_s-N correlation was used to determine the shear wave velocity of the selected locations. The acceleration magnification factor was in the range of 1.56 to 2.36. Site-specific GRA considering the effect of local soil condition was emphasised in their study.

Nath et al. (2014) performed probabilistic seismic hazard assessment with 10% probability of exceedance in 50 years for microzonation of Kolkata city using EL GRA and reported the surface level PGA in the range of 0.176g to 0.253g.

Shylamoni et al. (2014) evaluated ground response adopting EL approach for KK-NPP site in Japan and obtained results matching well with the recorded aftershocks data.

Site-specific probabilistic SHA at four important sites of Mumbai city has also been performed by Desai and Choudhury (2015) using three different levels of input motion. It was observed that the surface level acceleration magnified in the range of 1.75 to 4.14 with respect to the MBRA depending on the frequency range of the input motions. Also, the response obtained at bed rock and surface level were distinctly different from recommendation of relevant Indian standard code of practices.

Shiuly et al. (2015) presented probabilistic seismic micro zonation of Kolkata city by performing EL GRA using SHAKE. Various maps for PGD, PGV, PGA and spectral acceleration at different time period range were presented for geotechnical and structural seismic design engineers. The maximum PGA at bedrock level was reported as 0.12g and at surface level was reported in the range of 0.095g to 0.18g for return period of 72 years.

Chatterjee and Choudhury (2016) studied the impact of local soil on seismic GRA adopting EL method. Five numbers input motions having significant variation of earthquake parameters were used to perform GRA at 16 different locations in Kolkata city. Maximum magnification of 4.1 was observed for input motions at surface level indicating the significant effect of local soil deposit in seismic GRA.

Satyam and Towhata (2016) employed 1D EL method and microtremor testing for GRA of Vijayawada city and developed seismic hazard maps. Also, liquefaction susceptibility of the city has been assessed using SPT-based empirical methodology.

Vivek and Mohanty (2016) carried out 1D EL and NL GRA of Bhubaneswar using SHAKE & Cyclic1D respectively. NL method was preferred against EL method for GRA. Also, liquefaction susceptibility of the city was assessed using results of GRA. It was shown that Bhubaneswar soil is not liquefiable under small to moderate earthquake.

Ajom and Bhattacharjee (2017) conducted effective-stress based GRA using NL approach for saturated layered soil profile using OpenSees software. It was shown that the surface acceleration is de-magnified with respect to the bed-rock level acceleration in loose to medium dense saturated sand.

Chatterjee (2017) performed EL GRA using derived V_s-N correlation for Kolkata city. Six different borehole locations and five different input motions were considered in his study. It was shown that the alluvial soil of Kolkata city is susceptible to magnification of response at ground surface and the magnification factor varied from 1.7 to 2.5.

Puri et al. (2018) adopted EL method for GRA at various locations of the state Haryana using DEEPSOIL software. Standard correlations were used for determination of initial shear modulus of each layer. Significant amplification of bedrock level acceleration indicated the necessity of performing site-specific GRA.

Recently, Rao and Choudhury (2020) proposed new correlation between SPT-N and shear wave velocity for proposed NPP site at Haryana considering 142 numbers locations of the proposed power plant. The proposed correlation was verified with available geophysical test data and good matching was observed.

Rao and Choudhury (2020) performed probabilistic SHA and Rao and Choudhury (2021) conducted deterministic SHA for the proposed NPP site at north-western part of Haryana state in India. Seismotectonic map was proposed considering the nearby fault and all possible earthquakes of magnitude more than three. These maps are very useful for seismic design of structures in future.

The liquefaction phenomenon is generally occurred in saturated loose cohesionless soil during strong ground motions due to loss of soil shear strength. The liquefaction assessment using safety factor based on simplified deterministic method has been reported by many researchers (Seed and Idriss 1971; Seed et al. 1985; Boulanger and Idriss 2014). Filali and Sbartai (2017) showed that the simplified deterministic method which is based on empirical correlation sometimes overestimate or underestimate the liquefaction potential with compared to exact dynamic method.

The behaviour of the soil during strong excitations is highly nonlinear. However, most of the studies reported in literature have not considered the nonlinearity of soil in seismic GRA. Nonlinear GRA of Kanpur, Bhubaneswar and Guwahati soil have been done by the previous researchers. Also, liquefaction susceptibility and post-liquefaction settlement using results of GRA has been done for Kanpur region only. The studies so far performed for Kolkata region are mainly based on linear and equivalent linear analysis. As RCD soil of Kolkata city mainly composes with loose to medium-dense sand below ground water table (GWT), nonlinear GRA of Kolkata soil considering the effect of local soil condition is very much essential.

2.2 Past Research on Laterally Loaded Pile Foundation in Non-liquefiable Soil

For years, the behaviour of single pile and pile groups have been investigated by several researchers through experimental, analytical and numerical approaches. In this section, a

literature review of representative investigations of laterally loaded pile foundations is presented.

2.2.1 Experimental Investigation

Full-scale field tests are best reliable way to understand the behaviour of laterally loaded pile foundations. But due to high-cost involvement, model tests (Mcvay et al. 1995,1998) are generally adopted for most experimental investigations. Also, most of the experimental studies have been focused on response of single piles. Relatively few full-scale tests (Brown et al. 1988; Rollins et al. 1998; Rollins et al. 2006) were performed on laterally loaded pile groups. These studies are used by several investigators for verification of their analytical research.

2.2.2 Analytical Investigation

A number of analytical methods have been developed for analysis of laterally loaded piles during last six decades. The research of Matlock and Reese (1960) is the pioneering work of the analysis of laterally loaded piles. They have presented the solutions of both short and long piles in non-dimensional form. The limit state method (Hansen 1961; Broms 1964a,b) calculates the ultimate lateral resistance of piles in cohesive and cohesionless soils based on the assumed distribution of ultimate soil pressure along the pile. Reese and Welch (1975) presented two simple expressions for determination of ultimate lateral soil resistance at any depth for cohesive soil. Randolph (1977) developed analytical expression using method of characteristics for the ultimate soil resistance.

The Elastic method (Poulos 1971a, b; Banerjee and Davies 1978; Poulos and Davis, 1980) assumes that the soil is elastic and continuous. The soil Young's modulus varies with the level of stress at the pile-soil interface.

The analytical methods are simplified and semi-empirical in nature. This approach cannot take account the soil continuum and nonlinearity at a time. Also, incorporation of soil layering and nonlinearity in the analytical formulation makes the solution more complicated. Hence, numerical formulation using finite element method can be used efficiently.

2.2.3 Numerical Investigation

Numerical approaches enable investigators to consider various parameters together in a detailed way for analysis of laterally loaded piles. Normally, two main approaches are used

for numerical investigation such as: the Winkler spring (p-y spring) method or subgrade reaction method or beam-on-foundation approach and the Finite Element Method (FEM) or Boundary Element Method.

a) The Winkler Spring Model/Subgrade reaction method

One of the earliest attempts to model the soil-pile interaction by idealizing the soil as a series of independent springs using Winkler spring method. In this model, coupling of soil resistance from point to point along the pile length is not considered. This method is quite accurate and less expensive from computational point of view. Soil nonlinearity can be easily incorporated in this method. The subgrade reaction method was adopted by the various researchers on laterally loaded piles (Allotey and El Naggar 2008, Zhang 2009, Reese et al. 1984, Davisson 1970, Broms 1964a, b, Matlock and Reese 1960, Reese and Matlock 1956).

Further modification of the Winkler approach led to the p-y method. Where p is the soil resistance per unit length of pile and y is the lateral relative soil-pile displacement. Today, the p-y method is widely used method for calculating the response of laterally loaded piles in practice (Matlock 1970; Reese et al. 1974, 1975; Reese and Welch 1975; Reese and Wang 1986). This method uses a beam to represent the pile and independent nonlinear springs along the pile to take account for the soil resistance. The p-y method is often used for the analysis of pile groups using p-multiplier. The different values of p-multiplier have been proposed by various researchers (Brown et al. 1991, McVay et al. 1998, Reese et al. 2006).

While oversimplified, this method is widely used because of its simplicity and the possibility to incorporate factors such as nonlinearity, variation of subgrade reaction and layered soil (Kumar et al. 2006).

b) The Finite Element method (FEM) or Boundary Element Method

The computer-aided finite element method is a powerful and versatile tool for analysis of laterally loaded pile foundation using advanced soil constitutive model. Today, the most versatile continuum-based method of analysis available is the finite element method. It allows to incorporate soil nonlinearity and non-homogeneity easily. However, this method is very complicated and time consuming from computational point of view and is generally used for important project and research-oriented work. On the other hand, boundary element method is framed in frequency domain and is based on linear material behaviour.

Several researchers have analysed laterally loaded piles and pile group using different forms of FEM (Randolph 1981; Kooijman and Vermeer 1988; Bhowmik and Long 1991; Bezgin et al. 2004). The complex mechanism of soil-pile interaction can be simulated using finite element method.

The response of a pile-group with a nonlinear soil model using 3D finite element method was investigated by Muqtadir and Desai (1986). Interaction between the piles in pile group and relative slip, debonding were discussed. The predicted results of pile displacement, bending moment using numerical method was compared with laboratory model test results and good agreement was found.

Brown and Shie (1990) studied the response of laterally loaded closely spaced piles in pile group using two different plasticity soil models. Frictional interface elements were considered to simulate slippage and debonding. They showed that the stiffness of piles in trailing row of pile group reduces significantly under lateral load. This was in line with the observed field tests.

Zhang et al. (1999b) performed 3D finite element analysis using FLPIER to predict response of both the single pile and pile groups. Single pile and 3x3 to 7x3 pile group configurations were considered in their study. The proposed model was validated with experimental results from prototype test. Good agreement between numerical method and model test was observed for predicting pile response.

2.2.4 Simplified or Approximate Method

Different methods are available in the literature which ranges from very simple model to complex nonlinear model to analyse the kinematic response of pile foundations.

Dobry and O'Rourke (1983), Nikolaou and Gazetas (1997), Mylonakis (2001), Nikolaou et al. (2001) proposed simplified methods for computing approximate kinematic bending moment at the interface between two-layers having remarkably different shear modulus. These methods are derived using Winkler model assuming each soil is homogeneous, isotropic, linearly elastic and identical static stress field is acting on soil.

Unlike dynamic or equivalent static analysis for inertial loading, there is no generalized methodology for analysis of pile foundation subjected to kinematic loading. Miura et al. (1989), Liu and Dobry (1995), JRA (2002), AIJ (1998), Liyanapathirana and Poulos (2005a, b) and Elahi et al. (2010) proposed simple but reasonably accurate pseudo-static approach for

analysis of pile foundations in potentially liquefiable soil under earthquake loading. This method is extensively used in engineering practice.

2.3 Past Research on Pile Foundation in Non-liquefiable Soil under Combined Vertical and Lateral load

Various experimental, analytical and numerical studies were performed by several researchers to predict the response of laterally loaded single piles under vertical load.

Karasev et al. (1977) conducted field test to predict the response of laterally loaded single piles under vertical loads. They have conducted full-scale test of cast-in-situ piles and concluded that the vertical response of pile is also influenced by lateral load on pile foundation.

The effect of soil nonlinearity on vertical and lateral response of pile foundation under cyclic loading was investigated by Trochanis et al. (1991). 3D finite-element based elastoplastic model considering soil-pile slippage and separation was considered. Results from numerical study showed that nonlinear behaviour of soil significantly alters the pile and soil response for laterally loaded piles under vertical load. Soil-pile slippage is prevalent for purely vertically loaded pile, whereas soil nonlinearity and soil-pile separation are the key parameters for laterally loaded piles.

Anagnostopoulos and Georgiadis (1993) performed series of model tests to evaluate the effect of interaction between vertical and lateral load on piles in clay. The effect of vertical load on the lateral response of pile was reported as less crucial. They have also suggested that 3D FE or FD method is preferable over subgrade reaction method for analysis of pile foundation under combined action of vertical and lateral loads.

Karthigeyan et al. (2006, 2007) carried out 3D finite-element analysis to evaluate the effect of vertical load on laterally loaded pile foundation in both uniform clay and sandy soil. It was showed that lateral load carrying capacity of pile increases in sandy soil and marginal decreases in clayey soil in presence of vertical load.

Achmus and Thieken (2010) reported using 3D FEM that combined load induces interaction effects in sandy soil. The mobilization of passive earth pressure and shaft resistance at a time due to combined action of vertical and lateral load causes interaction effects.

Hussien et al. (2011, 2014) used simplified soil-pile interaction FE models for uniform sandy soil to evaluate the effect of vertical load on lateral response of 3x5 group piles. The results showed that lateral capacity of leading pile does not vary significantly in presence of the vertical load. However, the response of other piles depends on the relative position of the pile within the group.

The static response of laterally loaded single piles under vertical load in cohesionless soil is studied by Chatterjee and Choudhury (2015). They have used both analytical (modulus of subgrade reaction) method and numerical method using MIDAS GTS. It was shown that presence of vertical load increases bending moment of piles irrespective of soil type and pile length. Also, the increase of maximum bending moment is observed for free headed piles in saturated loose sand.

Chatterjee et al. (2015a) conducted dynamic field testing at three different places of Kolkata city to develop load-settlement curves and time-history of force-velocity. Also, numerical study using FLAC3D has been carried out to simulate field conditions for same soil-pile system. Field and numerical results were differed by 9% for determination of net pile displacement and ultimate pile capacity indicating high efficiency of FLAC3D for analysis of piles under impact loading.

Chatterjee et al. (2015b) have developed an efficient pseudo-static method (analytical approach using FEM) to evaluate the response of single piles under combined loading in both homogenous (saturated and dry) and typical layered soil. The forced based approach with varying lateral pseudo-static loads along depth is considered. It was showed that the pile response increases with an increase of amplitude of earthquake motion for piles having length to diameter ratio 40 and founded in dry dense sand.

Hazzar et al. (2017) have studied the influence of vertical loads on lateral response of pile foundations in sandy soil, clayey soil and two-layer soil-strata using 3D FD analysis. Results showed that lateral resistance of piles does not change significantly with vertical load in sandy soil. However, the presence of vertical load is detrimental to its lateral capacity in uniform or nonuniform clay soil. Also, the effects of vertical load on lateral response of piles in two-layer soil strata depends on characteristics of soil surrounding the piles as well as soil beneath their tips.

It is understood from the above discussion that the analysis of piles under combined action of vertical and lateral loads in layered soil is still scanty in the literature. The studies conducted

so far are mainly considering homogeneous clay, sandy soil or idealized two-layer soil system. Also, these studies lead to inconsistent results with regards to the effect of vertical loads on the lateral response of piles. Hence, the response of laterally loaded pile foundation under the influence of vertical loading in multi-layered soil deposit which is mostly encountered in practical situation becomes extremely necessary.

2.4 Practices and Research on Laterally Loaded Pile Foundation in Liquefiable Soil

2.4.1 Codal Provisions for Piles in Liquefiable Soil

A brief review of design methods in the major codes of practice is presented. All the national and international code provisions for seismic design of pile foundation in liquefiable soil are comprehensively reviewed and summarized herein.

2.4.1.1 Eurocode 8 (EN 1998-5:2004)

The Eurocode 8 (EN 1998-5:2004) identify clearly that the piles should primarily be designed to remain elastic but formation of plastic hinge may be allowed at pile head under certain circumstances. The code advices to consider extra forces on the pile foundation in liquefiable soil due to lateral spreading, specifically in existence of non-liquefiable soil layer overlying liquefiable soil layer. Also, the contribution of liquefiable soil strata to evaluate the pile capacity should be neglected.

2.4.1.2 JRA code (2019)

The failure mechanism of piles in liquefiable soil as per the Japanese Highway Specification, JRA (2019) is shown in Figure 2.1. The code advices design engineers to design the piles based on bending failure mechanism. It assumes that pile experienced passive earth pressure by non-liquefiable layer while the pressure on a pile due to liquefiable soil layer is equal to 30% of total overburden pressure. The code also advices design engineers to check the bending failure of piles for kinematic forces and inertial forces individually. Hence, checking of bending failure due to combined action of kinematic and inertial forces are not necessary.

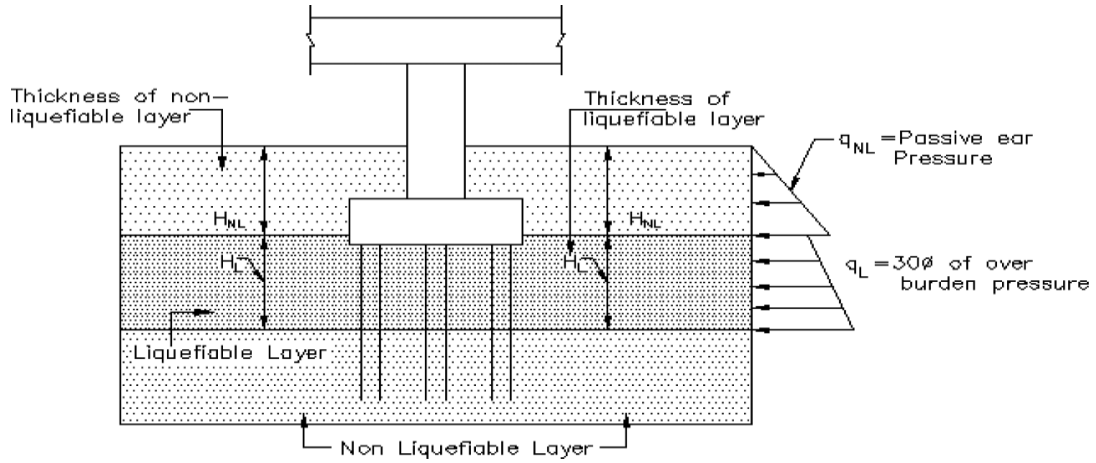

Fig. 2.1 Seismic design of foundation as per JRA code of practice (Pradhan MK et al. 2022)

2.4.1.3 ASCE 7 (2022)

ASCE 7-2022 standards of United States do not give any particular methodology for designing of pile in liquefiable soils. However, the code specifies that pile foundation should be designed to resist deformations due to both earthquake motions and structural response. Also, the code recommends to evaluate the effects of both inertial and kinematic interaction for designing of pile foundation in liquefiable soil.

2.4.1.4 AASHTO (2020)

This code specifies that pile should be analysed and designed for liquefied and non-liquefied conditions in Seismic Zone 4 where the acceleration coefficient is more than 0.5g. The piles should primarily be designed to remain elastic but formation of plastic hinge may be allowed at pile head under certain conditions. Large inelastic deformation may be allowed in the piles for expected liquefaction-induced lateral spreading site. However, the elastic moment capacity should not exceed more than 2.

2.4.1.5 ISO-23469 (2005)

The issues of liquefaction and dynamic SSI is addressed by this code using performance-based design framework. The effects of liquefaction are assessed in simplified equivalent static analysis by incorporating reduction factor for subgrade reaction and effects of ground displacement. Allowable deflection of pile cap, use of high margins to elastic limits of shear force and bending moment at pile head are the criteria for performance-based design for pile foundations.

2.4.1.6 IS 1893 (2016)

Indian design code IS 1893: Part 1 (2016) specifies that pile foundations may be adopted for foundation in liquefiable soil but the pile should be anchored in stronger strata well below the liquefiable layer. Piles should be designed for lateral loads neglecting the lateral resistance of liquefiable soil. The code suggests to perform detailed soil-structure interaction (SSI) analysis for pile founded in liquefiable soil. However, any specific guidelines of SSI analysis are not available in the code.

2.4.1.7 NEHRP (2020)

The USA code NEHRP (2020) focus on the bending strength of the pile. This code notes that "If an unloaded pile were placed in the soil, it would be forced to bend similar to a pile supporting a building. The primary requirement is stability, and this is best provided by piles that can support their loads while still conforming to the ground motions and, hence the need for ductility". Fig.2.2 shows the schematic drawing of kinematic and inertial action as per this code.

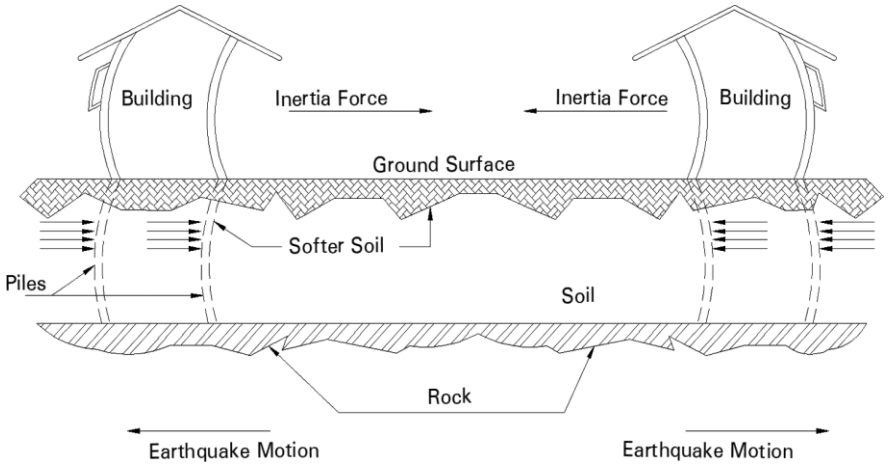

Fig. 2.2 Schematic drawing of kinematic and inertial action as per NEHRP code (Bhattacharya 2003)

2.4.1.8 Caltrans (2011)

Due to limited guidance of analysis methodology of pile foundations, Caltrans (2011) provides more detailed and comprehensive methods of analysis. Although the Caltrans (2011) is a guidance documents of the U.S states of California, not a code of practice. The Caltrans

guidelines for pile foundations is appropriate for both piles in laterally-spreading ground as well level ground.

2.4.2 Past Research on Laterally Loaded Pile Foundation in Liquefiable Soil

After 1964 Niigata and Alaska earthquakes, several efforts have been made to understand the seismic response of pile foundations in liquefiable soil. However, the research into the failure mechanisms of pile foundation was intensified after widespread damages of various pile-supported structures during the 1995 Kobe earthquake using experimental, analytical and numerical procedures.

2.4.2.1 Experimental Investigation

Researchers have performed physical model test to evaluate the effects of soil liquefaction on seismic response of pile foundations using shake table and centrifuge testing.

Investigation using Shake table test

Feng and Wang (2006) proposed scaling factor for p-y curve of liquefiable soil in between 0.25 to 1.0 corresponds to EPWP ratio 0.80 to 0.2 using Aluminium model pile in shake table testing. Model size was 5x5 m and base excitation considered was 0.3g.

Cubrinovski et al. (2006) showed that lateral load on pile from top non-liquefiable layer is almost 4.5-times Rankine's passive pressure and stiffness of liquefiable soil is within the range of 0.033 to 0.013 times stiffness in non-liquefiable condition. Also, it was reported that the response of flexible and rigid pile behaviour was determined by the ground displacement and lateral load from top non-liquefiable crust layer respectively.

Su and Li (2006) investigated the effect of intensity of input motions in seismic response of single piles in liquefiable soil. They showed that development of EPWP is greatly dependent on intensity of input motions. Also, build-up of high EPWP in soil decreases bending moment in pile because of reduction of soil strength.

Dungca et al. (2006) performed shake table test for evaluating the resistance of piles against liquefaction-induced lateral spreading. It was seen that the resistance increases with an increase of loading rate. Also, it was showed that the soil dilatancy and density increases with an increase of shaking in front of pile.

Li et al. (2006) showed that the mode shape alters significantly and natural frequency of soil-pile system reduced by 20-60% in liquefiable condition. Pore water pressure was observed to be increased with base excitation.

Elgamal et al. (2006) evaluated the effect of lateral spreading on single pile using large laminar box. The laminar box was inclined 2^0 with the horizontal. They recommended the soil pressure on pile in the range of 20-40 kPa due to lateral spreading.

He et al. (2008) evaluated the shadowing and group effects of pile group in liquefiable soil. It was shown that the lateral spreading load at trailing row piles reduces 60% due to shadowing effect.

Tang et al. (2009) performed seismic soil-pile-structure interaction in liquefiable soil. It was showed that both the low and elevated cap piles magnify the input acceleration at the pier top in liquefiable condition.

Motamed and Towhata (2010) evaluated the behaviour of pile group under lateral spreading condition and a new parameter 'contribution index' is proposed to calculate the share of each pile against total lateral force.

Haeri et al. (2012) evaluated shadowing and neighbouring effect of pile group in liquefiable soil and it was shown that the soil pressure on each pile is dependent on the location within pile group.

Chen et al. (2012) showed using shake table test with laminar box and aluminium piles that the peak acceleration of soil occurred just before the occurrence of liquefaction. The peak acceleration reduces suddenly after liquefaction.

Motamed et al. (2013) performed shake table test of pile group with superstructure using hollow steel pile. They evaluated the lateral pressure of liquefiable soil on pile group. It was observed that the lateral displacement of soil decreases significantly with the position of quay wall.

Ling et al. (2014) showed that acceleration of pile cap magnify under strong shaking and de-magnify under moderate shaking in liquefiable soil. Also, acceleration at the bottom of pile, surface level and superstructure level magnified under moderate to strong shaking.

Hall et al. (2018) evaluated vibration characteristic of pile group in liquefiable soil. It was showed that predominant period elongates significantly during soil liquefaction. As a result, structural response may be amplified due to resonance effect.

Zhanfang et al. (2020) perform shake table test for 3x3 pile group. It was showed that when pile spacing increases from 3d to 4d (d=pile diameter) in pile group, liquefaction performance is decreased.

Investigation using Centrifuge test

Wilson (1998) investigated the response of piles in liquefiable soil using centrifuge testing and presented dynamic p-y curves using back analysis.

Haigh (2002) evaluated the effect of pile flexibility and pile head fixity condition on seismic response of piles in liquefiable soil. Lateral pressure on rigid pile is found to be greater than flexible pile.

Boulanger et al. (2003) examined the behaviour of piles in non-liquefiable crust layer overlying liquefiable layer considering the effect of lateral spreading. It is shown that peak kinematic load due to lateral spreading coincides with the inertial load of superstructure.

Abdoun et al. (2003) performed centrifuge testing and showed that the maximum kinematic bending moment occurs at boundary between liquefiable and non-liquefiable layer. Also, pile bending moment decreases with shaking duration after increasing at initial stage due to strain-softening behaviour of soil.

Iai and Tobita (2004) observed large-scale residual displacement of soil-pile system in liquefiable soil in comparison with non-liquefiable soil under same inertial loading.

Hung et al. (2014) investigated the effect of pile head mass on seismic response of piles in liquefiable and non-liquefiable soil. Different natural frequency of soil-pile system was observed for different pile head mass.

Zhang et al. (2020a) showed that axial load carrying capacity of pile decreases with an increase of lateral inertial force when buckling effect is considered.

2.4.2.2 Analytical Investigation

The seismic response of laterally loaded pile foundations in non-liquefiable and liquefiable soil under the combined action of lateral and vertical load has been evaluated by Chatterjee et al. (2015) using analytical method following pseudo-static approach. Stiffness degradation factor was considered to represent liquefiable soil condition.

Chatterjee and Choudhury (2017) proposed an analytical procedure to evaluate the influence of combined loading on pile response considering typical soil profile of Kolkata city using pseudo-static approach. They concluded that both the kinematic interaction due to free field motion and inertial interaction due to vertical load should be considered for accurate estimation of seismic response of piles in liquefiable soil.

2.4.2.3 Numerical Investigation

Pile foundations are conventionally designed for inertial load neglecting the effects of kinematic loading. However, for seismic analysis of pile foundations in liquefiable ground consideration of both kinematic and inertial interaction effects is very much essential. The inertial interaction effect is predominant at 10d to15d (d=pile diameter) from ground surface and kinematic interaction is responsible for pile response at deeper depth (Mylonakis 2001).

The effects of kinematic interaction on pile response have been studied by various investigators (Flores-Berrones and Whitman 1982; Dobry and O'Rourke 1983; Kavvadas and Gazetas 1993; Poulos and Tabesh 1996; Nikolaou et al. 2001; Dobry et al. 2003; Maiorano et al. 2009; Sica et al. 2011; Di Laora et al. 2011) following the early research of Margason and Halloway (1977). The kinematic pile response considering nonlinearity of soil has also been investigated (Wu and Finn 1997; Bentley and El Naggar 2000; Cai et al. 2000; Maheshwari et al. 2005) in the past.

Some of the latest numerical studies related to seismic response of pile foundations in liquefiable soil are summarized in Table 2.1.

Table 2.1 Brief of latest numerical studies of pile foundations in liquefiable soil

Authors	Method of numerical study	Objective	Major findings
Cubrinovski et al. (2004)	3D finite-element analysis using DIANA	Comparison of numerical results with shake table test for piles in lateral spreading ground	The estimated soil and pile responses are matching well with observed results from experiment.
Kerciku et al. (2008)	3D continuum analysis using ABAQUS	Buckling and fixity of pile foundation in liquefiable soil	Buckling of pile is controlled by depth of liquefaction, free head length and degradation of soil stiffness.
Dash et al. (2008)	3D BNWF model using SAP2000	To review various methods of developing p-y curves	Proposed more realistic p-y curves for liquefiable soil.

Ren et al. (2008)	3D finite-difference analysis using FLAC3D	To investigate liquefaction depth and bending moment in piles for clay layer underlain by saturated sand	Liquefaction occurs easily at shallow depth and strain at the top of the pile is higher than bottom.
Cheng and Jeremic (2009)	3D FEM based model using OpenSees	To calculate pile bending moment considering soil-pile-column interaction in liquefiable soil	Pile bending moment profile is symmetrical in level ground but slightly asymmetrical in sloping ground.
McGann et al. (2011)	3D (p-y) using OpenSees	To evaluate the accuracy of adopting traditional p-y curves for lateral spreading analysis	Conventional p-y curves are not suitable for large pile displacement.
Maheshwari and Sarkar (2011)	Finite-element code developed using MATLAB	Response of superstructure considering soil-pile-structure interaction	Soil-pile-structure interaction increases the time period of structure and reduces peak response of superstructure.
Rahmani and Pak (2012)	3D FEM using OpenSees	To perform parametric study for investigating the dynamic response of piles in liquefiable soil	Pile head fixity condition, depth of liquefiable layer and frequency of seismic motion are important parameters for piles in liquefiable soil.
Phanikanth et al. (2013)	Finite-difference code developed using MATLAB	To evaluate the impact of existence and depth of liquefiable layer on pile response.	Pile bending response is significantly influenced by the depth of liquefiable layer and peak moment occurred at the boundary between

			liquefiable and non-liquefiable layer.
Choudhury et al. (2014)	3D finite-difference analysis using FLAC3D	To evaluate the effect of input motion on soil and pile response in liquefiable soil	PGA magnification is more for ground motion having larger bracketed duration and frequency. The peak bending moment in pile is occurred at the boundary when the thickness liquefiable layer is about 60% of pile length.
Wang and Orense (2014)	2D nonlinear p-y analysis using OpenSees	To evaluate the response of raked pile in liquefiable soil	Negative batter pile is more effective at interface and positive batter pile is effective at pile head for reducing bending moment for fixed head pile during lateral spreading.
Finn (2015)	3D FEM using PILE3-D	To provide intensive overview of seismic response of pile foundations in liquefiable and non-liquefiable soil.	EPWP, nonlinear behaviour of soil, kinematic and inertial effect are important factors for pile response in liquefiable soil.
Janalizadeh and Zahmatkesh (2015)	2D BNWF model using OpenSees	To evaluate the effect of kinematic and inertial loading in lateral spreading ground	Response of piles in liquefiable soil can be estimated effectively using degraded p-y curves approach.

Lombardi and Bhattacharya (2016)	2D Nonlinear BNWF model using SAP2000	To investigate the effects of soil liquefaction on damping and frequency characteristics of pile supported structures	Soil-pile interaction in complete liquefiable state using p-y curves with strain-hardening proposed by authors gives reasonably good prediction.
Wang et al. (2016)	3D FEM using OpenSees	To evaluate the seismic response of piles in liquefiable soil	Dynamic response of pile is significantly affected by pile cap, lateral spreading and top non-liquefiable crust layer.
Oliaei et al. (2017)	3D FEM using OpenSeesPL	To evaluate the response of large diameter piles in liquefiable layer under clay layer	Frequency of input motion, existence of clay layer and pile diameter significantly affects the dynamic response of piles in liquefiable soil.
Chatterjee (2018)	BNWF approach using MATLAB code	To evaluate the response of piles passing through liquefiable and non-liquefiable soil of Kolkata city considering kinematic and inertial effect	Inertial loading should also to be considered in addition to the kinematic loading for pile passing through liquefiable soil. Also, pile response is profoundly influenced by the depth of liquefiable layer.
Saeedi et al. (2018)	Finite difference method	To investigate the effect of pile and soil properties on dynamic response of piles in	Pile stiffness, relative density of soil, relative stiffness of soil-pile

		liquefiable soil	system and predominant frequency of input motion significantly influence the pile response. However, impact of densities of pile material are not significant on dynamic response of piles.
Zhang et al. (2018)	3D FEM using OpenSees	To evaluate the effect of input motion parameters on soil-pile response in liquefiable and non-liquefiable soils	PGV is the more influential ground motion parameter for dynamic response of pile and near-field input motion is more dangerous than far-filed for pile damages in liquefiable ground.
Ali (2019)	3D FEM using OpenSeesPL	To investigate the response of piles during liquefaction stage	Response of piles closing to ground level is controlled by mass of superstructure, pile stiffness, relative density of soil and bed rock level acceleration of input motion. But, deeper part of pile response is governed by ground slope.
Chatterjee et al. (2019)	3D FDM using FLAC 3D	To perform dynamic analysis of single piles in liquefiable soil incorporating P-delta effect	Both kinematic and inertial effect should be considered for accurate evaluation of seismic

			response of piles in liquefiable soil.
Lopez Jimenez et al. (2019)	3D FDM using FLAC 3D	To investigate the effect of kinematic and inertial interaction on seismic response of soil-pile-structure system in liquefiable soil	Response of structure is significantly influenced by relative density, pile length and frequency of input motion.
Li et al. (2019)	3D FDM using FLAC 3D	To evaluate the effectiveness of X-shaped cross-section pile group in liquefiable sloping ground to mitigate slope displacement	X-shaped pile group is more effective than circular pile for reducing lateral slope displacement. Also, pile head fixity condition and spacing play vital role in deformation response.
Fiky et al. (2020)	3D FE Model using Ansys	To evaluate the effect of horizontal and vertical motion on seismic response of piles in liquefiable soil	Lateral pile displacement decreases with an increase of depth of top non-liquefiable curst.
Zhang et al. (2020)	2D (p-y) using OpenSees	To assess the combined effect of lateral and vertical load on pile buckling in liquefiable soil	Buckling load reduces with an increase of lateral inertial load.
Rajeswari and Sarkar (2020)	3D FEM using OpenSees	To simulate transient force on pile in liquefiable soil for various input motions	The maximum force on pile observed when EPWP varies from 0.5 to 0.75 for homogenous soil and 0.6 to 0.9 for layered soil deposit.
Sinha et al.	FDM using	Flexural response of pile	Bending and buckling

(2020)	MATLAB	foundations in liquefiable soil considering both kinematic and inertial effects	failure of pile can be avoided by selecting appropriate pile geometry neglecting the resistance of liquefiable layer.
Kwon and Yoo (2020)	3D FDM using FLAC 3D	To compute the dynamic response of soil-pile system in liquefiable soil	The dynamic response of pile is influenced by the thickness and relative density of liquefiable layer. Also, kinematic loading due to ground deformation is predominant in liquefiable soil.
Mehdi et al. (2021)	3D FEM using ABAQUS	To investigate the response of soil-pile system in liquefying soil	The relation between pile response and input motion is nonlinear. Effective stress-based GRA is recommended for seismic response analysis of piles in liquefiable soil.
Pradhan et al. (2022)	Literature review	Comprehensive review of pile response in liquefiable soil	For design of pile foundations in liquefiable soil, proper ground improvement techniques to alleviate liquefaction potential should be adopted instead of proposing massive foundation.

Recently, Bhattacharya (2003), Knappett and Madabhusi (2005) and Kimura and Tokimatsu (2007) established an alternative theory of possible pile failure in liquefiable soil based on buckling mechanism. They showed that pile behaves as an unsupported column because of loss of lateral confinement during liquefaction. This axially-loaded column is prone to buckling failure in the direction of least bending stiffness even without lateral spreading loading. So, pile in liquefiable soil may be assumed as laterally loaded slender column and Euler's buckling criteria must be satisfied for analysis of piles in liquefiable soil. Also, vulnerability of pile foundations due to bending-buckling interaction in liquefiable soil has been studied by several researchers (Bhattacharya et al. 2004; Dash et al. 2010; Knappett and Madabhushi 2012). They concluded that both bending and buckling failure mechanism must be considered for designing of pile foundations in liquefiable soil. Bhattacharya et al. (2005) have recently introduced new procedure for evaluating buckling failure mechanism using two main parameters. The evaluation procedure includes determination of Critical depth on account of buckling as capacity and laterally unsupported length of pile as demand. Bhattacharya and Goda (2013) have illustrated this method using probabilistic approach.

2.4.3 Past Research on Laterally Loaded Pile Foundation in Sloping Ground

Mezazigh and Levacher (1998) performed centrifuge test to study the effect of slopes on p-y curve in dry cohesionless soil. It was observed that the lateral pile displacement and bending moment increases when pile is placed near the crest. The displacement and bending moment of pile increased 1.6 and 1.25 times more with respect to the horizontal ground surface for sloping ground of side slope 2 in 1.

Yasuda et al. (2000) investigated the response of piles in level as well as sloping ground using shake table test. It was observed that pile rigidly connected with pile head fails at both top and bottom end but pinned connected pile fails at bottom end only. Also, piles in sloping ground failed due to liquefaction-induced lateral spreading.

Boominathan and Ayothiraman (2007) conducted model experimental study for static and dynamic bending response of single piles in soft clay. The peak bending response in dynamic condition was 1.5 times greater than the peak bending response during static condition.

Muthukkumaran et al. (2008) performed laboratory model tests for evaluating the effect of slopes on p-y curves in dry sandy soil under surcharge loading. The effect of different ground slopes and relative densities of soil have been studied using the same model for soil and pile

response. The non-dimensional p-y curves were proposed for piles in sloping ground under various surcharge loading.

Georgiadis and Georgiadis (2010) analysed the response of piles having different diameter and length in cohesive soil in sloping ground using 3D FE analysis under lateral load. Various undrained shear strength of soil was considered. Analytical expressions for ultimate lateral load and initial stiffness of p-y curves were proposed for piles in clay soil. These curves were used to compare the response with the conventional method and good agreement was found.

Liyanapathirana and Poulos (2010) analysed the pile behaviour in liquefiable sloping ground using Winkler model. Free-filed ground displacement and degraded strength of soil was first evaluated conducting effective stress-based ground response analysis. Then, dynamic analysis was carried out for the soil-pile system. The generation of pore water pressure and strength of the soil evaluated using stress-path model were compared with the results of simple shear test in liquefiable level and sloping ground. It was showed that the proposed method was reasonably competent for evaluating the pile response.

Sawant and Shukla (2014) carried out 3D FE analysis in clay soil to evaluate the effect of slope on laterally loaded pile response. It was observed that proposed model is capable to predict the pile behaviour in the sloping as well as level ground.

Muthukkumaran (2014) studied the effect of slope and loading direction on LLP in cohesionless soil and showed that if piles are placed at a distance of 15-times pile diameter from the slope crest, slope effects in lateral load capacity of pile can be neglected. Muthukkumaran and Almas Begum (2015) investigated the response of laterally loaded single piles in sloping ground experimentally. A series of laboratory tests were performed to develop p-y curves for level and sloping ground. It was concluded that the soil resistance increases with an increase of relative density of soil and embedment depth of pile.

Deendayal et al. (2016) performed static load test of laterally loaded single piles in soft clay on sloping ground. The results of experimental study have been compared with the numerical analysis and reasonable agreement was found.

Jegatheeswaran and Muthukkumaran (2016) analysed the behaviour of pile due to combined loading in slopping ground. The showed that lateral load carrying capacity of pile is decreased and lateral deflection is increased with an increase of slope angle.

Deendayal et al. (2017) evaluated the effect of slopes and embedment depth to diameter ratio on non-dimensional p-y curves in clayey soil. A series of laboratory model test was conducted on a single model pile. New p-y curves were proposed for laterally loaded pile foundation in non-dimensional form.

Deendayal et al. (2018) carried out finite-element based numerical study for group of piles located in layered sloping ground. The response of front, middle and back rows pile under lateral load with various slope angles were studied. It was observed that the front row piles resist lower load in comparison with the middle and back row piles in sloping ground.

Peng et al. (2019) evaluated the behaviour of LL piles in sloping ground using modified strain wedge approach. The soil resistance was assessed using the proposed model. Two divisions of the modified strain wedge and their calculation were proposed. The reliability of the proposed model was verified by performing in-situ testing.

2.5 Summary of Past Works

From the significant number of cases of failure and/or damages of piles and pile-supported structures during recent past earthquakes it has been evidenced that response of soil to earthquake loads plays major role in the damages. The behaviour of the soil during strong excitations is highly nonlinear. However, most of the studies reported in literature have not considered the nonlinearity of soil in seismic ground response analysis. The studies so far performed for Kolkata region are mainly based on equivalent linear analysis.

The effects of vertical load on lateral response of single pile foundation in homogeneous soil have been studied by several researchers. Also, bending failure of pile due to lateral load and buckling failure due to axial load in liquefiable soil have been studied separately by various researchers. However, the response of pile foundations in liquefiable multi-layered soil considering both vertical and lateral load is limited in the literature.

Pile foundations are significantly influenced by both the motion of supporting soil (kinematic interaction) and superstructure (inertial interaction) during earthquakes. However, conventional design practice neglects the effects of kinematic interaction. The presence of mild slope may significantly influence on kinematic pile bending. Past earthquakes also demonstrated that pile-supported structures are vulnerable to kinematic bending failure in

liquefiable sloping ground. However, interaction between kinematic and inertial interaction of piles in liquefiable layered sloping ground is still scanty in the literature.

The response of pile foundations in liquefiable soil using simplified methods based on pseudo-static approach needs various numerical assumptions and not able to predict the accurate values of time-dependent soil stiffness and damping. Besides, due to large shear strain is likely to be developed during soil liquefaction, dynamic analysis of pile considering nonlinear SSI is extremely necessary for seismic response of pile foundations in liquefiable soil.

Chapter 3

Nonlinear Ground Response Analysis

3.1 Introduction

Earthquakes are naturally occurring seismic hazard causing tremendous damage of property, death and injuries of lives. During earthquakes, elastic waves propagate from the focus and produce ground vibration lasting from few seconds to minutes. The magnification of ground motion at any location is depended on seismicity of the area, bed rock type, topography of the site, water table depth, geological and geotechnical properties of the site. Ground vibration is the primary seismic hazard as all other hazards like structural damages, liquefaction of soil, landslides, Tsunami are associated with strong ground vibration. The local soil condition plays important role in the seismic ground response analysis (GRA). The seismic GRA is performed to obtain various parameters like magnification of ground motion, response spectra, stresses and strains in dynamic condition for seismic design of structures and evaluation of liquefaction hazard. 1D, 2D or 3D GRA can be performed depending upon the dimensionality of the problems (Kramer 2005). 1D technique is most popular in geotechnical earthquake engineering practice and widely used for level or mildly-inclined infinite sloping sites with parallel material boundaries. It requires less computational effort. The 2D and 3D methods are suitable for irregular ground surface and presence of embedded structures. Further linear, equivalent linear or nonlinear methods can be employed for 1D GRA (Kramer 2005).

It is evident from the literature review that all the studies of GRA of Kolkata Soil are based on either linear or equivalent linear methods but actual behaviour of soft, alluvial soil of Kolkata under strong ground motions is nonlinear in nature. Nonlinear GRA has been performed in this study for two different sites of Kolkata city having two distinct soil types using the nonlinear finite element program Cyclic1D (Elgamal et al. 2006; Yang et al. 2004) considering the influence of variation of ground water level (*GWT*) and mildly-inclined infinite-sloping site. The 1D GRA technique can be effectively used for liquefaction analysis of Kolkata city as it lies on plain terrain in Gangetic West Bengal (Chatterjee and Choudhury

2016). The liquefaction potential of Kolkata soil has been assessed using the results of 1D nonlinear GRA with the help of both simplified & dynamic methods. The post-liquefaction settlement profile at one location of Kolkata city has also been evaluated.

3.2 Area under Study

The Kolkata metropolitan city, is a portal to north-east India. It is third-most populated city in India. Originally, Kolkata city was developed towards the east side of the river Hooghly. But due to increasing population and scarcity of vacant land, infrastructures are often constructed without proper town planning on reclaimed lands in the Salt Lake and Rajarhat areas. More than 80% of the city area has covered with different types of important heritage building, school, hospital buildings in unplanned way. The altitude of the city above MSL is 5.8 to 6.1 m and *GWT* is located near surface level (Govindaraju and Bhattacharya 2012). The soil of Kolkata city is mainly alluvial in nature having two different soil structures, i.e., Normal Kolkata Deposit (NKD) and River Channel Deposit (RCD). NKD soil mainly compose with silty clay or clayey silt of soft to stiff consistency with sandy deposit at intermediate layer. NKD soil is existed in central Kolkata region like Sealdah, Beliaghata, Ultadanga and Park circus area. The RCD soil mainly composes with medium to dense compactness sand deposit up to significant depth along the existing old Adiganga channel (Roy et al 2018). RCD soil is predominant in south Kolkata region like Tollygunge, Alipore and Kasba area. Kolkata city falls in the Zone III & IV according to zonation map of Indian standard design code IS:1893, Part-I (2016). The Kolkata city is located on the important regional basement fault Eocene Hinge Zone. The width of Eocene Hinge Zone is about 25 km and extended about 45 km below ground level (Roy and Sahu 2012). Kolkata, in the past, has suffered tremendous damages due to near and far field earthquakes. The local soft, alluvial soil of Kolkata city magnify the earthquake ground motion.

3.3 Geotechnical Data

Seismic GRA study requires complete geotechnical data of the selected site. In the present study, geotechnical bore hole data of Kolkata city has been selected from previous study (Roy et al. 2018). The subsoil profile at Ultadanga site (Latitude 22.5948 ^{o}N, Longitude 88.3869 ^{o}E) having NKD soil and Tollygunge Metro site (Latitude 22.4986 ^{o}N, Longitude 88.3454 ^{o}E) having RCD soil have been chosen as shown in Fig. 3.1. The depth of borehole is 50 m for

both the sites. The velocity of shear wave (V_s) of each soil layer is required as input for seismic GRA using Cyclic1D. In absence of in-situ data, SPT-N values are used to calculate V_s using derived co-relation, $V_s = 78.21 * N^{0.38}$, appropriate for all type of soil deposit of Kolkata city developed by Chatterjee and Choudhury (2013), where V_s is in m/s. The co-relation has high value of regression co-efficient indicating accurate prediction of V_s from field SPT values. Friction angles (φ) for cohesionless soils and undrained shear strength (C_u) for cohesive soil are calculated using the co-relation of SPT-N with φ for cohesionless soil and SPT-N with C_u for cohesive soils (Das 1983). Fine contents (FC) of top clay layer is almost 80% and sandy layer varies from 10-30% for depth up to 30.0 m of RCD soil. The values of various soil properties of two typical soil are shown in Tables 3.1 and 3.2 (Roy et al. 2018). The GWT is located at surface level. Average shear wave velocity (V_s^{30}) for 30 m soil column is important parameter for geotechnical site classification as per NEHRP (2020). Vs^{30} for NKD and RCD soil of Kolkata city obtained in the present study using Table 3.1 and 3.2 are 161.0 m/sec and 263.0 m/sec respectively. It is evident that Ultadanga site (NKD soil) falls under class-E (V_s^{30}<180 m/sec) and Tollygunge Metro site (RCD soil) falls under class-D2 (V_s^{30} : 240-300m/sec) which are nearly same as site classification performed by Nath et al. (2014).

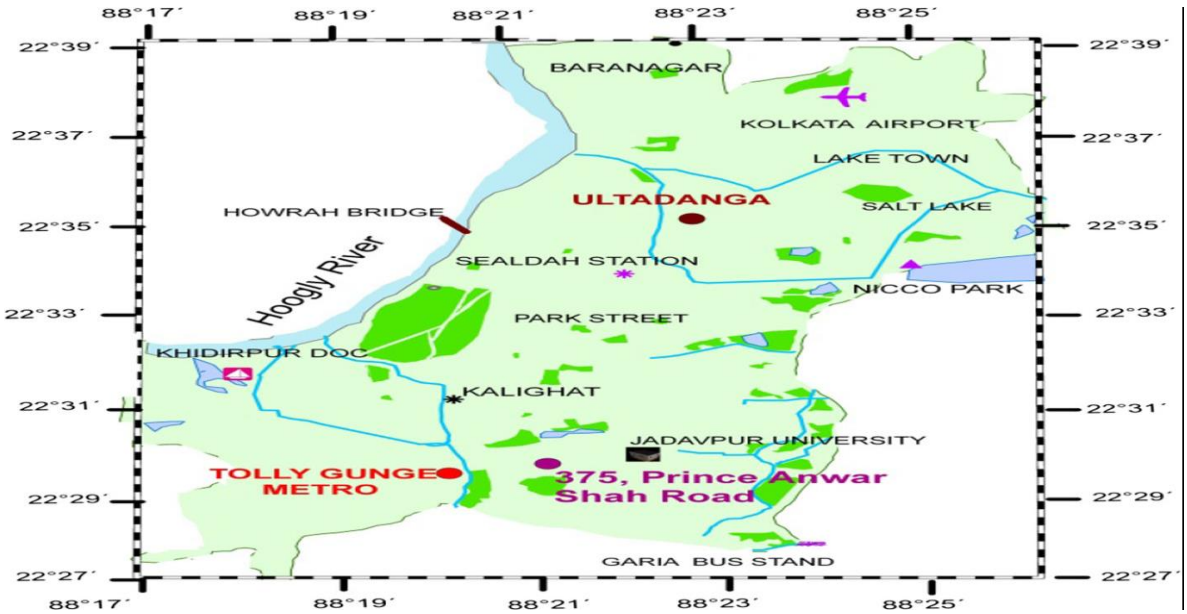

Fig. 3.1 Selected Borehole locations in Kolkata City (Roy et al 2018)

Table 3.1 Typical soil properties of NKD soil of Ultadanga site (after Roy et al. 2018)

Depth(m)	SPT-N value	Unit weight (kN/m3)	V_s (m/sec)	Φ(degree)	C_u (kN/m2)
0.0-3.0	2	19.30	101.8	-	18
3.0-10.0	2	17.00	101.8	-	18
10.0-16.0	8	19.90	172.3	-	37
16.0-26.0	31	19.70	288.4	-	75
26.0-31.0	14	20.00	213.2	-	37
31.0-39.0	22	19.80	253.1	31.4	-
39.0-42.5	29	20.10	281.2	-	75
42.3-46.5	50	19.70	345.8	35.0	-
46.5-50.0	69	20.30	390.9	40.0	-

Table 3.2 Typical soil properties of RCD soil of Tollygunge Metro site (after Roy et al. 2018)

Depth(m)	SPT-N value	Unit weight (kN/m3)	V_s (m/sec)	Φ(degree)	C_u (kN/m2)
0-1.25	2	14.10	101.8	-	18
1.25-5.00	16	16.40	224.3	31.4	-
5.00-11.25	17	18.50	229.5	31.4	-
11.25-15.00	32	19.00	291.9	35.0	-
15.00-18.00	36	19.00	305.2	40.0	-
18.00-30.50	48	19.00	340.5	40.0	-
30.50-32.50	30	19.00	284.8	-	75
32.50-37.00	29	19.50	281.2	-	75
37.00-40.00	40	19.80	317.7	-	75
40.00-45.75	50	19.00	345.8	-	75
45.75-48.50	54	20.30	356.1	-	75
48.50-50.00	67	21.00	386.5	40.0	-

3.4 Input Ground Motions

The input ground motions considered for present analysis are Imperial valley (IMV), Bhuj (BHJ) and Sikkim (SIKM) earthquakes with significant variation in moment magnitude, maximum bedrock level acceleration (MBRA), strong motion duration and frequency content as tabulated in Table 3.3. The input motions are selected in such a way that the MBRA value remain within the reported range of 0.1g to 0.34g in Kolkata city (Mohanty and Walling 2008; Roy and Sahu 2012; Akhila et al. 2012; Govindaraju and Bhattacharya 2012). Strong motion record of IMV earthquake is adopted from the database of Cyclic1D, whereas the BHJ and SIKM earthquakes are adopted from strongmotioncenter.org and www.pesmos.com respectively. The input earthquake motions used in present analysis are shown in Fig. 3.2(a) to (c). The various parameters of these input motions have been estimated using SEISMOSIGNAL (Seismosoft 2012) and are tabulated in Table 3.3.

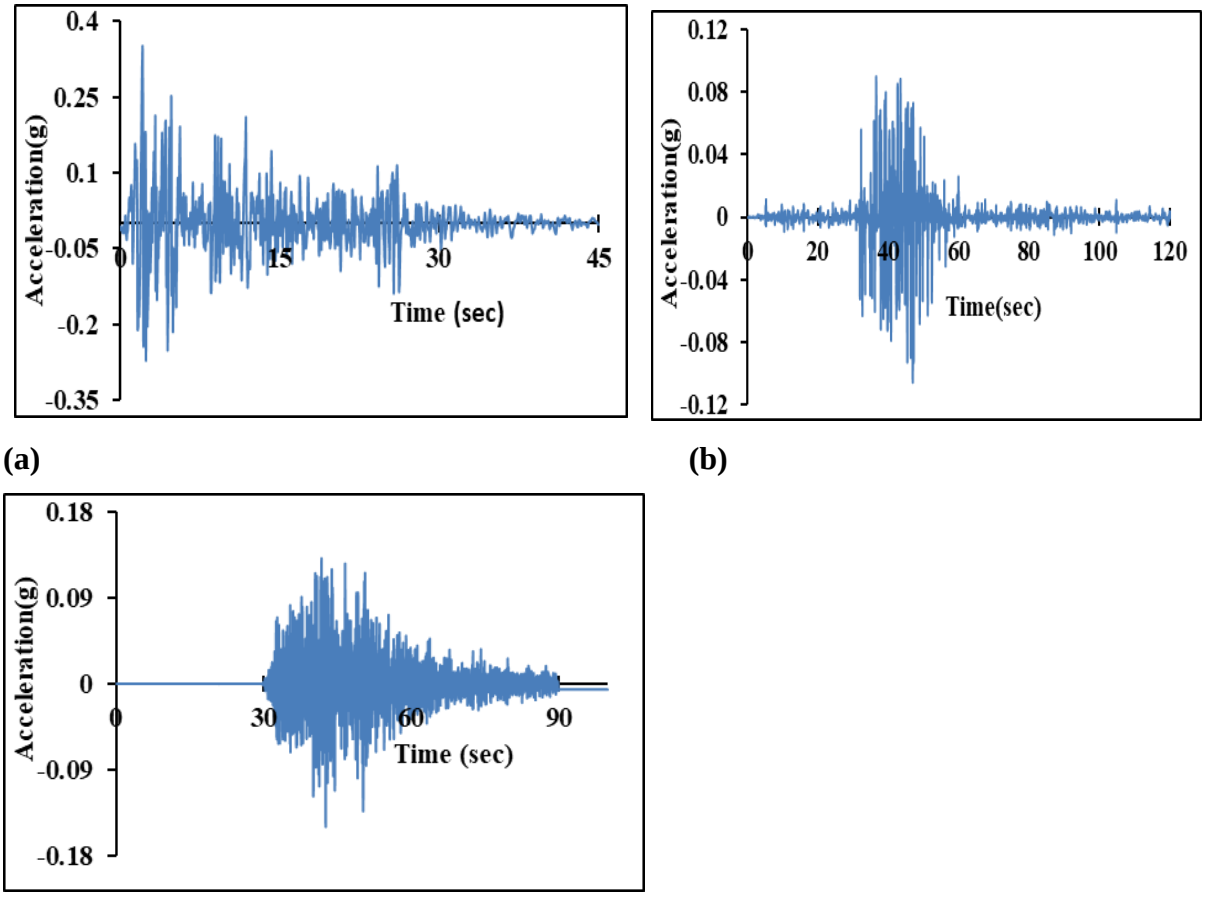

Fig.3.2 Acceleration time-history of **a** IMV **b** BHJ and **c** SIKM input motions

Table 3.3 Various parameters of the considered earthquake motions in the present study

Parameters	Imperial Valley (IMV)	Bhuj (BHJ)	Sikkim (SIKM)
Date	18/05/1940	26/01/2001	18/09/2011
Earthquake Magnitude (M_w)	6.9	7.7	6.8
Name of Recording Station	El Centro site, Imperial Valley	Ahmedabad Passport office	Gangtok
Source to station distance (km)	8.0	230	68
Epicentre of Earthquake	32.733^0N 115.5°W	23.419°N 70.232°E	22.723°N 88.064°E
Max. Bedrock level acceleration(g)	0.348	0.106	0.149
Mean period(sec)	0.488	0.598	1.05
Bracketed duration(sec)	29.67	69.50	71.76
Significant duration(sec)	8.92	16.98	31.75
Predominant period(sec)	0.14	0.27	0.15

3.5 Methodology

1D GRA has been carried out for predicting the layered soil response subjected to input ground motion at bedrock level. It is assumed that response generated is mainly because of vertical propagation of horizontally polarised shear waves and all the boundaries are flat (Kramer 2005). The methods of 1D ground response analysis may be classified as linear, equivalent linear and nonlinear. All the methods have different assumption of the soil rigidity modulus and damping properties. The present study utilizes the nonlinear methods of analyses through computer program Cyclic1D (Elgamal et al. 2015). The soil models available in Cyclic1D have also been implemented in OpenSees (McKenna and Fenves 2001), a software framework for developing applications to simulate the performance of structural and geotechnical systems subjected to earthquakes. Incremental plasticity model is used to simulate the nonlinearity of soil. It allows to model permanent deformation and hysteretic damping. The finite elements are assigned for both dry and saturated soil strata under formulation of fully-coupled fluid-soil system (Elgamal et al. 2015). In time domain based nonlinear analysis the following dynamic equation of motion is solved at every time step with

the help of Newmark time integration method by specifying two user defined coefficients Beta *(β)* and Gama *(γ)* (Newmark 1959):

$[M]\{\ddot{u}\} + [C]\{\dot{u}\} + [K]\{u\} = -[M]\{I\}\ddot{u}_b$ *(3.1)*

where *[M]*, *[C]*, *[K]* are the global mass, damping and stiffness matrix respectively; {ü}, {u̇}, {u} are nodal relative acceleration, velocity and displacement vector respectively; $\ddot{u}_b$ is the acceleration of base motion and *{I}* is the unit vector. Incremental response of soil layers is used to combine *[M]*, *[C]* and *[K]* matrices.

Cyclic1D has been developed for 1D wave propagation analysis using pressure-dependent and pressure-independent soil constitutive models. The constitutive model of soil in Cyclic1D has the capability to narrate the development and dissipation of pore water pressure. The liquefaction model within Cyclic1D (Parra 1996; Yang 2000) is built under multi-yield-surface plasticity framework (Prevost 1985).

A finite element model in the present study is defined in Cyclic1D by specifying the total height of soil profile of 50m.The multi-layered soil profile layer has been divided into total 200 numbers of elements, each of 0.25m thick after convergence analysis. User defined clay without pore pressure effects 'U-Clay' material and user defined saturated granular soil including pore-pressure effects 'U-LiqSand' materials are chosen in present study for defining clay and sand deposit respectively (Elgamal et al. 2003). The shear response of U-Clay material is independent of confinement and can be defined using shear wave velocity *(V_s)*, shear strength *(C_u)*, lateral earth pressure co-efficient at rest *(K_0)*, Maximum shear strain percentage *(y_{max})*, Number of yield surfaces *(NYS)*. The relationship between K_0 and Poisson's ratio *(μ)* is given by the following equation:

$$K_0 = \frac{\mu}{1-\mu} \quad (3.2)$$

The confinement-dependent U-LiqSand material can be defined by specifying reference shear wave velocity *(V_{sr})* in m/s, reference effective mean confinement in kPa *(p_{ref})*, co-efficient of Confinement dependence (*n*), lateral earth pressure co-efficient at rest (K_0), friction angle (Φ) in degree, Maximum shear strain percentage (y_{max}), Number of yield surfaces (*NYS*), Dilation or Phase Transformation (*PT*) angle (φ_{PT}) in degree, Contraction co-efficient (c_1 and c_2), Dilation co-efficient (d_1 and d_2), Liquefaction co-efficient (*Liq*) and co-efficient of Permeability (*k*) in m/sec. The variation of shear wave velocity (V_s) with confinement (*p*) is given by the following expression:

$$V_s = V_{sr}\left(\frac{p}{p_{ref}}\right)^{n/2} \quad (3.3)$$

Shear strength (τ_{max}) at a confinement *p* is expressed by the following equation:

$$\tau_{max} = c + p\sin\Phi \quad (3.4)$$

where, cohesion (*c)* is the shear strength corresponds to zero confinement.

Shear-induced volume contraction and dilation response is separated by Dilation angle (Elgamal et al. 2003). Below PT surface, the contraction scaling function is given in the form: $c_1 \exp(\frac{c_2 p'}{p_a})$

where p_a is atmospheric pressure and c_1 and c_2 are contraction co-efficient dictating rate of pore pressure development and overburden pressure effect respectively.

Above the *PT* surface, the dilation scaling function is dictated in the form: $d_1 \exp(d_2 \gamma_d)$

where d_1 and d_2 are dilation co-efficient and γ_d is cumulative octahedral plastic strain. Dilation parameter d_1 and d_2 dictates the rate of volume expansion and accumulated shear strain effects on dilation respectively. Liquefaction co-efficient (*Liq*) indicates the range of shear strain accumulation.

Recommended range of values of c_1, c_2, d_1, d_2 and *Liq* are 0.3-0.0, 0.2-0.6, 0.0-0.6, 10 and 0.025-0.0 respectively for very loose sand to very dense sand (Elgamal et al. 2003). The values of various input parameters considered from Cyclic1D user manual (Elgamal et al. 2015) based on soil type and properties of each layer of two sites are summarized in Tables 3.4 and 3.5.

A rigid bedrock base is considered for soil layer and inclination angle of model is assumed as zero. *GWT* location at 0.00 m (surface level) is considered initially for both types of soil. Parametric variation of GWT and ground slope has been conducted for RCD soil under Bhuj earthquake motion. The amplitude of the input ground motions of BHJ is scaled by the factor 0.9 for analysis of NKD soil. For all other cases, the scale factor is taken as unity.

Soil nonlinear hysteretic response generates damping in Cyclic1D. Mass and stiffness proportional Rayleigh-type damping of the following form is used in this study:

$$C = A_m M + A_k K \quad (3.5)$$

A_m and A_k are two user-defined constants.

The below equation is used to estimate the damping ratio curve (ξ) using frequency *(f):*

$$\xi = \frac{A_m}{4\pi f} + A_k \pi f \quad (3.6)$$

To define damping coefficients a general damping ratio of 5% along with two close frequencies 1Hz and 6Hz are used. In current study, average acceleration method (γ=0.50, and β=0.25) has been used in Cyclic1D. A convergence tolerance of 10^{-5} is used for computation at any time step. Consistent mass matrix is considered in present analysis.

Table 3.4 Parameter values for the soil materials models of NKD soil (Ultadanga site) (Elgamal et al. 2015)

Depth	$\varphi_{PT(^o)}$	c_1	c_2	d_1	d_2	*Liq*	*k* (m/sec x10^{-5})	p_{ref} (kPa)	*Co-eff*	K_0	y_{max} (%)	*NYS*
3.0	-	-	-	-	-	-	-	-	-	0.5	5	20
10.0	-	-	-	-	-	-	-	-	-	0.5	5	20
16.0	-	-	-	-	-	-	-	-	-	0.5	5	20
26.0	-	-	-	-	-	-	-	-	-	0.5	5	20
31.0	-	-	-	-	-	-	-	-	-	0.5	5	20
39.0	26.5	0.19	0.2	0.2	10	0.015	6.60	80	0.5	0.5	5	20
42.5	-	-	-	-	-	-	-	-	-	0.5	5	20
46.5	24.0	0.06	0.5	0.4	10	0.01	6.60	80	0.5	0.5	5	20
50.0	22.0	0.01	0.6	0.6	10	0.003	6.60	80	0.5	0.5	5	20

Table 3.5 Parameter values for the soil materials models of RCD soil (Tollygunge Metro site) (Elgamal et al. 2015)

Depth	$\varphi_{PT(^o)}$	c_1	c_2	d_1	d_2	*Liq*	*k* (m/sec x10^{-5})	p_{ref} (kPa)	*Co-eff*	K_0	y_{max} (%)	*NYS*
1.25	-	-	-	-	-	-	-	-	-	0.5	5	20
5.00	26.5	0.19	0.2	0.2	10	0.015	6.60	80	0.5	0.5	5	20
11.25	26.5	0.19	0.2	0.2	10	0.015	6.60	80	0.5	0.5	5	20
15.00	26.5	0.19	0.2	0.2	10	0.015	6.60	80	0.5	0.5	5	20
18.00	24.0	0.06	0.5	0.4	10	0.01	6.60	80	0.5	0.5	5	20
30.50	24.0	0.06	0.5	0.4	10	0.01	6.60	80	0.5	0.5	5	20
32.50	-	-	-	-	-	-	-	-	-	0.5	5	20
37.00	-	-	-	-	-	-	-	-	-	0.5	5	20
40.00	-	-	-	-	-	-	-	-	-	0.5	5	20
45.75	-	-	-	-	-	-	-	-	-	0.5	5	20
48.50	-	-	-	-	-	-	-	-	-	0.5	5	20
50.00	22.0	0.01	0.6	0.6	10	0.003	6.60	80	0.5	0.5	5	20

3.6 Validation of Present Model

The present model is validated by comparing the results of PGA profile and PGA magnification profile obtained using Cycic1D software with that obtained using SHAKE 2000 computer program (Chatterjee 2017). PGA magnification is defined as the ratio of maximum PGA at ground surface to the maximum bedrock level acceleration. BHJ earthquake as shown in Fig. 3.2(b) is used as input motion. The soil profile of Borehole and typical dynamic soil properties of Kolkata city (Chatterjee 2017) has been considered for analysis in Cyclic1D as shown in Table 3.6. The values of surface level PGA observed are 0.24g and 0.21g in the reference study and the present study respectively against considered maximum bedrock level acceleration (MBRA) 0.106g. Also, the magnification of PGA at surface level obtained are 2.28 and 2.0 using the reference study and the present study respectively. Figs. 3.3(a) and (b) show the comparison of the profile of PGA and PGA magnification using both the codes. It is found that the results of Cyclic1D are co-relates well with the results of SHAKE 2000 except top 2 m. The top 2m soil is mainly soft soil. The difference of soil response is because of large hysteretic stress-strain behaviour due to soil nonlinearity at low confining pressure near surface level. Both the methods produce same results for stiff soil where strain level is low (Kramer 2005). The slight deviation in results at greater depth may be reasonable due to different analysis procedures and soil model which are estimated based on soil descriptions by two authors. SHAKE uses equivalent linear analysis, whereas Cyclic1D is based on nonlinear analysis. Hence, the present model can be efficiently used for seismic GRA and liquefaction hazard assessment.

Table 3.6 Soil profile of Borehole considered in the present study (after Chatterjee 2017)

Depth (m)	*SPT-N*	Unit weight (kN/m3)	V_s(m/sec)	Material model	Model parameters
0.0-1.05	6	17.6	154.5	*U-Clay*	K_0=0.5, C_u=37kPa, y_{max}=5%, *NYS*=20
1.05-7.4	3	16.3	118.7	*U-Sand*	p_{ref}=80kPa, *co-eff*=0.5, K_0=0.5, $\Phi=29^0$, y_{max}=5%, *NYS*=20.
7.4-11.9	5	17.8	144.2	*U-Clay*	K_0=0.5, C_u=37kPa, y_{max}=5% , *NYS*=20
11.9-14.15	10	18.7	187.6	*U-Sand*	p_{ref}=80kPa, *co-eff*=0.5, K_0=0.5, $\Phi=30^0$, y_{max}=5%, *NYS*=20.
14.15-18.4	8	19.6	172.4	*U-Sand*	p_{ref}=80kPa, *co-eff*=0.5, K_0=0.5, $\Phi=30^0$, y_{max}=5%, *NYS*=20.
18.4-23.6	18	20.7	234.6	*U-Clay*	K_0=0.5, C_u=75kPa, y_{max}=5%, *NYS*=20
23.6-30.0	24	19.8	261.7	*U-Sand*	p_{ref}=80kPa, *co-eff*=0.5, K_0=0.5, $\Phi=35^0$, y_{max}=5%, *NYS*=20.

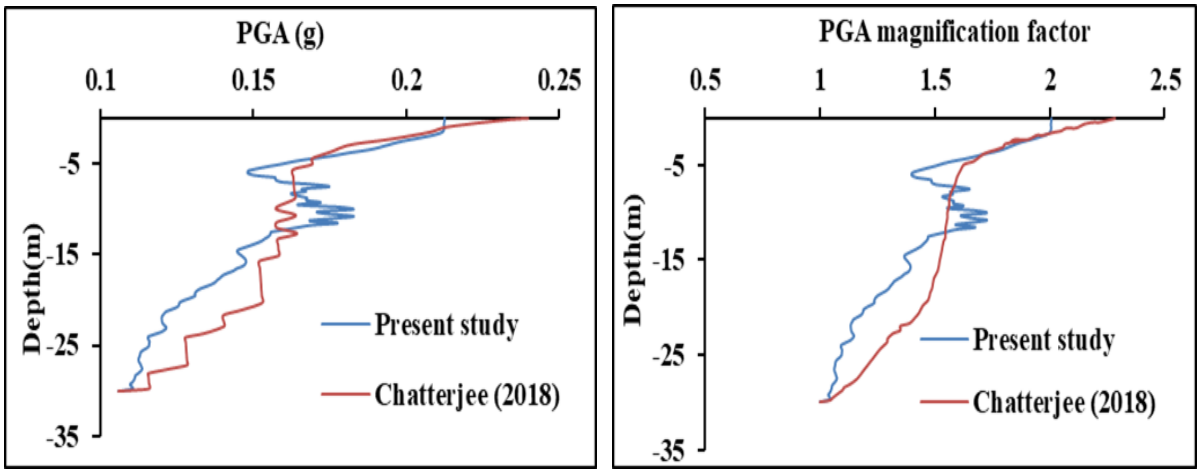

(a) **(b)**

Fig.3.3 Profile of **a** PGA and **b** PGA magnification factor

3.7 Results and Discussions

Nonlinear GRA is performed for two different sites of Kolkata metropolitan city having NKD and RCD soil type using Cyclic1D. Three different input motions namely, IMV, BHJ and SIKM earthquakes with significant variation in moment magnitude, MBRA, strong motion duration and frequency content have been used in this study. The results obtained from GRA are presented in the subsequent section. In addition, liquefaction potential has been evaluated for RCD soil using both simplified deterministic and dynamic methods along with post-liquefaction settlement profile.

3.7.1 Profile of PGA and its Magnification Factor

The profile of PGA for two soil types are presented in Figs. 3.4 (a) and (b) respectively. The PGA at surface level for IMV, BHJ and SIKM earthquake motions are 0.119g, 0.109g, 0.118g for NKD soil against MBRA 0.348g, 0.095g, 0.149g respectively. Also, PGA at surface level for RCD soil using same earthquake motions are 0.091g, 0.075g, 0.072g against MBRA 0.348g,0.106g ,0.149g respectively. It is seen that surface acceleration is de-magnified with respect to MBRA for NKD soil for all the earthquake motions except BHJ earthquake motion. The input acceleration is magnified by 1.15 times when subjected to BHJ motion in the same soil profile because of comparatively low amplitude input ground motion. For RCD soil, reduction of output acceleration is observed for all the earthquake motions. The ground motion magnification occurs in the stiffer soils under lower MBRA and reduction occurs in the soft soils under higher MBRA as soft soil undergoes large hysteretic stress-strain behaviour and dissipates energy under strong motion causing reduction of PGA. The PGA magnification factor of two types of soil for all the ground motions are shown in Table 3.7. The magnification factors for all the layers are higher in BHJ and SIKM earthquake motions than high amplitude IMV motion. It is to be noted that all the MBRA converges to almost same PGA at ground surface for both types of soil. Hence, MBRA has less influence over the same. The PGA and its magnification factor obtained in the present study using nonlinear method are compared with the results of previous researchers using linear and equivalent linear (EL) method and tabulated in Table 3.8. The PGA values obtained in this study (0.072g to 0.119g) are matching well with the reported PGA of Kolkata city by Shiuly et al. (2015) as well as codal value of 0.08 to 0.12g for zone-III & IV of IS 1893 part I (2016)**.** As per the Global Seismic Hazard Assessment Program (GSHAP) (Giardini et al. 1999), the PGA values

of Kolkata city with 10% probability of exceedance in 50 years range from 0.08g to 0.13g, which is closely matching with the current results. However, the PGA obtained in the present study is significantly less than predicted by Mohanty and Walling (2008), Nath et al. (2014) and all other researchers for Kolkata city. It is seen that linear and EL method of analysis overestimates the PGA and its magnification factor as shown in Fig. 3.5. Also, linear or EL method of analysis cannot truly represent the hysteric stress-strain relationship of soil. The EL method is based on total stress analysis and does not consider the effects of ground water table. Nonlinear method of GRA is most appropriate for soft alluvium soil of Kolkata city as GWT is located near ground surface.

Figs. 3.6(a) and (b) show the comparison of surface level acceleration time-history response between NKD and RCD soil profile for IMV and BHJ earthquake motions respectively. The acceleration response of NKD soil is higher than RCD soil under both the motions. As the stiffness of top soil of RCD is comparatively lower than NKD soil, the reduction of MBRA is more at surface of RCD soil. Ground motion magnification or de-magnification is a function of both dynamic soil properties and magnitude of ground motions.

Table 3.7 PGA magnification factor (PGA at surface/MBRA) for selected earthquakes at two different sites of Kolkata

Site	IMV	BHJ	SIKM
NKD soil	0.34	1.15	0.79
RCD soil	0.26	0.70	0.48

Table 3.8 Comparison of response obtained using present study with previous researchers for Kolkata city

Parameters	Mohanty and Walling (2008)	Akhila et al. (2012)	Govindaraju and Bhattacharya (2012)	Roy and Sahu (2012)	Nath et al. (2014)	Shiuly et al. (2015)	Chatterjee and Choudhury (2016)	Chatterjee (2018)	Present study
Software & type of analysis	Attenuation model	DEEPSOIL (*L*)	SHAKE (*EL*)	SHAKE (*EL*)	DEEPSOIL (EL)	SHAKE (*EL*)	SHAKE (*EL*)	SHAKE (*EL*)	Cyclic1D (*NL*)
MBRA considered (g)	-	0.1-0.34	0.154-0.21	0.136-0.141	0.124-0.178	0.12	0.106-0.372	0.106-0.372	0.106-0.348
PGA at surface level(g)	0.1-0.34	0.40-0.73	0.24-0.30	0.223-0.278	0.176-0.253	0.095-0.18	0.438-0.68	0.24-0.63	0.072-0.119
PGA magnifi-cation factor	-	1.5-3.80	1.34-1.73	1.64-1.97	2.51-4.22	0.80-1.50	1.63-4.10	1.7-2.5	0.26-1.15
Spectral acceleration (g)	-	-	0.78-0.95	0.32-1.26	0.48-0.52	0.014-0.88	0.41-0.86	0.46-0.75	0.33- 0.67

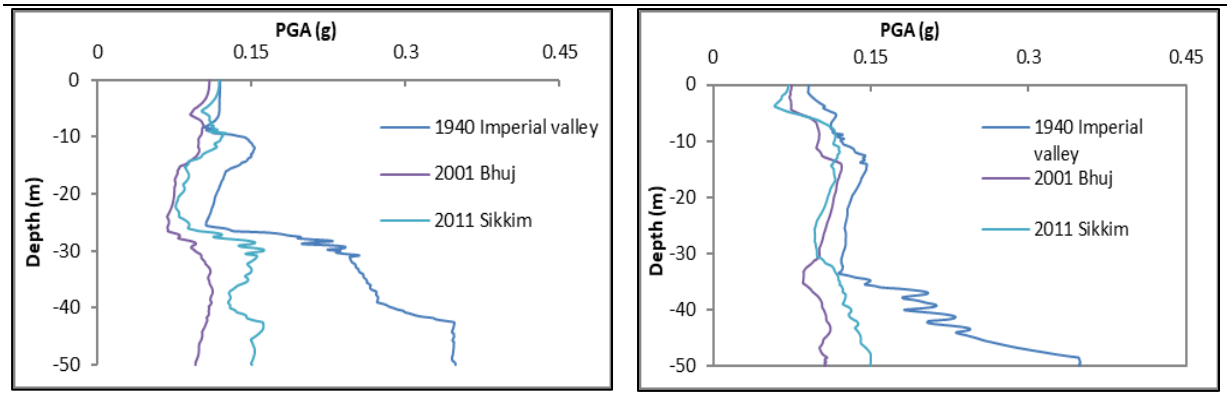

(a) **(b)**

Fig.3.4 PGA Profile of **a** NKD soil and **b** RCD soil

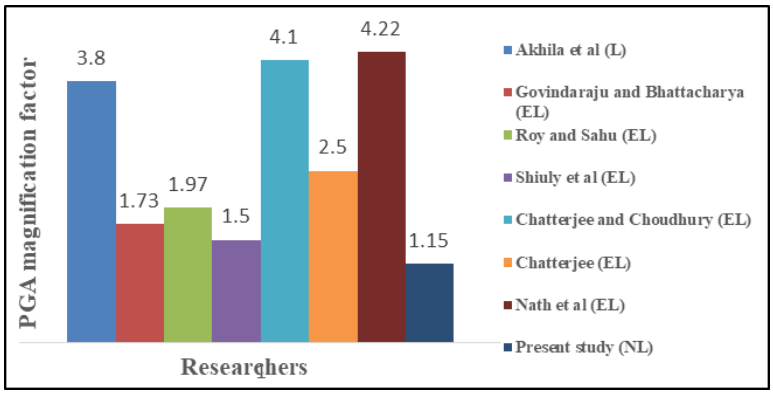

Fig. 3.5 Comparison of maximum PGA magnification factor obtained by various researchers

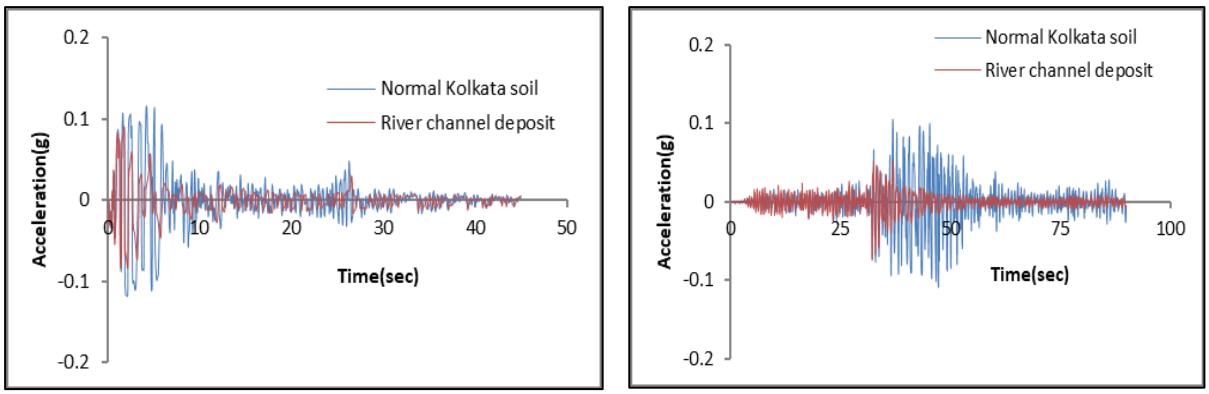

(a) **(b)**

Fig. 3.6 Comparison of surface level acceleration response at the surface between NKD and RCD soil for **a** IMV and **b** BHJ earthquake motion

3.7.2 Peak Shear Stress & Shear Strain profile

Figs. 3.7 (a) and (b) demonstrate the variation of shear stress with depth of NKD and RCD soil respectively for various earthquake motions. The shear stress is linearly increasing over depth and peak values obtained are 82.77 kPa and 86.10 kPa respectively for NKD and RCD at bottom of soil profile under IMV earthquake motion. The shear stress value obtained for all other ground motions for same soil profile are less than that of IMV earthquake motion. Hence, shear stress is depended on soil profile and amplitude of earthquake motions. The shear strain profile of NKD and RCD soil are shown in Figs. 3.8 (a) & (b) respectively for three different earthquake motions. It is seen that the top 12.0 m of RCD soil consisting mainly fine to medium dense sand undergoes large strain under IMV and SIKM input motions. The peak strain value obtained is 1.33% for NKD soil (2nd layer from top) and close

to 5.00 % for RCD soil (3rd layer from top) under IMV earthquake. Higher strain value indicates the more energy dissipation during earthquake loading and the liquefaction susceptibility of the considered site.

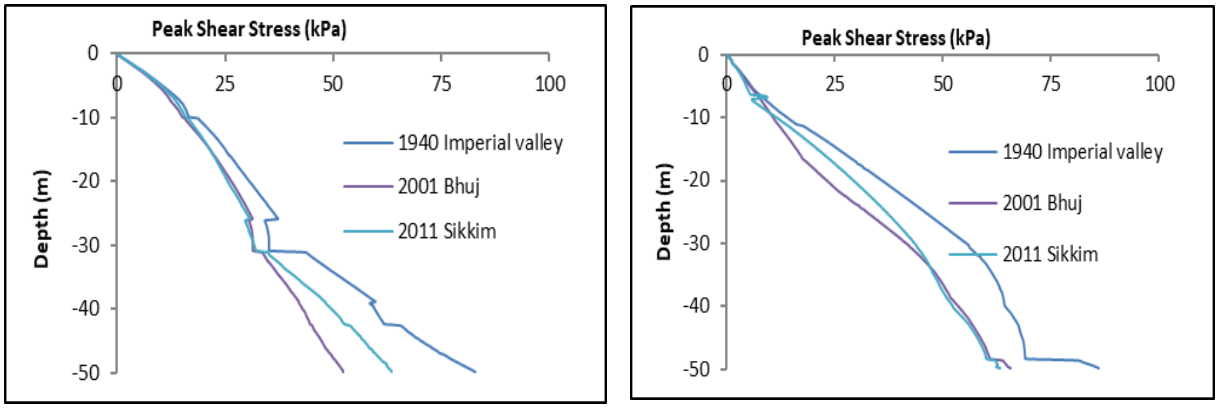

(a) **(b)**

Fig.3.7 Peak shear stress profile for **a** NKD and **b** RCD soil

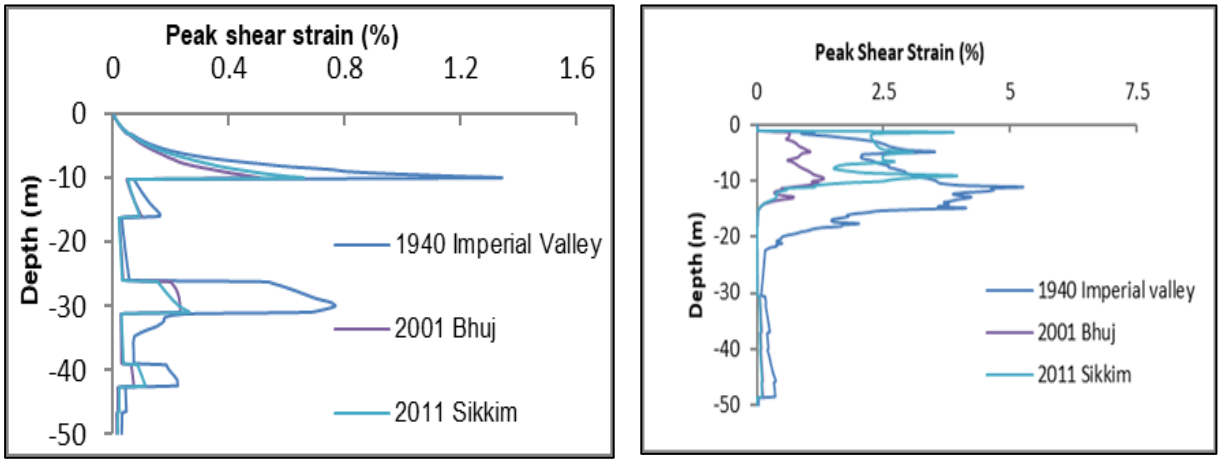

(a) **(b)**

Fig.3.8 Peak shear strain profile for **a** NKD and **b** RCD soil

3.7.3 Peak Ground Displacement (PGD) Profile and Time-history

From Fig. 3.9(a), it is observed that the PGD relative to the base of NKD is almost uniform for depth 31.0 m from ground level for all the considered ground motions. The relative displacement below depth 31.0 m decreasing linearly and becomes negligible. The relative displacement of RCD soil for IMV and BHJ motions are almost uniform to depth 40.0 m and

becomes negligible thereafter. PGD value for SIKM motion decreases linearly from ground surface to 11.25m and then follow uniform pattern up to 40.0 m as shown in Fig 3.9(b). Figs. 3.10 (a) and (b) represent the displacement time-history under BHJ motion for NKD soil and RCD soil respectively. It is noticed that RCD soil shows more residual displacement at the end of loading cycle because of its liquefaction susceptibility. More residual displacement of RCD soil indicating probability of earthquake-induced lateral spreading. The PGD at surface of NKD soil are 0.082, 0.035 and 0.083 m for IMV, BHJ and SIKM motions respectively. For RCD soil the values are 0.078, 0.059, 0.252 m respectively.

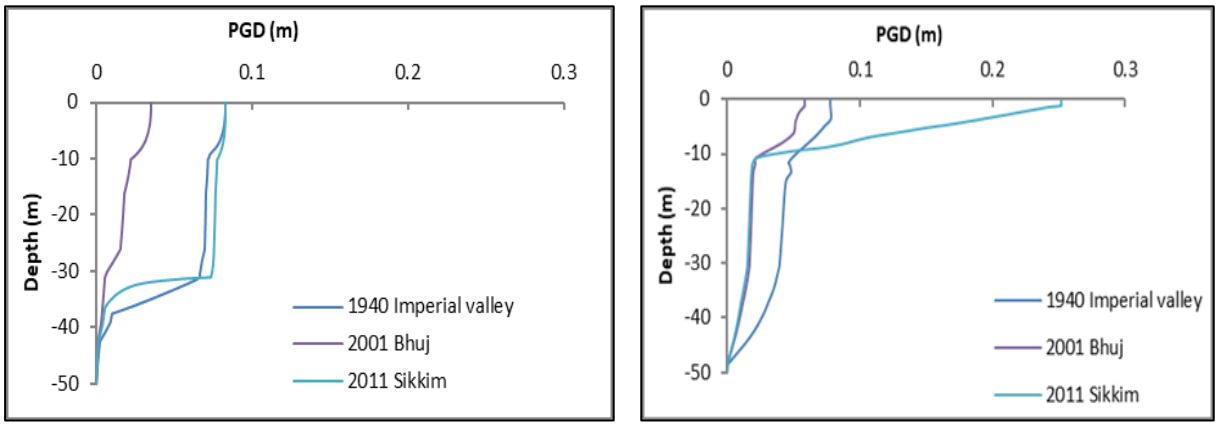

(a) **(b)**

Fig.3.9 Peak ground displacement (PGD) profile for **a** NKD and **b** RCD soil

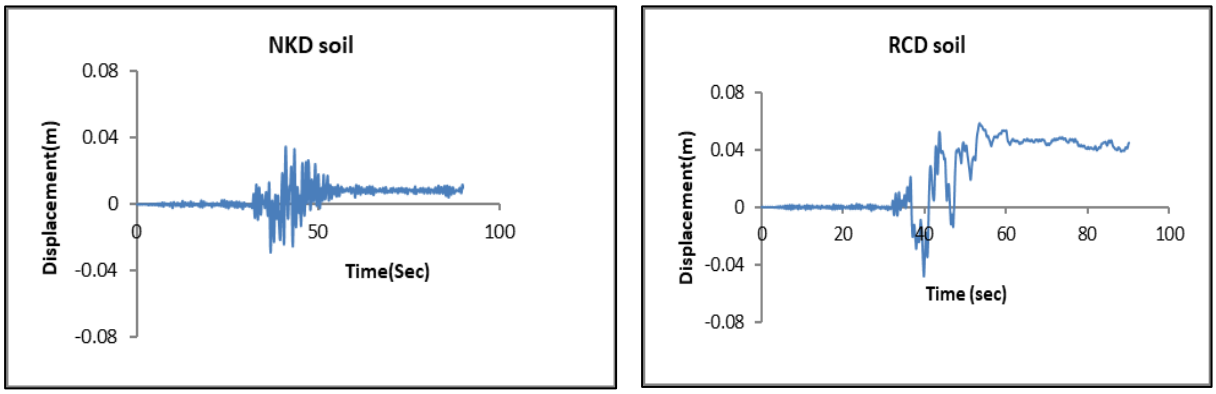

(a) **(b)**

Fig.3.10 Peak ground displacement (PGD) time-history at ground surface for **a** NKD and **b** RCD soil under BHJ earthquake motion

3.7.4 Shear stress vs. Shear Strain Variation

The hysteretic loop of shear stress vs. shear strain curve is key to identify the soil nonlinearity in seismic GRA. Figs. 3.11 (a) and (b) show the hysteretic loop at 24.88m depth of NKD soil and 34.88 m depth of RCD soil respectively under BHJ earthquake motion. These figures indicate that nonlinear method is capable to calculate unrecoverable plastic strains of soil. First cycle of hysteresis loop is bigger in area and shear stress and shear strain attain their highest values. Shear stress amplitude got attenuated with the passage of time. Similar trends are noticed at different soil layer for both NKD and RCD soil.

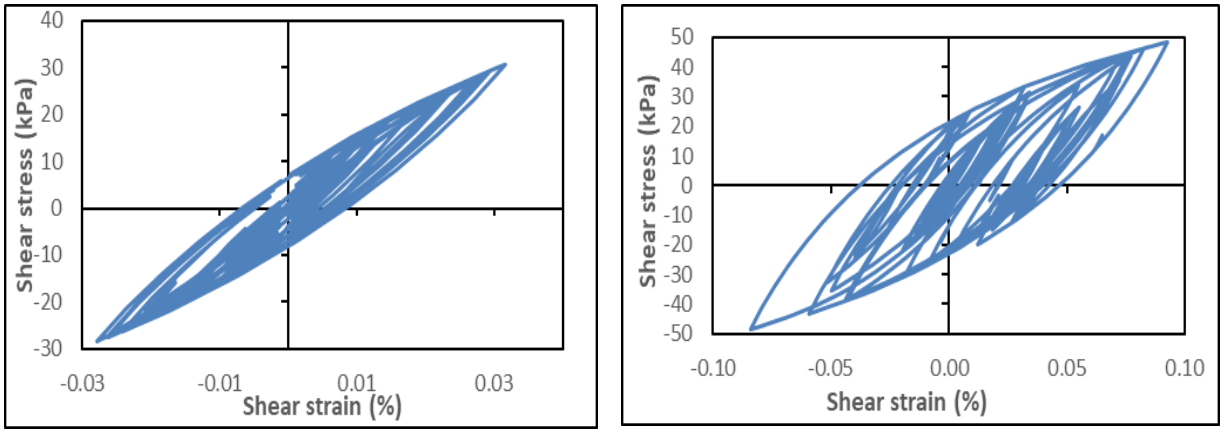

(a) **(b)**

Fig. 3.11 Shear Stress vs. Shear Strain of **a** NKD soil (Depth: 24.88 m) and **b** RCD soil (Depth: 34.88 m) for BHJ motion

3.7.5 Acceleration Response Spectrum vs. Period

The evaluation of response spectrum curve is vital step in GRA for seismic design of structure. The acceleration response spectrum curves at ground surface for various input earthquake motions by considering 5% damping ratio are illustrated in Figs. 3.12(a) & (b) for NKD and RCD soil respectively. The peak spectral acceleration values obtained for IMV, BHJ and SIKM earthquake motions are 0.67g, 0.53g, 0.51g at 0.86 sec, 0.77 sec and 0.14 sec, respectively for NKD soil. The peak spectral acceleration values 0.46g, 0.33g, 0.34g at 0.58 sec, 0.72 sec and 0.26 sec respectively are obtained for RCD soil. The values of spectral acceleration obtained using present nonlinear GRA are matching well with the results of previous researchers as shown in Table 3.8 and Fig. 3.13. So, the IMV and BHJ motions have

detrimental effect on high rise structures resting on soft soil and SIKM motions are vulnerable for short period structure resting on soft soil, respectively.

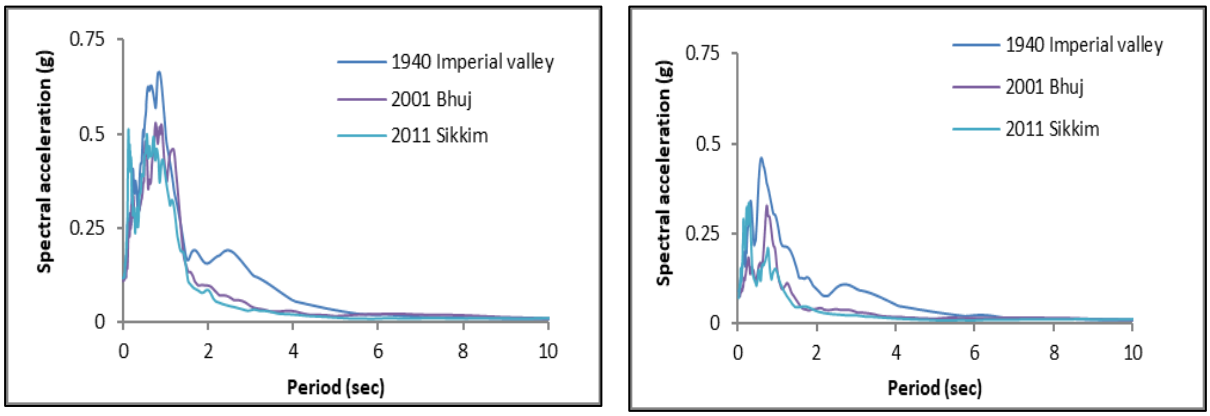

(a) **(b)**

Fig. 3.12 Response spectrum curves for 5% damping for **a** NKD and **b** RCD soil

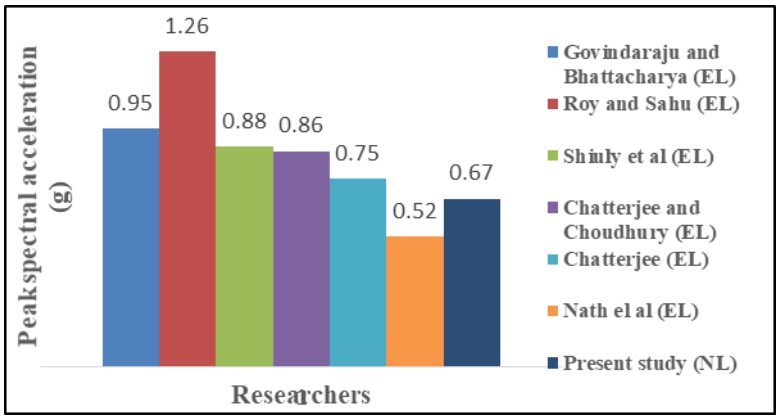

Fig. 3.13 Comparison of peak spectral acceleration obtained by various researchers

3.7.6 Effect of Ground Water Table (*GWT*)

During seismic conditions, increasing pore pressure will reduce effective stress of saturated loose to medium dense sand which may lead to considerable differences on the magnification of PGA at the surface when compared with same soil deposits without *GWT* consideration. The depth of *GWT* at various location of Kolkata city ranges from surface level to 3.0 m (Akhila et al. 2012; Govindaraju and Bhattacharya 2012; Chatterjee 2017). In this study the effect of fluctuation of *GWT* from ground surface to 5.0 m depth has been investigated for RCD soil. The influence of location of *GWT* on seismic nonlinear GRA has shown in Table 3.9 and Figs. 3.14 (a), (b) & (c). PGD value decreases by almost 37% when level of *GWT* changes from 0.0 m to 5.0 m depth below ground surface for BHJ motion as shown in Fig. 3.14(a). PGA value increases by almost 39% for fluctuation of *GWT* from surface to 5.0 m below surface for the same motion. Settlement profile decreases drastically with lowering

GWT as shown in Fig 3.14(c). The variation of various parameters with fluctuation of water table location is tabulated in Table 3.9.

Table 3.9 Variation of PGA and magnification factor, PGD, Settlement with *GWT* location of RCD soil for BHJ earthquakes

GWT (Below *GL*)	Various parameters			
	PGA (g)	Magnification factor	*PGD* (m)	Settlement (m)
0 m	0.075	0.70	0.059	0.0203
2.5m	0.117	1.11	0.052	0.0096
5.0 m	0.123	1.16	0.037	0.0043

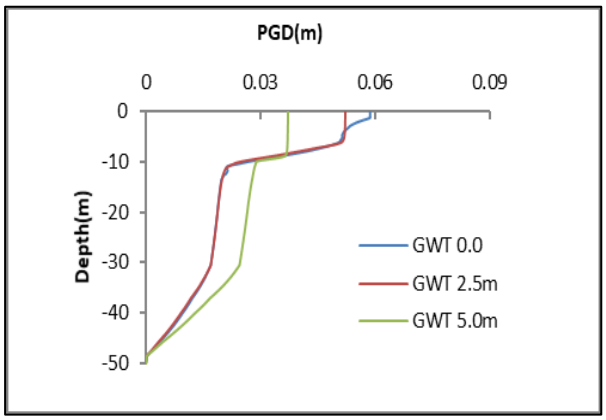

(a)

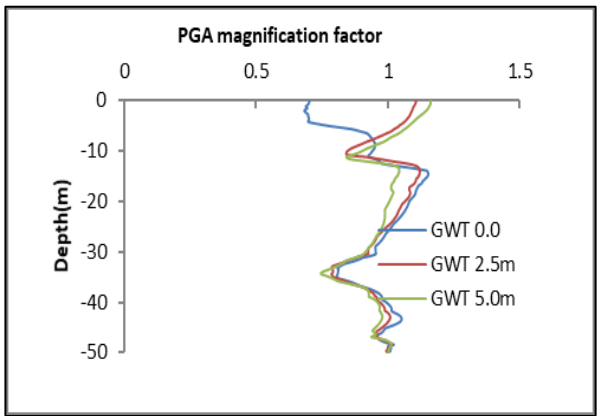

(b)

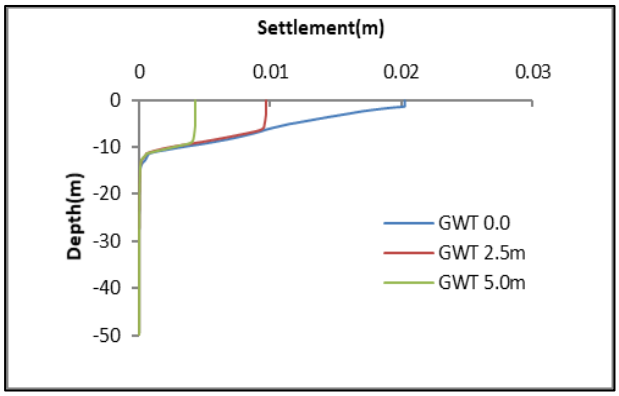

(c)

Fig. 3.14 Profile of **a** PGD **b** PGA magnification factor and **c** settlement with variation of *GWT* location of RCD soil using BHJ motion

3.7.7 Effect of Mildly-inclined Infinite Slope

The effect of mildly-inclined infinite sloping site on seismic GRA has been carried out for RCD soil. Parametric study has been conducted considering Slope(*S*)=0, 2.5 and 5 degree. *S*=0 degree corresponds to level ground. The PGA value obtained at surface level are 0.075g, 0.160g, 0.117g for BHJ motion for slope 0, 2.5 and 5 degree respectively. The PGA & PGD profile for various sloping sites under BHJ motion are demonstrated in Figs. 3.15(a) and (b) respectively. It is also to be noticed that peak ground displacement (PGD) relative to base increases significantly with small increase of slope for BHJ earthquake motion. So, the mildly-inclined slope at river channel soil deposit is prone to liquefaction-induced lateral spreading. PGD vales are 0.059m, 1.68m and 1.31 m for *S*=0,2.5 and 5% respectively under BHJ motion.

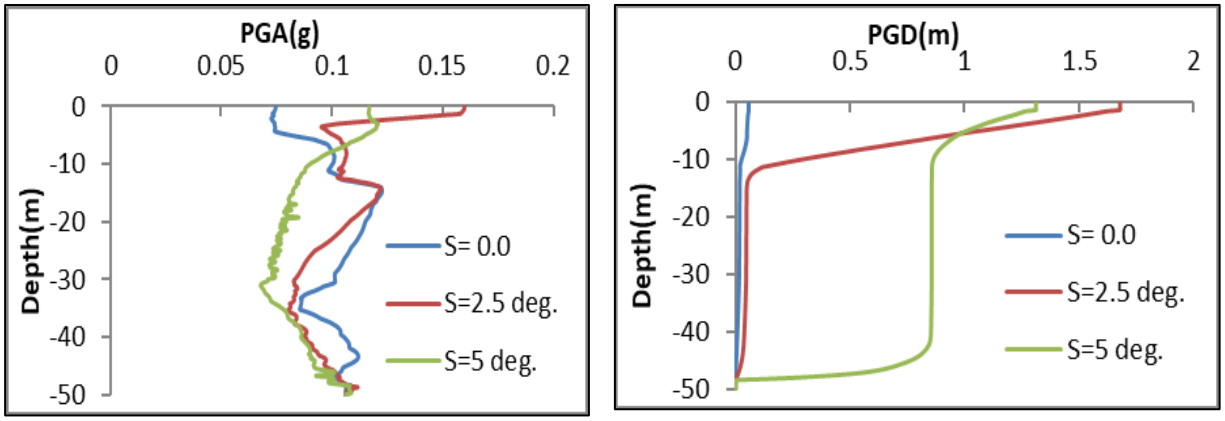

(a) **(b)**

Fig. 3.15 Variation of **a** PGA and **b** PGD with slope of RCD soil under BHJ motion

3.7.8 Assessment of Liquefaction Potential

The liquefaction analyses have been carried out using excess pore pressure ratio for both NKD and RCD soil. The values of excess pore pressure ratio are evaluated at each depth. The soil is termed as liquefiable if the ratio exceeds one. The excess pore pressure profile of NKD and RCD soil for IMV, BHJ and SIKM earthquake motions are presented in Figs. 3.16 (a) and (b) respectively. The excess pore pressure ratio is less than 1 in all the soil layers of NKD soil.

However, the excess pore pressure ratio is more than 1 for top 12.0 m depth of RCD soil for all the earthquake motions. So, the RCD soil is prone to liquefaction.

As the RCD is prone to liquefaction, liquefaction potential of this soil has also been studied using Simplified deterministic method (Seed and Idriss 1971; Seed et al. 1985; Boulanger and Idriss 2014) and nonlinear dynamic method (Filali and Sbartai 2017) for BHJ earthquake motion. In simplified deterministic method, the factor of safety for liquefaction potential (FOS) which is ratio of cyclic resistance ratio (CRR) to cyclic stress ratio (CSR/CSRD) is evaluated along depth. The RCD soil profile as shown in Table 3.2 has been considered for liquefaction analysis. CRR is evaluated from corrected SPT-N value and fines content (FC) percentage (Boulanger and Idriss 2014). The PGA at surface and shear stress reduction co-efficient profile (R_d) obtained from nonlinear GRA has been utilized for evaluating the CRR. Also, in dynamic method CSRD is evaluated at each depth using maximum shear stress obtained from the dynamic analysis. Fig. 3.17 shows the variation of FOS and FOSD along depth for BHJ earthquake motion. It is clear from graph that the FOS is less than 1 for top 12.0 m soil for all the motions. FOS using dynamic method for BHJ motion shows the similar results. It is also seen that FOS increases with depth but it start decreasing beyond 20.0 m depth. CRR value is more up to 20 m depth due to high fines content in the soil. Beyond 20 m depth, factor of safety decreasing due to decrease of CRR value but it is more than 1 which indicates non-liquefied condition. Nath et al. (2014) reported liquefaction potential at various places of Kolkata city in their seismic microzonation study. The reported liquefaction potential index (LPI) of Ultadanga having NKD soil is 0 to 5.0 (low) and Tollygunge Metro site having RCD soil is 5.0 to 15.0 (high). Hence, the present finding is in line with the report of Nath et al. (2014).

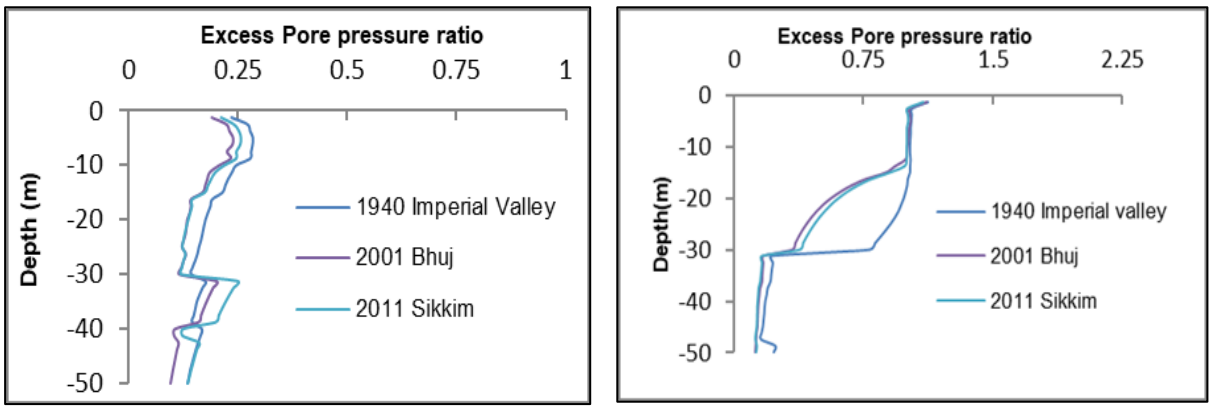

(a) **(b)**

Fig.3.16 Excess pore pressure ratio profile for **a** NKD and **b** RCD soil

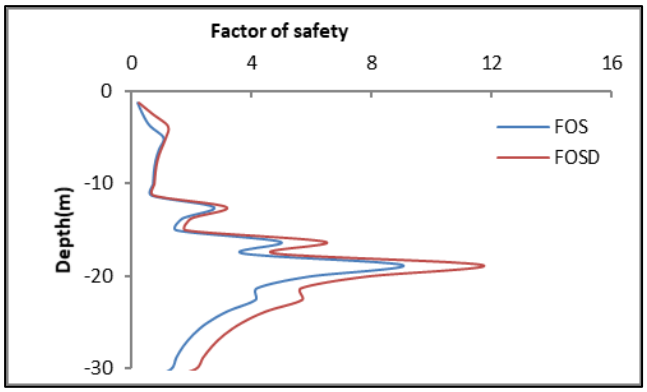

Fig.3.17 Comparison of Factor of Safety for liquefaction potential (FOS/FOSD) for RCD soil under BHJ motion

3.7.9 Evaluation of Post-liquefaction Settlement Profile

The post-liquefaction settlement profile of RCD soil is evaluated using Cyclic1D. Fig. 3.18 shows the settlement profile of RCD soil subjected to different earthquake motions. The settlement values observed of RCD soil at surface level are 0.066m, 0.020m and 0.057m for IMV, BHJ and SIKM earthquake motions respectively. This is also to be noted that top 12 m loose to medium fine sand mainly contributes the settlement.

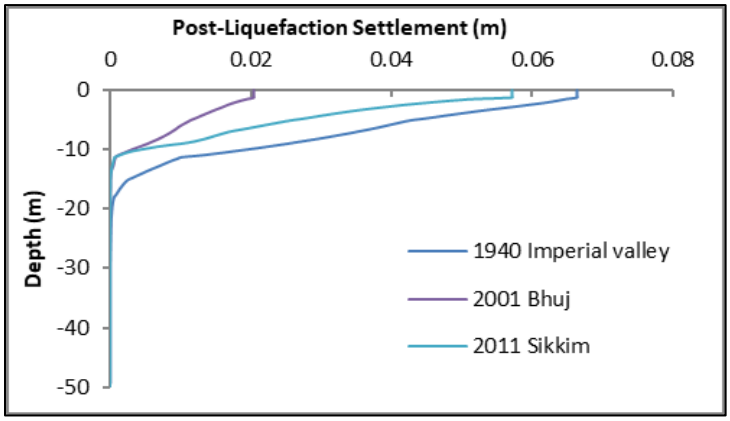

Fig. 3.18 Post-liquefaction settlement profile of RCD soil

3.8 A Case study of Liquefaction-induced Damage to a Port Building Supported on Pile Foundation

Liquefaction-induced damage to building supported on Pile foundation during earthquake is presented in this study using a reported case study on damages to the Kandla Port building during the 2001 Bhuj earthquake in India (Dash et al. 2009). Port structures are more vulnerable to seismic damages when built in seismically active area like Gujarat in India (Rajaram and Kumar 2014). The foundation of Port Structures is often constructed on reclaimed land which are potentially liquefiable. During the 2001 Bhuj earthquake the liquefaction of intermediate sandy layer, ground settlement, lateral spreading and resulted damages of Kandla port building have been reported (Dash et al. 2009). The effective stress-based ground response analysis (GRA) of the port site has been carried out using nonlinear finite element program Cyclic1D considering nonlinearity of soil.

3.8.1 Kandla Port Building: Liquefaction-induced Damage during Bhuj Earthquake

3.8.1.1 The Earthquake

The 2001 Bhuj earthquake (*Mw*=7.7) was the most devastating seismic hazard causing tremendous damages of lives and properties in urban area of India. It struck the Kutch area of Gujarat state of India on January26, 2001. The epicentre of the earthquake was situated at 23.419^{o}N, 70.232^{o}E located at a distance of 20 km North East of Bhuj in Gujrat. The maximum bedrock level acceleration (MBRA) was 0.106g. The acceleration time-history of the earthquake is shown in Fig. 3.2(b).

3.8.1.2 The Structural Details of the Kandla Port Building

Kandla Port is located in the Kandla Creek and is 50 km from the epicentre of the earthquake. The Kandla Port tower, a 22.0 m high six-storied building supported on combined pile-raft foundation is located proximate to waterfront. The building was supported by 12 numbers of column (0.45x0.45 m and 0.25x0.25 m) and 32 numbers RCC piles of diameter 0.4 m and length 18 m. The 0.5 m thick foundation mat was provided as a rigid pile cap.

3.8.1.3 The Geotechnical Properties of the Port Site

The Kandla port is built on inherent ground consisting of recent unconsolidated layer of clay, silt and sand. The ground slope is about 1.5-2.0 % towards seaside. The ground water table (*GWT)* is located at 1.2-3.0 m below ground surface. The soil of the site composes of 10 m

deep soft clay underlain by 12 m deep fine to medium dense sand and 10 m deep hard clay (Dash et al. 2009). The top clay layer having water content 42-47 % is highly plastic in nature. The SPT-N values of the upper fine sand layer is below 15, whereas the deep coarse sand layer is below 50. The fines content of sandy soils is in the range of 1-32%. The N-value below 15 and fines content 1-32% below GWT of intermediate sandy layer are prone to liquefaction under strong to moderate earthquake vibration.

3.8.1.4 Post-Earthquake Observations

The top of the considered pile-supported building was tilted about 0.30 m towards sea side. The ground adjacent to the building was settled about 0.3 m. Ejaculation of sand through ground cracking was observed near the building site which indicates the widespread liquefaction. A successive pattern of lateral spreading was noticed after earthquake. The maximum magnitude of lateral spreading reported was 0.80 to 1.0 m. Very little damage of superstructure was noticed and significant damages observed in the foundation. Fig. 1.6 shows the tilted building, schematic drawing of the building before and after earthquake respectively (Dash et al. 2009).

3.8.2 Nonlinear Ground Response Analysis of the Port Building Site

1D nonlinear GRA has been carried out for predicting the layered soil response of Kandla port building site using 2001 Bhuj earthquake input ground motion at bedrock level.

A finite element model in the present study is defined in Cyclic1D by specifying the total height of soil profile of 40m.The multi-layered soil profile layer has been divided into total 80 numbers of elements, each of 0.50m thick after convergence analysis. Predefined material models of clayey and sandy soils are chosen to define the soil profile of the site as shown in Table 3.10. A rigid bedrock base is considered for soil layer. Location of GWT is assumed at 1.50 m below ground surface. Mass and stiffness proportional Rayleigh-type damping (5%) has been considered. In current study, average acceleration method (γ=0.50, and β=0.25) has been used in Cyclic1D.

Table 3.10 Parameter values for the soil materials models of Kandla Port soil (Dash et al. 2009, Elgamal et al. 2006)

Depth (m)	*SPT-N*	Material model	Unit weight (kN/m3)	V_s (m/s)	Poisson's ratio	*k* (m/s)	Φ (deg.)	C_u (kPa)
0.0-10.0	5	Cohesive soft	13.00	100.0	0.4	1.0E-09	-	18
10.0-22.0	14	Medium, sand permeability	19.00	205.0	0.4	6.6E-05	31.5	-
22.0-32.0	35	Cohesive stiff	18.00	300.0	0.4	1.0E-09	-	75
32.0-40.0	50	Medium-dense, sand permeability	20.00	225.0	0.4	6.6E-05	35	-

3.8.3 Assessment of Liquefaction Potential

Figs. 3.19(a) and (b) show the profile of PGA and peak shear strain. The PGA at surface level for Bhuj earthquake motion is 0.107g against MBRA 0.106g**.** It is seen that surface acceleration is almost same with respect to MBRA for the Kandla port site. The soil strata at 10.0 m to 22.0 m depth consisting of fine to medium dense sand undergoes large strain. The peak strain value obtained is 1.05% at 13.25m depth from surface. Amplification of PGA reduces significantly at that stratum due to higher shear strain. Higher strain value indicates the liquefaction susceptibility of the site. The profile of excess pore pressure (EPP) ratio is evaluated at each depth of Kandla Port site as shown in Fig. 3.20(a). The EPP ratio is almost 1 for soil layer of 10.0 to 22.0 m depth under the Bhuj earthquake. So, the intermediate fine to coarse sandy strata is prone to liquefaction.

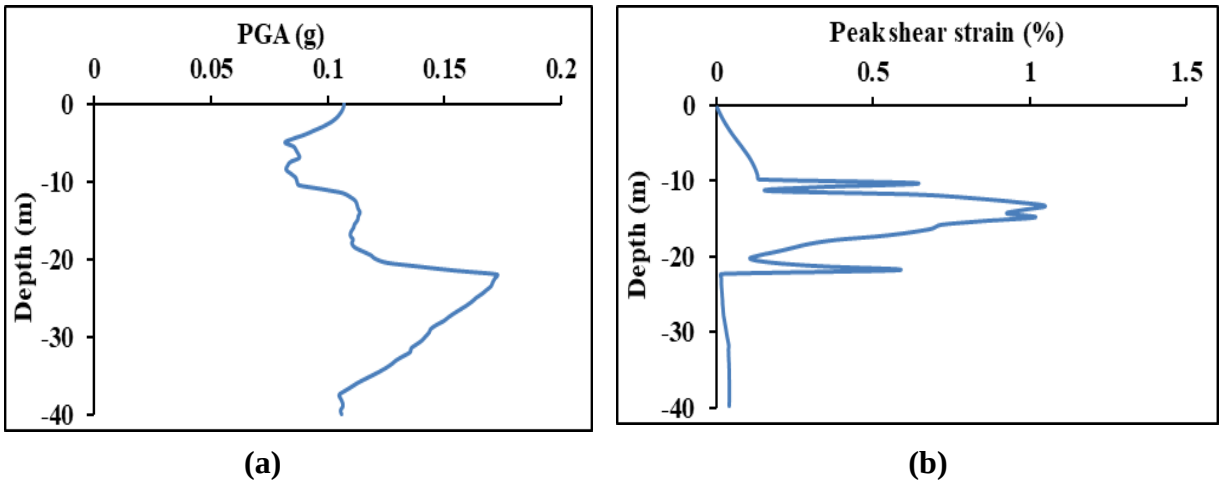

(a) **(b)**

Fig. 3.19 Profile of **a** PGA and **b** peak shear strain

Simplified deterministic method is used to assess the liquefaction susceptibility of the port site as shown in Fig 3.20(b). The factor of safety to liquefaction (FOS) which is ratio of cyclic resistance ratio (CRR) to cyclic stress ratio (CSR) is evaluated along depth. CRR is evaluated from corrected SPT-N value and fines content (FC) percentage. The PGA at surface and shear stress reduction co-efficient profile (R_d) obtained from nonlinear GRA has been utilized for evaluating the CRR. The FOS evaluated from the results obtained using Cycic1D software is compared with that obtained using SHAKE 2000 computer program (Dash et al. 2009), which uses equivalent linear analysis. Fig. 3.20(b) shows the comparison of FOS along depth using both the codes. It is found that the results of Cyclic1D are co-relates well with the results of SHAKE 2000. The slight deviation in results at intermediate depth may be reasonable due to different analysis procedures and soil model which are estimated based on soil descriptions by two authors.

It is clear from graph that the FOS is less than 1 for top clay (1.5-10.0 m) and intermediate sandy layer (10.0-22.0 m) under Bhuj motion. So, the upper clay stratum experiences ground deformation and cracking due to cyclic failure. Moreover, intermediate sand layer (10.0-22.0 m) suffers ground settlement and lateral spreading due to liquefaction. So, the results of GRA argues the ejaculation of liquefiable fine sand through ground cracking near the building site.

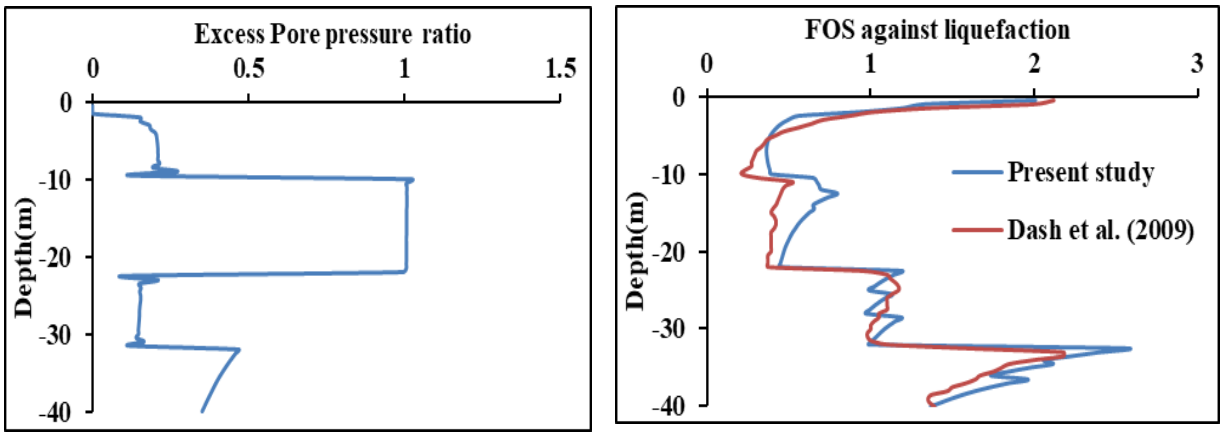

(a) **(b)**

Fig. 3.20 Profile of **a** Excess pore pressure ratio and **b** Factor of Safety for liquefaction potential (FOS)

3.8.4 Evaluation of Post-Liquefaction Settlement

Post liquefaction settlement of saturated sand depends on a number of factors such as relative density, maximum volumetric strain and excess pore pressure. Figs. 3.21(a) and (b) show the profile of volumetric strain and settlement of the port site under Bhuj earthquake motion. The peak value of volumetric strain obtained is 0.49% at 10.25 m depth. The post-liquefaction settlement profile of port site is evaluated using Cyclic1D. The total post-liquefaction settlement calculated using present model, previous study (Dash et al. 2009) and field observation are illustrated in Table 3.11. The settlement values obtained from the present analysis (0.288 m) are matching well with the previous author as well as post-earthquake observed settlement of 0.3 m. Hence, the present study justifies the liquefaction phenomenon of the port site at Kandla.

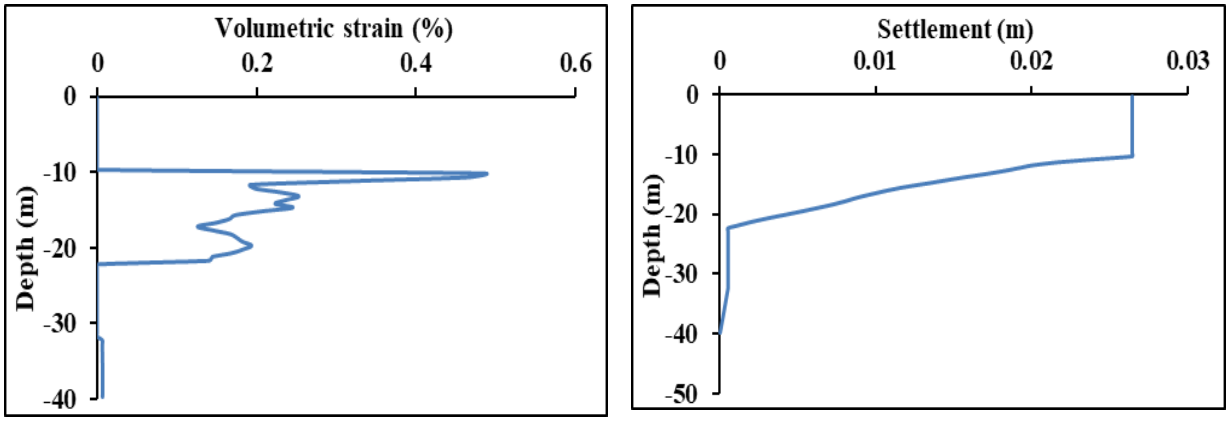

(a) **(b)**

Fig.3.21 Profile of **a** volumetric strain and **b** post-liquefaction settlement

Table 3.11 Post-liquefaction settlement

Depth(m)	Settlement (m)	Settlement (m) (Dash et al. 2009)		Observed settlement (m) (Dash et al. 2009)
		Method-I	Method-II	
10-22	0.283	0.241	0.345	
32-40	0.005	0.070	0.028	
Total settlement	0.288	0.311	0.373	0.300

3.8.5 Lateral Spreading of the Site

Lateral spreading is generally defined as permanent lateral displacement of gently sloping ground due to earthquake-induced liquefaction. Various empirical and semi-empirical methods are available in the literature (Kramer and Smith 1997, Bray et al. 1998, Bray and Travasarou 2007, Escudero 2017) for predicting the amount of lateral spreading. In this study, simplified semi-empirical relationship (Dash et al. 2009) is used to estimate the amount of lateral spreading for probability of exceedance of 16% and 84% respectively. The value of yield co-efficient of soil slope considered is 0.052 assuming 5% ground slope. Additionally, the following values have been considered for evaluation of lateral spreading: earthquake

magnitude M_w=7.7, Average shear wave velocity=175 m/sec, Initial time period of ground *Ts*=0.23 sec, spectral acceleration at *1.5Ts*= 0.44g. The amount of lateral spreading evaluated in the present study is presented in Table 3.12 along with the values calculated by Dash et al. (2009) and observed post-earthquake observation. The obtained value is comparable with the estimated value and post-earthquake observed value.

Table 3.12 Liquefaction-induced lateral spreading

	Present study		Dash et al. (2009)		Observed value
	16% probability	84% probability	16% probability	84% probability	
Lateral spreading (cm)	18.43	73.73	24	91	80-100

The peak ground displacement (PGD) is almost uniform for depth 10.0 m from ground surface as shown in Fig. 3.22(a). The PGD below depth 10.0 m decreasing linearly and becomes negligible at the bottom of liquefiable layer. Fig. 3.22(b) represents the displacement time-history of the site under Bhuj motion. It is noticed that soil shows residual displacement at the end of loading cycle indicating probability of earthquake-induced lateral spreading under strong motion. The PGD at surface of soil are 0.590 m.

The results of the present analysis are compared with the post-earthquake observations as well as the analyses reported in the literature. The current results are matching well with the field observations at port building site.

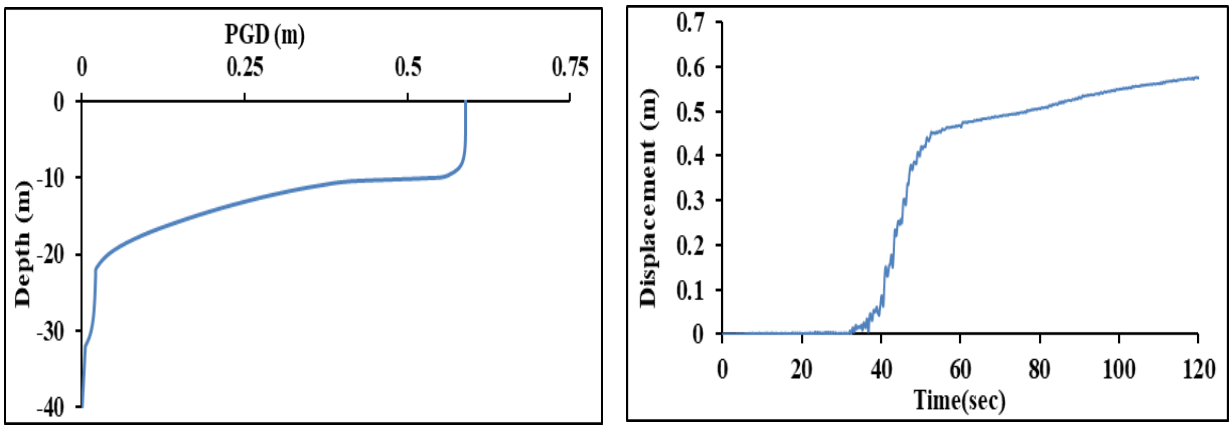

(a) **(b)**

Fig.3.22 a PGD profile and **b** displacement time-history

Chapter 4

Pseudo Static Analysis of Piles

4.1 Analysis of Laterally Loaded Single Pile in Non-Liquefiable Homogenous Cohesionless Soil

The solution of laterally loaded pile (LLP) foundation is complex problem and involves nonlinear soil-structure interaction (SSI) effects. The exact solution of LLP foundation is not well established unlike vertically loaded piles (VLP). Ultimate lateral resistance of soil and maximum allowable lateral displacement of pile are the two principal criteria for design of laterally loaded pile (LLP) foundation. The ultimate lateral resistance of a single pile depends on both geotechnical properties of soil and structural properties of pile. The pattern of failure of short and long piles are also different. The failure of short pile is due to rigid body translation or rotation whereas that of long pile is by forming one or more plastic hinges. Only approximate solutions based on theoretical analysis are presented in Indian standard code of pile foundations IS-2911-Part I (1984). The effects of SSI are neglected in conventional design practice assuming fixed base condition to avoid complexity of the problem. However, this assumption valid for low rise structures resting on stiff soil. The consideration of SSI becomes compulsory for laterally loaded high rise structures resting on soft soil. The flexibility of the supporting soil medium affects the time period and damping properties of the structure. So, the seismic response of structure may not be accurate by neglecting or oversimplifying the SSI effects. The effects of nonlinear SSI on free and fixed head single pile under lateral load in cohesionless soil is investigated in the current study using Beam on nonlinear Winkler foundation (BNWF) model. Fig. 4.1 (a) and (b) presents the basic Winkler hypothesis for beam on elastic foundation. The Winkler model for laterally loaded soil-pile system is shown in Fig. 4.1(c). The simplified BNWF model is capable to incorporate nonlinear SSI effects accurately with less computational operation. The effects of various soil types on pile and soil response are investigated for single pile considering nonlinear SSI effects. The effects of (L/d) ratio and pile head fixity condition are also studied for loose sand.

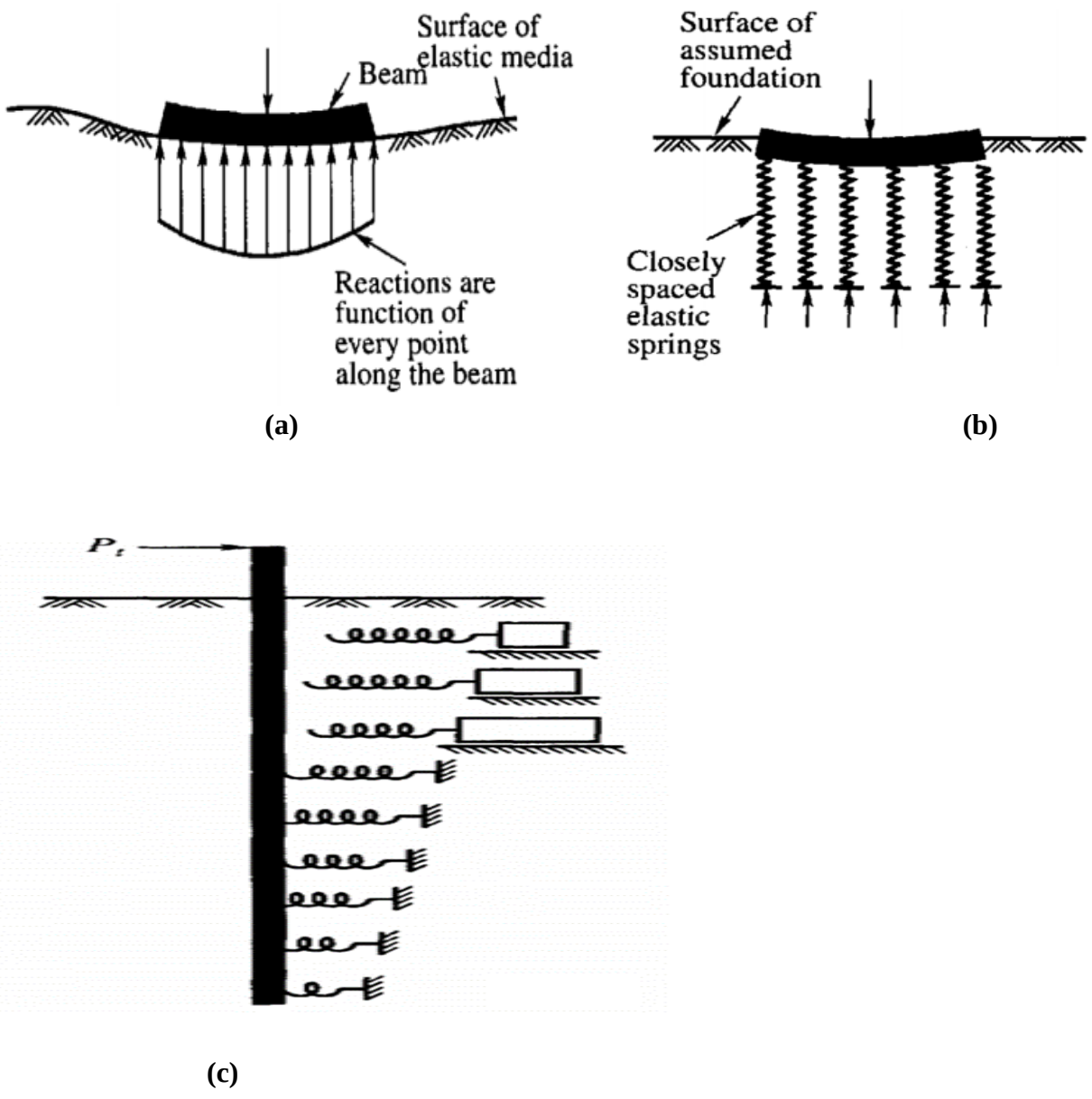

Fig 4.1 a,b Winkler hypothesis and **c** Winkler model for LLP (Murthy 2018)

The basic differential equation of LLP under axial load *P* is given by:

$$EI\frac{d^4y}{dz^4} + P\frac{d^2y}{dz^2} + E_s y = 0 \quad (4.1)$$

where, E_s=-p/y, E_s (soil elastic modulus) and soil resistance (*p*) are dependent on pile displacement (*y*).

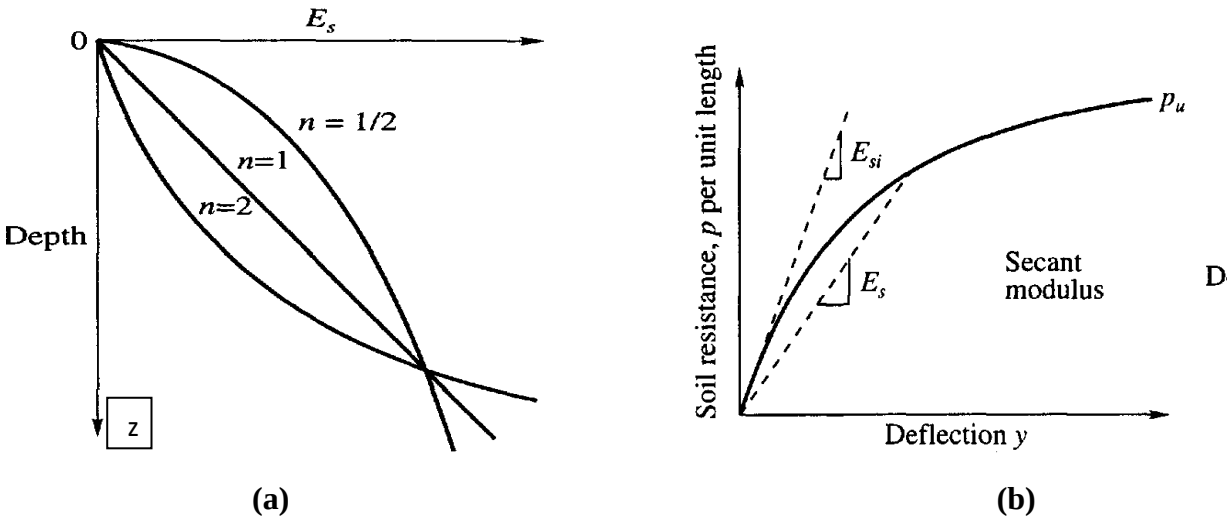

Fig 4.2 a Variation of soil elastic modulus with depth and **b** p-y curve (Murthy 2018)

E_s varies with depth (z) as shown in Fig. 4.2(a) in the following form:

$$E_s = n_h z^n \quad (4.2)$$

where, n_h is co-efficient of soil elastic modulus.

The variation of soil resistance (p) with pile displacement for a particular depth is also shown in Fig. 4.2(b) in the form of *p-y* curve.

The differential equation 4.1 may be solved using analytical or numerical techniques.

Analytical solutions can only be obtained for constant E_s with depth.

4.1.1 Model Description

A 3D soil-pile model has been built using open-source finite element-based code, OpenSees (McKenna and Fenves 2001) BNWF model is used to model the interaction between pile and soil as shown in Fig. 4.3. Pile and soil are simulated by displacement-based beam element and nonlinear spring element respectively. *p-y* curves based on API procedures (API 2007) are used for simulating nonlinear behaviour of soil. The model is developed with three different sets of nodes: fixed spring nodes, slave spring nodes and pile nodes. The finite element mesh is generated using element length of 0.5 m. The three-dimensional spring nodes having three translational degrees of freedom are generated. Zero-length elements are used to define soil springs using fixed and slave-nodes. Distinct uniaxial material objects are used in the lateral and vertical directions. The *p-y* springs oriented in lateral direction represent lateral resistance of soil-pile interface. On the other hand, vertically-oriented t-z and Q-z springs represent skin friction along pile length and end bearing at pile base, respectively. The *p-y*, *t-z* and *Q-z*

springs are defined using the PySimple1, TzSimple1 and QzSimple1 uniaxial materials, respectively. The detail backbone equations and parameters of these springs are presented by Boulanger et al. (1999) and Boulanger (2000). The three-dimensional pile nodes are created with six degrees of freedom. Both translational and rotational degrees of freedom of pile nodes are considered. Orientation of the pile is done by specifying a linear coordinate transformation object. The topmost pile head node is simulated as free head condition to apply lateral load. The pile nodes are connected with slave nodes of soil springs using equal degree of freedom command. Here the pile nodes are considered as master nodes. Both the nodes share equal degrees of freedom in lateral and vertical direction. Elastic behaviour of pile is considered using elastic section object.

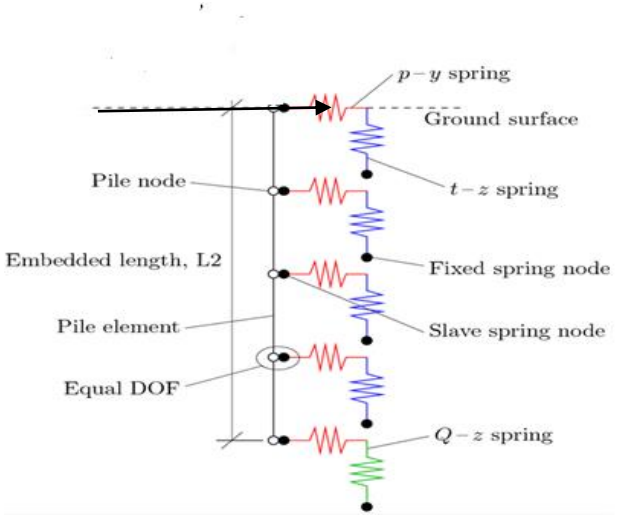

Fig. 4.3 BNWF modelling approach adopted for soil-pile interaction (McKenna and Fenves 2001)

4.1.2. Validation of the Present Numerical Model

The reliability of the present finite element based numerical model is verified by comparing results with the theoretical solution of Reese and Matlock (1956). A laterally loaded single pile of length 10 m and diameter 0.5 m resting in loose sand is analysed using present model. The modulus of subgrade reaction is taken as 6800 kN/m3 (Matlock and Reese 1960). Lateral load of magnitude 150 kN is applied at pile top. Figs. 4.4(a), (b) and (c) present the comparison of lateral displacement, shear force and bending moment profile of pile using the present model and theoretical solution. The present results are matching well with the theoretical solutions available in the literature. The slight deviation in results may be equitable due to different analysis methodology and soil model which are considered based on soil

descriptions. Hence, the BNWF model implemented in OpenSees can be efficiently used for lateral response of pile foundation.

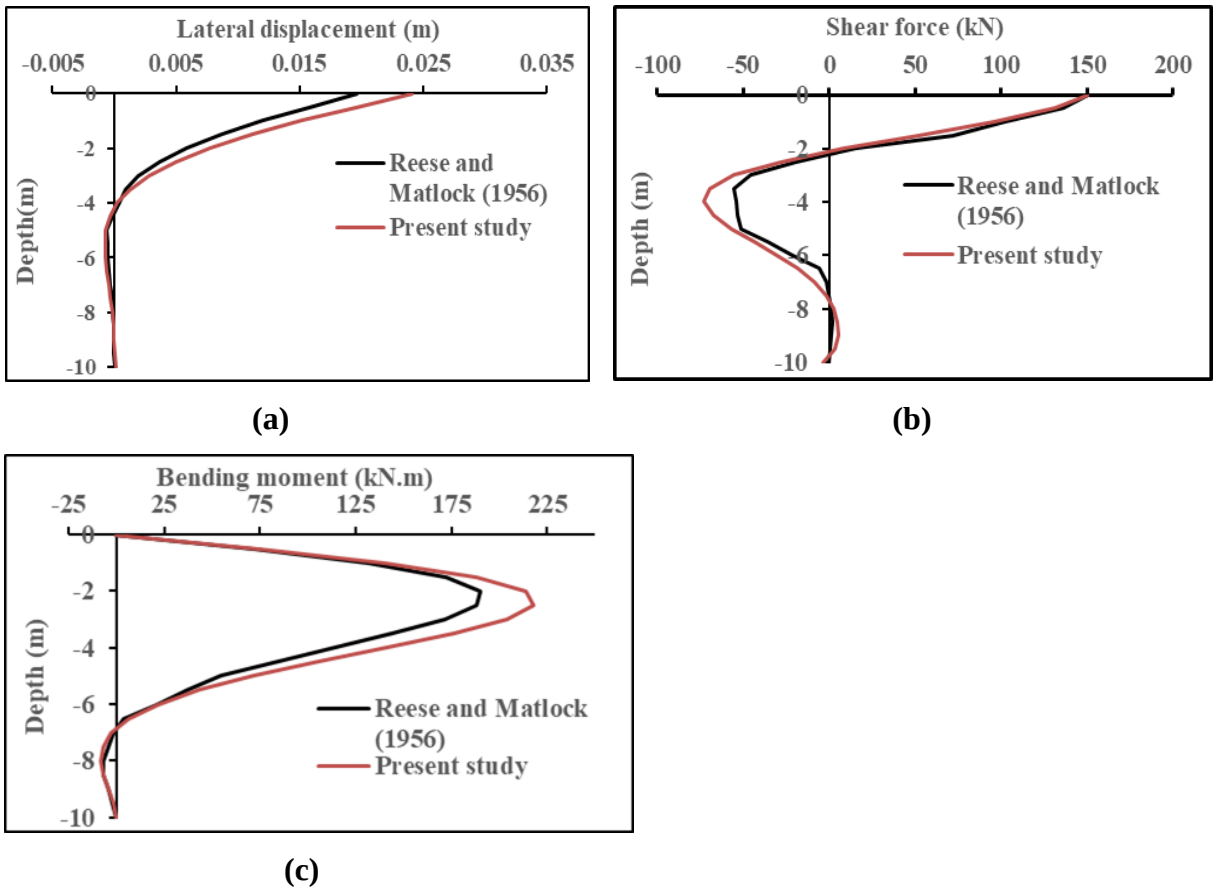

Fig. 4.4 Comparison of **a** lateral displacement and **b** shear force and **c** bending moment and response of pile obtained from present study with Reese and Matlock (1956)

4.1.3 Parametric Studies

The behaviour of LLP foundation depends on a number of parameters. The effects of various soil types on pile and soil response are investigated using present model for single pile. The effects of slenderness ratio (*L/d*) of pile and pile head fixity are also studied. The length of pile is varied from 5.0 m to 15.0 m keeping diameter constant (0.5 m) for parametric study. Tables 4.1 and 4.2 summarises the properties of pile and soil used in the study respectively. The properties of pile and soil are taken from IS 456-2000 and Das (1983) respectively. Single layer cohesionless soil is considered and the ground water table is considered well below the tip of the pile. Pile head is located at ground surface. Lateral load of 150 kN is applied linearly from 0 kN to 150 kN over a 10 sec at topmost pile node using plain pattern

with elective time-series parameters. The load-controlled integrator is used to conduct the analysis.

Table 4.1 Pile parameters considered in the present study (IS 456-2000)

Particulars	Values
Length of pile (L)	15 m
Diameter of pile (d)	0.5 m
Lateral load	150 kN
Grade of concrete	M30
Young's Modulus of Pile (E)	27400 MPa
Poisson's ratio of pile (μ_p)	0.2
Moment of inertia of pile (I)	0.003066 m4

Table 4.2 Soil parameters considered in the present study (Das 1983)

Soil type	Unit weight, γ_s (kN/m^3)	Young's Modulus, E_s (MPa)	Poisson's ratio,μ_s	Friction angle, ϕ (°)
Loose sand	17	18	0.25	29
Medium sand	19	25	0.30	33
Dense sand	21	50	0.35	40

4.1.3.1 Influence of Soil Type on Pile and Soil Response

Static analysis for 15.0 m long pile (L/d=30) has been performed for loose, medium and dense soil types and the results are presented. Variation of lateral displacement profile of pile is presented in Fig. 4.5(a) for various soil types**.** It is observed that the maximum lateral displacements at free end for loose, medium and dense sand under same lateral load of 150 kN are 24.12, 9.33 and 4.22 mm respectively**.** Maximum lateral displacement is reduced by 82.50% when the soil type changes from loose to dense sand. So, the significant reduction of lateral displacement of pile is observed with the increase of stiffness of soil.

The variation of shear force and bending moment of the pile along depth are shown in Figs. 4.5(b) and 4.5(c) respectively. The peak value of shear force obtained is 150 kN at free head of the pile**.** The depths correspond to point of inflection are 2.5 m, 1.5 m, 1.5 m for loose, medium and dense sand respectively. The maximum values of bending moment are also

affected by the stiffness of soil. The maximum bending moments are 218.18 kN-m, 170.33 kN-m and 128.58 kN-m for loose, medium and dense sand respectively. The depth correspond to peak bending moment is dependent on soil type. The peak value of bending moment of pile is reduced by 41.10% when the soil type changes from loose to dense sand. The depth of point of contraflexure from ground surface decreases with the increase of relative density of soil. Fig. 4.5(d) presents the soil reaction profile for various soil types. The response is negative from the ground surface to about 4.5 m, 3.0 m and 2.5 m depth, then transitions to positive until about 9.0 m 6.0 m and 5.0 m depth, for loose, medium and dense sand, has a second smaller negative section, and then is nearly zero near the tip of the pile. The peak value of soil reaction obtained for loose, medium and dense sand are 44.12, 70.87 and 95.98 kN/m respectively. Also, the soil reaction of dense sand is 35.40% more than loose sand under same lateral load.

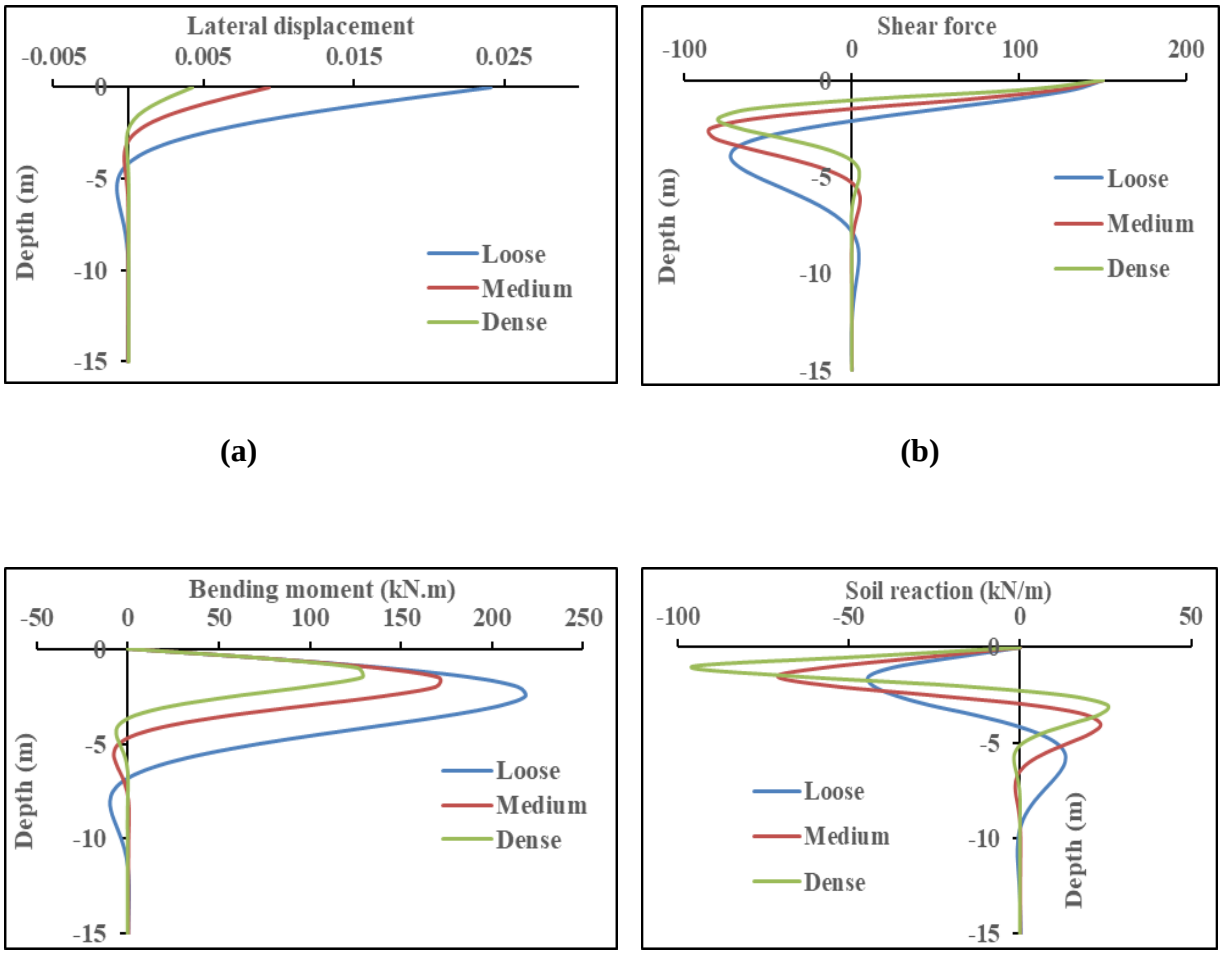

Fig. 4.5 Profile of **a** lateral displacement **b** shear force **c** bending moment of pile and **d** soil reaction response for various soil types

4.1.3.2 Influence of (*L/d*) Ratio on Pile and Soil Response

The behaviour of pile as short rigid or long flexible, response of pile and soil are highly influenced by *L/d* ratio of pile. Fig. 4.6(a) shows the impact of *L/d* on lateral displacement of pile in loose sand. The pile having *L/d* ratio 10 behaves like short rigid pile and tends to rotate with respect to point of inflection. The peak opposite displacement appeared at the bottom of short pile as shown in Fig. 4.6(a). The Piles having *L/d* ratio 15, 20 and 30 behaves like long flexible piles and the maximum negative displacement occurred in between inflection point and the base of pile. Also, the negative tip displacement is more for short pile with compared to long pile.

It is observed that the maximum bending moment are 211.55 kN-m for *L/d* ratio 10 and 218.18 kN-m for *L/d* ratio more than 10 in loose sand. Also, the maximum bending moment of pile decreases along length for L/d ratio 10 and 15. However, the negative bending moment occurs near the point of contraflexure and finally becomes zero at base of pile for *L/d* ratio 20 and 30 as shown in Fig. 4.6(b).

The soil reaction profile for various *L/d* ratio of pile in loose sand are presented in Fig. 4.6(c). The soil reaction is 46.80% more for pile having *L/d* ratio 10 than other *L/d* ratios resting in loose sand. Also, soil reaction for the pile having *L/d* ratio 10 transitions to positive and becomes maximum at the pile tip. When *L/d* ratio exceeding 10 the reaction changes to positive and has a second smaller negative and tends to zero near the base of pile.

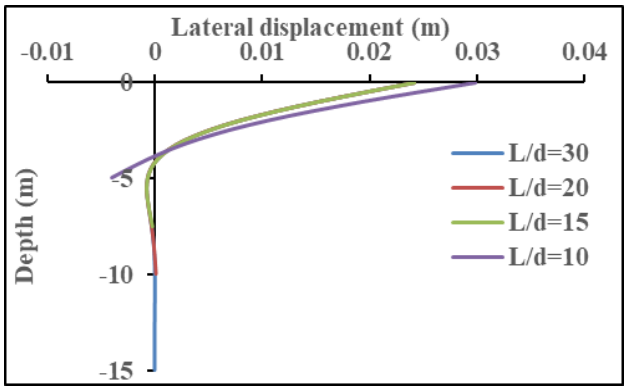

(a)

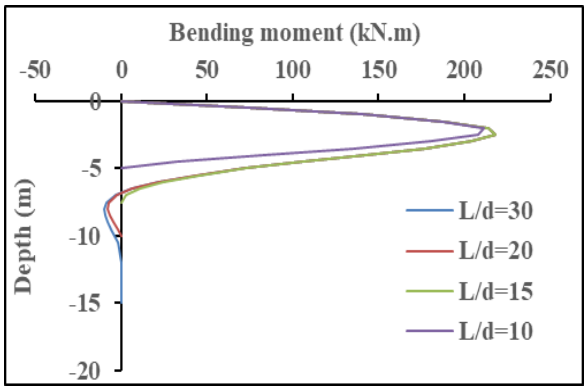

(b)

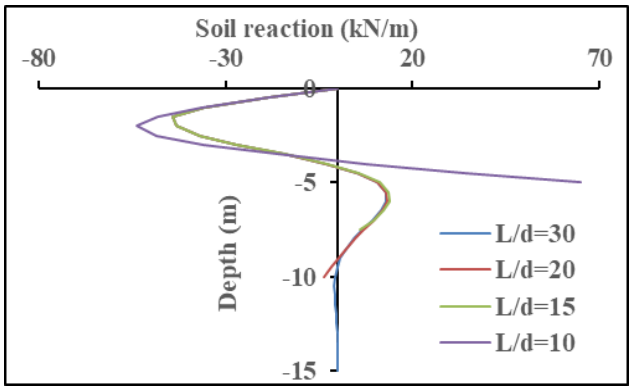

(c)

Fig. 4.6 Profile of **a** lateral displacement **b** bending moment of pile and **c** soil reaction response in loose sand for various pile *L/d* ratio

4.1.3.3 Influence of Pile Head Fixity Condition on Pile and Soil Response

The effects of pile head fixity on lateral displacement response of *L/d* ratio 10 and *L/d* ratio 30 for loose and dense sand are presented in Fig. 4.7(a) and (b) respectively. The rigid behaviour showing rigid body rotation is noticed for free and fixed head pile (*L/d*=10) in loose sand. But, in dense sand the flexible type behaviour was observed for same pile for both free and fixed head condition. However, the behaviour of *L/d* ratio 30 is always flexible type for all types of soils and pile head fixity condition as shown in Fig. 4.7(b). Also, it is observed that the lateral displacement of pile decreases significantly when the pile head fixity changes from free head to fixed head condition. The lateral displacement of pile having *L/d*=30 for loose and dense sand is decreased by 69.75% and 73.90% respectively when the pile head fixity changes from free to fixed head condition.

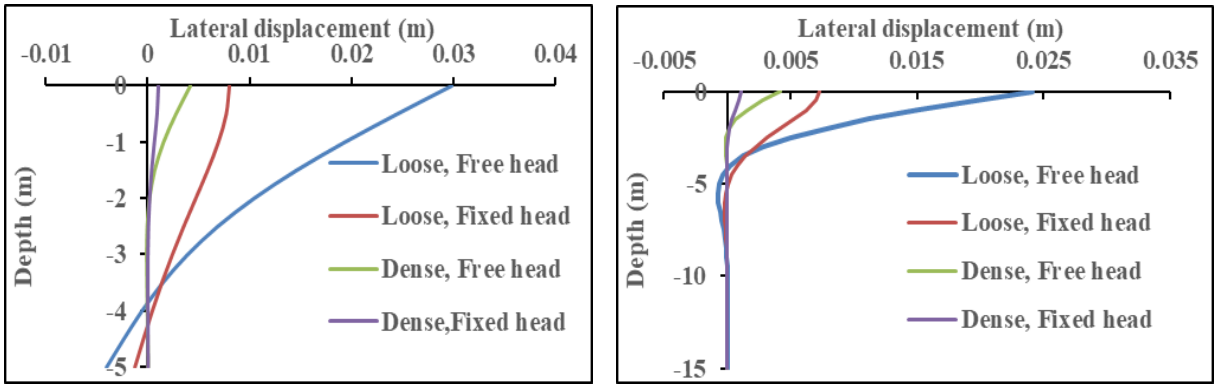

(a) **(b)**

Fig. 4.7 Lateral displacement profile for **a** pile (*L/d*=10) and **b** pile (*L/d*=30)

The bending moment profiles of short and long pile for different pile head condition and soil type are presented in Fig. 4.8(a) and (b) respectively. The pile head fixity condition and L/d ratio have profound influence on bending moment profile. The depth corresponds to maximum bending moment are also different for free and fixed head pile. The maximum bending moment of free head and fixed head long pile is reduced by 41.10% and 45.60% respectively for changes of relative density of soil from loose to dense.

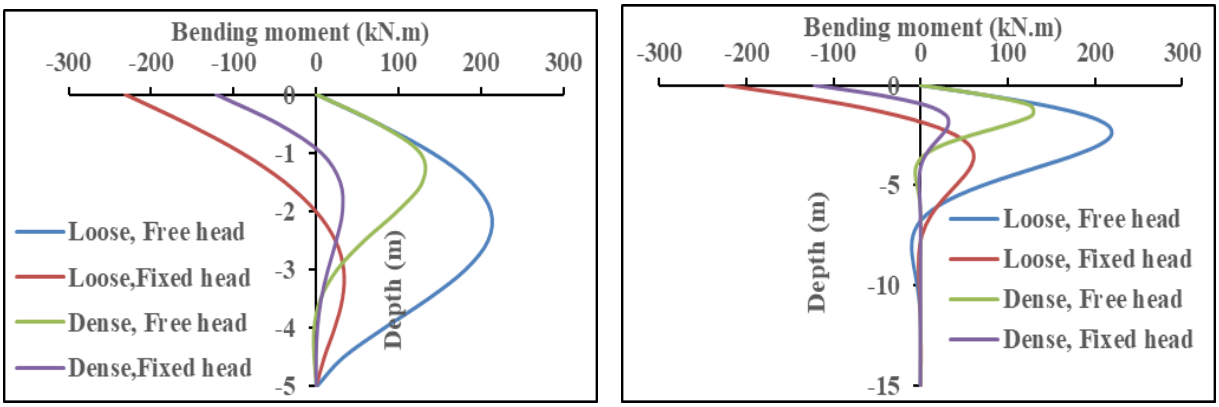

(a) **(b)**

Fig. 4.8 Bending moment profile for **a** pile (*L/d*=10) and **b** pile (*L/d*=30)

The soil response is also dependent on pile head fixity condition for various *L/d* ratios of pile. Figs. 4.9(a) and (b) illustrate the soil reaction profile for pile *L/d* ratio 10 and 30 respectively embedded in loose and dense sand. The pattern of soil reaction of free and fixed head pile having *L/d* ratio 10 in loose sand is completely different with that of pile having *L/d* ratio 30.

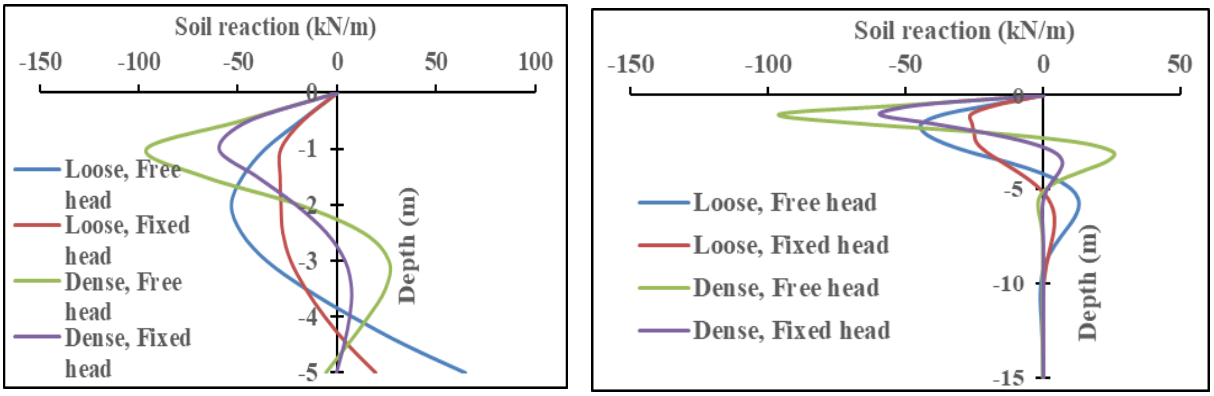

(a) **(b)**

Fig. 4.9 Soil response profile for **a** pile (*L/d*=10) and **b** pile (*L/d*=30)

4.2 Seismic Response of Laterally Loaded Single Piles in Liquefiable Multi-Layered Sloping Ground

The seismic response of pile foundation in liquefiable soil is a complex nonlinear soil-structure-interaction (SSI) problem. It involves evaluation of inertial interaction between super-structure and pile foundation, kinematic interaction between soil and pile foundation as well as degraded strength and stiffness of soil due to liquefaction. The degradation of strength and stiffness of liquefiable soil in sloping ground may develop considerable amount of shear force and bending moment in the pile due to lateral spreading, leading pile failure (Finn and Fujita 2002). A significant number of damages and/or collapses of pile foundations and pile-supported structures in level and mild sloping liquefiable ground during past major earthquakes such as San Francisco (1906), Niigata (1964), Northridge (1994), Kobe (1995), Chi-Chi (1999), Bhuj (2001) and Sumatra (2004) pose great concern to the geotechnical earthquake engineering community.

In traditional practice, the piles are analysed and design based on inertial load from super-structure during earthquake neglecting the effects of kinematic interaction. However, for seismic design of pile foundations in liquefiable soil both kinematic and inertial loading needs to be considered. The base of super-structure does not follow the free-field motion during travelling of seismic waves from bedrock level to the ground level due to presence of embedded piles. This difference in response of soil-pile system from the free-field motion will develop bending moment in the pile foundation even in absence of super-structure and is termed as kinematic interaction. It is to be separated from inertial interaction due to presence of mass of the super-structure. The response of pile due to inertial interaction diminish rapidly below depth of 10 to 15 times pile diameter from ground level (Mylonakis 2001). So, the kinematic response of pile is responsible for failure of piles at greater depth.

The presence of mild slope may significantly influence on kinematic pile bending. Past earthquakes also demonstrated that pile-supported structures are vulnerable to kinematic bending failure in liquefiable sloping ground. However, interaction between kinematic and inertial interaction of piles in liquefiable sloping ground is still scanty in the literature. Therefore, the aim of this study is to investigate the seismic response of single piles in liquefiable sloping ground using pseudo-static approach based on beams on nonlinear Winkler foundation (BNWF) model considering nonlinearity of soil. Then parametric studies have been conducted for evaluating the effects of ground slope, slenderness ratio of pile, pile

head fixity condition, existence of liquefiable layer, depth of liquefiable soil layer and embedment depth of pile on seismic response of layered soil-pile system.

4.2.1 Current Design Approaches

In this pseudo-static method, a free-field ground response analysis is conducted in stage I to evaluate the peak ground displacement (PGD) profile and peak ground acceleration (PGA) at surface level. In stage II, a static analysis is performed for the pile subjected to PGD profile obtained in stage I and pseudo-static lateral load at pile head. The lateral load is calculated by multiplying the PGA at surface level with the maximum axial load acting on pile head and lateral load co-efficient. In the present study, a similar method is adopted for estimation of seismic response of pile foundations in liquefiable sloping ground.

4.2.2 Methodology

In the present study, a finite-element based numerical approach has been adopted for seismic analysis of single pile embedded in liquefiable multi-layered sloping ground using open-source finite element-based computational platform OpenSees. This software framework allows for developing applications to simulate the performance of structural and geotechnical systems subjected to earthquake loading. The various steps for seismic response analysis of pile are summarized below:

(1) 1D nonlinear ground response analysis (GRA) has been carried out for predicting the layered soil response using input ground motion at bedrock level. From this analysis, PGA at ground surface and PGD profile along pile depth can be calculated. The present study utilizes the nonlinear methods of analyses through computer program Cyclic1D. Cyclic1D has been developed for 1D wave propagation analysis using pressure-dependent and pressure-independent soil constitutive models. The constitutive model of soil in Cyclic1D has the capability to narrate the development and dissipation of pore water pressure.

(2) The maximum axial load on pile during earthquake will be increased due to additional dynamic axial load for inertial action of the superstructure. If P_s is the static axial load acting on each pile head from superstructure and α is the dynamic axial load factor, then the maximum axial load (P_d) can be estimated using equation (4.3) as proposed

by Bhattacharya (2006). α may vary from 0.1 to 0.5 depending up on the type of superstructure, supporting soil condition, characteristics of input earthquake motion.

$$P_d = P_s\,(1 + \alpha) \tag{4.3}$$

(3) If m_1 is the peak ground acceleration (PGA) at ground surface obtained from nonlinear GRA in step 1 and a is the lateral load co-efficient, then the lateral inertial load at pile head can be calculated as below (Chatterjee and Choudhury 2017):

$$H = (a * P_d) * m_1 \tag{4.4}$$

(4) A 3D model based on BNWF method has been built (Fig. 4.10) using open-source finite element-based code, OpenSees to incorporate the interaction between pile and soil in liquefiable three-layered sloping ground with slope angle α and pile length L below ground. The thickness of top non-liquefiable (NL) crust, intermediate liquefiable layer and bottom stiff NL base layer are L_1, L_{Liq} and E respectively. Displacement-based beam element and nonlinear spring element are used for simulating pile and soil respectively. The pile axis is oriented in z-coordinate direction and x-coordination is the direction of lateral loading. Zero length elements are used to represent the soil spring. Fixed spring nodes, slave spring nodes and pile nodes are used to create the model. The soil end and pile end of the spring elements are considered as completely fixed and only free in direction of loading respectively. The pile nodes are connected to the pile end of soil springs as slave nodes in the direction of loading using equal degree of freedom command. The pile nodes are considered as fixed against translation in the y-direction and rotation out of the plane of loading. The base of the pile is also assumed as fixed against vertical translation. The *p-y* springs oriented in lateral direction represent lateral resistance of soil-pile interface. The *p-y* springs are defined using the PySimple1 uniaxial materials. The detail backbone equations and parameters of these springs are presented by Boulanger et al. (1999) and Boulanger (2000). The input parameters for defining PySimple1 material are ultimate lateral resistance of soil (P_{ult}) and displacement at 50% lateral capacity (y_{50}). P_{ult} values of soft clay and sand are calculated using procedure proposed by Matlock (1970) and Brinch Hansen (1961) respectively.

P_u is calculated using the smaller of the values given by the equations below for soft clay under *GWT*:

$$P_u = \left[3 + \frac{\gamma'}{C_u} z + \frac{J}{d} z\right] C_u * d \quad (4.5a)$$

$$P_u = 9 C_u d \quad (4.5b)$$

where,

d = diameter of the pile (m)

z= depth below ground surface (m)

γ' = effective unit weight (kN/m3)

J = factor determined experimentally by Matlock equal to 0.5

C_u = undrained shear strength at depth *z* (kPa)

P_u for sand is defined as per the method of Brinch Hansen (1961) as follow:

$$P_u = \left[\gamma * z * K_{qD} + C * K_{cD}\right] * d \quad (4.6)$$

Where, K_{qD} and K_{cD} are the earth pressure coefficient for overburden pressure and cohesion respectively as functions of friction angle and depth to diameter ratio (*z/d*) of pile.

PySimple1 material formulated with P_{ult} as a force, not force/length, multiply by tributary length

$$P_{ult} = [P_u * dz] \quad (4.7)$$

Where, *dz* is the element length in finite element mesh which is 0.5 m in present case.

y_{50} values of clay and sand are calculated using procedure proposed by Matlock (1970) and recommendation by the API (2007) respectively. The y_{50} value of soft clay can be calculated using equation (4.8). The strain corresponding to one-half the maximum principal stress difference (ε_{50}) to be taken as 0.020 for soft clay (Matlock 1970).

$$y_{50} = 2.5 * \varepsilon_{50} * d \quad (4.8)$$

p-y curves based on API procedures are used for calculating of y_{50} of sandy soil. The *p-y* curves for non-liquefiable cohesionless soil are defined by the following hyperbolic equation based on API procedure:

$$p = AP_u * \ tanh(\frac{kz}{AP_u} y) \quad (4.9)$$

where *k* is the coefficient of subgrade reaction and *A* is loading type (cyclic or static) and initial tangent stiffness is obtained as $k_T=kz$ by derivation of equation (4.9) with respect to *y* at *y*=0.

The values of *k* of sands above and below *GWT* are recommended by API based on relative density and friction angle. The value of *k* increases with increasing friction angle nonlinearly. So, the linear variation of *k* as recommended by API does not illustrate the true soil response gives overestimation at greater depth. The value of API subgrade reaction modulus (*k*) has been modified with depth using parabolic variation after Boulanger et al. (2003) as:

$$k^* = k_{API} C_\sigma \quad (4.10)$$

where,

*k** = corrected modulus of subgrade reaction,

k_{API} =API recommended initial modulus of subgrade reaction,

C_σ = overburden stress correction factor,

$$C_\sigma = (\sigma_{ref}'/(\ \sigma_v'))\text{^}0.5 \quad (4.11)$$

σ_{ref}' = reference stress at which k was calibrated, taken as 50 kPa.

σ_v' = effective overburden stress.

The value of y_{50} can be evaluated for sand based on ultimate lateral resistance (p_u), loading type coefficient (*A*) and corrected subgrade modulus (*k**). When half of full resistance has been mobilized, *p(y50)/Pult = 0.5*

$$y_{50} = [\frac{0.5\left(\frac{p_u}{A}\right)}{(k^*z)} * \text{atanh(x)}\ ] \quad (4.12a)$$

$$atanh(x) = \frac{1}{2} * ln((1+x)/(1-x)), |x| < 1 \quad \text{where, } x=0.5 \quad (4.12b)$$

Loading-type coefficient *A* for given depth-to-diameter ratio (*z/d*) values are obtained from a figure as recommended by API.

(5) In case of soil liquefaction, stiffness of soil is significantly reduced. The effects of liquefaction on p-y curves of sand can be considered in three different ways. At first, the lateral resistance of sandy soil under liquefiable condition can be neglected and supposed to be zero. This method is highly conservative and not economic from design point of view (Janalizadeh and Zahmatkesh 2015). Secondly, liquefiable sand can be treated as undrained soft clay and undrained shear strength can be obtained from initial effective overburden pressure (σ_v) and relative density (Boulanger et al. 2003):

$$P_{u,liq} = N_p * S_u * d \quad (4.13)$$

where:

$p_{u,liq}$ = ultimate soil resistance of liquefiable soil,

N_p= 9 considering plane strain condition,

S_u = mobilized shear resistance of the liquefied soil

The shear resistance ratio (S_u/σ_v') depends on relative density of sand and loading history. This ratio for loose liquefiable sand may be considered to be:

$$S_u/\sigma_v' = 0.07 \quad (4.14)$$

In the third method, reduction factor or *p*-multiplier is used to degrade the soil stiffness due to liquefaction. A multiplication factor varying from 0.01 to 0.3 is generally used for the *p-y* curves of sandy soil under liquefied state (Janalizadeh and Zahmatkesh 2015; Boulanger et al. 2003; Brandenberg et al. 2007). In the present study, second method using equation (4.13) and (4.14) has been adopted for evaluating P_{ult} of liquefiable sand and the constant degradation factor 0.10 has been

considered to reduce the API recommended initial modulus of subgrade reaction (k) for y_{50} calculation.

(6) The whole procedure is completed by conducting pseudo-static analysis using static load control integrator using open-source finite element-based code, OpenSees. The laterally loaded single pile is analysed using BNWF model subjected to kinematic loading from lateral ground displacement only (H=0) as shown in Fig. 4.10. The free-field PGD profile obtained in step 1 is employed incrementally to the soil end of the *p-y* springs to simulate lateral spreading. Also, the pile response for inertial loading (H) alone at pile head as equivalent static load from vibration of the superstructure may be evaluated. The combined pile response due to kinematic and inertial interaction may be obtained using principal of superposition. The combined response can be obtained by square root of sum of squares (SRSS) of individual response when natural period of structure (T_b) is greater than natural period of ground (T_s) and by adding the individual response algebraically at various nodes along pile depth when T_b is less than T_s (Tokimatsu et al. 1998).

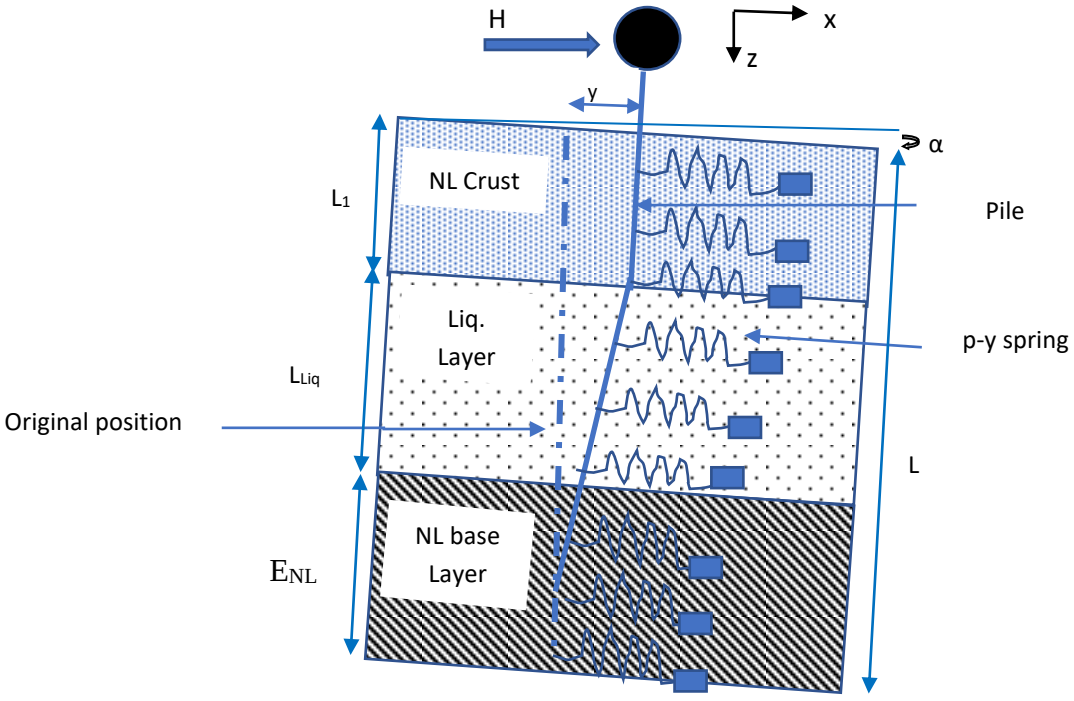

Fig. 4.10 A beam on the nonlinear Winkler foundation (BNWF) model for pseudo-static analysis

4.2.3 Validation of the Present Numerical Model

The performance and reliability of the present finite element based numerical model is verified by comparing results with the established theoretical solution and past case study. A

laterally loaded single pile of length 15 m and diameter of 0.5 m resting in loose sand is analysed using present model. The modulus of subgrade reaction is taken as 6800 kN/m3 (Matlock and Reese 1960) Lateral inertial load of magnitude 150 kN is applied at pile top. Figs. 4.11(a) and (b) present the comparison of lateral displacement and bending moment profile of pile using the present model and theoretical solution of Reese and Matlock (1956). The present results are matching well with the theoretical solutions available in the literature. The slight deviation in results may be equitable due to different analysis methodology and soil model which are considered based on soil descriptions. Hence, the BNWF model implemented in OpenSees can be efficiently used for lateral response of pile foundation due to inertial loading.

The kinematic pile response obtained using present methodology is compared with the filed observation of Niigata Family Courthouse (NFCH) building during 1964 Niigata earthquake. The building is a three-storied pile-supported RC structure with pile length *(L*) and diameter (*d*) of 7.0 m and 0.350 m respectively as reported by O'Rourke et al. (1992). The top 8.0 m soil of the building site was loose sandy deposit with SPT N values below 10. The location of ground water table was reported at 2.0 m below ground level. Hence, the pile tip was founded in liquefiable deposit with upper 2.0 m composed with non-liquefiable crust. O'Rourke et al. reported that the Niigata earthquake (Magnitude 7.5) induced lateral spreading and PGD as per field observation was about 660 mm. Kinematic pile lateral displacement and bending moment have been evaluated in the present study using reported ground displacement by O'Rourke et al. The value of Young's modulus of pile used in the study is 27400 MN/m2 (Phanikanth et al. 2013). The lateral pile displacement and bending moment obtained using present model with API procedure for non-liquefiable soil and method recommended by Boulanger et al. (2003) for degradation of strength of liquefiable soil are shown in Figs. 4.12(a) and (b) respectively. Also, exponentially variable degradation factor of 0.1 (top of liquefiable crust) to 1.0 (bottom of liquefiable crust) has been considered using exponential decay function as proposed by Janalizadeh and Zahmatkesh (2015) in the form of:

$$R_f = R_0 * e^{\frac{z}{L_{Liq}} ln(-R_0)} \quad (4.15)$$

Where *R* is the degradation factor at depth *z* from top of layer; L_{Liq} is the depth of liquefiable crust; R_o is the degradation factor at the top of liquefiable crust and are compared with analytical results of Meera et al. (2007) and field observation of O'Rourke et al. (1992) as shown in Figs. 4.12 (a) and (b) respectively. The variation of pile displacement from PGD reported in literature is due to non-availability of actual soil data of top 2.0 m layer to

incorporate in the present model. It is seen from the displacement profile that though the ground displacement is trapezoidal, pile behaviour is rigid which is justified as the maximum depth co-efficient (*L/T*) is 3.40 <4.0 (IS2911 Part I/Sec II: 2010), where relative stiffness factor, $T = (\frac{EI}{n_h})$^0.2; *EI*= flexural rigidity of pile, n_h=coefficient of subgrade reaction=0.1x5400=540 kN/m^3 for loose sand below *GWT* (Matlock and Reese 1960). The maximum pile kinematic bending moment obtained in the present study are 58.72 kN-m and 69.24 kN-m for constant degradation factor Boulanger et al. (2003) and exponential variable degradation factor (Janalizadeh and Zahmatkesh 2015) respectively. The maximum bending moment estimated by Meera et al. (2007) was 53.8 kN-m and filed bending moment by O'Rourke et al. (1992) was 55.9 kN-m.

It is observed that the results obtained in this study using constant degradation factor agree well with the analytical results and field observation. Hence, the present numerical model is validated for both inertial and kinematic loading with previous authors. The use of constant degradation factor approach for liquefied state has been adopted for subsequent analysis of piles in liquefiable soil.

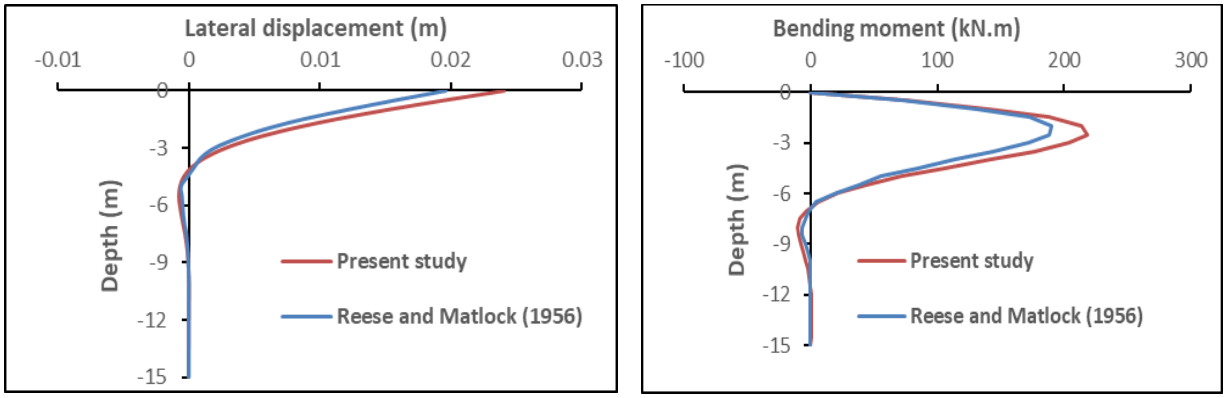

(a) **(b)**

Fig. 4.11 Comparison of present study with theoretical solution of Reese and Matlock (1956) **a** lateral displacement and **b** bending moment response of pile for inertial loading

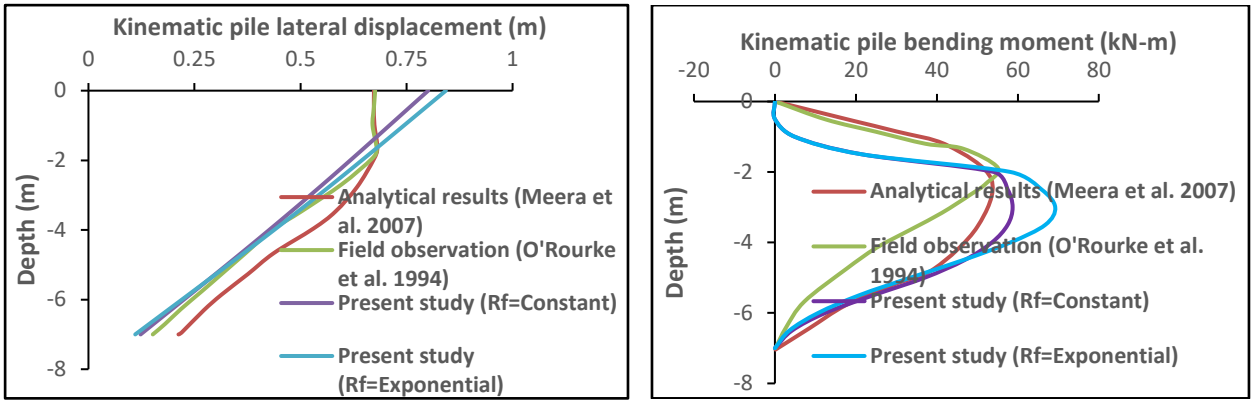

(a) **(b)**

Fig. 4.12 Comparison of present study with analytical results and field observation **a** kinematic pile lateral displacement and **b** kinematic pile bending moment response

4.2.4 Present Study

The seismic behaviour of a single pile in liquefiable multi-layered sloping ground subjected to both inertial and kinematic loading is studied in the present study using Kandla Port case study (Dash et al. 2009) as shown in Fig. 4.13. Each pile in the pile group of Kandla Port building is represented by black circle in plan view as shown in Fig. 4.13(b). The BNWF model considered for this study is shown in Fig.4.14. The boundary conditions considered here are similar to the Fig. 4.10. The soil end of *p-y* springs is considered as completely fixed and pile end of *p-y* springs is only free in direction of loading. The pile nodes are connected soil springs in the direction of loading using equal degree of freedom. The pile nodes are considered as fixed against translation in the y-direction and rotation out of the plane of loading. The base of the pile is also assumed as fixed against vertical translation. Elastic section properties are assigned to model the pile foundation. The length of each beam element of pile considered is 0.5 m. Kandla Port is located in the Kandla Creek and is 50 km from the epicentre of the earthquake. The Kandla Port tower, a 22.0 m high six-storied building supported on combined pile-raft foundation is located proximate to waterfront. The building was supported by 12 numbers of column (0.45x0.45 m and 0.25x0.25 m) and 32 numbers RCC piles having diameter 0.4 m and length 18 m. The 0.5 m thick foundation mat was provided as a rigid pile cap. The pile properties and structural details of Kandla Port building are tabulated in Table 4.3 and 4.4 respectively (Dash et al. 2009; IS 456-2000). The typical soil profile of Kandla Port site at Gujarat state of India (Dash et al. 2009) is consisting of recent unconsolidated layer of clay, silt and sand. The ground slope of Kandla Port site is

about 5-degree towards seaside. The ground water table (*GWT*) is located at 1.5 m below ground surface. The input motion considered is the 2001 Bhuj earthquake. The 2001 Bhuj earthquake (*Mw*=7.7) was the most devastating seismic hazard causing tremendous damages of lives and properties in urban area of India. The maximum bedrock level acceleration (*MBRA*) was 0.106g. The acceleration time-history of the earthquake is shown in Fig. 3.2(b). Four distinct ground slopes of 0, 2.5, 5.0 and 8.0 degree are also considered for parametric study.

1D effective-stress based free-field nonlinear GRA has been carried out for predicting the layered soil response of Kandla port building site with various ground slope using 2001 Bhuj earthquake input ground motion at bedrock level through computer program Cyclic1D. A finite element model in the present study is defined in Cyclic1D by specifying the total height of soil profile of 40m.The multi-layered soil profile layer has been divided into total 80 numbers of elements, each of 0.50m thick after convergence analysis. Predefined material models of clayey and sandy soils are chosen to define the soil profile of the site as tabulated in Table 3.10.

The depth of liquefaction of the port site has been assessed using the results obtained from nonlinear GRA. The profile of excess pore pressure (EPP) ratio is evaluated at each depth of Kandla Port site as shown in Fig. 3.20(a). The EPP ratio is almost 1 for soil layer of 10.0 to 22.0 m depth under the Bhuj earthquake. So, the intermediate fine to coarse sandy strata is prone to liquefaction. Also, simplified deterministic method is used to assess the liquefaction susceptibility of the port site as shown in Fig 3.20(b). It is clear from graph that the FOS is less than 1 for top clay (1.5-10.0 m) and intermediate sandy layer (10.0-22.0 m) under Bhuj motion. So, the upper clay stratum experiences ground deformation and cracking due to cyclic failure. Moreover, intermediate sand layer (10.0-22.0 m) is susceptible to liquefaction.

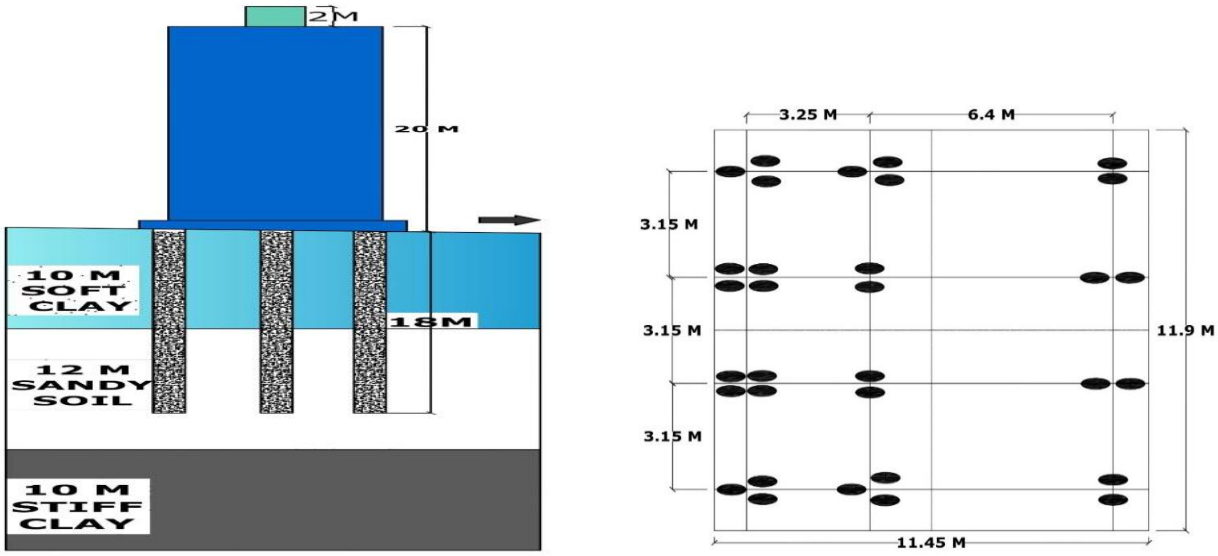

(a) **(b)**

Fig. 4.13 Details of **a** Kandla Port Building and **b** foundation layout plan (Dash et al. 2009)

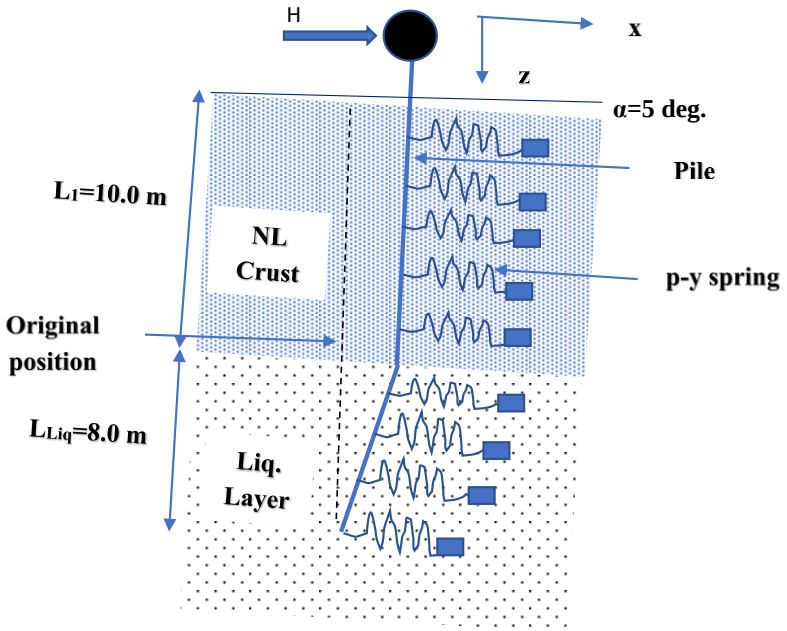

Fig.4.14 BNWF model considered in the present study for pseudo-static analysis of pile foundation of Kandla Port building

Table 4.3 Pile properties considered in the present numerical study (Dash et al. 2009; IS 456-2000)

Properties	Values
Characteristic compressive strength of concrete (f_{ck})	30 MPa
Young's Modulus (E)	30 GPa
Poisson's Ratio (μ)	0.30
Unit weight (γ_p)	25 kN/m^3
Length of pile (L)	18.0 m
Diameter of pile (d)	0.4 m

Table 4.4 Structural details of Kandla Port building (Dash et al. 2009)

Description	Values
Number of stories	6 nos.
Building height (h)	22.0 m from GL
Building type	RCC frame structure
Building dimensions at plinth level (l x b)	9.6 m x 9.8 m
Foundation type	Combined piled-raft
Foundation-raft dimensions	11.45 m x 11.9 m x 0.5 m
Numbers of pile	32 nos.
Total weight of building	10749 kN
Load on each pile	336 kN

The different input parameters calculated for seismic nonlinear soil-structure interaction analysis of single piles in liquefiable sloping ground are illustrated in Table 4.5. The variation of stiffness factor *(T*) and depth co-efficient (*L/T*) with depth for liquefied and non-liquefied condition are shown in Fig 4.15(a) and (b) respectively. It is noticed that depth coefficient (*L/T*) for soil-pile system in Kandla port building site varies from 10.9 to 12.5 for non-liquefied condition and 6.8 to 12.5 for liquefied condition. So, flexible pile behaviour can be expected in both non-liquefiable and liquefiable condition as per IS 2911-Part I (1984).

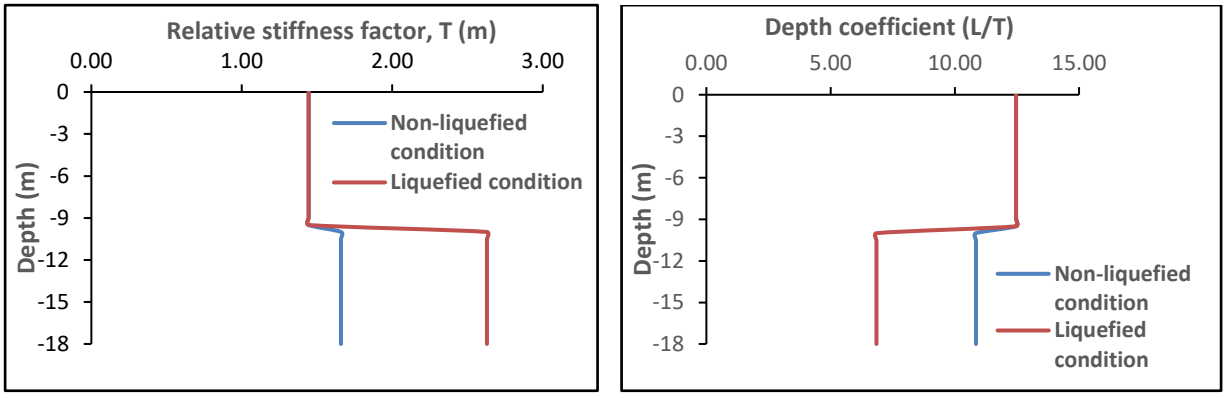

(a) **(b)**

Fig. 4.15 Variation of **a** relative stiffness factor and **b** depth coefficient with depth under non-liquefied and liquefied condition

Table 4.5 Input parameters for soil-pile interaction analysis in liquefied condition

Depth (m)	p_u (kN/m)	p_{ult} (kN)	A	C_σ	k_{API} (kN/m^3)	k^* (kN/m^3)	y_{50} (m)
0.5	15.74	7.87					0.020
1.0	19.48	9.74					0.020
1.5	23.21	11.61					0.020
2.0	26.95	13.48					0.020
2.5	30.69	15.35					0.020
3.0	34.43	17.21					0.020
3.5	36.00	18.00					0.020
4.0	36.00	18.00					0.020
4.5	36.00	18.00					0.020
5.0	36.00	18.00					0.020
5.5	36.00	18.00					0.020
6.0	36.00	18.00					0.020
6.5	36.00	18.00					0.020
7.0	36.00	18.00					0.020
7.5	36.00	18.00					0.020
8.0	36.00	18.00					0.020
8.5	36.00	18.00					0.020
9.0	36.00	18.00					0.020
9.5	36.00	18.00					0.020

10.0	15.62	7.81	0.88	0.898	12487	1121.36	0.000435
10.5	16.53	8.27	0.88	0.873	12487	1090.16	0.000450
11.0	17.44	8.72	0.88	0.850	12487	1061.43	0.000466
11.5	18.34	9.17	0.88	0.829	12487	1034.85	0.000481
12.0	19.25	9.63	0.88	0.809	12487	1010.17	0.000496
12.5	20.16	10.08	0.88	0.790	12487	987.18	0.000510
13.0	21.07	10.53	0.88	0.773	12487	965.69	0.000524
13.5	21.97	10.99	0.88	0.757	12487	945.55	0.000537
14.0	22.88	11.44	0.88	0.742	12487	926.62	0.000550
14.5	23.79	11.89	0.88	0.728	12487	908.78	0.000563
15.0	24.70	12.35	0.88	0.714	12487	891.93	0.000576
15.5	25.60	12.80	0.88	0.701	12487	875.98	0.000588
16.0	26.51	13.26	0.88	0.689	12487	860.86	0.000600
16.5	27.42	13.71	0.88	0.678	12487	846.50	0.000613
17.0	28.32	14.16	0.88	0.667	12487	832.84	0.000624
17.5	29.23	14.62	0.88	0.656	12487	819.81	0.000636
18.0	30.14	15.07	0.88	0.646	12487	807.38	0.000647

4.2.5 Results and Discussions

The bending moment (*M)*, shear force (*F*) and lateral pile displacement (*y*) obtained in the present pseudo-static analysis are normalized with plastic moment capacity (*Mp*), plastic shear capacity (F_p) and pile diameter *(d*) and plotted in the form of dimensionless bending moment coefficient (*M/Mp*), shear force coefficient (F/F_p) and lateral pile displacement coefficient (y/d) against normalized depth coefficient (*z/L*) for single pile embedded in liquefiable multi-layered sloping ground. The effects of both kinematic and inertial interaction, ground slope, slenderness ratio of pile, pile head fixity condition, existence of liquefiable layer, depth of liquefiable soil layer and embedment depth on pile response are evaluated and presented graphically. The plastic moment capacity is evaluated using following expression (Haldar and Babu 2010; IS 456-2000):

$$M_p = Z_p * \sigma_y \tag{4.16}$$

Where, Z_p = Plastic section modulus= $d^3/6$ and σ_y = yield stress= $0.446 f_{ck}$

Similarly, shear force coefficient (F/F_p) of pile is calculated by dividing the shear force (F) with plastic shear capacity (F_p) of pile. The plastic shear capacity of RCC pile is estimated using IS 456:2000 as below:

$$F_p = F_{sy} + F_c \tag{4.17}$$

Where, F_{sy} = shear capacity of transverse reinforcement = $\frac{(0.87 * f_y * A_{sv} * d)}{S_v}$, considering strain hardening of steel and replacing 0.87 by 1.25:

$$F_{sy} = \frac{1.25 * f_y * A_{sv} * d}{S_v} \tag{4.18}$$

And F_c= shear capacity of concrete = $\delta \tau_c \left(\frac{\pi}{4}\right) d^2$,

Where, $\delta = 1 + \frac{3Pu}{Agfck} \leq 1.50$ and τ_c = critical shear stress which is based on percentage of steel as per IS :456-2000

The plastic moment capacity (Mp) and shear capacity (Fp) of M-30 grade RCC pile of diameter 0.4 m are calculated to be 143 kN-m and 460 kN respectively using equation (4.16) and (4.17).

4.2.5.1 Effects of Kinematic and Inertial Interaction

The PGD profile obtained from nonlinear GRA for various ground slope is shown in Fig. 4.16. Ground deformation pattern are almost constant for top non-liquefiable crust and linearly decreases in liquefiable layer and becomes negligible at the bottom of the liquefiable layer for 0, 2.5 and 5-degree ground slopes. However, for 8-degree slope, due to additional gravity component of the soil, whole liquefiable layer will displace laterally along with top non-liquefiable layer as a rigid mass movement owing to liquefaction-induced lateral spreading. However, top non-liquefiable layer displaces more with compared to the bottom liquefiable layer. The PGA at the ground surface obtained from the present analysis are 0.107g, 0.123g, 0.155g and 0.165g for 0. 2.5, 5.0 and 8.0 degree ground slope respectively. In this study, kinematic and inertial effects have been studied using Kandla Port case study with 5-degree ground slope. The PGD profile obtained from nonlinear GRA for 5.0-degree ground slope is employed to the soil end of the p-y springs for evaluating kinematic response of pile. The increase of axial load on pile due to inertial action of the superstructure during earthquake is estimated using equation (4.1).

Calculation of maximum axial load under dynamic condition (P_d)

The static axial load acting on each pile of Kandla Port building from superstructure (P_s) is 336 kN. At the beginning of the earthquake, inertial forces generated due to vibration of the superstructure transmitted to the pile foundations through the pile cap. The inertial force transmitted as lateral force and overturning moment to the pile through pile cap. The overturning moment is further transmitted as asymmetrical axial forces through pile cap. During soil liquefaction, the stiffness of soil-pile system changes significantly and period of the superstructure also changes. The additional axial load on pile foundations due to change of period of structure is calculated before and after soil liquefaction.

Before soil liquefaction, the fundamental period of RCC building is calculated as per IS 1893 (2016) as

$$T_b = (0.09 * h)/b\text{^}0.5 \quad (4.19)$$

Where h=height of building= 22.0 m and b= base dimension of the building at plinth level= 9.8 m for this case. The period calculated using equation (4.19) is 0.63 sec. The spectral acceleration coefficient (S_a/g) for time period between 0.10 sec to 0.67 sec is 2.50 for soft soil site Type-III as per IS 1893 (2016).

So, the base shear of Kandla Port building can be estimated as

$$V_b = A_h * W \quad (4.20)$$

Where A_h= seismic coefficient and W= total seismic weight of the building

$$A_h = \frac{Z}{2} * \frac{I}{R} * (\frac{S_a}{g}) \quad (4.21)$$

The values of Z=Zone factor=0.36 for zone V, I= Importance factor=1.5 and R= Response reduction factor=3.0 for Kandla Port building as per IS1893 (2016).

The value of A_h estimated to be 0.225 for this case and total seismic weight is calculated as

$$W = DL + 0.25\ LL \quad (4.22)$$

Where *DL*=Total dead load of the building= 9688 kN and *LL*=Total live load of the building= 983 kN (Dash et al. 2009).

Hence, total seismic weight of Kandla Port building obtained using equation (4.20) is 9933.75 kN.

Therefore, the base shear of Kandla Port building using equation (4.20) is evaluated to be 2235 kN.

The pile foundation is to be withstand this base shear and lateral load on each pile is 70 kN. According to Davisson and Robinson (1965), laterally load pile foundations may be assumed to be fixed at depth of *1.8T* below ground level, where *T* is the relative stiffness factor may be calculated using the following equation:

$$T = (EI/n_h)\text{^}0.2 \quad (4.23)$$

Where, *EI* = Flexural rigidity of pile and n_h=coefficient of modulus of subgrade reaction of soil.

The value of n_h can be taken as 6000 kN/m^3 for soft clay from IS 2911-Part 1 (2010).

The relative stiffness factor (*T)* can now be evaluated using equation (4.23) as 1.44 m. Thus, the depth of fixity may be assumed at 2.60 m below ground level as shown in Fig. 4.17(a). Now, the rocking moment in pile foundation may be evaluated as

$$M_R = 2235 * 2.60 = 5811\ kN.m \quad (4.24)$$

The extra axial compressive load on each pile may be estimated using following formula:

$$P_{ext} = \frac{M_R * r_i}{\sum {r_i}^2} = 74.32\ kN \quad (4.25)$$

using the values of r_i= 11.9/2=5.95 m and Σr_i^2= 402.68 m from foundation plan of Kandla port building (Fig. 4.13b). So, the maximum increase of axial load at corner pile of one side of the pile cap is close to 22.12 %.

During liquefaction, **t**he period of vibration of Kandla Port building is calculated at liquefied condition. The top 10 m of pile is passing through non-liquefiable crust and bottom 8 m is passing through in liquefiable soil. Hence, depth of fixity of pile is estimated based on

degraded stiffness of soil. The relative stiffness factor (*T*) is evaluated using equation (4.23) as 2.06 m considering average degraded stiffness value of 1000 kN/m3 from Table 4.5. So, the depth of fixity of pile will be 3.7 m from interface of liquefiable and non-liquefiable crust (Davisson and Robinson 1965) and 13.7 m below ground level (Fig. 4.17b) during liquefaction stage.

The stiffness of Kandla Port building during liquefied condition may be estimated using L_f=13.7 m by following equation:

$$k_s = 32 * \frac{12EI}{L_f^3} = 5627.05 \text{ kN/m} \quad (4.26)$$

Here the total stiffness of soil-pile system is supposed to be mainly contributed by stiffness of pile foundations as stiffness of liquefiable soil is negligible with compared to RCC piles. The time period of Kandla Port building at liquefied condition is now calculated using following equation:

$$T_{b,liq} = 2\pi \left(\frac{M}{k}\right)^{0.5} = 2.77\ sec \quad (4.27)$$

Where, *M*= Mass of Kandla Port building =10749 kN

So, the period of vibration of the building is increased by 4.40 (2.77/0.63) times and the spectral acceleration coefficient (S_a/g) for time period of 2.77 sec would be $\frac{1.67}{2.77} = 0.603$ according to IS1893 (2016).

The value of A_h will be now 0.054 for S_a/g= 0.603 using equation (4.21). Therefore, the base shear would be 536.0 kN using equation (4.20). The maximum increase of axial load on corner pile is calculated using equation (4.25) as

$$P_{ext} = \frac{(536 * 13.7) * 5.15}{402.68} = 93.9 \text{ kN} \quad (4.28)$$

The increase of axial load is around 27.95 %. Thus, the axial load on pile may be increased up to 30% due to soil liquefaction. Here, the dynamic axial load factor (α) is considered as 0.35 for calculation of the maximum axial load (P_d) during dynamic condition and the maximum axial load (P_d) estimated using equation (4.3) is 454 kN. Now, lateral inertial load at pile head is estimated using equation (4.4) as 49.0, 56.0, 71.0 and 75.0 kN for 0. 2.5, 5.0- and 8.0-

degree ground slope respectively considering lateral load co-efficient as 0.1 (Chatterjee et al. 2015).

During liquefied condition, the fixity point of the pile is assumed to be effectively held in position but not restrained against rotation and top is restrained against rotation but not held in position which is feasible as top non-liquefiable layer may move laterally with bottom liquefiable layer in sloping ground. So, effective length (L_e) of pile as per Table 28 of IS 456 (2000)= 2 x 13.7 =27.4 m.

The Euler's buckling load (P_{cr}) for 0.4 m diameter pile is calculated using following expression

$$P_{cr} = \frac{\pi^2 EI}{L_e^2} \tag{4.29}$$

The value of P_{cr} obtained using equation (4.29) is 495.0 kN. Therefore, the factor of safety (FOS) against buckling failure = 495/454 =1.09. Generally, a FOS 3 is preferred by structural engineers for linear elastic buckling taking account into eccentricities, decaying of elastic stiffness because of plastic yielding and inevitable imperfections of pile section. In this case, FOS obtained is 1.09. So, the pile is also prone to buckling failure during soil liquefaction.

Now, the pile response for inertial loading (H) alone at pile head as equivalent static load from vibration of the superstructure are evaluated for ground slope of 5-degree using static load control integrator.

The natural period of ground (T_s) is calculated as below:

$$T_s = 4\,\Sigma\frac{H_{30}}{V_s} = 0.74 \text{ sec (for } H_{30}=30 \text{ m top soil)} \tag{4.30}$$

As the natural time period of the building (T_b) is less than T_s, kinematic and inertial effects have been studied separately and combined response is evaluated by the algebraic summation of individual response at various nodes along pile depth. The lateral pile displacement due to inertial loading is significantly less with compared to kinematic loading in liquefiable sloping ground as seen from Fig. 4.18(a). It is observed from Fig. 4.18(b) that the bending response at pile head is mainly governed by the inertial loading and it diminishes rapidly below depth of 25-times pile diameter from ground level. So, the kinematic response of pile is of great importance at greater depth. However, the combination of kinematic and inertial loading

determines the critical load for pile foundation during earthquake shaking. The variation of shear force coefficient (*F/Fp*) with normalized depth for various kinematic, inertial and combined loading is shown in Fig. 4.18(c). In the present study, peak lateral displacement coefficient, bending moment coefficient and shear force coefficient obtained are 1.87 at ground surface, 2.33 at 6.5 m depth and 0.19 at 11.0 m depth respectively for combined action of kinematic and inertial action. So, the bending moment developed in the pile exceeds the capacity of the pile and shear force demand is less than shear capacity of pile. Hence, the pile is safe against shear failure and unsecured against bending failure. Formation of plastic hinge is anticipated at the interface between liquefiable and non-liquefiable crust.

4.2.5.2 Failure Due to Dynamic Amplification

During soil liquefaction, the time period of Kandla port building increases to 1.73 sec which is far away from the mean period of 0.598 sec of 2001 Bhuj earthquake motion. So, the possibility of pile failure due to dynamic amplification owing to resonance effect is not expected in this case.

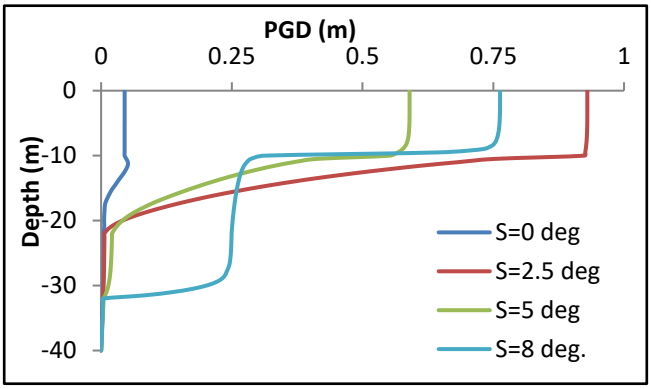

Fig. 4.16 PGD profile for various ground slope

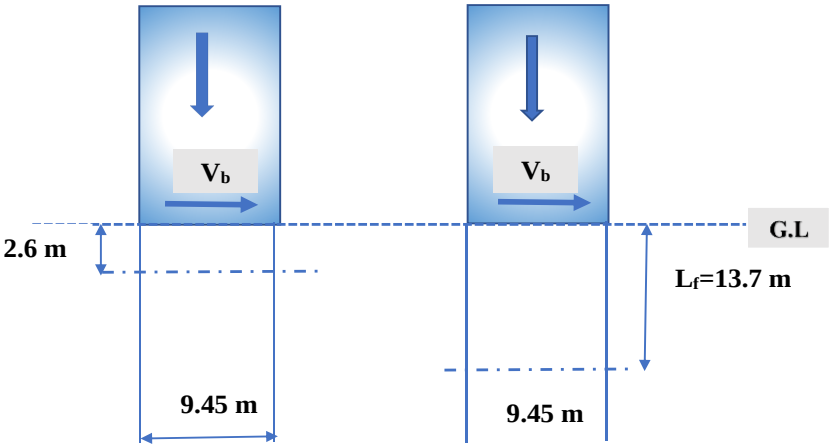

(a) **(b)**

Fig.4.17 Depth of fixity of pile (a) before; and (b) after full liquefaction

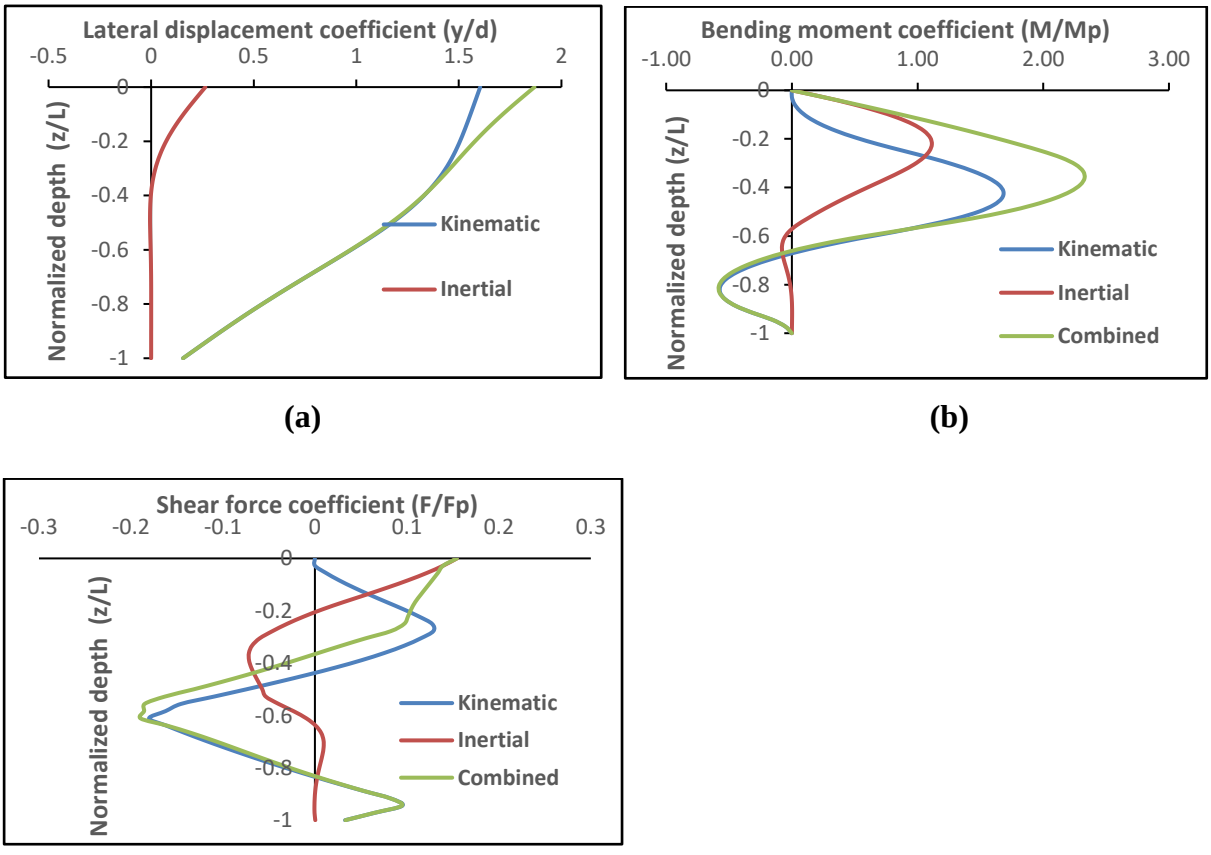

(a) **(b)**

(c)

Fig. 4.18 Variation of **a** lateral displacement coefficient **b** bending moment coefficient and **c** shear force coefficient with normalized depth for kinematic, inertial and combined loading

4.2.5.3 Effects of Degradation of Strength and Stiffness of adjacent Non-Liquefiable Layer at Interface due to Intermediate Liquefiable Layer

Analysis has been carried out for 18 m long and 0.4 m diameter pile resting in Kandla port soil profile to demonstrate the effects of degradation of strength and stiffness of adjacent non-liquefiable layer at interface due to intermediate weaker liquefiable layer. The strength and stiffness values computed in this study are modified using the method proposed by McGaan et al. (2011) and results are shown in Fig 4.19(a), (b) and (c). It is observed that maximum pile head displacement does not change significantly. However, the maximum bending moment and shear force coefficient are reduced from to 1.68 to 1.45 and 0.18 to 0.15 respectively,

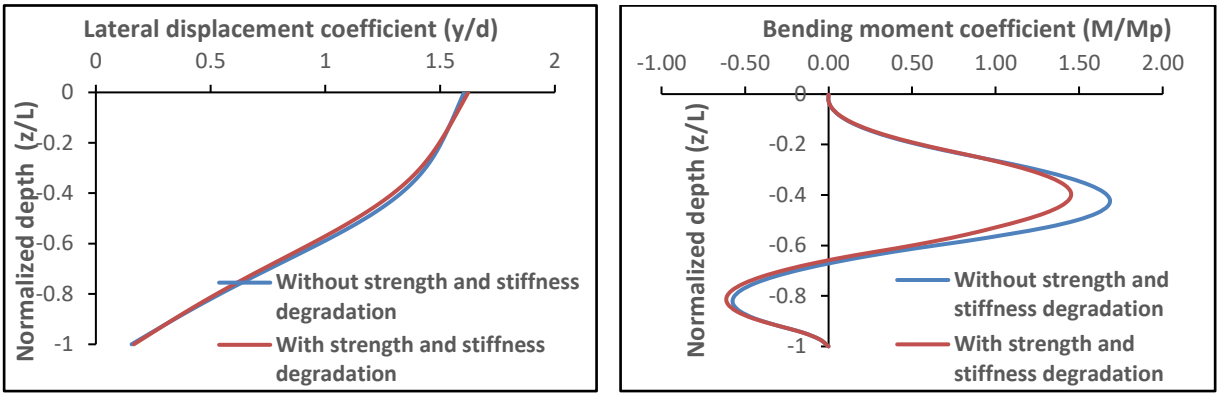

(a) **(b)**

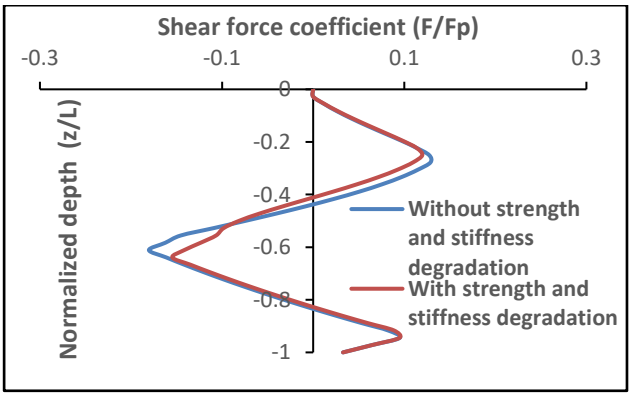

(c)

Fig. 4.19 Comparison of **a** lateral displacement coefficient **b** bending moment coefficient and **c** shear force coefficient with normalized depth with and without degradation of strength and stiffness of adjacent non-liquefiable layer at interface

thereby showing a reduction of maximum shear force and kinematic pile bending moment of almost 14% with considering the strength and stiffness degradation of adjacent non-liquefiable (NL) layer at interface due to intermediate liquefiable layer.

4.2.5.4 Comparison of Response of Pile for p-y Curve with Conventional P-Multiplier Method and p-y Curve Considering Shear Hardening

In the recent literature, p-y curve has been developed for pile in liquefiable soil layer considering shear hardening (Lombardi et al. 2017). It is recognised that liquefiable soil dilates upon application of undrained shearing. As a result, excess pore water pressure gradually decreases and subsequently strength and stiffness increases. A comparative plot of lateral displacement coefficient, bending moment coefficient and shear force coefficient of pile against normalized depth are presented for *p-y* curve with conventional p-multiplier method and p-y curve considering shear hardening as shown in Fig 4.20(a), (b) and (c). It is seen that lateral pile head displacement does not change at all. However, and maximum negative bending moment and shear force coefficient are increased from 0.57 to 1.32 and 0.18 to 0.37 respectively, thereby showing an increase of maximum kinematic pile bending moment and shear force of almost 132% and 105% respectively for kinematic analysis of pile using *p-y* curve considering shear hardening with compared to conventional *p*-multiplier method.

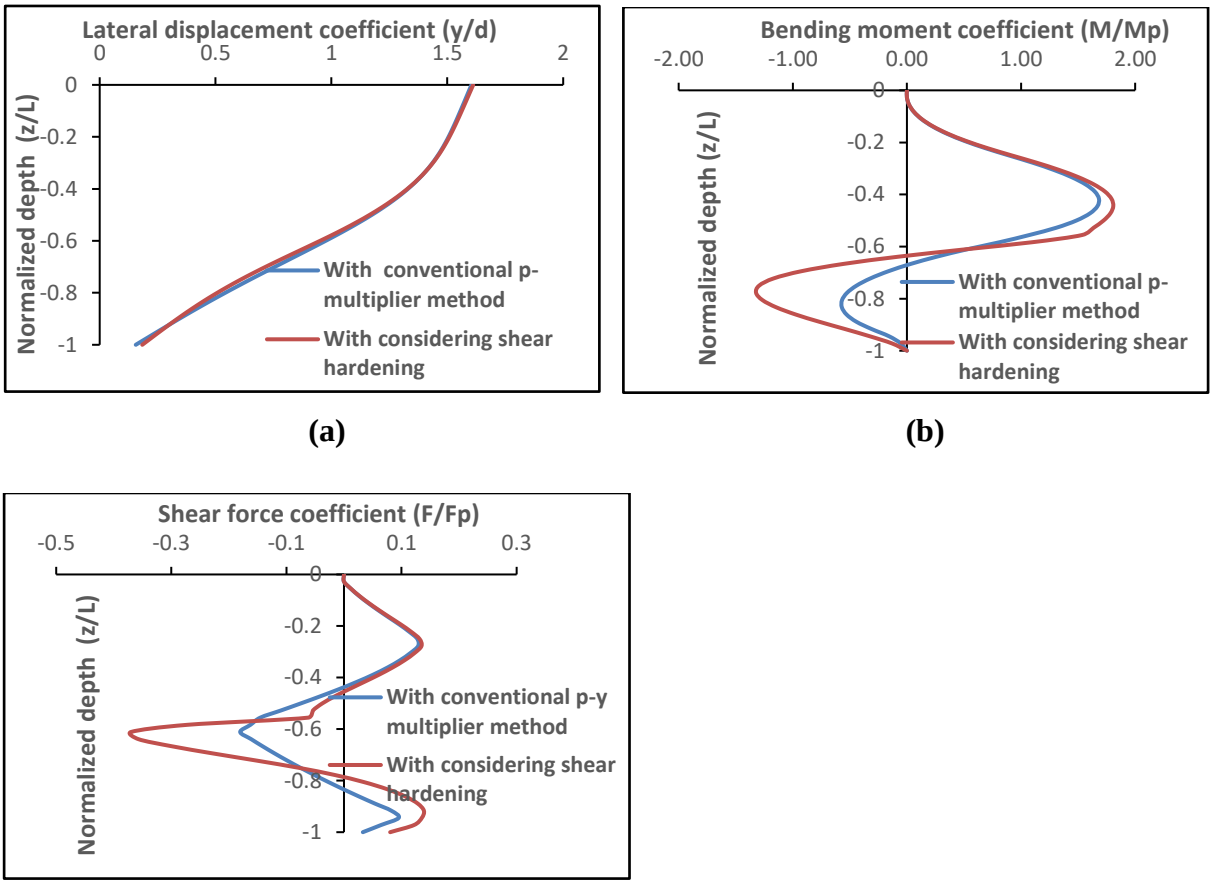

Fig. 4.20 Comparison of **a** lateral displacement coefficient **b** bending moment coefficient and **c** shear force coefficient with normalized depth for p-y curve with conventional p-multiplier method and p-y curve considering shear hardening

4.2.5.5 Effects of Ground Slope

It is seen from the free-field GRA (Fig. 4.16) that peak ground displacement (PGD) of sloping ground increases several times with respect to the level ground (S=0 degree). So, large lateral force may be developed in the pile in sloping ground during liquefaction, which is generally termed as lateral spreading. The highest PGD value observed for 2.5-degree ground slope. The PGD values are almost constant for top non-liquefiable crust and linearly decreases in liquefiable layer and becomes negligible at the bottom of the liquefiable layer for all the ground slopes except 8-degree. The variation of kinematic lateral displacement coefficient and bending moment coefficient of pile with normalized depth for various ground slopes are presented in Figs. 4.21(a) and (b) respectively. The results show that peak lateral

displacement coefficient increases significantly with ground slope due to kinematic loading and values are 0.11, 2.54, 1.60 and 2.1 for ground slope of 0, 2.5, 5 and 8.0 degree respectively. The peak kinematic bending moment coefficients corresponds to 2.5, 5.0 and 8.0 degree ground slope are 4.7, 3.3 and 3.0 times more than level ground respectively. Higher inclination (5 degree and 8 degree sloping grounds) caused earlier mobilization of soil movement during initial stage of earthquake and subsequent increase of passive resistance of soil with passage of time. However, for mild slope (2.5 degree), the displacement increases with the passage of time due to comparative less passive resistance when subjected to long duration Bhuj earthquake motion. So, the peak values of lateral displacement and bending moment for 2.5 degree sloping ground are greater than 5 degree and 8 degree sloping grounds. More detailed investigation is required for more quantitative reasoning of this interesting result. The sliding of non-liquefiable crust overlying liquefiable layer in sloping ground may impose large lateral load on pile. Hence, pile foundation in liquefiable sloping ground is susceptible to kinematic bending failure.

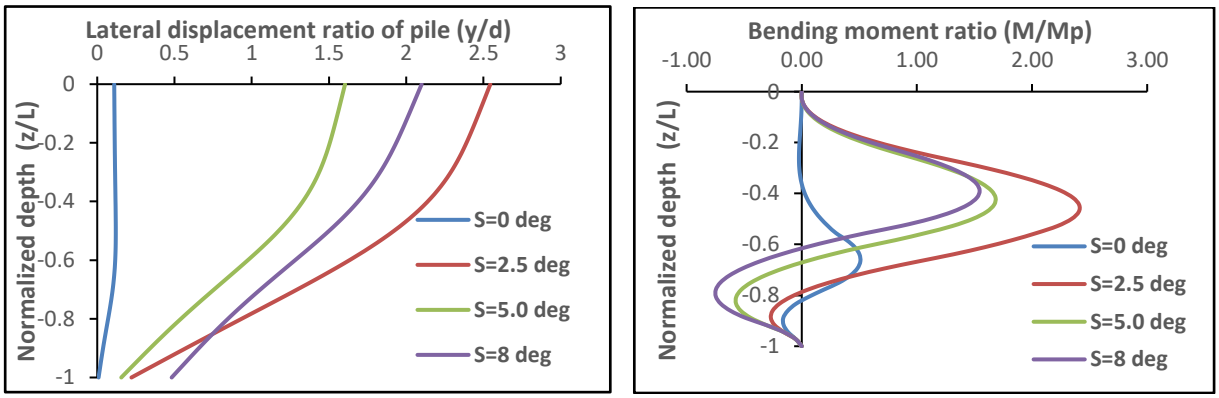

(a) **(b)**

Fig. 4.21 Variation of **a** lateral displacement coefficient and **b** bending moment coefficient with normalized depth for various ground slope for kinematic loading

4.2.5.6 Effects of L/d Ratio of Pile

The effects of *L/d* ratio on kinematic pile response for pile having constant length (*L*) of 18 m and diameter (*d*) of 0.4 m, 0.6 m, 0.75 m and 1.0 m with corresponding *L/d* ratio of 45, 30, 24 and 18 are considered in the present study. From Fig. 4.22(a), it is noticed that maximum lateral pile displacement coefficient decreases from 1.60 to 0.77 which is almost 52% when the pile diameter increases from 0.4 m to 1.0 m. The variation of bending moment coefficient (M/M_p) with normalized depth coefficient for various pile diamter is presented in Fig 4.22(b).

The plastic moment capacity (M_p) of 0.4 m, 0.6 m, 0.75 m and 1.0 m diameter M-30 grade RCC piles are calculated to be 143 kN-m, 482 kN-m, 941 kN-m and 2230 kN-m respectively using equation (4.16). The maximum bending moment developed in the pile increases from 240.22 kN-m to 631.44 kN-m (almost 163%) due to change of pile diamter from 0.4 m to 1.0 m and the maximum bending moment coefficient (M/M_p) obtained are 1.68, 0.84, 0.55, 0.28 for pile diamter of 0.4 m, 0.6 m, 0.75 m and 1.0 m respectively. So, the bending moment coefficient decreases by 83.33 % due to change of pile diamter from 0.4 m to 1.0 m. M/M_p ratio more than 1.0 for pile diameter of 0.4 m indicates the kinematic bending failure of pile of Kandla port building using Bhuj earthquake. So, use of large diameter pile is recommended to avoid kinematic bending failure in liquefiable sloping ground.

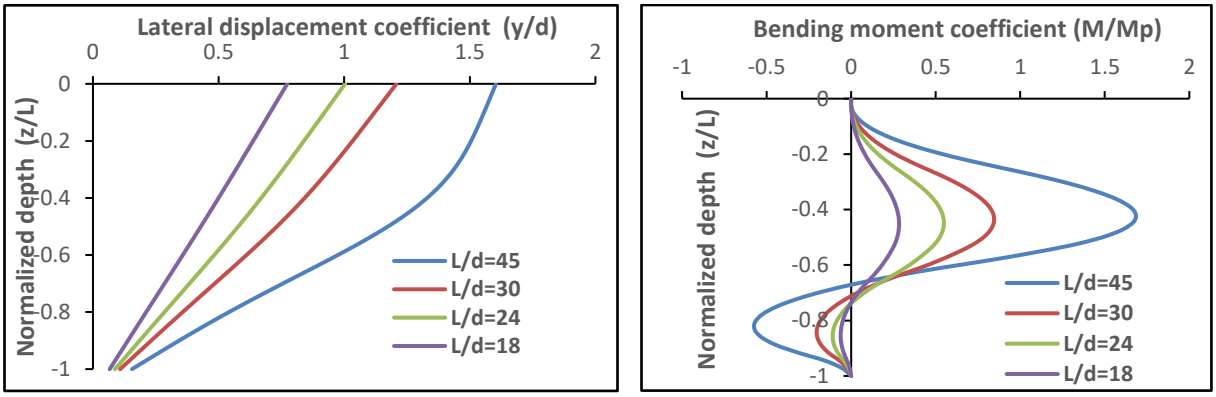

(a) **(b)**

Fig. 4.22 Variation of **a** lateral displacement coefficient and **b** bending moment coefficient with normalized depth for various L/d ratio of pile

4.2.5.7 Comparison of Pile Response in Liquefied and Non-Liquefied Condition

The lateral displacement and bending moment of pile are significantly influenced by the existance of liquefiable crust within pile length. The effects of ground water table has been neglected and stiffness degradation factor is assumed to be 1 to simulate non-liquefiable condition. From Fig. 4.23, it is found that maximum lateral displacement coefficient is increased from 0.45 to 1.60 due to change of soil condition of inermediate sandy layer of Kandla Port site from non-liquefiable condition to liquefiable condition. Hence, magnification factor which is the ratio of maximum lateral displacement of pile in liquefiable condition to that in non-liquefiable condition obtained is 3.5 considering kinematic effects only. The maximum kinematic bending moment in liquefiable condition and non-liquefiable condition are 240.22 kN-m (M/Mp=1.68) and 298 kN-m (M/Mp=2.09) respectively. The maximum displacement coefficient in liquefied condition is increased because of reduction of soil

strength and stiffness owing to liquefaction. However, the maximum kinematic bending moment is more in case of non-liquefiable condition because maximum bending moment at the interface depends on stiffness contrast between liquefable and non-liquefiable crust. In this case, the top 10 m soil is soft clay with less stiffness and liquefiable condition of intermediate layer also reduces the stiffness of 12 m sandy layer. Thus, stiffness contrast between the top non-liquefiable and intermediate liquefiable soil reduces significaly and less bending moment developed with compared to non-liquefiable condition. The maximum The pattern of variation of bending moment with depth also differers in both the condition.

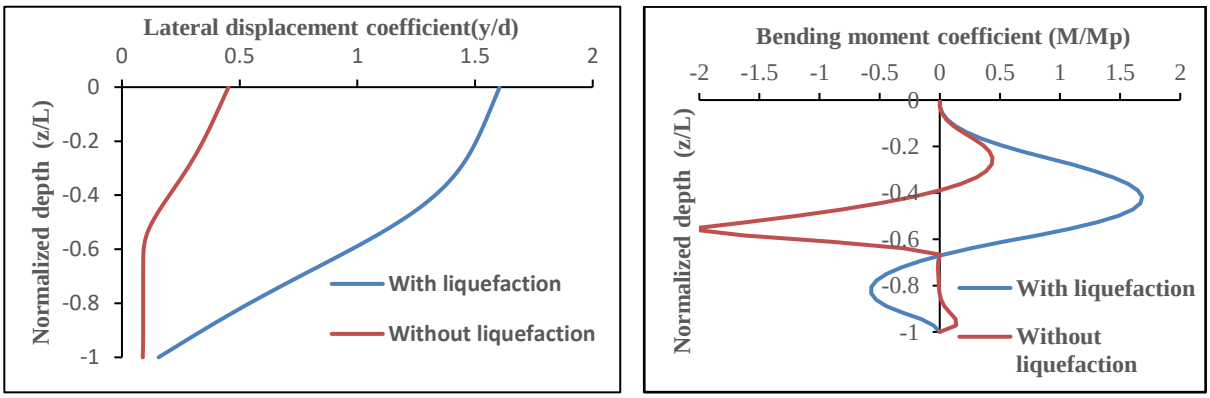

(a) **(b)**

Fig. 4.23 Variation of **a** lateral displacement coefficient and **b** bending moment coefficient with normalized depth under liquefied and non-liquefied condition

4.2.5.8 Effects of Pile Head Fixity Condition on Pile Response

The pile head fixity condition has a profound effect on pile response. The lateral displacement coefficient of the pile does not significantly influence by the pile head fixity conditions as shown in Fig. 4.24(a). Fixed head means free to translate and restrained against rotation (full rotational fixity) has been considered in this study. The maximum lateral displacement coefficient of free head and fixed head piles are 1.60 and 1.53 respectively. However, for free head pile, the maximum bending moment (240.22 kN-m) occurs near the interface of liquefiable and non-liquefiable layer. For fixed head pile, the maximum bending moment occurs at two positions: one at the pile head (71.43 kN-m) and other near the interface of liquefiable and non-liquefiable interface (261.05 kN-m) as shown in Fig. 4.24(b).

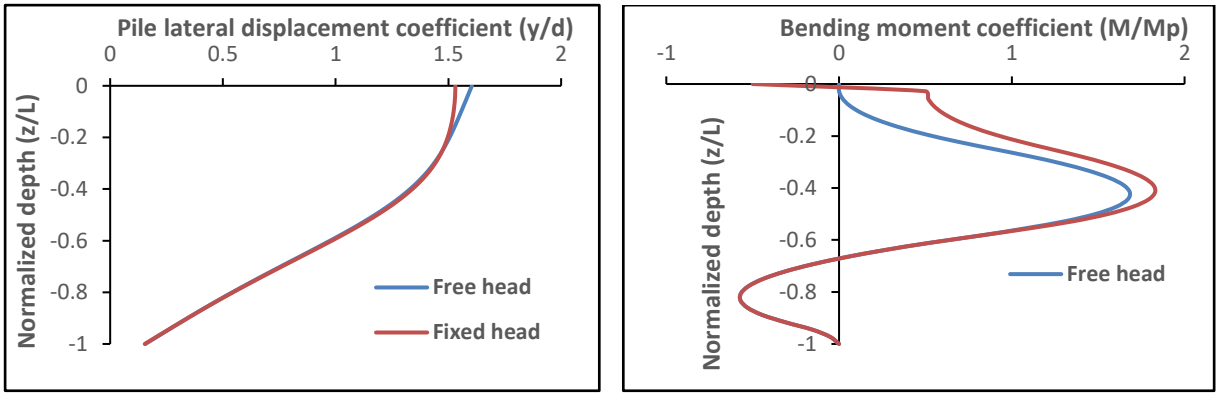

(a) **(b)**

Fig. 4.24 Variation of **a** lateral displacement coefficient and **b** bending moment coefficient with normalized depth for different pile head fixity condition

4.2.5.9 Effects of Depth of Liquefiable Soil Layer

In this study, the effects of depth of liquefiable soil layer on kinematic pile response has been studied for single free headed pile embedded in three-layer soil profile as shown in Fig. 4.25. The soil profile adopted for parametric study is slightly modification of original soil profile of Kandla Port site. The total length (L) and diameter (d) of pile are 18 m and 0.4 m respectively which are same as foundation of Kandla Port building. The thickness of top non-liquefiable crust (L_1=6.0 m) is kept constant and the thickness of liquefiable layer (L_{Liq}) varies in the form of (L_{Liq}/L) from 0.22 to 1.0 by changing the depth of embedment (E_{NL}) of pile at bottom stiff non-liquefiable layer from 0d to 20d as shown in Fig.4.25. It is observed from Fig. 4.26(a) that the maximum lateral displacement coefficient of pile is 2.81 for L_{Liq}/L= 0.55. The displacement coefficient reduces to 1.42 when the entire soil layer is liquefiable (L_{Liq}/L= 1.0). The kinematic bending moment response for various ratios of L_{Liq}/L is shown in Fig. 4.26(b). The peak bending moment coefficient is 5.50 near the boundary between liquefiable and non-liquefiable layer for L_{Liq}/L= 0.22. The peak bending moment coefficient reduces thereafter with increase of L_{Liq}/L ratio and becomes minimum when L_{Liq}/L= 0.66. With the increase of L_{Liq}/L ratio, the embedment depth (E_{NL}) of pile decreases and kinematic bending moment decreases. Hence, peak bending moment co-efficient also decreases. When L_{Liq}/L becomes 0.66, the embedment depth (E) of pile becomes zero and peak bending moment coefficient becomes minimum.

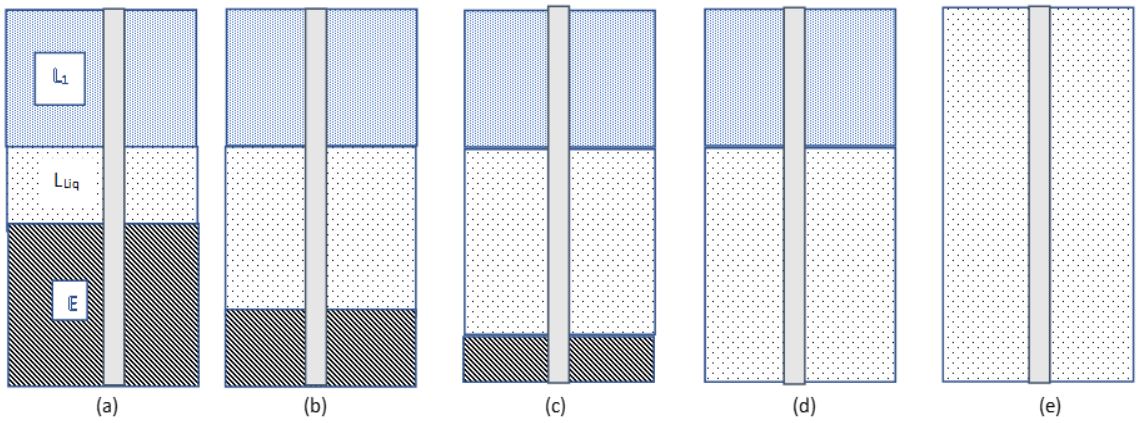

Fig. 4.25 Variation of depth of liquefiable layer **a** Case I (L_{Liq}/L=0.22, E_{NL}=20d) **b** Case II (L_{Liq}/L=0.44), E_{NL}=10d **c** Case III (L_{Liq}/L=0.55, E_{NL}=5d) **d** Case IV (L_{Liq}/L=0.67, E_{NL}=0d) and **e** CaseV (L_{Liq}/L=0.1.0, E_{NL}=0d)

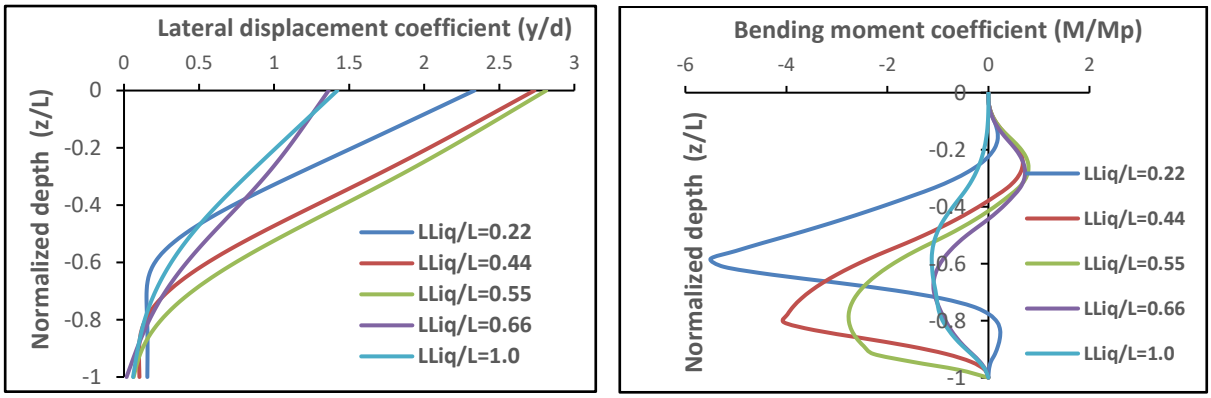

(a) **(b)**

Fig. 4.26 Variation of **a** lateral displacement coefficient and **b** bending moment coefficient with normalized depth for different depth of liquefiable soil layer

4.2.5.10 Effects of Depth of Embedment of Pile

The kinematic pile lateral displacement, shear force and bending moment coefficient for various embedment depth of pile are shown in Fig. 4.27 (a), (b) and (c) respectively. It is observed that peak displacement coefficient 2.81 occurs for embedment depth of five times the pile diameter and reduces for further increase of embedment depth. However, the shear force and bending moment coefficient are increased with the increase of depth of embedment of pile. The maximum shear force and bending moment coefficients obtained are 0.79 and 5.5 for embedment depth of twenty times the pile diameter respectively. The kinematic pile

bending and shear in liquefiable sloping ground increases with increasing embedment depth of pile.

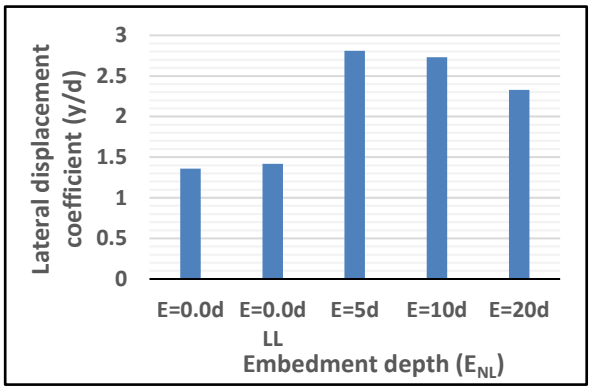

(a)

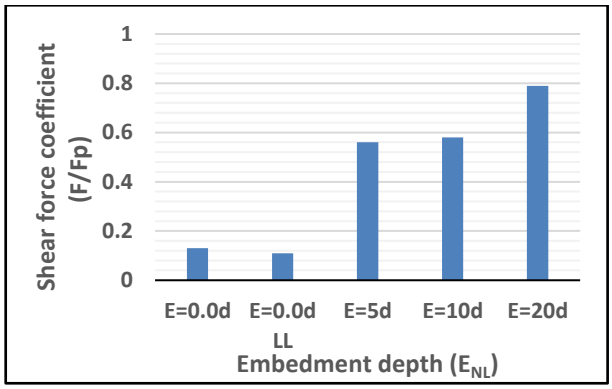

(b)

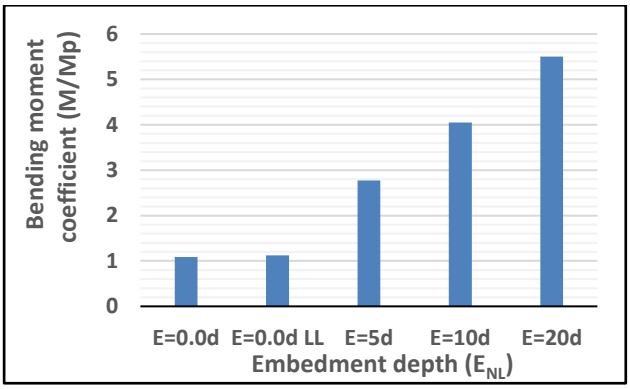

(c)

Fig. 4.27 Comparison of **a** lateral displacement coefficient **b** shear force coefficient and **c** bending moment coefficient with different embedment depth of pile

4.2.5.11 Comparison of Present Numerical Methodology with the Simplified Formulation in the Literature

The maximum kinematic pile bending moment developed at the interface between two-layers having remarkably different shear modulus using present numerical methodology is compared with simplified formulations of Dobry and O'Rourke (1983), Mylonakis (2001), Dobry et al. (2003) and Abdoun et al. (2003). The same pile and soil properties as considered in case I of Fig. 4.25 for 18.0 m long and 0.4 m diameter pile resting in level ground have been used to compute the maximum kinematic pile bending moment at interface of liquefiable and non-liquefiable soil. The bending moment obtained at 14.0 m depth using present numerical methodology and simplified formulations are tabulated in Table 4.6. Slight variation of

maximum bending moment between present study and simplified formulations of previous researchers are observed. The simplified methods underestimate the maximum bending moment at the interface. This is because these methods are approximate method and derived using Winkler model assuming each soil is homogeneous, isotropic, and linearly elastic. The thickness of soil layers, characteristics of input motion are not considered in these simplified formulations.

Table 4.6 Comparison of results obtained using present study with the simplified formulation of previous researchers

Pile bending moment at interface	Present study	Dobry and O'Rourke (1983)	Mylonakis (2001)	Dobry et al. (2003)	Abdoun et al. (2003)
M_{max} (kN.m)	567.59	429.73	478.72	392.00	403.76

Chapter 5

Dynamic Analysis of Piles in Level Ground

5.1 Introduction

A significant number of damages and/or collapses of pile foundations and pile-supported structures are reported in liquefiable soil after past major earthquakes in spite of employing large factor of safety (FOS) in their design as per latest standard code of practices (Dash et al. 2010). So, it is challenging job for geotechnical earthquake engineers to ensure safe and economical design of pile foundation and pile-supported high-rise structures on liquefiable soil of metropolitan city like Kolkata, where rapid growing of population and infrastructure makes it essential.

The effects of soil liquefaction on seismic response of pile foundations have been studied by various researchers and showed that the pile response is strongly affected by type of soil, nature of input motions, inertial effects of superstructure and kinematic effects due to soil displacement. Simplified 1D, 2D and 3D numerical studies performed by several researchers using robust numerical codes and platforms due to spatial and economic limitations of physical model. The constitutive model considered for most of these numerical studies are very simple and based on uncoupled formulation of soil-fluid interaction. This approach is incapable to simulate direct pore water pressure development and changing of shear strength due to shear deformation of soil.

It is clearly understood from literature review that the simplified methods based on pseudo-static approach needs various numerical assumptions and not able to simulate the complex dynamic response of piles during earthquake. Besides, due to large shear strain is likely to be developed during soil liquefaction, nonlinearity of soil needs to be considered for seismic analysis of pile foundations in liquefiable soil. Bending and buckling are two distinct approaches of structural design. Buckling criteria will not be fulfilled automatically by designing the pile against bending criteria. Bending is stable failure mode which depends on bending strength of material (Plastic moment capacity, *Mp*). Contrariwise, buckling is

unstable failure mode which depends only on geometric characteristics of the member. Hence, in present study, seismic response of pile foundations in liquefiable layered soil of Kolkata city is carried out through numerical simulation of dynamic nonlinear soil-pile interaction under influence of axial loading to incorporate bending and buckling interaction. An advanced soil constitutive model, implemented in fully-coupled *u-p* formulation (where *u* and *p* are soil skeleton displacement and pore water pressure respectively) is adopted using nonlinear finite-element based computer program OpenSeesPL (Elgamal et al. 2010; Lu et al. 2011) for soil-fluid interaction and pore water pressure development reasonably. The finite-element model is three dimensional with consideration of *P-delta* effect. There are others computer program also like FLAC or ABAQUS for numerical analysis of pile foundations. FLAC is finite volume-based software, whereas, ABAQUS and OpenSeesPL are finite element-based software. There are many advanced soil constitutive models in OpenSees framework for simulating dynamic nonlinear behaviour of soil. Also, the OpenSeesPL is an open-source software and the user interface is easier to use than ABAQUS and FLAC. Hence, in the present study OpenSeesPL based on finite element method is selected for dynamic analysis of soil-pile system.

5.2 Study Area

The Kolkata metropolitan city, is a gateway to north-east India. It is third-most populated city in India. Originally, Kolkata city was developed towards the east side of the river Hooghly. But due to increasing population and scarcity of vacant land, infrastructures are often constructed without proper town planning on reclaimed lands in the Salt Lake and Rajarhat areas. More than 80% of the city area has covered with different types of important heritage building, school, hospital buildings in unplanned way. The soil of Kolkata city is mainly alluvial in nature having two different soil formations such as Normal Kolkata Deposit (NKD) and River Channel Deposit (RCD). NKD soil mainly compose with silty clay or clayey silt of soft to stiff consistency with sandy deposit at intermediate layer. The RCD soil mainly composes with medium to dense compactness sand deposit up to significant depth along the existing old Adiganga channel (Roy et al. 2018). In the present study, geotechnical bore hole data of Kolkata city has been selected from Roy et al. (2018) and details are described in chapter 3. The depth of borehole is 50 m for both the sites. Friction angles (φ) for cohesionless soils and undrained shear strength (C_u) for cohesive soil are calculated using the co-relation of SPT-*N* with φ for cohesionless soil and SPT-*N* with C_u for cohesive soils

(Das 1983). The values of various soil properties of two typical soil are shown in Fig.5.1. Fines content (FC) of each layer of RCD soil is also indicated in Fig. 5.1.

Kolkata city falls in the Zone III & IV according to zonation map of Indian standard design code IS:1893 (2016). The Kolkata city is located on the important regional basement fault Eocene Hinge Zone. Kolkata, in the past, has suffered tremendous damages due to near and far field earthquakes. The local soft, alluvial soil of Kolkata city magnify the earthquake ground motion. The input ground motions considered for present analysis are Imperial valley (IMV) and Bhuj (BHJ) earthquakes with significant variation in moment magnitude, maximum bedrock level acceleration (*MBRA*), strong motion duration and frequency content as tabulated in Table 3.3. The input earthquake motions used in present analysis are shown in Fig. 3.2(a) and (b).

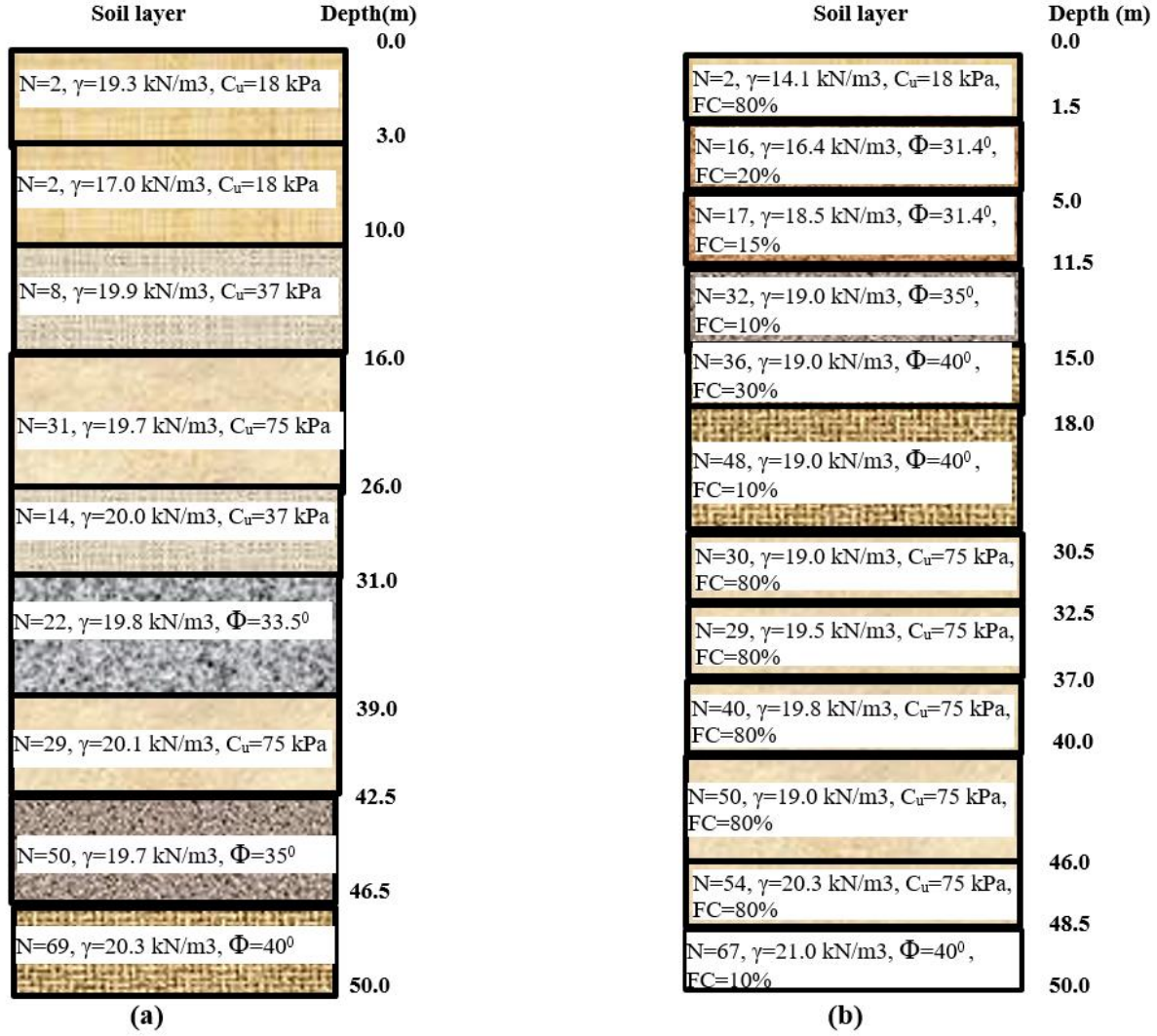

Fig.5.1 Typical soil profile of Kolkata city **a** NKD soil (Ultadanga site) **b** RCD soil (Tollygunge Metro site) (after Roy et al. 2018)

5.3 Descriptions of the Present Numerical Model

Full 3D numerical model is built using finite-element based program OpenSeesPL as shown in Fig. 5.2 to simulate coupled soil-pile system. All the simulations in OpenSeesPL are performed using open-source finite element-based computational platform OpenSees (McKenna and Fenves 2001). Due to symmetric condition, only half of the soil domain is modelled. A floating pile of Length *L* and diameter *d* is embedded in the layered soil. The soil domain is modelled with 8-node brick elements and elastic beam-column element is used to model the pile. Each soil and pile node has four and six degrees-of-freedom (*DOF*) respectively. The first three *DOFs* of soil node illustrate translation of soil skeleton and the fourth *DOF* represents pore water pressure. Rigid connecting element having similar material properties of the pile is used to implement the physical modelling of the pile. Each 3D brick element of soil domain is connected to the adjacent pile element at same elevation using outer nodes of these rigid links through equal *DOF* command and transfer the forces from pile to soil and vice versa. Fine mesh size is used for pile zone and mesh size becomes comparative larger near domain boundaries to prevent reflection of seismic waves. The total length of mesh in each horizontal direction considered is 40d from the middle of the pile. The total depth of the soil profile (50 m) is considered for the dimension of model in vertical direction. Also, the maximum size of element in dynamic analysis considered is less than $\lambda/10$ (λ=wave length) to prevent filtration of parts of the seismic waves (Oliaei et al. 2017).

All the soil nodes at the base of the model are considered as completely fixed in all directions. The pore water pressure *DOF* on ground surface is fixed for drain out water and is open in the rest of the nodes for free variation of pore water pressure (*PWP*). Side nodes orthogonal to the direction of base excitation are considered as fixed in this direction and are set free parallel to the direction of excitation. Nodes at the boundaries parallel to the base excitation are constrained orthogonal to the excitation direction and are set free to move in the excitation direction. Ground motions are applied at assumed bed rock level (50 m depth) in longitudinal direction (x-axis) and its amplification has been considered for dynamic analysis of soil-pile system.

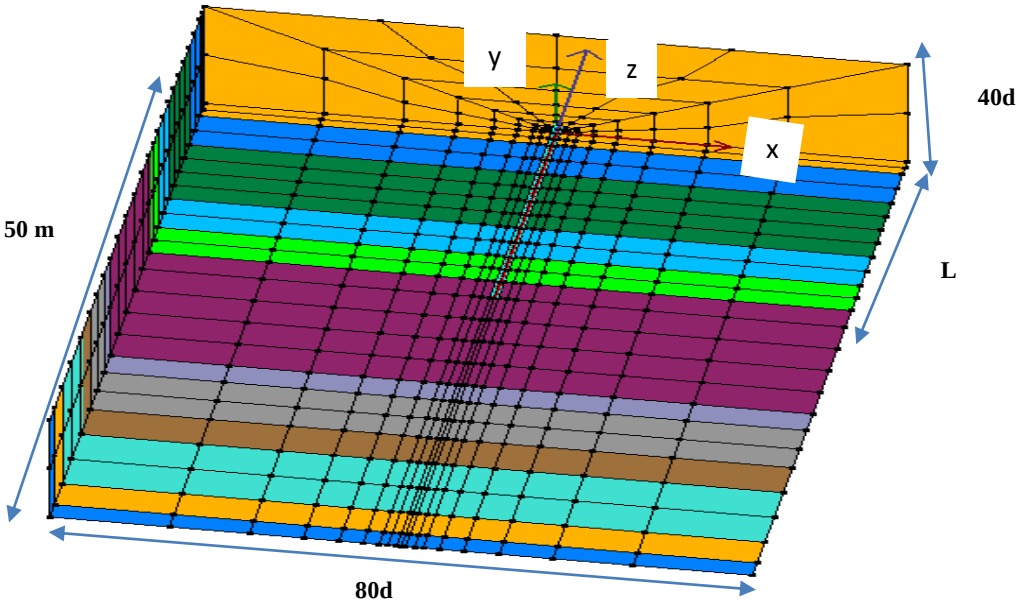

Fig. 5.2 3D FE model used in the present study

The plasticity model used in the present study is based on pressure-dependent multi-yield surface approach to model the cyclic hysteretic response (Elgamal et al. 2003; Yang et al. 2003) of frictional cohesionless soil. Yield function (*f*) is defined in the following form (Prevost 1985):

$$f = \frac{3}{2}(s - (p' + p_0')\alpha) : (s - (p' + p_0')\alpha) - m^2(p' + p_0') = 0 \quad (5.1)$$

where, $s = \sigma' - p'\delta$ is the deviatoric stress tensor, p' is mean effective stress and p_0' is the small positive constant for finite size of yield surface at $p' = 0$. Parameters α and m are the second order kinematic deviatoric tensor and size of yield surface respectively (Elgamal et al. 2003).

Multi-yield surface plasticity constitutive model has several features. The yield surface is pressure-dependent and nested cone shape in principal stress space. The peak shear strength of soil is represented by the outermost surface. The hardening zone is formed by the nested yield surfaces with regards to multi-surface plasticity for simulating nonlinear soil response. Shear-induced dilatancy during liquefaction is modelled using this constitutive model. A new adequate flow rule is developed to incorporate the contractive, completely plastic and dilative stages. In this respect, effort is placed to the coupling of deviatoric volumetric strain under cyclic loading, which is responsible for cyclic mobility. Shear-induced dilation or contraction

is defined by the volumetric component $P"$ of the normal to the plastic potential. Along the phase transformation (PT) surface, the stress ratio $\eta=\tau/p'$ is indicated by η_{PT}. Clear contractive or dilative characteristics are simulated through the following equations of P'' based on the value of η in comparison to η_{PT} and the sign of $\dot{\eta}$ (time rate of η):

$$P" = \frac{1-(\eta/\eta_{PT})^2}{1+(\eta/\eta_{PT})^2} c_1 \qquad \text{(for contraction)} \tag{5.2}$$

where c_1=non-negative parameter indicating the rate of shear-induced volume contraction or pore-pressure build up and

$$P" = \frac{1-(\eta/\eta_{PT})^2}{1+(\eta/\eta_{PT})^2} d_1 exp(d_2\gamma_d) \qquad \text{(for dilation)} \tag{5.3}$$

where d_1 and d_2=non-negative parameters indicating the rate of shear-induced volume dilation and γ_d=octahedral shear
strain build up throughout dilation cycle.

So, the following cycles of response are simulated under undrained situations (Fig. 5.3):

1. the contractive cycle within the *PT* surface ($\eta < \eta_{PT}$, cycles 0–1 and 3–4) and also outside during shear unloading ($\eta > \eta_{PT}$ with $\eta <0$, cycle 2–3);
2. the dilative cycle during shear loading outside the *PT* surface ($\eta > \eta_{PT}$ with $\eta >0$, cycle 1–2); and
3. a neutral cycle (P"=0, cycle 4–5) between the contraction (P" >0, cycle 3–4) and the dilation (P" <0, cycle 5–6) cycles. This cycle is important only at small confinement.

The principal component of this modelling approach is the prior calibration of the employed soil model under liquefaction and lateral spreading scenario. The Pressure dependent *multi-yield02 (PDMY02)* type material model (Yang et al. 2003) is used in the present study for modelling the liquefiable sands which is modified form of Pressure dependent multi-Yield material. Extra parameters (*c3* and *d3*) are required to account for effect of overburden pressure (K_σ effect). Parameter *c2* is required to include the effect of past dilation history on consequent dilation tendency. Mass density *(*ρ), Friction angles (φ) and reference mean effective confining pressure (P_{ref}), pressure dependent coefficient (*d*), reference low-strain shear modulus *(*G_r), reference low-strain bulk modulus (B_r), peak shear strain (y_{max}) at which highest shear strength is achieved and number of yield surfaces (*NYS*) are the principal input parameters for this material model. The variation of shear modulus (*G*) and bulk modulus (*B*) with effective confining pressure (p') is defined using the reference G_r and B_r as follows:

$$G = G_r(\frac{p'}{p'_{ref}})^d \tag{5.4}$$

$$B = B_r(\frac{p'}{p'_{ref}})^d \tag{5.5}$$

Soil dilatancy is defined by specifying phase transformation angle (Φ_{PT}), contraction (c_1, c_2 and c_3) and dilation parameters (d_1, d_2 and d_3). These parameters monitor the rate of pore water pressure accumulation in soil during liquefaction.

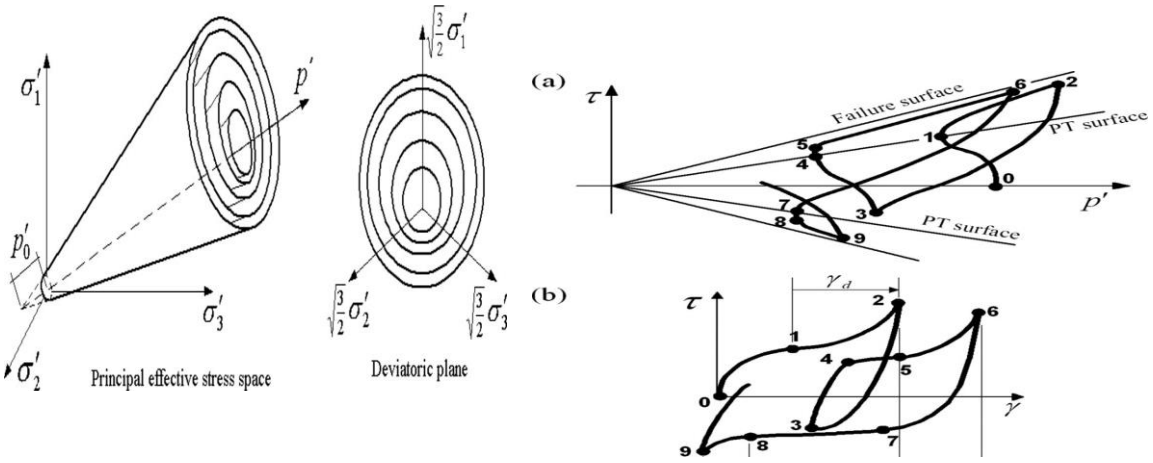

(a) Multi-yield yield surface in principal stress space and deviatoric plane

(b) Stress path and shear stress-strain

Fig. 5.3 Pressure-dependent multi-yield-surface plasticity constitutive model (Elgamal et al. 2003; Yang et al. 2003)

Nonlinear hysteretic material model is used for modelling clay material using Von Mises multi-surface kinematic plasticity model as shown in Fig. 5.4 (Yang et al. 2003; Parra 1996; Yang 2000). Simulating the soil hysteretic elasto-plastic shear response is focused in this model. Plasticity develops only in the deviatoric stress-strain response for this material. The volumetric stress-strain response is linear-elastic and is free from the deviatoric response. This constitutive model simulates monotonic or cyclic response of materials having shear response is independent to the confinement variation. Multi-surface approach is used to formulate the plasticity with an associative flow rule based on Prevost approach. The nonlinear hyperbolic shear stress-strain (τ- γ) relationship at constant confinement p'_r for clay model is defined using the two material parameters, low-strain shear modulus (G_r) and

ultimate shear strength(τ_f) as given in equation (5.6) and (5.7). *Pressure independent multi-yield (PIMY)* type material is used for modelling the cohesive soils.

$$\tau = \frac{G_r \gamma}{1+\left(\frac{G_r}{\tau_f}-\frac{1}{\gamma_{max}}\right)\gamma} \tag{5.6}$$

$$\tau_f = \frac{2\sqrt{2}sin\varphi}{3-sin\varphi} p_r' + \frac{2\sqrt{2}}{3} c \tag{5.7}$$

Mass density (ρ), cohesion (c) and reference mean effective confining pressure (P_{ref}), pressure dependent coefficient (*Co-eff*), reference low-strain shear modulus (G_r), reference low-strain bulk modulus (B_r), peak shear strain (y_{max}) at which highest shear strength is achieved and number of yield surfaces (*NYS*) are the principal input parameters for this material model. The values of various input parameters for modelling each layer are considered from OpenSees user manual (Lu et al.2011; Mazzoni et al. 2006) based on soil type of each layer of NKD and RCD soil and summarized in Tables 5.1 and 5.2 respectively. The values of fluid mass density, combined bulk modulus, permeability of clay and sandy soil considered are 1.0 Mg/m^3, $2.2x10^6$ kN/m^2, $1x10^{-09}$ and $6.6x10^{-05}$ m/s respectively (Lu et al.2011).

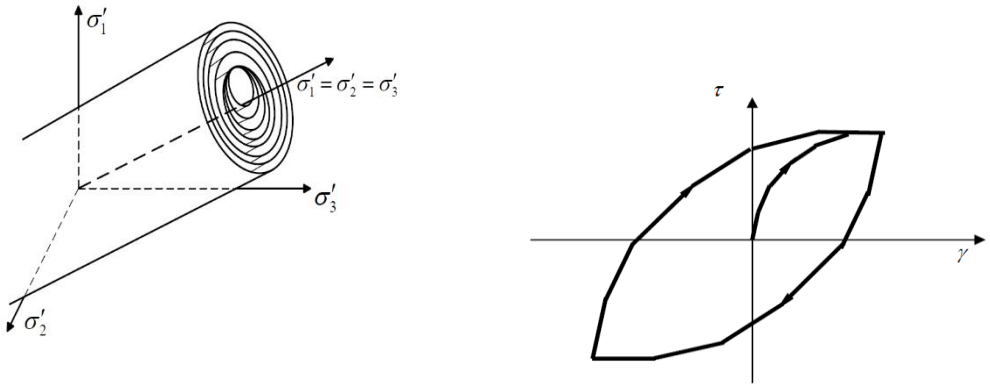

(a) Von Mises multi-surface (b) Hysteretic shear response.

Fig. 5.4 Von Mises multi-surface kinematic plasticity model (Parra et al. 1996; Elgamal et al. 2003)

An advanced soil constitutive model implemented in fully-coupled *u-p* formulation is adopted for soil-fluid interaction and pore water pressure development reasonably. The matrix form of fully-coupled *u-p* formulation for dynamic problem is given by:

$$M\ddot{U} + \int_v B^T \sigma' dV - QP - f^{(s)} = 0 \quad (5.8)$$

$$Q^T \dot{U} + HP + S\dot{P} - f^{(p)} = 0 \quad (5.9)$$

where *M, B, Q, S* and *H* are mass, strain-displacement, coupling, compressibility and permeability matrices respectively. The vectors $f^{(s)}$ and $f^{(p)}$ represent body and surface forces in soil and fluid respectively. The above equations are solved numerically using Newmark's algorithm which is implemented in OpenSees.

Table 5.1 Values of model parameters for NKD soil of Ultadanga site

Depth (m)	P_{ref} (kPa)	*Co-eff*	G_{max} (kPa x10^4)	B_{max} (kPa x10^4)	y_{max} (%)	*NYS*	Φ_{PT} (^{0})	c_1	c_2	c_3	d_1	d_2	d_3
0-3.0	100	0	1.3	6.5	10	20	-	-	-	-	-	-	-
3.0-10.0	100	0	1.3	6.5	10	20	-	-	-	-	-	-	-
10.0-16.0	100	0	6	30	10	20	-	-	-	-	-	-	-
16.0-26.0	100	0	15	75	10	20	-	-	-	-	-	-	-
26.0-31.0	100	0	6	30	10	20	-	-	-	-	-	-	-
31.0-39.0	101	0.5	10	23.3	10	20	25.5	0.045	5	0.15	0.06	3	0.15
39.0-42.5	100	0	15	75	10	20	-	-	-	-	-	-	-
42.5-46.5	101	0.5	13	26	10	20	26.0	0.028	5	0.05	0.1	3	0.05
46.5-50.0	101	0.5	13	26	10	20	26.0	0.013	5	0	0.3	3	0

Table 5.2 Values of model parameters for RCD soil of Tollygunge Metro site

Depth (m)	P_{ref} (kPa)	*Co-eff*	G_{max} (kPa x10^4)	B_{max} (kPa x10^4)	y_{max} (%)	*NYS*	Φ_{PT} (^{0})	c_1	c_2	c_3	d_1	d_2	d_3
0-1.5	100	0	1.3	6.5	10	20	-	-	-	-	-	-	-
1.5-5.0	101	0.5	9	22	10	20	26	0.067	5	0.23	0.06	3	0.27
5.0-11.5	101	0.5	9	22	10	20	26	0.067	5	0.23	0.06	3	0.27
11.5-15.0	101	0.5	11	24	10	20	26	0.028	5	0.05	0.1	3	0.05
15.0-18.0	101	0.5	13	26	10	20	26	0.013	5	0	0.3	3	0
18.0-30.5	101	0.5	13	26	10	20	26	0.013	5	0	0.3	3	0
30.5-32.5	100	0	15	75	10	20	-	-	-	-	-	-	-
32.5-37.0	100	0	15	75	10	20	-	-	-	-	-	-	-
37.0-40.0	100	0	15	75	10	20	-	-	-	-	-	-	-
40.0-46.0	100	0	15	75	10	20	-	-	-	-	-	-	-
46.0-48.5	100	0	15	75	10	20	-	-	-	-	-	-	-
48.5-50.0	101	0.5	13	26	10	20	26	0.013	5	0	0.3	3	0

5.4 Methodology

The effects of axial loading in addition to the input earthquake motion on dynamic response of laterally loaded single piles in liquefiable layered soil of Kolkata city considering nonlinearity of soil is evaluated in the present study using finite-element based program OpenSeesPL. The properties of pile section (Chatterjee and Choudhury 2017; IS 456-2000) considered in this study are presented in Table 5.3. A circular pile of total length 21m with free head length of 1 m and embedded length of 20 m is selected for the study. Pile head is pinned and linear elastic material behaviour is considered. The geometric configuration along with the boundary conditions of the soil-pile system adopted in this study is shown in Fig. 5.5. The modulus of elasticity (E) of the pile is calculated from IS:456 (2000) using following equation:

$$E = 5000\sqrt{f_{ck}} \tag{5.10}$$

where f_{ck} is the characteristic strength of concrete

The value of M_p is calculated using the following expressions based on recommendations of IS 456-2000:

$$M_p = Z_p * \sigma_y \quad (5.11)$$

where, Z_p = Plastic section modulus= $d^3/6$ and σ_y = yield stress= $0.446 f_{ck}$

Table 5.3 Pile properties considered in the present numerical study (Chatterjee and Choudhury 2017; IS 456-2000)

Characteristic compressive strength of concrete (f_{ck}) (MPa)	20	30			40
Diameter of pile (d) (m)	0.5	0.5	0.75	1.0	0.5
Young's Modulus (E) (GPa)	22.36	27.4	27.4	27.4	31.63
Poisson's Ratio (μ_p)	0.2	0.20	0.2	0.2	0.2
Mass Density (ρ) (kN/m3)	25	25	25	25	25
Plastic moment capacity (M_p) (kN.m)	186	279	941	2230	372

The allowable load carrying capacity (P_{all}) of 20 m embedded piles of various diameters in NKD and RCD soil are computed by dividing the ultimate capacity of pile with a factor of safety of 2.5 based on IS 2911 (1984) and shown in Fig. 5.6. The three different masses, describing superstructure, equivalent of 30%, 50% and 100% of P_{all} are connected to the pile head to assess the effects of axial load on flexural response of pile foundation in liquefiable and non-liquefiable condition. The depth of liquefaction and reduction of shear strength are evaluated using finite-element simulation. The detailed depth and time-varying effects of kinematic and inertial forces on pile foundation are also assessed.

During ground shaking, the effective stress of saturated cohesionless soil decreases due to increase of pore water pressure. When the effective stress becomes zero, the soil loses its shear resistance and behaves like liquid. The pile becomes laterally unsupported during liquefaction stage and becomes prone to buckling failure under axial loads. Critical buckling load of concrete piles are computed using Euler's buckling equation:

$$P_{cr} = \frac{\pi^2 EI}{L_e^2} \quad (5.12)$$

where L_e and EI are the effective length and flexural rigidity of the pile respectively. The effective length of pile depends on the end conditions and length of pile.

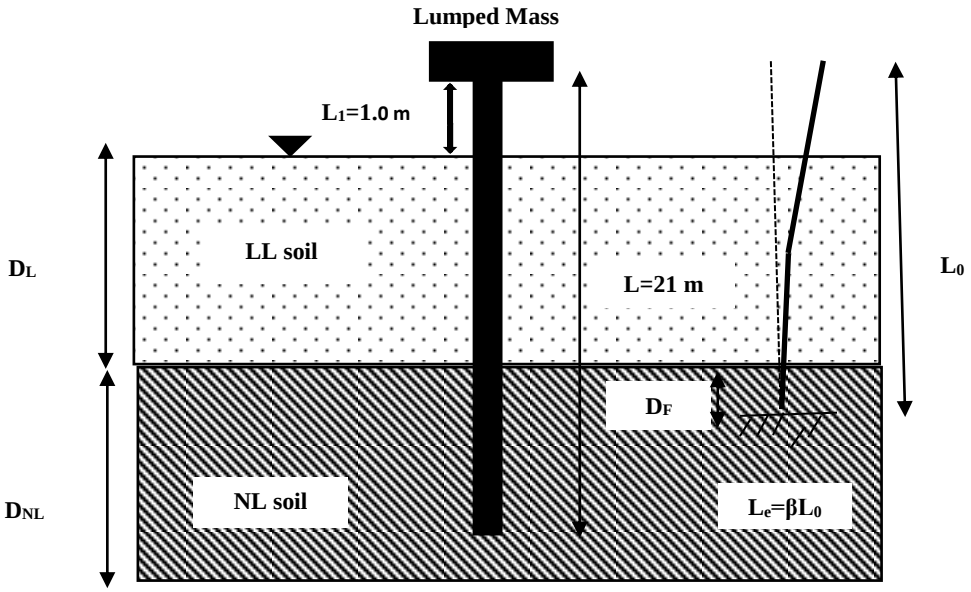

Fig. 5.5 Schematic diagram of soil-pile system considered in the present study

In the present study, the effective length of pile is estimated using the following expression:

$$L_e = \beta L_0 \tag{5.13}$$

where β is the factor which depends on end conditions of pile and L_0 is the length of pile in buckling zone. According to Davisson and Robinson (1965), laterally load pile foundations may be assumed to be fixed at depth of *1.8T* (D_F) below the interface between liquefiable and non-liquefiable layer, where T is the relative stiffness factor may be calculated using the following equation:

$$T = (EI/n_h)\text{^}0.2 \tag{5.14}$$

Where, n_h=coefficient of modulus of subgrade reaction of soil.

The value of n_h considered in this study is 4500 kN/m^3 for non-liquefiable sand (N=32) from IS 2911 (1984).

The value of L_0 is the depth of liquefiable layer (D_L) plus depth of fixity (D_F). Also, the boundary condition of top end of pile is assumed to be restrained against rotation but not held in position. The bottom boundary condition is assumed to be effectively held in position but not restrained against rotation (i.e., pinned type) when depth of embedment of pile in bottom non-liquefiable layer is less than five times pile diameter and effectively held in position and restrained against rotation (i.e., fixed type) when depth of embedment of pile in bottom non-liquefiable layer is more than five times pile diameter (Bhattacharya 2006). The values of β considered from Table 28 of IS 456 (2000) depending on the boundary conditions of top and bottom ends of pile foundation.

The effects of axial load on seismic response of pile foundations in liquefiable soils are next evaluated. Bhattacharya (2003) suggested the following effects of axial load:

(i) Increasing the possibility of buckling instability

Bhattacharya et al. (2005) proposed buckling failure mechanism based on Euler's and Rankine's buckling criteria by investigating the seismic performance of pile foundations in liquefiable soil using dynamic centrifuge tests. They proposed slenderness ratio (λ) of pile is expressed by the following expression:

$$\lambda = L_e/r_{min} \tag{5.15}$$

where L_e is the effective length of the pile in liquefiable zone and r_{min} is the minimum radius of gyration which is the ratio between moment of inertia about weakest section (I_{min}) and cross-sectional area of pile (A_{cs}).

The Euler's buckling criteria which is applicable for long column is given by the following equation:

$$P_{cb} = \frac{\pi^2 E I_{min}}{L_{eff}^2} \tag{5.16}$$

$$\sigma_{cb} = \frac{P_{cb}}{A} = \frac{\pi^2 E}{\lambda^2} \tag{5.17}$$

where P_{cb} is the critical buckling load and σ_{cb} is the elastic critical buckling stress.

Rankine's buckling criteria which is applicable for both short and long column is expressed by the following equation:

$$\frac{1}{\sigma_f} = \frac{1}{\sigma_y} + \frac{1}{\sigma_{cb}} \tag{5.18}$$

where σ_f is the Rankine's failure stress considering both crushing and buckling criteria, σ_y is the yield stress of material.

Bhattacharya (2003) and Bhattacharya et al. (2005) reported that the possibility of buckling instability of pile in liquefiable layer is dependent on slenderness ratio of pile. Liquefaction-induced lateral spreading is not necessary for buckling instability.

(ii) Reduction of plastic moment capacity of piles

A hinge may be formed within a pile section under the coupled action of axial load (*P*) and moment (*M)*. The combined action of axial load and moment in plastic moment capacity of pile is governed by the following equation (Sinha et al. 2020):

$$(\frac{P}{P_y})^n + \left(\frac{M}{M_p}\right) = 1 \quad (5.19)$$

where P_y is the squash load without bending; M_p is the plastic moment capacity without axial load and n=1.5 for circular section.

The value of P_y is calculated using the following expressions based on recommendations of IS 456-2000:

$$P_y = \sigma_c * A \quad (5.20)$$

where σ_c= Compressive strength= $0.67f_{ck}$

P-M interaction curve can be plotted for any pile section having particular diameter and grade of concrete. The plastic moment capacity of any pile section decreases in presence of axial load in liquefiable soil layer.

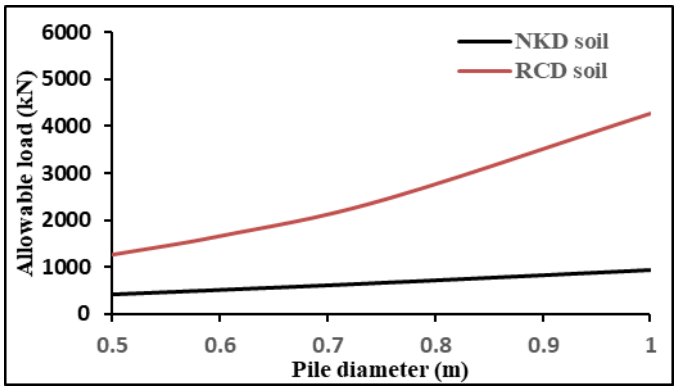

Fig. 5.6 Allowable load carrying capacity (P_{all}) of piles with various diameters in NKD and RCD soil

5.5 Validation of the Present Numerical Model

The suitability of the present FE model is carried out by comparing the results with the dynamic centrifuge tests conducted by Wilson (1998) prior to conducting parametric study to evaluate the effects of various parameters on dynamic response of pile foundations. The model was consisted with two horizontal layers of saturated, fine and uniformly graded Nevada sand having 9.1 m thick upper medium dense sand (*Dr*=55%) and 11.4 m thick lower dense sand (*Dr*=80%) at the prototype scale. A single steel pile having diameter of 0.67 m and wall thickness of 19 mm was used to model the pile. The pile head was extended 3.8 m from the ground level and a superstructure load of 480 kN was applied on pile head. The embedded depth of pile was about 16.8 m. This model was excited to the Kobe (1995) earthquake motion (Wilson 1998) with peak acceleration value scaled to 0.22g as shown in Fig. 5.7. The

measured and calculated excess pore pressure (EPP) ratio and bending moment time history at 2.3 m depth are presented in Fig. 5.8 (a) and (b) respectively. Also, Fig. 5.8(c) displays the measured and calculated acceleration time history of the superstructure. The pile displacement profile at 11.2 sec after earthquake loading is shown in Fig. 5.9.

It is observed that the excess pore pressure ratio and bending moment time-history at 2.3 m depth obtained from the present numerical model are fairly matching with the results of centrifuge test. The difference of results may be attributed to the use of constant value of permeability in the present study, but in real case, it increases several times during liquefaction. The dilative response of soil is noticed in the present study for the first few cycles (prior to complete liquefaction) due to sharp reduction of *EPP*. The reduction of *EPP* due to soil dilation increases soil shear modulus and corresponding stiffness. As a result, big acceleration spikes are transmitted to the superstructure through the field during earthquake and higher acceleration response is observed. On the other hand, the maximum bending moment is generated in the pile with the softening of soil due to rise of *EPP*. Hence, the maximum bending moment is noticed at 6.1 sec after applying of earthquake motion due to abrupt change of *EPP*. Also, Fig. 5.9 shows the comparison of the lateral displacement profile of pile at 11.2 sec after applying of earthquake motion. The results are matching well. The slight deviation in results for the first few cycles may be reasonable due to the distinction between frequency content of the Kobe earthquake record originated for the centrifuge test and considered for the present study. Hence, the present model can be efficiently used to predict soil and pile response under seismic loading condition.

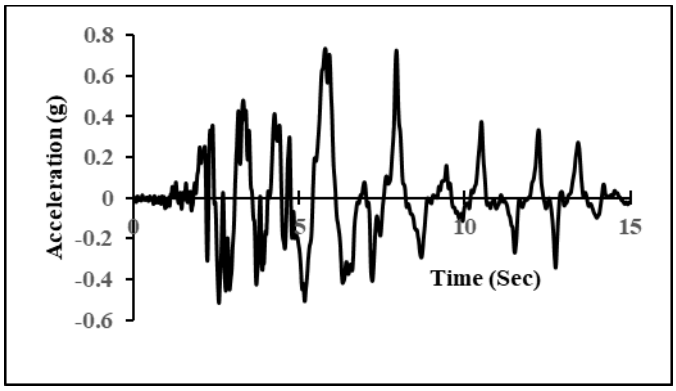

Fig. 5.7 Acceleration time-history of 1995 Kobe earthquake motion (Wilson 1998)

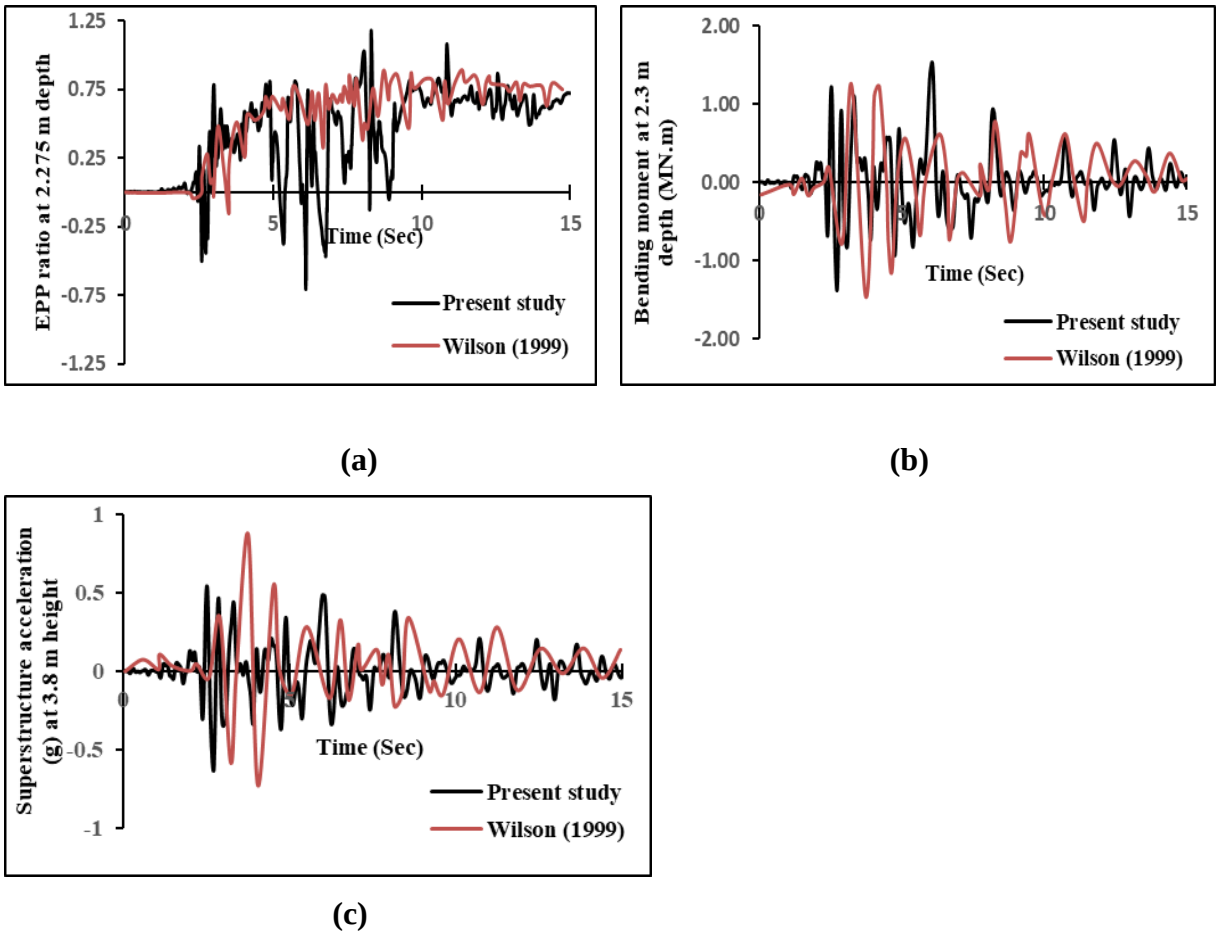

Fig. 5.8 Comparison of present study with dynamic centrifuge tests conducted by Wilson (1998) **a** *EPP* time-history **b** bending moment time-history and **c** superstructure acceleration time-history

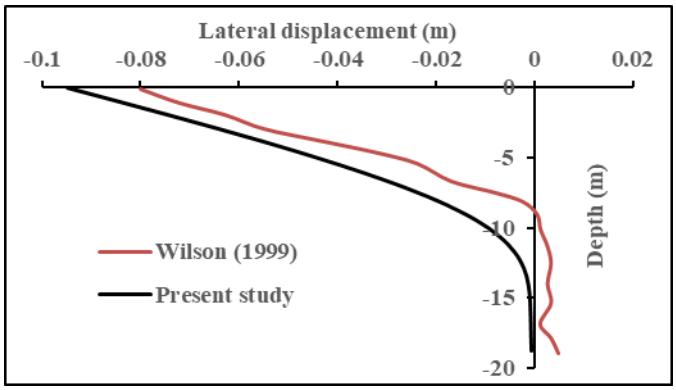

Fig. 5.9 Comparison of lateral displacement profile obtained from present study with dynamic centrifuge tests (Wilson 1998)

5.6 Results and Discussions

A parametric study has been conducted using the present numerical model for evaluating the effects of axial load on flexural response of pile foundation in liquefiable and non-liquefiable soil of Kolkata city considering nonlinearity of soil using finite-element based computer program OpenSeesPL and the results are presented and discussed graphically.

5.6.1 Assessment of Liquefaction Potential and Response of Soil

Flexural response of pile foundation is greatly dependent on adjacent soil conditions. The axially-loaded pile becomes unsupported during soil liquefaction due to significant reduction of shear strength of soil. The determination of unsupported length of pile is needed to calculate critical buckling load (P_{cr}). So, the assessment of liquefaction potential for the considered site is essential. The depth of liquefaction may alter depending upon the type of soil and input motion characteristics. In the present study, liquefaction assessment is conducted using a practical parameter excess pore pressure (*EPP*) ratio (R_u). R_u is defined as the ratio of *EPP* to the initial effective vertical stress. The soil is termed as liquefiable when R_u becomes unity. To evaluate the influence of various parameters on the generation and distribution of time and depth varying *EPP* ratio (R_u), different figures are plotted and discussed. The near-field and far-field soil response are also compared graphically.

The variation of R_u with depth for NKD and RCD soil at 0.25 m and 13.2 m horizontal distance from centre of pile representing near and far-field soil response for various input motions are shown in Fig. 5.10 and 5.11 respectively. It is seen that depths of liquefaction (D_L) are 10 m, 16 m and 16 m for NKD soil and 8.25 m, 11.5 m and 11.5 m for RCD soil under BHJ, scaled IMV and IMV motion respectively in case of near-field response. The same is observed as 1 m, 10 m and 13 m for NKD soil and 8.25 m, 9.87 m and 13.25 m for RCD soil in case of free-field response. The depth of liquefaction is dependent on both soil types and characteristics of input motions. From the Fig. 5.10 and 5.11, it is clear that R_u value decreases with increasing depth due to increasing soil stiffness. The relative density of soil for top portion of the model is relatively low which causes more vibrations of soil grains during seismic event. Accordingly, pore water pressure increases due to densification of soil's structure. The rapid increase of R_u is observed near ground for all the cases because of presence of low permeability clay layer at the top of granular layer. During seismic excitation, top clay layer prevents to drain out the pore water from deeper layer.

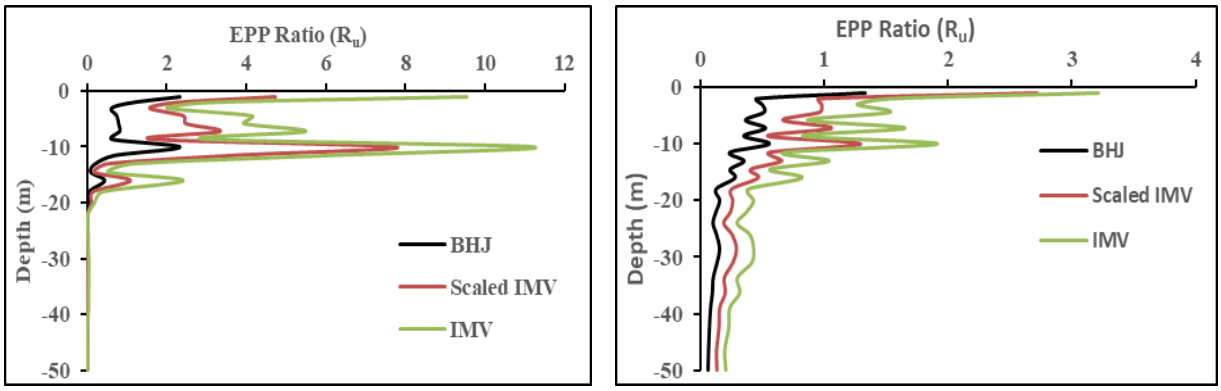

(a) **(b)**

Fig. 5.10 Profile of R_u in NKD soil **a** near field and **b** far field for various input motions

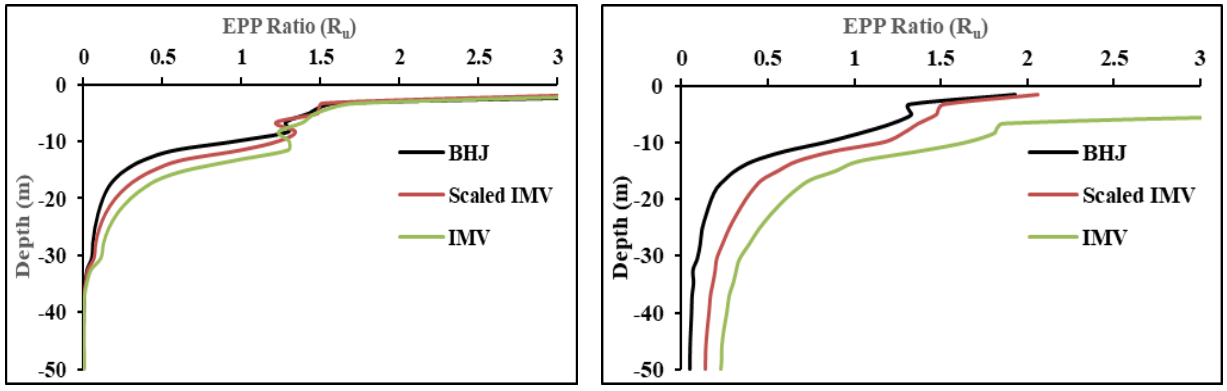

(a) **(b)**

Fig. 5.11 Profile of R_u in RCD soil **a** near field and **b** far field for various input motions

The weight of the super structure on pile foundation has profound influence on depth of liquefaction. The near-field variation of R_u with depth for different pile head mass under scaled IMV input motion is presented in Fig. 5.12. It is noteworthy that the depth of liquefaction decreases significantly adjacent to the pile with an increase of superstructure weight except top of the soil profile because of sudden increase of EPWP due to existence of clay layer. The clay layer obstructs to drain out the pore water during seismic shaking due to low permeability and EPWP ratio becomes more for higher superstructure weight. The depth of liquefaction (D_L) decreases from 11.5 m to 1.5 m adjacent to the pile when the superstructure weight increases from 0 kN to 1327 kN. This is due to densification of soil adjacent to pile during earthquake with an increase of pile head mass or superstructure weight. Fig. 5.13 shows the time-dependent near-field variation of R_u at 5 m, 9.87 m, 11.5 m and 20 m depth of RCD soil for the scaled IMV input motion. It is noteworthy that liquefaction begins at distinct times over depth, usually, from top to bottom layers.

Liquefaction starts after 2.66 sec, 5.05 sec, 26.36 sec of application of input motion for depth of 4.63 m, 9.53 m, 11.16 m respectively.

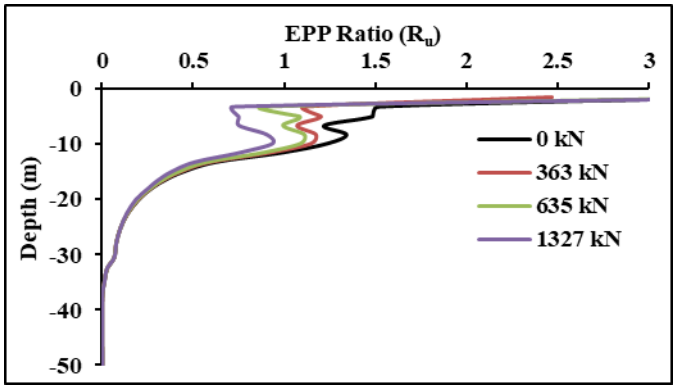

Fig. 5.12 Profile of R_u of RCD soil under scaled IMV motion for various superstructure weight

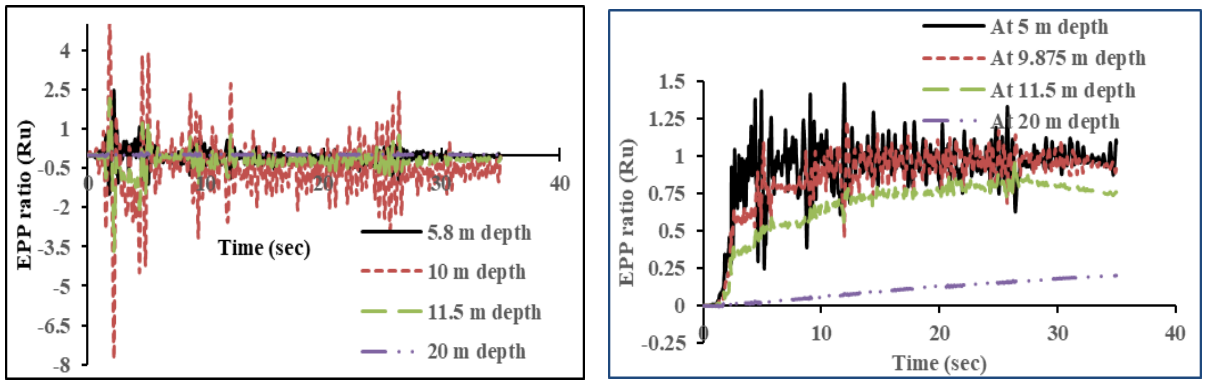

(a) **(b)**

Fig. 5.13 Comparison of time history of R_u at various depths **a** NKD soil and **b** RCD soil using scaled IMV motion

Assessment of undrained residual strength (S_r) of liquefiable soil is a vital issue in earthquake geotechnical engineering. It involves the complicated nonlinear soil response during earthquake loading. Several empirical correlations are available in the literature based on SPT-N value for estimating S_r [80]. Cyclic shear stress vs shear strain plot of RCD soil under scaled IMV motion at various depths obtained from present finite element analysis are shown in Fig. 5.14. It is noteworthy that the S_r value at various depths tends to zero at liquefaction phase. Hence, it can be concluded that liquefiable soil loses its strength and consequently pile becomes laterally unsupported susceptible to buckling failure under axial load.

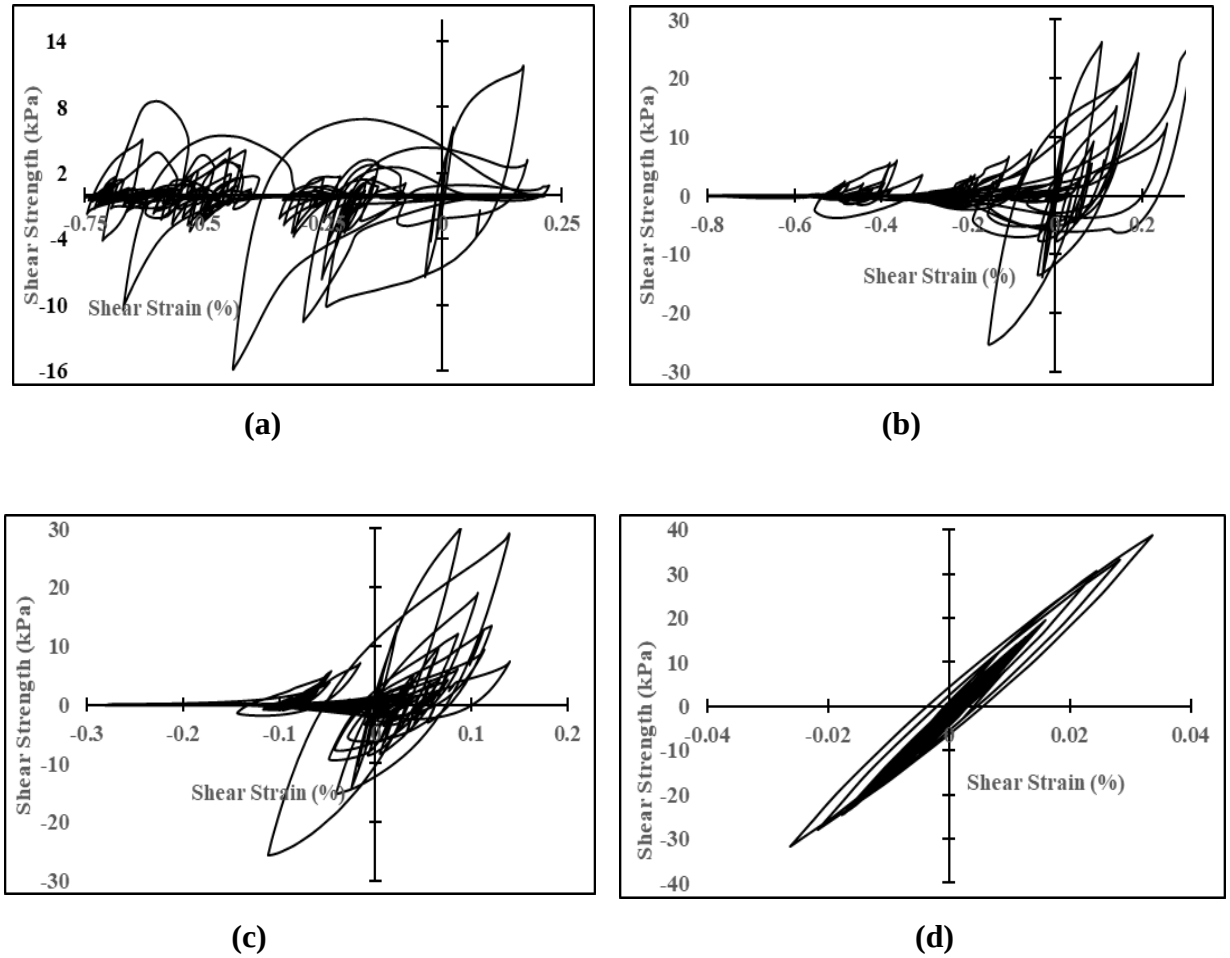

Fig. 5.14 Shear stress vs shear strain relationship for RCD soil under scaled IMV motion **a** 4.63 m **b** 9.53 m **c** 11.16 m and **d** 19.58 m depths

5.6.2 Response of Pile

The lateral displacement (y) and bending moment (M) of pile obtained in the present dynamic analysis are normalized with pile diameter (d) and available plastic moment capacity (M_p') and plotted in the form of dimensionless lateral pile displacement coefficient (y/d) and bending moment coefficient (M/M_p') against depth.

5.6.2.1 Response of Pile Displacement

Fig.5.15(a) and 5.16(a) presents the variation of kinematic peak lateral displacement coefficient (y/d) of pile with depth in NKD and RCD soil respectively for 0.5 m diameter M-30 grade concrete pile when subjected to the BHJ, Scaled IMV and IMV earthquake motions. It

is observed that kinematic peak lateral displacement co-efficient increases dramatically with an increase of PGA.

5.6.2.2 Response of Pile Bending Moment

The variation of peak bending moment co-efficient (M_{max}/M_p') of pile with depth in NKD and RCD soil are represented by the Fig.5.15(b) and 5.16(b) respectively. The kinematic peak bending moment co-efficient is maximum at 10 m depth of NKD soil which is near the boundary between liquefiable and non-liquefiable layer and its maximum values are 1.53, 1.06 and 0.32 for IMV, scaled IMV and BHJ earthquake motion respectively. However, for RCD soil the maximum kinematic bending moment co-efficient are 0.68 at 11.5 m depth, 0.41 at 9.87 m depth and 0.28 at 9.87 m depth under IMV, scaled IMV and BHJ earthquake motion respectively. The maximum kinematic bending moment developed in the pile exceeds the plastic moment capacity in NKD soil for IMV, scaled IMV earthquake motions. So, formation of plastic hinge is expected for 0.5 m diameter M-30 grade concrete piles in NKD soil under IMV, scaled IMV earthquake motion. However, the same pile when embedded in RCD soil is safe against kinematic bending failure under same earthquake motions. So, kinematic bending failure is dependent on both soil type and input motion characteristics. Also, due to increase of free length, large bending moment is developed for pile embedded in RCD soil when subjected to IMV and scaled IMV motion in comparison with the BHJ motion.

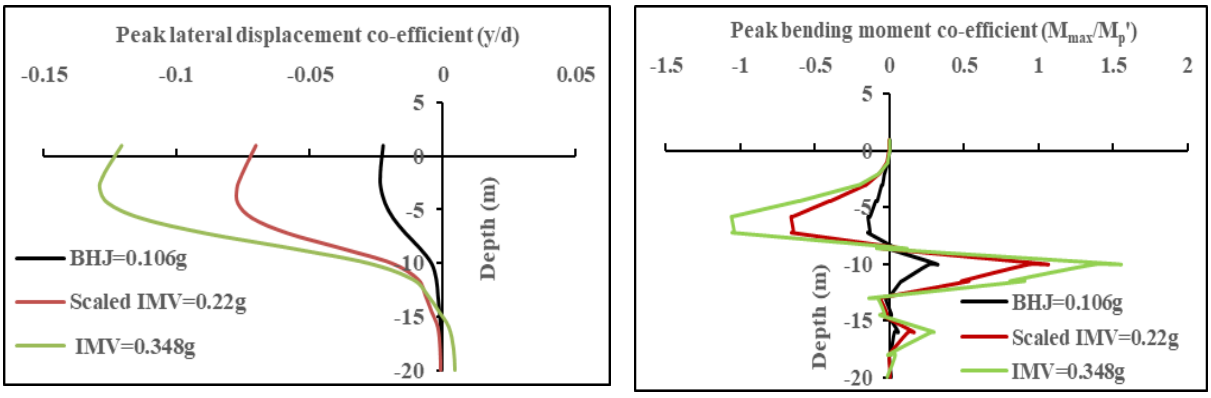

(a) **(b)**

Fig. 5.15 Kinematic **a** peak lateral displacement and **b** peak bending moment of pile in NKD soil under various input motions

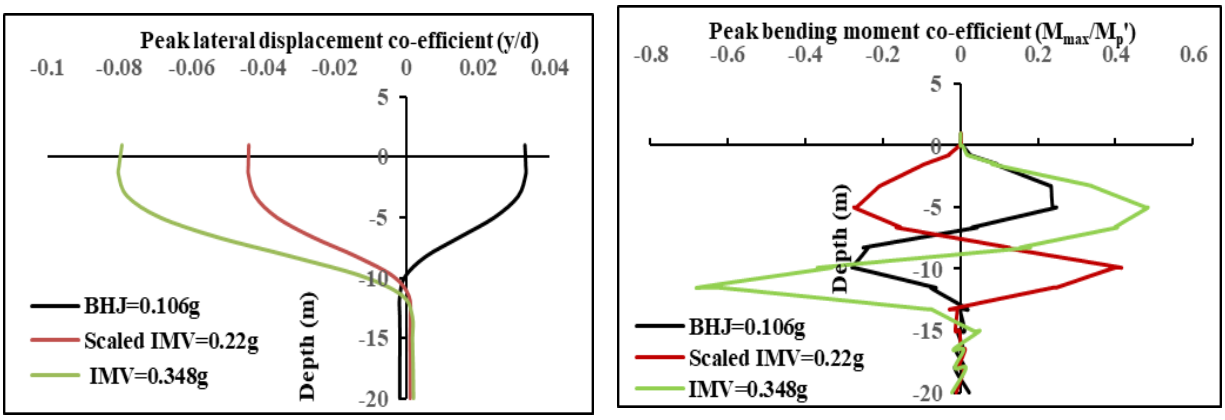

(a) **(b)**

Fig. 5.16 Kinematic **a** peak lateral displacement and **b** peak bending moment of pile in RCD soil under various input motions

5.6.3 Effect of Axial Load on Pile Response

Pile supports superstructure which are generally multi-degree of freedom (MDOF) systems. These MDOF systems are assumed as lumped mass at the pile head for simplification of analysis during design of pile foundations. During travelling of seismic waves from bedrock level to the ground, the inability of the embedded pile to follow the free field motion develops bending moment in the pile foundation even in absence of lumped mass and is termed as kinematic interaction. On the other hand, inertial force is generated due to the vibration of the lumped mass i.e., super-structure during seismic shaking. So, for accurate estimation of the maximum bending moment developed in the pile foundation for soil-pile system with lumped mass during earthquake event, the combined effect of kinematic and inertial interaction should be considered. Fig.5.17 shows the effect of axial load on dynamic response of pile foundation. The four different masses, describing superstructure, equivalent of 0%, 30%, 50% and 100% of P_{all} (0, 363, 635 and 1327 kN) are connected to the head of 0.5 m diameter M-30 grade concrete pile to assess the effects of axial load on flexural response of pile foundation in RCD soil using scaled IMV earthquake motion. The comparative lateral pile displacement and bending moment response along pile between kinematic and combined kinematic and inertial soil-pile interaction are provide in Fig. 5.17(a) and (b) respectively. It is observed that the maximum lateral displacement co-efficient under kinematic loading is significantly less than the combined kinematic and inertial loading. The lateral displacement co-efficient under combined loading increases by 29.5%, 102.3% and 154.5% with respect to kinematic lateral displacement co-efficient when the axial load increases from 0 to 363 kN, 635 kN and 1327

kN respectively. Also, the peak value, position and incidence time of kinematic pile bending response in liquefiable soil is markedly dissimilar from combined response. In case of kinematic interaction, pile follows the imputed motion of liquefiable soil. Hence, the peak bending moment occurs at deeper depth during post-liquefaction stage. The maximum kinematic bending moment obtained is 115.4 kN-m (M/M_p=0.41) at 9.87 m depth. The maximum bending moments due to combined loading obtained are 218.62 kN-m (M/M_p=0.81) at 0.75 m depth, 326.81 kN-m (M/M_p=1.25) at 0.75 m depth and 667.45 kN-m (M/M_p=2.97) at 1.5 m depth when the axial loads are 363, 635 and 1327 kN respectively. The maximum pile bending moment increases by 89.4%, 184.2% and 478.4% with respect to kinematic bending moment when the axial load increases from 0 kN to 363, 635 and 1327 kN respectively. The increase of maximum bending moment in the pile due to inertial loading before liquefaction is dependent on the mass of the superstructure. The maximum bending moment at ground level increases significantly with the presence of superstructure as shown in Fig. 5.18 (a) and (b) for NKD and RCD soil respectively. The significant increase of maximum bending moment in presence of superstructure mass for both the soil profile is due to the inertial loading.

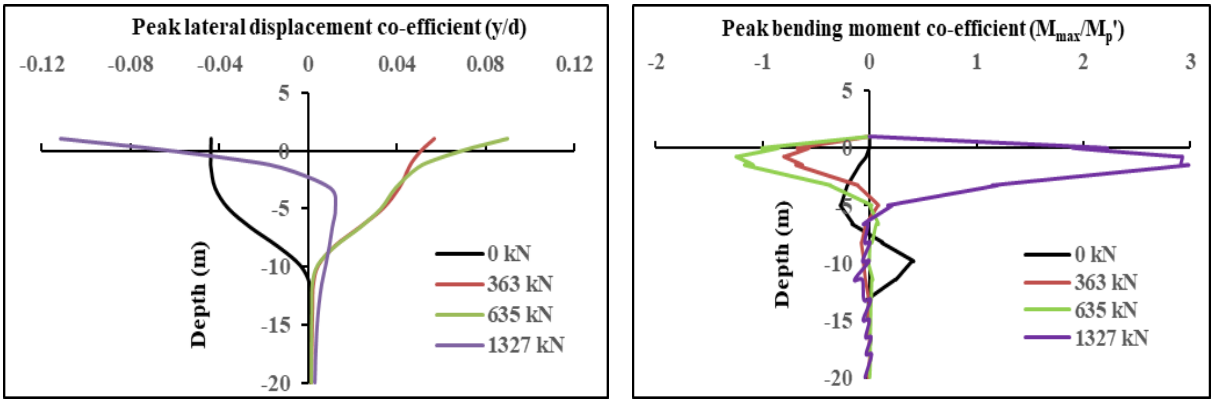

(a) **(b)**

Fig. 5.17 Variation of **a** peak lateral displacement and **b** peak bending moment of pile for different combinations of vertical loading in RCD soil when subjected to scaled IMV motion

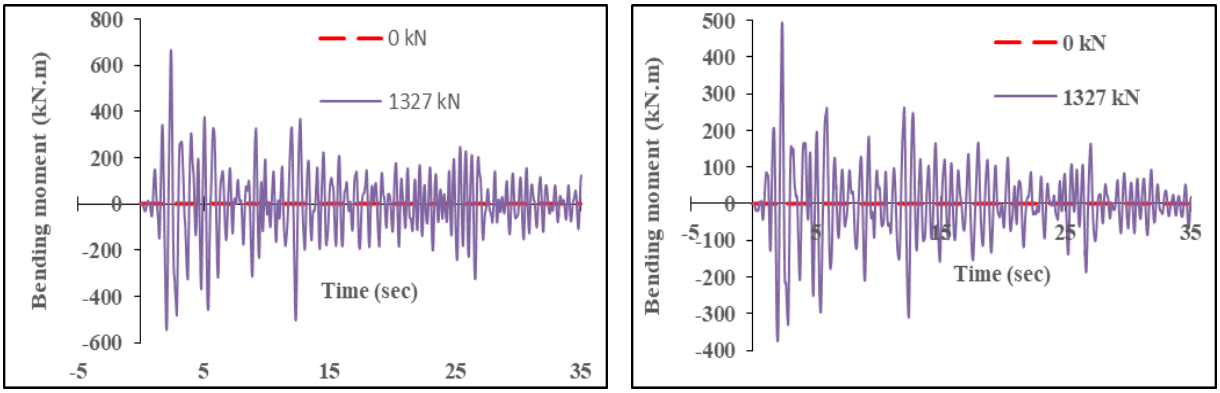

Fig. 5.18 Comparison of peak bending moment time-history of pile at ground level with and without vertical loading in **a** NKD soil and **b** RCD soil when subjected to scaled IMV motion

5.6.4 Seismic Design of Pile Foundation as per IS 1893:2016

As per Indian seismic design code IS 1893 (2016), piles should be designed for lateral loads neglecting the lateral resistance of liquefiable soil. Hence, a comparative study has been conducted for RCD soil with and without considering the shaft resistance of the liquefiable layer in the present study for calculation of pile capacity. The allowable load carrying capacity (P_{all}) of of 0.5 m diameter and 21 m length (1.0 m free head length) in RCD soil is obtained as 991 kN based on IS 2911 Part 1: Section 4 (1984) neglecting the shaft resistance of liquefiable layer. Fig. 5.19 (a) and (b) shows the profile of peak lateral displacement and bending moment co-efficient when subjected to scaled IMV earthquake motion with full superstructure weight of 1327 kN and 991 kN which represents with and without consideration of skin friction of liquefiable layer respectively for calculating P_{all}. The peak lateral displacement co-efficient does not change and peak bending moment decreases by 19.4% (M/M_p decreases 44.1%) without considering the skin resistance of liquefiable layer. However, M/M_p value for both the cases is more than 1, hence pile is not safe against kinematic bending even without consideration of skin friction of liquefiable layer as per provision of IS 1893-2016.

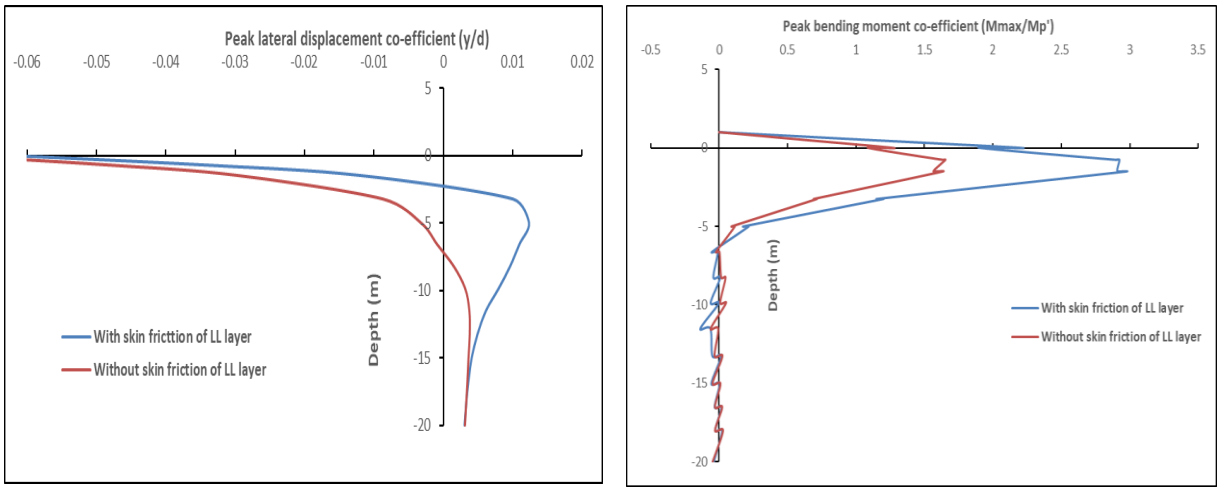

(a) **(b)**

Fig. 5.19 Variation of **a** peak lateral displacement **b** peak bending moment of pile with and without considering skin friction of liquefiable layer (LL) in RCD soil when subjected to scaled IMV motion

5.6.5 Comparison of Pile Response in Liquefiable and Non-Liquefiable Conditions

The effect of the axial load on dynamic response of pile foundation for different soil condition is evaluated in this study by comparing the peak lateral displacement and bending moment co-efficient profile in liquefiable and non-liquefiable condition of RCD soil. Fig. 5.20(a) and (b) shows the profile of peak lateral displacement and bending moment co-efficient of pile founded in non-liquefiable condition of RCD soil for four distinct axial loads. It is seen that pattern of peak lateral displacement and bending moment co-efficient profile for kinematic loading is remarkably different from others. Kinematic force is induced due to deformation of ground, on the other hand, inertial force is developed by the vibration of superstructure. The peak lateral displacement co-efficient under various axial loads are shown in Fig. 5.21 (a) and (b) in non-liquefiable and liquefiable condition respectively. Similarly, Fig. 5.22(a) and (b) shows the peak bending moment co-efficient of pile under various axial loads in non-liquefiable and liquefiable condition respectively. The peak lateral displacement decreases by 83.2% in non-liquefiable condition and 60.71% in liquefiable condition due to decrease of axial load from 1327 kN to 0 kN. Also, peak bending moment developed in the pile decreases by 97.2% in non-liquefiable condition and 82.7% in liquefiable condition when axial load reduces from 1327 kN to 0 kN. So, kinematic force is predominant in liquefiable soil condition and inertial force is prevalent in non-liquefiable condition and mainly accountable for peak bending moment in the vicinity of pile head.

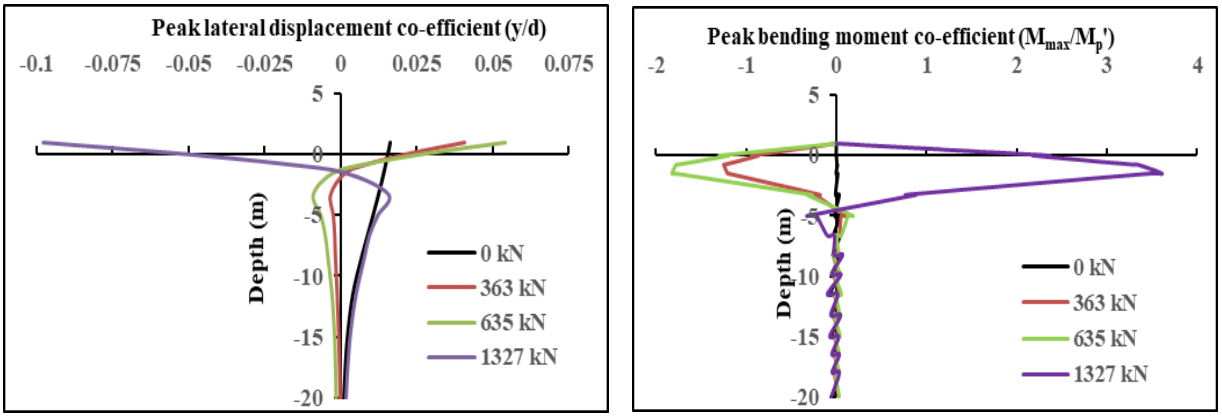

(a) **(b)**

Fig. 5.20 Variation of **a** peak lateral displacement and **b** peak bending moment co-efficient of pile for different combinations of vertical loading in non-liquefiable condition of RCD soil when subjected to scaled IMV motion

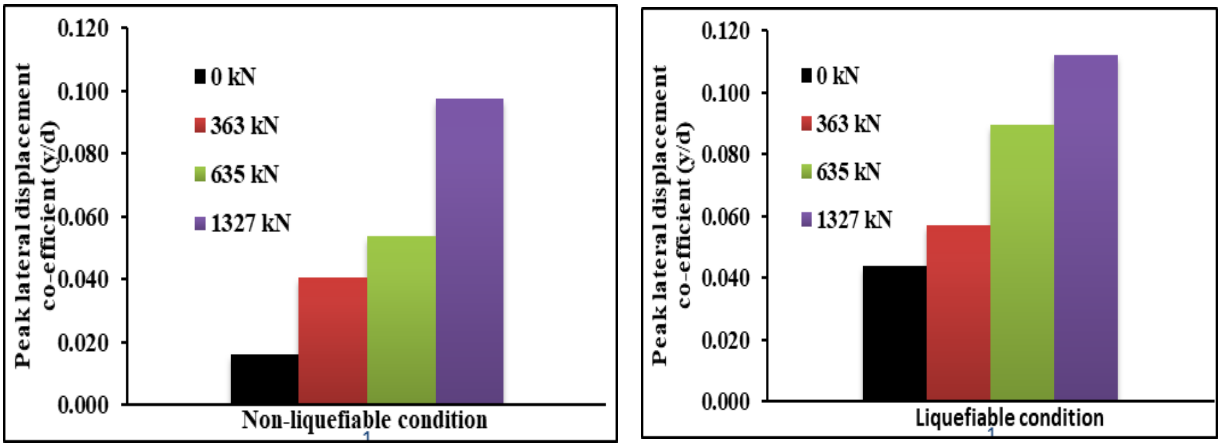

(a) **(b)**

Fig. 5.21 Comparison of peak lateral displacement co-efficient of pile for **a** non-liquefiable and **b** liquefiable soil condition of RCD soil when subjected to scaled IMV motion

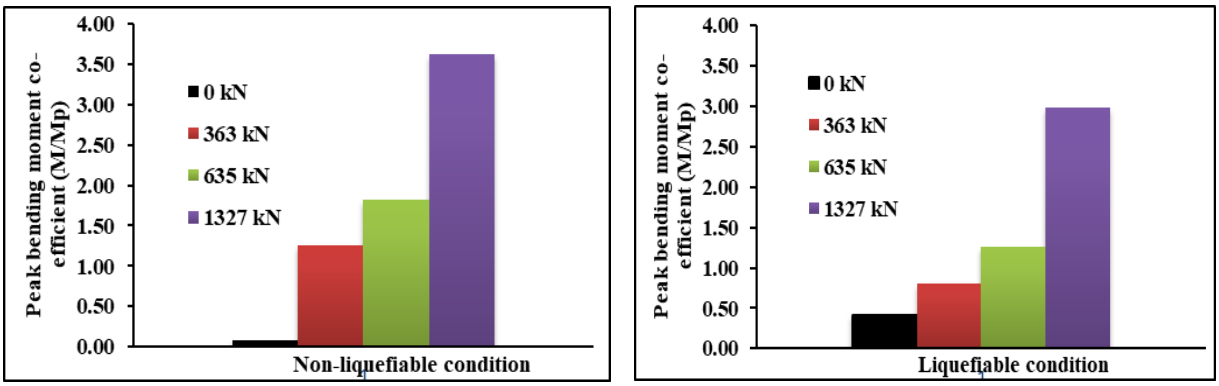

(a) **(b)**

Fig. 5.22 Comparison of peak bending moment co-efficient of pile for **a** non-liquefiable and **b** liquefiable soil condition of RCD soil when subjected to scaled IMV motion

5.6.6 Bending and Buckling Interaction Analysis

After reliable estimation of unsupported length of the pile, bending and buckling failure criteria can be checked using procedure discussed before. When the stress on pile due to axial load (σ) exceeds the Rankine's failure stress (σ_f), buckling failure may be occurred and when the maximum bending moment (M) developed in the pile section exceeds the available plastic moment capacity (M_p), bending failure may be occurred. So, failure due to bending-buckling interaction may be occurred when both criteria exceeded. Pile may be considered as safe when both bending moment co-efficient (M/M_p') and buckling co-efficient (σ/σ_f) are less than 1. Table 5.4 and 5.5 shows the results obtained for analysis of bending and buckling failure criteria of 21 m long (free head length=1 m) M-30 grade concrete pile with various diameters embedded in RCD soil of Kolkata city under scaled IMV earthquake motion and Fig. 5.23 presents bending-buckling interaction graph for the same. The bending-buckling interaction graph is the plot of σ/σ_f and M/M_p' for a particular analysis case. This graph is necessary for identifying a probable failure mode of pile foundation under combined vertical and lateral loads. It is noticed from Fig.5.23 that the maximum bending moment of pile increases with an increase of axial load on pile for a particular diameter of pile because of buckling and P-delta effects. With an increase of pile diameter buckling co-efficient of pile reduces significantly and bending moment co-efficient changes slightly. Hence, it may be interpreted that larger diameter pile can be used in liquefiable soil to avoid buckling failure mode. The capacity against bending of a pile can be greatly improved by using high grade of concrete or steel having high flexural strength. However, buckling capacity of pile does not change significantly with the grade of concrete. Significant improvement of buckling capacity can be

achieved by increasing the diameter as it is connected with the geometrical properties of pile section.

Table 5.4 Checking against bending failure mechanism of various diameter pile of M-30 grade in RCD soil under scaled IMV motion

d (m)	P (kN)	f_{ck} (MPa)	P_y (kN)	M_p (kN-m)	Mp' (kN-m)	M_{max} (kN-m)	M_{max}/Mp'
0.5	0	30	3944.6	279	279.00	115.40	0.41
	363				271.21	218.62	0.81
	635				260.98	326.81	1.25
	1330				224.38	667.45	2.97
0.75	0	30	8875.40	941	941.00	363.53	0.39
	730				918.80	550.45	0.60
	1210				893.63	848.82	0.95
	2430				806.19	1668.76	2.07
	0	30	15778.5	2230	2230.00	825.10	0.37
1.0	1284				2178.23	1196.52	0.55
	2140				2118.61	1636.91	0.77
	4280				1914.95	3116.88	1.63

Table 5.5 Checking against buckling failure mechanism of various diameter pile of M-30 grade in RCD soil under scaled IMV motion

d (m)	P (kN)	E (GPa)	D_L (m)	D_F (m)	L_0 (m)	β	L_e (m)	r_{min} (m)	λ	σ_y (Mpa)	σ_{cb} (Mpa)	σ_f (Mpa)	σ (Mpa)	σ/σ_f
0.50	0	27.4	11.5	3.2	15.7	2	31.4	0.125	251.2	13.38	4.28	3.24	0	0
	363					2							1.85	0.57
	635					2							3.24	1.0
	1330					2							6.78	2.09
0.75	0	27.4	11.5	4.5	17.0	2	34.0	0.187	181.3	13.38	8.22	5.09	0	0
	730					2							1.65	0.32
	1210					2							2.74	0.54
	2430					2							5.50	1.08
1.0	0	27.4	11.5	5.6	18.1	2	36.2	0.25	144.8	13.38	12.88	6.56	0	0
	1284					2							1.64	0.25
	2140					2							2.73	0.42
	4280					2							5.45	0.83

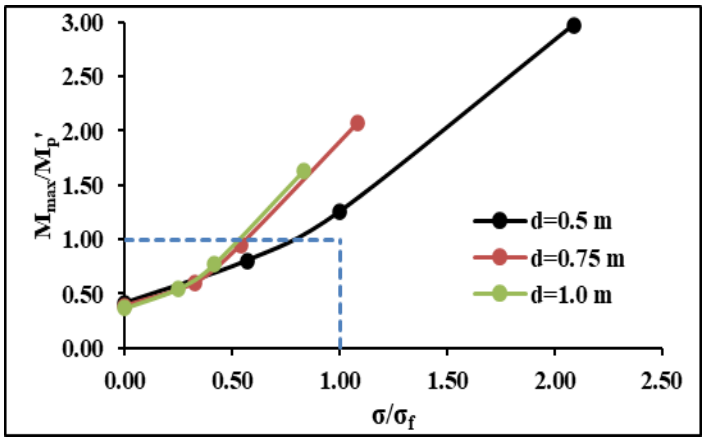

Fig. 5.23 Bending-buckling interaction graph of various diameter piles in RCD soil due to the scaled IMV motion

Similarly, Table 5.6 and 5.7 presents result of bending-buckling interaction and Fig. 5.24 shows the corresponding graph for the 0.5 m diameter concrete pile under BHJ, scaled IMV and IMV earthquake motions having different PGA. It is observed that amplitude of the input

motions has profound influence on seismic response of pile foundations. Higher amplitude of input motions enhances the inertial forces working on pile and develops higher bending moment in the pile. As the soil properties changes dramatically during liquefaction, the input motion characteristics have profound influence on bending and buckling failure criteria. Several dynamic forces may be developed within pile section based on the time period of pile-supported structures and the characteristics of liquefiable soil. Here, the 0.5 m diameter M-30 grade pile is safe against both bending and buckling for axial load equal to 50% of P_{all} under BHJ earthquake motion but the same pile is unsafe at same axial load when subjected to scaled IMV and IMV input motions having higher PGA.

Table 5.6 Checking against bending failure mechanism of 0.5 m diameter pile of M-30 grade in RCD soil under various input motions

Input Motions	P (kN)	f_{ck} (MPa)	P_y (kN)	M_p (kN-m)	Mp' (kN-m)	M_{max} (kN-m)	M_{max}/Mp'
BHJ	0	30	3944.6	279	279.00	78.29	0.28
	363				271.21	184.67	0.68
	635				260.98	168.86	0.65
	1330				224.38	307.24	1.37
Scaled IMV	0	30	3944.6	279	279.00	115.40	0.41
	363				272.21	218.62	0.81
	635				260.98	326.81	1.25
	1330				224.38	667.45	2.97
IMV	0	30	3944.6	279	279.00	189.85	0.68
	363				272.21	236.63	0.87
	635				260.98	434.06	1.66
	1330				224.38	953.32	4.25

Table 5.7 Checking against buckling failure mechanism of 0.5 m diameter pile of M-30 grade in RCD soil under various input motions

Input Motions	P (kN)	E (GPa)	D_L (m)	D_F (m)	L_0 (m)	β	L_e (m)	r_{min} (m)	λ	σ_y (Mpa)	σ_{cb} Mpa)	(σ_f (Mpa)	σ (Mpa)	σ/σ_f
BHJ	0	27.4	8.25	3.2	12.45	2	24.9	0.125	199.2	13.38	6.81	4.51	0	0
	363					2							1.85	0.41
	635					2							3.24	0.72
	1330					2							6.78	1.50
Scaled IMV	0	27.4	11.5	3.2	15.7	2	31.4	0.125	251.2	13.38	4.28	3.24	0	0
	363					2							1.85	0.57
	635					2							3.24	1.0
	1330					2							6.78	2.09
IMV	0	27.4	11.5	3.2	15.7	2	31.4	0.125	251.2	13.38	4.28	3.24	0	0
	363					2							1.85	0.57
	635					2							3.24	1.0
	1330					2							6.78	2.09

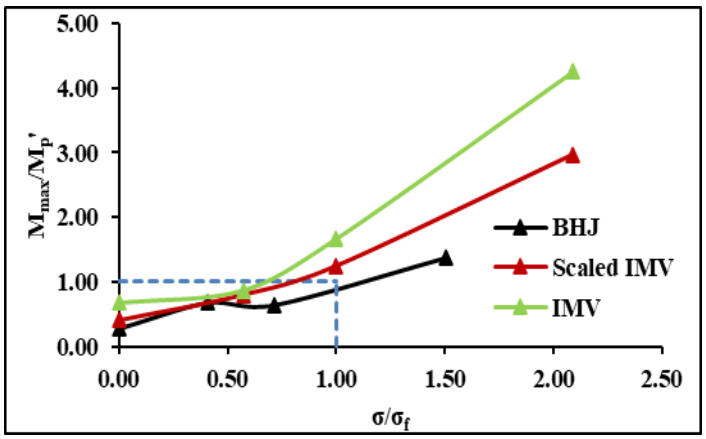

Fig. 5.24 Bending-buckling interaction graph of 0.5 m diameter pile in RCD soil due to the BHJ, scaled IMV and IMV motions

Finally, bending-buckling interaction results for the 0.5 m diameter concrete piles of various grade under scaled IMV earthquake motion are given in Table 5.8 and 5.9. Fig.5.25 shows the interaction graph for the same. It is noticed that the buckling capacity is slightly improved by using higher grade of concrete but the bending capacity is increased significantly by selecting

higher grade of concrete pile. Here, the 0.5 m diameter M-20 grade pile is unsafe against bending for axial load equal to 30% of P_{all} under scaled IMV earthquake motion but the same pile is safe against bending and buckling at 30% of P_{all} and 50% of P_{all} for M-30 grade and M-40 grade concrete pile respectively. So, bending and buckling failure mode can be avoided by selecting a suitable combination of material strength and pile geometry.

Table 5.8 Checking against bending failure mechanism of 0.5 m diameter pile of various grades under scaled IMV earthquake motion in RCD soil

Grade	P (kN)	f_{ck} (MPa)	P_y (kN)	M_p (kN-m)	Mp' (kN-m)	M_{max} (kN-m)	M_{max}/Mp'
M-20	0	20	2631.0	186	186.00	99.63	0.54
	363				176.47	205.25	1.10
	635				163.95	340.99	1.83
	1330				119.15	599.08	3.22
M-30	0	30	3944.6	279	279.00	115.40	0.41
	363				271.21	218.62	0.81
	635				260.98	326.81	1.25
	1330				224.38	667.45	2.97
M-40	0	40	5259.5	372	372.00	127.78	0.34
	363				365.25	227.13	0.62
	635				356.39	350.01	0.98
	1330				324.69	718.79	2.21

Table 5.9 Checking against buckling failure mechanism of 0.5 m diameter pile of various grades under scaled IMV earthquake motion in RCD soil

Grade	P (kN)	E (GPa)	D_L (m)	D_F (m)	L_0 (m)	β	L_e (m)	r_{min} (m)	λ	σ_y (Mpa)	σ_{cb} (Mpa)	σ_f (Mpa)	σ (Mpa)	σ/σ_f
M-20	0	22.4	11.5	3.2	15.7	2	31.4	0.125	251.2	8.92	3.49	2.51	0	0
	363					2							1.85	0.74
	635					2							3.24	1.29
	1330					2							6.78	2.70
M-30	0	27.4	11.5	3.2	15.7	2	31.4	0.125	251.2	13.38	4.28	3.24	0	0
	363					2							1.85	0.57
	635					2							3.24	1.0
	1330					2							6.78	2.09
M-40	0	31.6	11.5	3.2	15.7	2	31.4	0.125	251.2	17.84	4.94	3.87	0	0
	363					2							1.85	0.48
	635					2							3.24	0.84
	1330					2							6.78	1.75

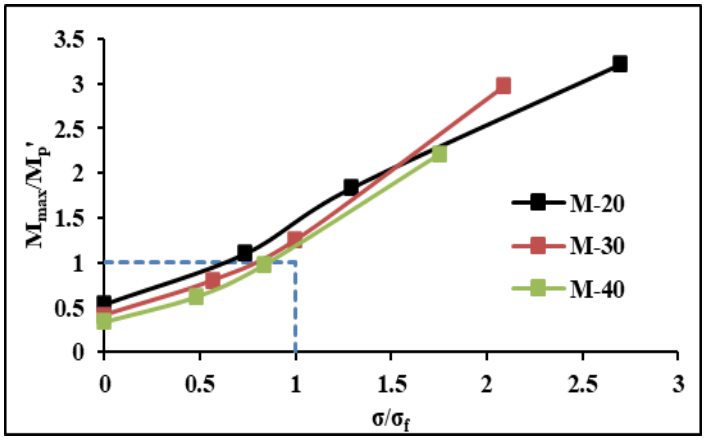

Fig. 5.25 Bending-buckling interaction graph of 0.5 m diameter pile of various grade of concrete in RCD soil due to the scaled IMV motion

5.6.7 Effect of liquefaction on natural time period of the soil-pile system

The natural frequency (f_n) of the soil-pile system is calculated using the following expression (Thomson 1996):

$$f_n = \frac{3.515}{8\pi}\frac{d}{L_0^2}\sqrt{\frac{E}{\rho}} \quad (5.17)$$

The total stiffness (k_s) of soil-pile system in liquefiable condition is contributed mainly by pile foundation due to negligible stiffness of liquefiable soil. The time period of the soil-pile system in liquefiable condition (T_{Liq}) can be calculated using the following equation (Bhattacharya 2006):

$$T_{Liq} = 2\pi\sqrt{\frac{M_s}{k_{NL}}} \quad (5.18)$$

where, M_s is the lumped mass at the pile head and stiffness

$$k_{NL} = \frac{12EI}{L_0^2} \quad (5.19)$$

The natural time period of soil-pile system obtained for 0.5, 0.75 and 1.0 m diameter M-30 grade concrete pile in RCD soil using Table 5.3 and 5.5 are 3.37, 2.63 and 2.24 sec respectively.

The time period of the soil-pile system in liquefiable condition are presented in Table 5.10 for various diameter M-30 grade concrete piles under different superstructure weight in RCD soil.

Table 5.10 Natural time period of soil-pile system in liquefiable condition for M-30 grade concrete pile of various configuration

Diameter (m)		0.5			0.75			1.0	
Superstructure Weight (kN)	363	635	1330	730	1210	2430	1284	2140	4280
Time period (sec)	2.37	3.13	4.53	1.68	2.16	3.07	1.38	1.78	2.52

It is observed from table 3.3 and 5.10 that predominant periods of the considered scenario earthquake motions are far away from the natural frequency of soil-pile system in liquefiable condition for 0.5, 0.75 and 1.0 m diameter M-30 grade concrete pile embedded in RCD soil.

Hence, possibility of happening resonance in dynamic loading due to liquefaction for the considered case is not expected. However, proper assessment of natural frequency of soil-pile system in liquefiable condition depending on the pile properties and the superstructure weight is very much essential for safe design of pile foundation.

Chapter 6

Dynamic Analysis of Piles in Sloping Ground

6.1 Introduction

In many practical conditions, bridge abutments are constructed on or near sloping ground for accommodating grade separations and also pile-supported buildings and bridges in hilly regions are built in sloping ground. Hence, it is extremely necessary to evaluate the seismic response of pile foundations in liquefiable sloping ground. The maximum lateral displacement and bending moment of piles are the two prevailing criteria in designing of laterally loaded piles rather than its ultimate lateral capacity.

The present pseudo-static analysis for single piles in liquefiable multi-layered sloping ground showed that pile response is significantly influenced with the ground slopes in liquefiable layered soil deposit. However, pseudo-static method is based on various numerical assumptions and unable to evaluate the complicated dynamic response of piles accurately during earthquake. As soil liquefaction causes development of high shear strain, nonlinear SSI is extremely required for seismic response of piles in liquefiable soil.

Also, present 3D nonlinear finite element based dynamic analysis of soil-pile system in liquefiable multi-layered level ground under the influence of axial loading shown that bending and buckling failure mode of piles in liquefiable soil can be avoided by choosing suitable combination of material strength and pile geometry.

It is clear from the literature review that most of the previous works have been directed towards static and dynamic response of single piles and pile groups in level ground surface. Also, static response of piles in sloping ground has been done by several researchers but there are very few studies of dynamic response of piles in multi-layered sloping ground, and there are even fewer studies on dynamic response of pile foundations in liquefiable multi-layered slopping ground considering the effects of static axial load as well as ground motions simultaneously. Thus, the present numerical study is adopted to fill up this research gap. Full-scale field tests are best reliable way to understand the behaviour of laterally loaded pile foundations. But due to high-cost involvement and technical difficulties, it is not always

feasible to perform field tests. Numerical approaches enable investigators to consider various parameters together in a detailed way. In this study, a single pile is modelled using 3D nonlinear finite-element based computer program OpenSeesPL (Elgamal et al. 2010; Lu et al. 2011). The present numerical model is validated and parametric study has been conducted to evaluate the effect of ground slope, soil type, input ground motion, pile slenderness ratio, pile head fixity condition and depth of ground water table (*GWT*) on dynamic response of soil-pile system.

6.2 Modelling Methodology

6.2.1 Material Properties

The field bore-log data of two typical sites of Kolkata metropolitan city in India have been considered in this study. Basically, Kolkata city was augmented along east direction of the river Hooghly and the soil is typically alluvial in nature. The ground water table is located near surface level. Normal Kolkata Deposit (NKD) and River Channel Deposit (RCD) are the two distinct soil formations of the city. Soft to stiff silty clay or clayey silt with intermediate sandy layer are the predominant composition of NKD soil. On the other hand, RCD soil consists mainly with medium to dense sand up to considerable depth beside old Adiganga canal. The field bore-log data of Ultadanga site and Tollygunge Metro site of Kolkata city representing NKD and RCD soil respectively are selected from the study of Roy et al. (2018) for evaluation of dynamic response of pile foundations. The detailed soil parameters like SPT-*N* value, unit weight (γ), Friction angles (φ) for cohesionless soils and undrained shear strength (C_u) for cohesive soil of these two typical sites considered from Fig. 5.1 of previous chapter.

The schematic layout of the soil-pile system in liquefiable multi-layered sloping ground considered in this study is shown in Fig. 6.1. A pinned headed circular single pile having total length (L) of 21.0 m with 1.0 m free head length (L_1) of M-30 grade concrete is embedded in the above soil profiles. D_L and D_{NL} representing depth of liquefiable and non-liquefiable layer respectively. The inclination angle is α with ground surface and depth of fixity of pile in non-liquefiable soil is (D_F). The effective length of pile (L_e) is dependent on factor (β) and pile length in liquefaction zone (L_0). The material behavior of the pile is selected to be liner elastic. The material and geometrical properties of pile section used in this study are considered from Table 5.3.

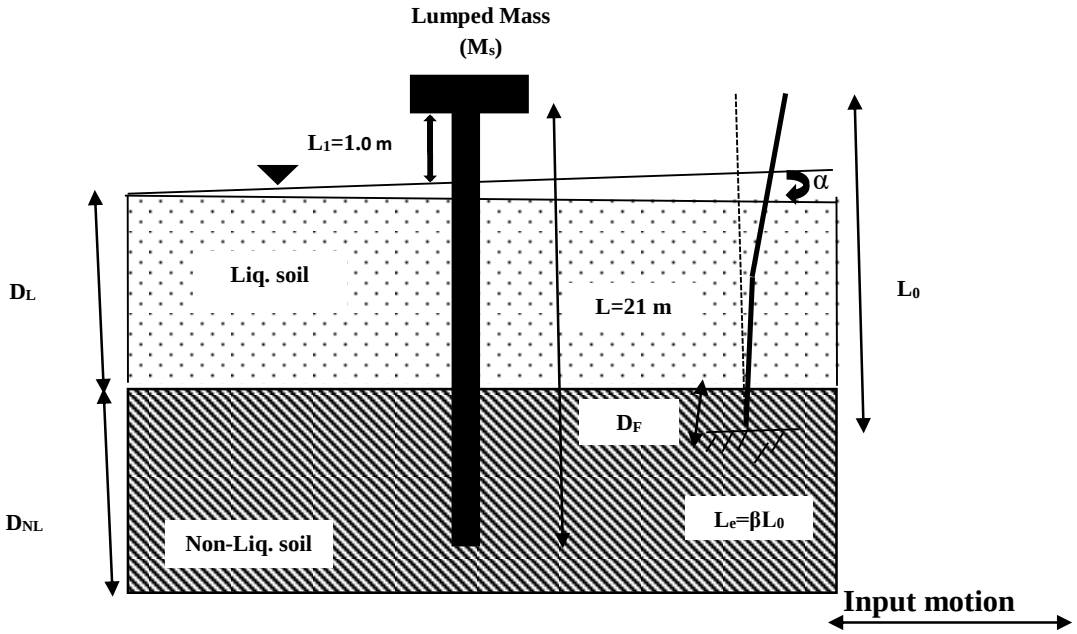

Fig. 6.1 Schematic layout of soil-pile system in liquefiable sloping ground considered in the present study

6.2.2 The Constitutive Model of Soil

The soil constitutive model used in this study is based on pressure-dependent multi-yield surface concept for cyclic hysteretic response (Elgamal et al. 2003; Yang et al. 2003).

The shape of the pressure-dependent multi-yield surface is conical shape in principal stress space. The utmost surface represents the maximum shear strength of soil. The conical yield surface forms hardening zone with respect to multi-surface plasticity to simulate soil nonlinearity. This constitutive model simulates the shear-induced dilative response due to liquefaction. The contractive, fully plastic, and dilative stages are incorporated by developing a new adequate flow rule.

In this study, *pressure dependent multi-yield02 (PDMY02)* type material model (Yang et al. 2003) is considered to model the liquefiable sands. Nonlinear hysteretic material model using Von Mises multi-surface kinematic plasticity model is employed to model the behavior of clay soil (Yang et al. 2003; Para 1996; Yang 2000). The cohesive soil is modelled using *pressure independent multi-yield (PIMY) type material* (Yang et al. 2003). The various model parameters are same as considered in chapter 5 (Table 5.1 and 5.2) for each layer of NKD and RCD soil.

The soil-fluid interaction and development of *EPWP* is accomplished using an advanced soil constitutive model implemented in fully-coupled *u-p* formulation as given in equation 5.8 and 5.9. The Newmark's algorithm is used to solve these equations numerically which is implemented in OpenSees.

6.2.3 Input Motions

The Kolkata city is located in between seismic zones III & IV as per Indian standard seismic code IS: 1893-2016. Enormous damage has occurred at Kolkata in the past due to near and far field earthquakes. The range of maximum bed rock level acceleration (MBRA) of Kolkata city varies from 0.1g to 0.34g with an average value of 0.22g (Mohanty and Walling 2008; Roy and Sahu 2012; Akhila et. al. 2012; Govindaraju and Bhattacharya 2012). In the present study, the input motions selected are Bhuj (BHJ), Imperial Valley (IMV) whose PGA values are well within the reported range of MBRA of the study area. The various parameters of BHJ and IMV earthquake motions are presented in Table 3.3. The acceleration time-history of BHJ and IMV motions are shown in Fig. 3.2(a) and (b) respectively.

6.2.4 Finite Element Model

Finite-element based program OpenSeesPL is used to create full 3D numerical model. Fig. 4 shows the 3D finite element model to simulate coupled soil-pile system in sloping ground. Open-source finite element-based computational platform OpenSees (Mazzoni et al. 2006) is used to perform simulations in OpenSeesPL. Only half of the soil domain is modelled owing to symmetry as shown in Fig.4. A floating pile having length *L* and diameter *d* is inserted into the layered NKD and RCD soil deposit. The soil and pile are modelled using 8-noded brick element and elastic beam-column element respectively. Every soil node has four and every pile node has six degrees-of-freedom (*DOF*). The fourth *DOF* of soil illustrates pore water pressure. The physical modelling of pile is employed using rigid link element with identical material properties of the pile. Each brick element of soil and surrounding pile element at same level is attached using outer nodes of the rigid link. Relatively fine mesh size has been considered near pile zone, which becomes coarser near domain boundaries. The present finite element model consists of 1700 numbers soil element and 141 numbers pile & link elements. The dimension of the soil model in longitudinal (x-direction) and transverse (y-direction) direction considered based on sensitivity analysis is 40d from the center of the pile. The

dimension in vertical direction (z-direction) considered is 50 m which is the total depth of soil profile used in this study. Mass and stiffness proportional Rayleigh damping (damping ratio 5%) has been considered. The model is inclined in longitudinal direction to represent sloping ground scenario. The optimum size of each finite-element considered in the model is not more than $\lambda/10$ (λ=wave length) to avoid filtration of portion of the seismic waves (Oliaei and Ghotbi Siabil 2017)

6.2.5 Boundary Conditions

Boundary conditions are very important for dynamic analysis of 3D numerical model to avoid reflection of seismic waves at the boundaries. Rigid box type boundary condition is selected for this study. All the base nodes of soil domain are selected to be fully fixed in x, y and z-directions. The 4th *DOF* of soil on the ground surface is fixed to drain out water. It is set open in the remaining nodes for free variation of E*PWP*. Boundary nodes perpendicular to the direction of input motion are considered as fixed in this direction. They are considered free parallel to the direction of input motion. Nodes at the sides parallel to the direction of input motion are constrained perpendicular to the motion direction and are considered free to move

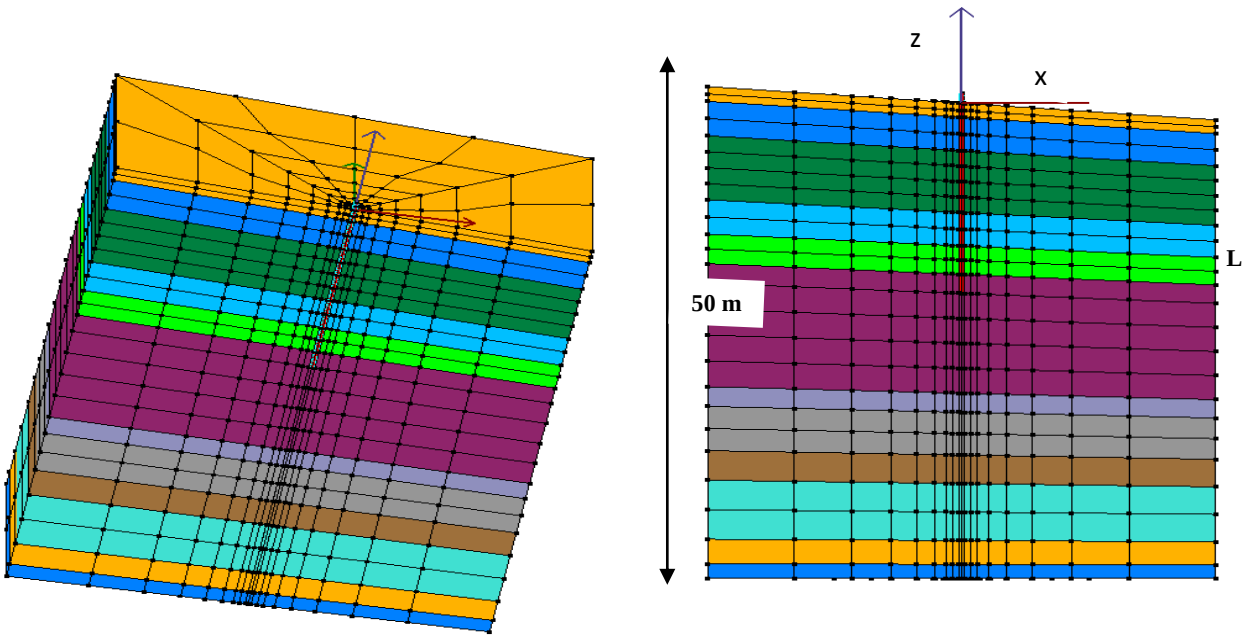

(a) **(b)**

Fig. 6.2 3D finite element model **a** 3D view **b** view in X-Z direction

in the motion direction. The bed rock level is assumed at the base of the soil model (50 m depth) and input motions are applied at that level in the longitudinal direction. Also, the magnification of ground motions during travelling from bed rock level to the surface level has been considered for dynamic analysis.

6.3 Validation of the Proposed Numerical Model

The results of the present model are compared with the centrifuge test results performed by Wilson (1998) to verify the applicability of the present model. The results obtained using the present FE model in terms of EPWP ratio, bending moment and superstructure acceleration time-history are compared with the measured values and shown in Figs. 5.8 (a) to (c). Fig.5.9 presents the variation of lateral displacement of pile with depth after 11.2 sec of earthquake duration. It is observed that the present results are matching well with the centrifuge test results. The slight variation of the results may be due to consideration of constant value of permeability in this study.

6.4 Present Study

In the present study, nonlinear dynamic response of laterally loaded single piles in liquefiable multi-layered slopping ground under the influenece of static axial load as well as ground motions simultaneously has been carried out to consider both kinematic and inertial interaction using finite-element based program OpenSeesPL.

The allowable load (P_{all}) of a particular diameter pile of 20 m embedded length in RCD soil is determined by dividing the ultimate load with a factor of safety of 2.5 as per IS 2911 (1984). A lumped mass (M_s) equivalent to allowable load carrying capacity of pile, representing the superstructure, is attached to the pile head to assess the effects of axial load on dynamic response of pile foundation. The allowable load on pile head calculated for 0.5, 0.75 and 1.0 m diameter piles are 1330, 2430, 4280 kN respectively.

The slopes of the ground (α) in the longitudinal direction varies from 0 to 10 degree to represent level and gently sloping ground scenario. The finite element simulation is used to calculate the depth of liquefaction (D_L) and degradation of shear strength of soil. The analysis is initially carried out in level and sloping ground for kinematic loading only, without considering the axial load on pile head. Then, the same analysis is conducted again for the combined kinematic and inertial loading by considering the axial load at pile head and ground

motions simultaneously. The variations of kinematic and combined response with time and depth in NKD and RCD soil are described in detail.

The presence of axial load reduces the plastic moment capacity of pile in liquefiable soil (Bhattacharya 2003). A hinge is generally formed within a pile section under the combined action of axial load (*P*) and moment (*M*) as shown in equation 5.19.

In the present study, bending failure of pile under combined loading in liquefiable soil is checked by comparing the maximum bending moment developed in the pile with the available plastic moment capacity computed using *P*-*M* interaction as given by equation 5.19.

The axial load also increases the buckling instability of piles in liquefiable soil (Bhattacharya 2003) owing to loss of lateral support during liquefaction. Critical buckling load of pile is estimated using Euler's buckling equation as given in equation 5.12.

The value of L_e is determined using equation 5.13. The fixity condition of top end of the pile is supposed to be pinned type. The bottom end of the pile is supposed to be pinned type for depth of embedment of pile less than 5d and fixed type for depth of embedment of pile more than 5d (Bhattacharya 2006). The values of β are taken from IS 456-2000 based on the fixity conditions of pile at both ends.

In this study, buckling failure of pile under combined loading in liquefiable soil is checked by comparing the maximum axial stress of the pile with the Rankine's failure stress as computed using equation 5.18.

Finally, bending-buckling interaction diagrams are produced from the above analysis for the piles located in level and sloping ground subjected to both the axial and lateral loads. This diagram is useful for seismic design of piles in liquefiable level as well as sloping ground.

6.5 Results and Discussions

A parametric study has been carried out using the proposed numerical model to evaluate the influence of ground slope, soil type, input ground motion, pile slenderness ratio, pile head fixity condition and depth of ground water table (*GWT*) on dynamic response of soil-pile system in liquefiable layered soil deposit considering the effect of both kinematic and inertial interaction. The results obtained for soil and pile responses are presented in tabular form and discussed graphically.

6.5.1 Response of Soil

6.5.1.1 Variation of Excess Pore Water Pressure Ratio (R_u)

R_u is an important practical parameter for the assessment of liquefaction potential of soil. When R_u approaches to unity, the soil loses its shear strength and term as liquefied soil. The effect of various parameters on the development and distribution of excess pore water pressure (EPWP) are evaluated and presented graphically.

It is seen from the Fig. 6.3(a) that the depth of liquefaction (D_L) in RCD soil for 0, 2.5, 5.0 and 10.0 degree ground slopes under scaled IMV motion are 10.8, 10.4, 9.9 and 10.2 m respectively. The values of D_L in RCD soil for 5-degree ground slope under BHJ, Scaled IMV and IMV ground motions are 10, 9.9 and 13.8 m respectively as shown in Fig. 6.3(b). Also, NKD soil is non-liquefiable except top 1.0 m depth for level ground condition and liquefiable up to depth of 10.75 m for 5-degree ground slope under scaled IMV motion as shown in Fig.6.3(c). Sudden increase of EPWP at top of both the soil profiles is observed due to existence of clay layer which obstructs to drain out the pore water. The value of D_L is significantly influenced by the depth of *GWT*. When the depth of *GWT* increases from 0 to 5.0 m, the thickness of top non-liquefiable layer increases but the bottom depths of liquefaction are 9.9, 11.5 and 11.5 m for *GWT* at 0, 2.5 & 5.0 m under scaled IMV motion as illustrated in Fig. 6.3(d). So, the value of D_L is dependent on topography of the ground, types of soil, ground motion characteristics and depth of *GWT*. It is clear from the above figures that the value of *EPWP* decreases with depth due to increase of stiffness of soil.

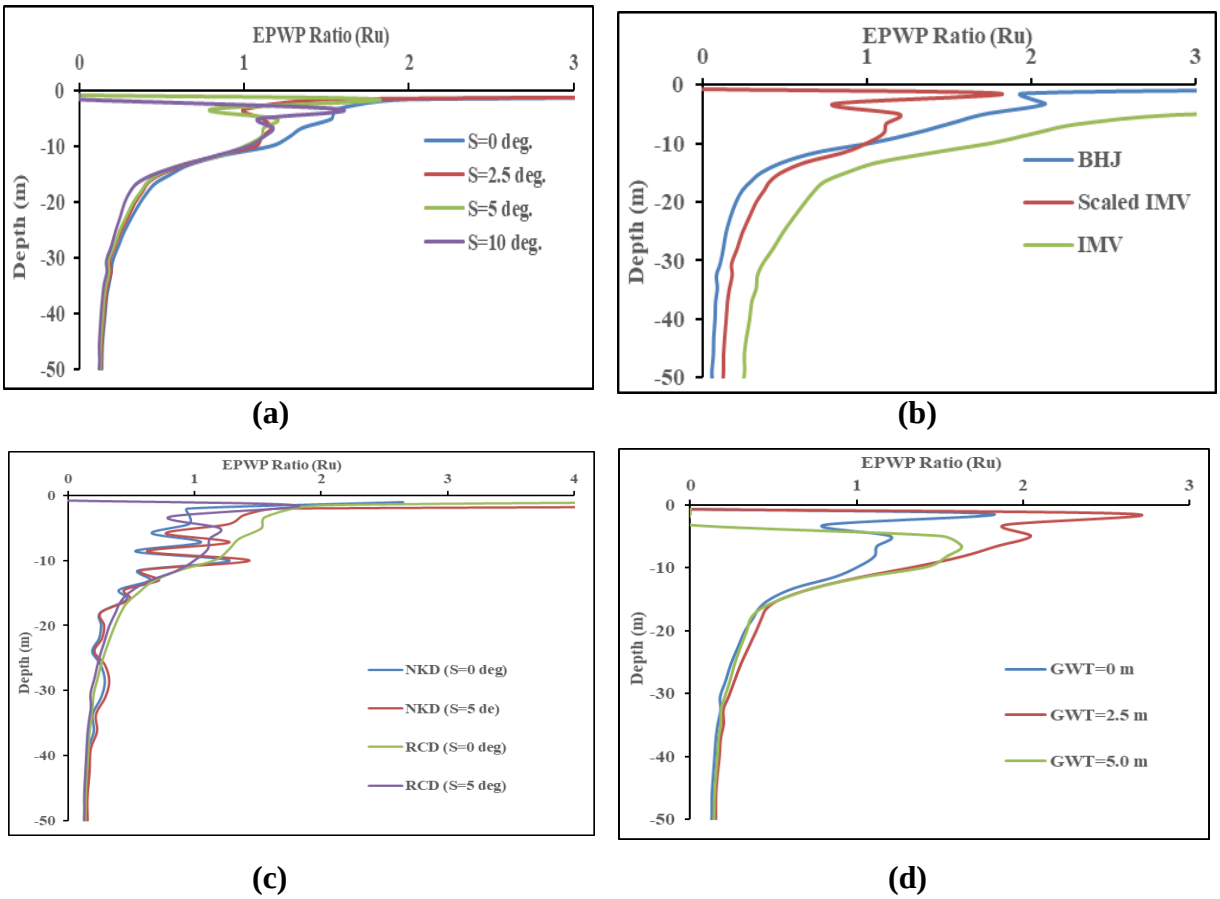

Fig. 6.3 Variation of R_u with depth **a** in RCD soil for different ground slopes under scaled IMV motion **b** in RCD soil for 5-degree ground slope under different ground motions **c** in NKD and RCD soil under scaled IMV motion and **d** in RCD soil for different depth of *GWT* under scaled IMV motion

6.5.1.2 Variation of Peak Ground Displacement (PGD)

Figs. 6.4(a) and (b) demonstrate the variation of PGD with depth in RCD soil for different ground slopes under scaled IMV motion and for 5-degree ground slope under different ground motions respectively. It is observed from Fig. 6.4(a) that the PGD value for top liquefiable soil layer increases with an increase of ground slopes under a particular ground motion. The maximum value of PGD observed at ground surface for level ground and near the boundary of liquefiable & non-liquefiable layer for sloping ground condition. The maximum value of PGD increase by 238 % due to increase of ground slope from 0 degree to 10 degree. The PGD value in sloping ground significantly increases with an increase of amplitude of input ground motions as shown in Fig. 6.4(b). The comparison of PGD profile in NKD and RCD soil for 5-

degree ground slope under scaled IMV motion is presented in Fig. 6.4(c). The PGD profile of NKD soil in sloping ground is totally different from RCD soil for top 11.5 m depth under same input motions. Hence, type of soil has profound influence on PGD profile. Also, PGD profile in sloping ground is significantly changes with variation of *GWT* as shown in Fig. 6.4(d). PGD is maximum when GWT is located at surface level.

Fig. 6.5(a) represents the PGD time-history at ground level in RCD soil for various ground slopes under scaled IMV motion. Residual soil displacement at the end of duration of input motion in sloping ground indicates the possibility of liquefaction-induced lateral spreading of the site. The residual displacement at ground level observed for 0, 2.5, 5.0 and 10.0 degrees sloping ground are 4.55, 9.65, 29.2 and 62.2 mm respectively. Similarly, the residual displacement increases with an increase of amplitude of input motions as shown in Fig. 6.5(b). Fig. 6.5(c) shows the comparison of PGD time-history at ground surface for 5-degree

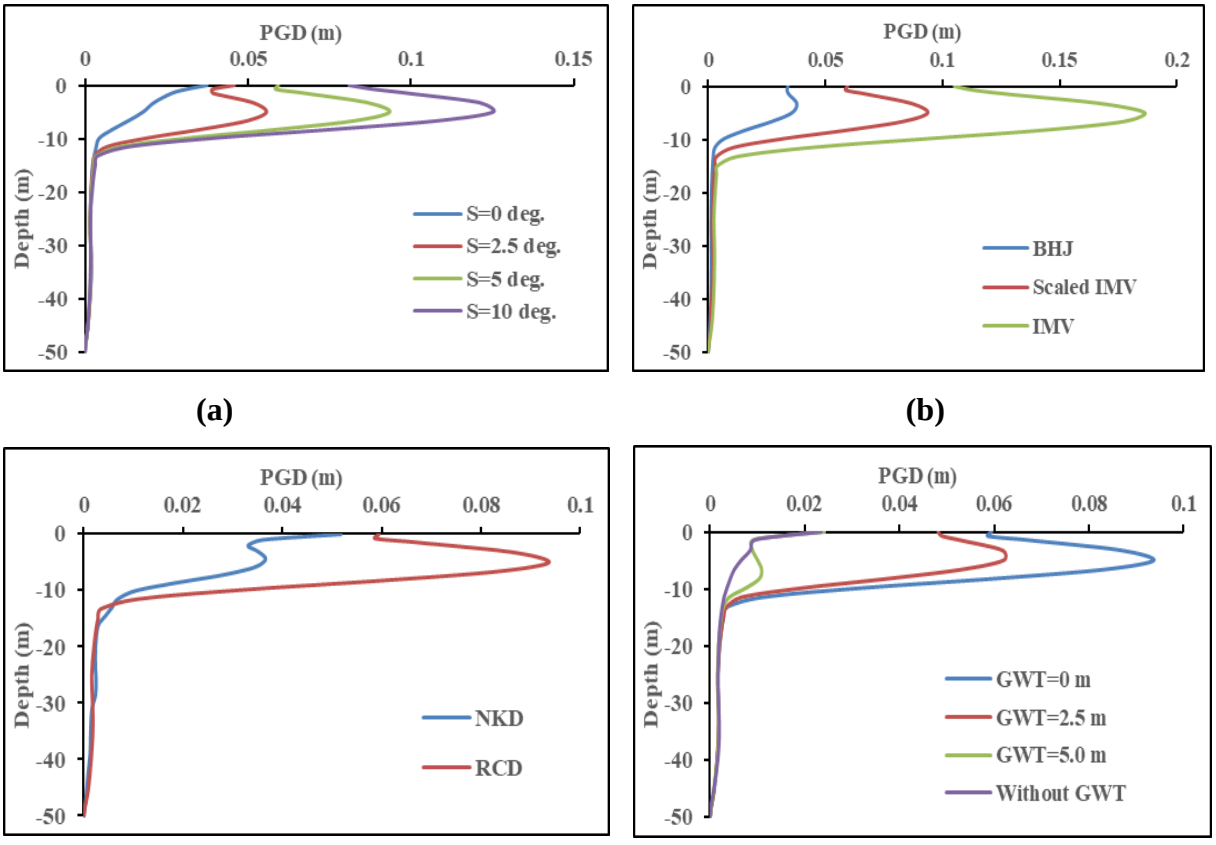

Fig. 6.4 Variation of PGD with depth **a** in RCD soil for different ground slopes under scaled IMV motion **b** in RCD soil for 5-degree ground slope under different ground motions **c** in NKD and RCD soil for 5-degree ground slope under scaled IMV motion and **d** in 5-degree sloping RCD soil for different depth of *GWT* under scaled IMV motion

ground slope in RCD soil for different depths of *GWT* under scaled IMV motion. It is noticed that residual displacement decreases significantly with an increase of depth of *GWT* from ground surface.

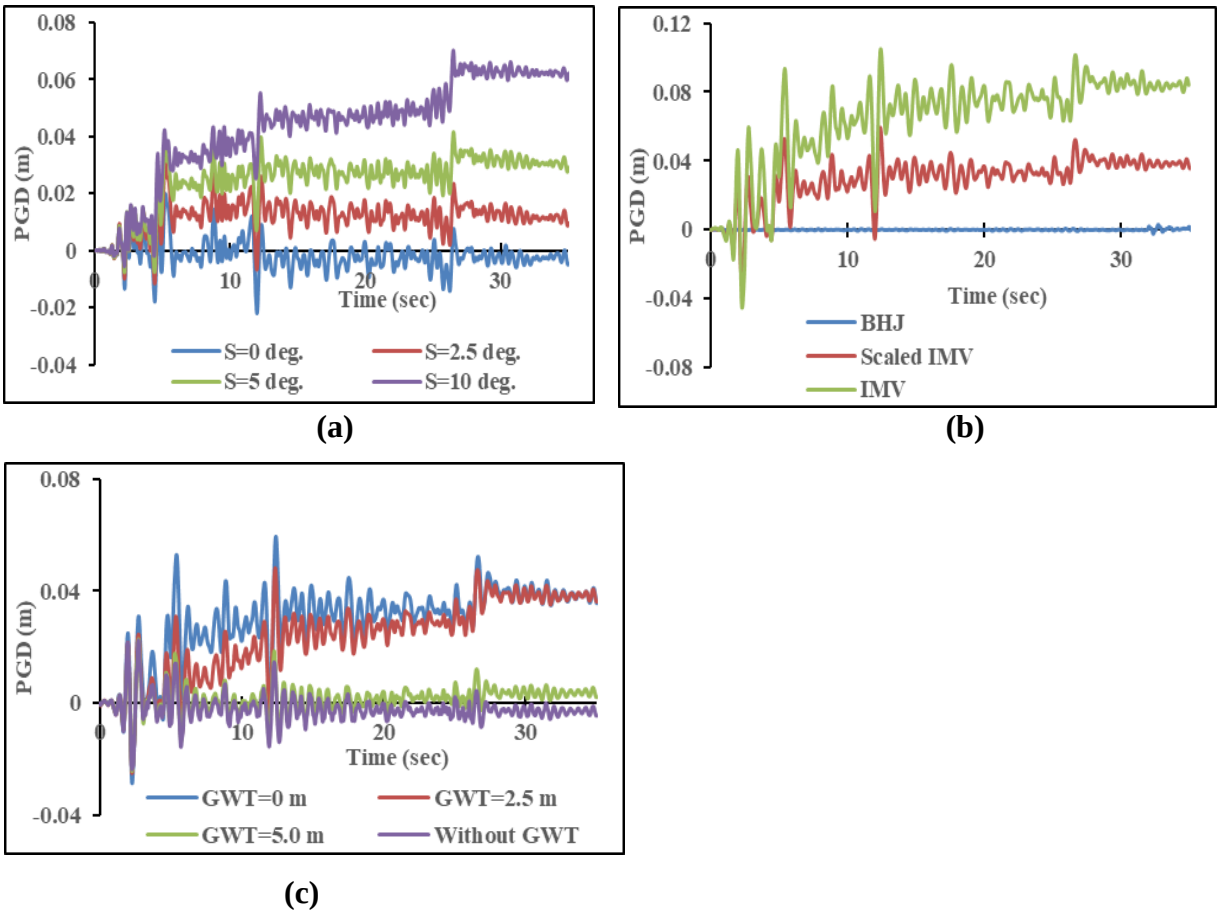

Fig. 6.5 PGD time-history at ground level **a** in RCD soil for various ground slopes under scaled IMV motion **b** in RCD soil for 5-degree ground slope under various ground motions and **c** in RCD soil for different depths of *GWT* under scaled IMV motion

6.5.1.3 Variation of Peak Ground Acceleration (PGA)

The variation of PGA with depth for different ground slopes in RCD soil under scaled IMV motion is shown in Fig. 6.6(a). The PGA amplification factor at ground surface does not change with ground slopes and the value is 1.26 for all the ground slopes under scaled IMV motion. But the amplification factor obtained are 1.26 for IMV & Scaled IMV and 1.60 for BHJ earthquake motion in RCD soil having ground slope of 5-degree as shown in Fig. 6.6(b). PGA amplification is comparative less for high amplitude input motion due to development of large hysteretic stress-strain response of top weak soil. However, for same ground slope of 5-

degree in RCD soil under scaled IMV motion, the PGA amplification factors obtained are 1.26, 9.15, 6.9 and 6.5 for *GWT* depth of 0, 2.5, 5.0 m and without *GWT* respectively as illustrated in Fig. 6.6(c). Hence, location of *GWT* significantly influence the amplification of PGA at surface level. When, *GWT* depth increases the top soil become non-liquefied and the strength of soil increases which causes PGA to amplify.

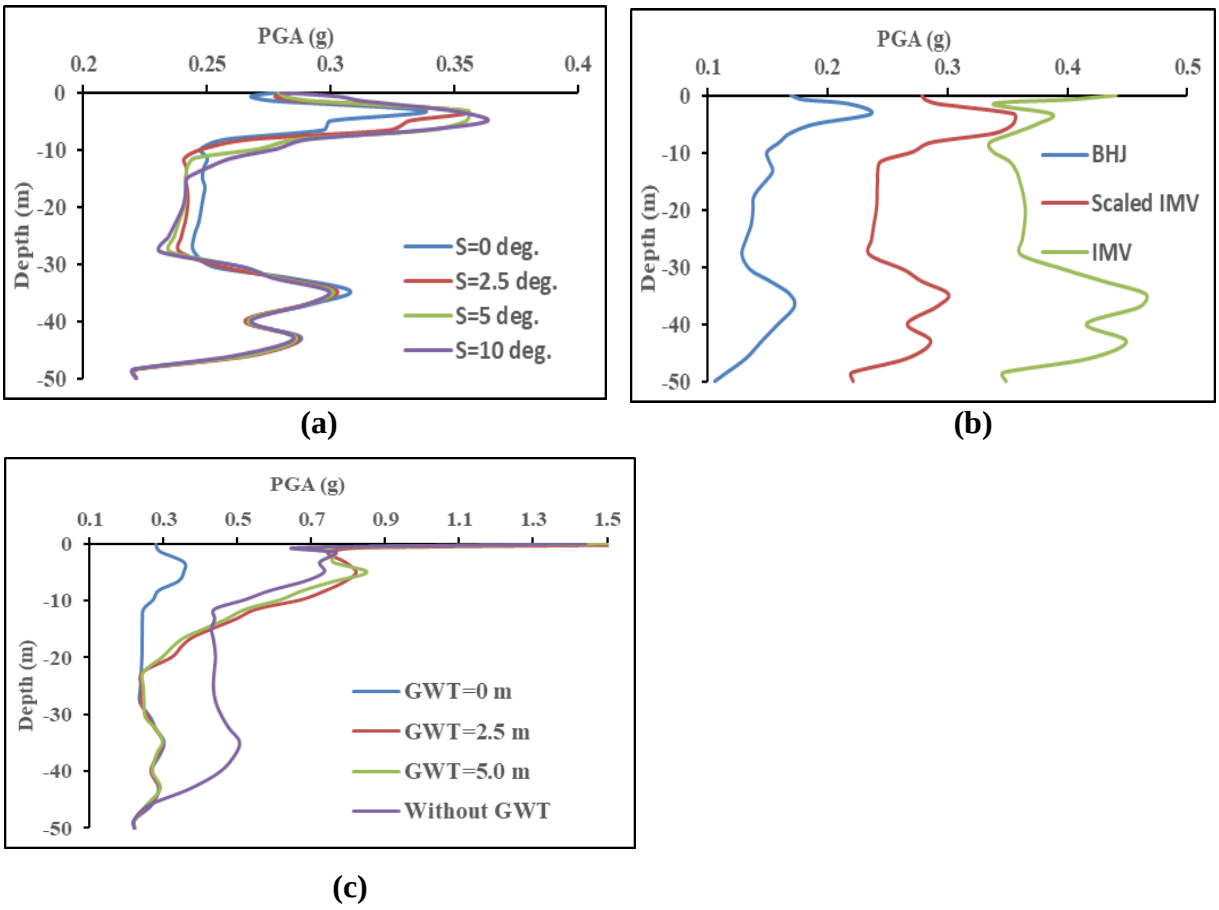

Fig. 6.6 Variation of PGA with depth **a** in RCD soil for various ground slopes under scaled IMV motion **b** in RCD soil for 5-degree ground slope under various ground motions and **c** in RCD soil for different depths of *GWT* under scaled IMV motion

6.5.2 Response of Pile

The dynamic response of piles obtained in this study are described in the form of variation of dimensionless lateral displacement co-efficient (*y/d*) and bending moment co-efficient (*M/Mp'*) against the depth for kinematic and combined kinematic and inertial loading conditions.

6.5.2.1 Influence of Ground Slopes

The variation of peak lateral displacement co-efficient along depth for 0.5 m diameter pile in different ground slopes of RCD soil under scaled IMV motion are shown in Figs. 6.7(a) and (b) for kinematic and combined loading respectively. It is observed that the both kinematic and combined peak lateral displacement co-efficient of pile in level ground is significantly less than that of the sloping ground under same earthquake motion. The peak lateral displacement co-efficient of pile with slopes are shown in Figs. 6.8(a) and (b) for kinematic and combined loading condition respectively. The amplification factors for sloping ground with respect to level ground due kinematic loading are 2.5, 4.3 and 5.6 for 2.5, 5.0 and 10.0 degree ground slopes respectively. The same values are 1.03, 1.7 and 2.2 due to combined kinematic and inertial loading. Hence, it can be inferred that the kinematic response of pile is significantly dependent on ground slopes.

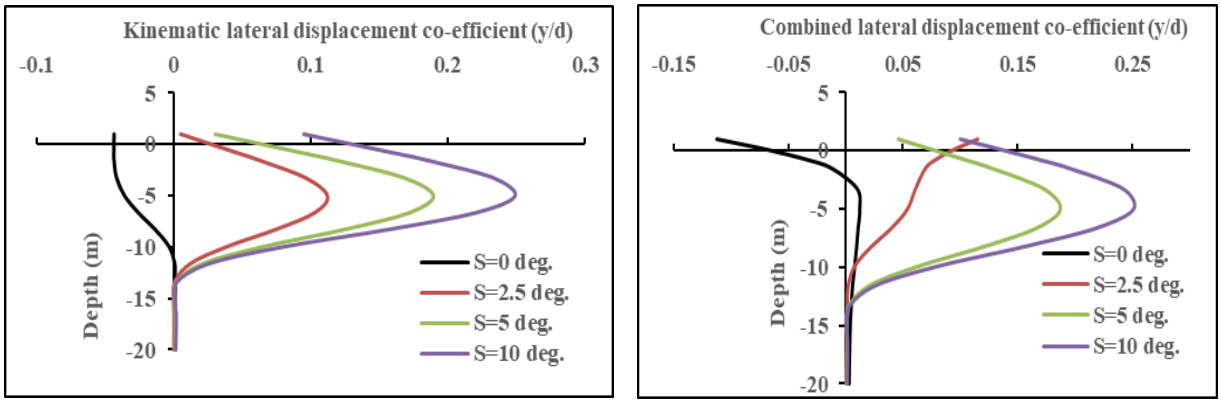

(a) **(b)**

Fig. 6.7 Variation of **a** kinematic and **b** combined lateral displacement co-efficient of pile with depth in RCD soil for different ground slopes under scaled IMV motion

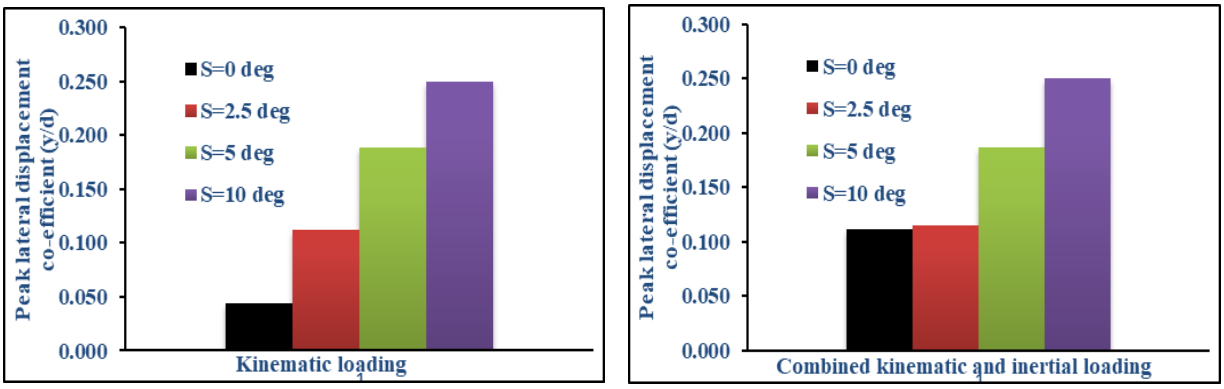

(a) **(b)**

Fig. 6.8 Peak lateral displacement co-efficient for **a** kinematic and **b** combined loading in RCD soil for different ground slopes under scaled IMV motion

Peak bending moment co-efficient due to kinematic loading only in RCD soil for 0, 2.5, 5.0 and 10.0 degree ground slopes under scaled IMV motion are 0.41, 1.44, 2.25 and 2.77 respectively as shown in Fig. 6.9(a). Hence, 0.5 m diameter pile is only safe in level ground of RCD soil under scaled IMV motion against kinematic bending failure. With mild increase of ground slope, the same pile is failed in kinematic bending. Fig. 6.9(b) shows the peak bending moment co-efficient due to combined loading for 0, 2.5, 5.0 and 10.0 degree ground slopes are 2.97, 3.24, 3.35 and 3.50 respectively. Hence, the inertial effect is predominant for combined response of pile. The maximum bending moment time-history at ground surface for different ground slopes due to kinematic and combined loading are shown in Fig. 6.10(a) and (b) respectively. It is observed that the maximum bending moment at ground surface increases significantly due to mass of the superstructure when combined response is considered. It is observed from Figs. 6.11(a) and (b) that the amplification factors of bending moment for sloping ground with respect to level ground are 3.50, 5.50, 6.75 due kinematic loading and 1.09, 1.13, 1.18 due to combined loading for 2.5, 5.0 and 10.0 degree ground slopes respectively.

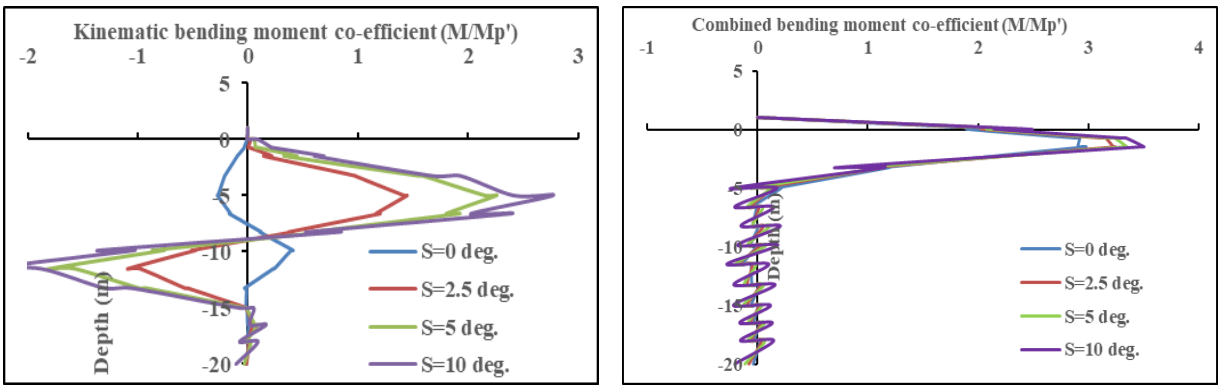

(a) **(b)**

Fig. 6.9 Variation of **a** kinematic and **b** combined bending moment co-efficient of pile with depth in RCD soil for various ground slopes under scaled IMV motion

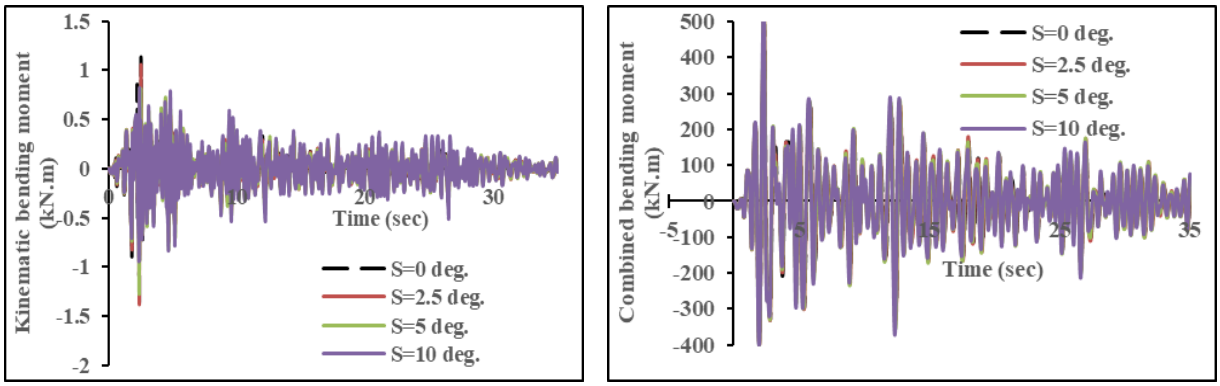

(a) **(b)**

Fig. 6.10 Comparison of **a** kinematic and **b** combined bending moment time-history at ground level in RCD soil for various ground slopes under scaled IMV motion

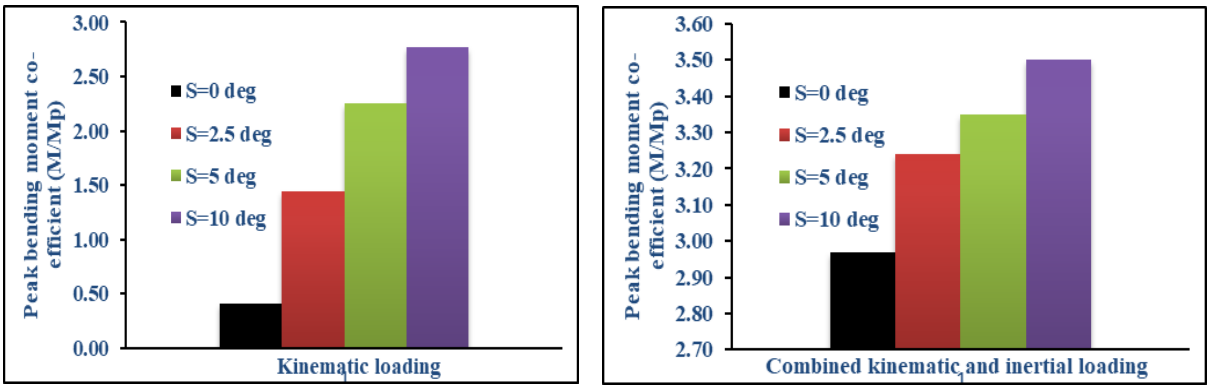

(a) **(b)**

Fig. 6.11 Peak bending moment co-efficient for **a** kinematic and **b** combined loading in RCD soil for different ground slopes under scaled IMV motion

6.5.2.2 Influence of Soil Types

From the combined response of peak lateral displacement and bending moment co-efficient as shown in Figs. 6.12(a) and (b) respectively, it is clear that response of pile is significantly different in NKD and RCD soil for 5-degree sloping ground under scaled IMV motion. Peak lateral displacement co-efficient for 0.5 m diameter pile obtained are 0.17 at surface level in NKD soil and 0.19 at 5.0 m depth in RCD soil. Similarly, peak bending moment co-efficient obtained are 4.1 at 1.0 m depth in NKD soil 3.35 at 1.5 m depth in RCD soil. Fig. 6.13 shows the comparison of maximum combined bending moment of 0.5 m diameter pile at ground surface in NKD and RCD soil for 5-degree sloping ground under scaled IMV motion. The response in NKD soil is more than RCD soil because of large inertial loading due to higher

PGA at surface level. Hence, the dynamic response of pile is profoundly influenced by the type of soil deposit.

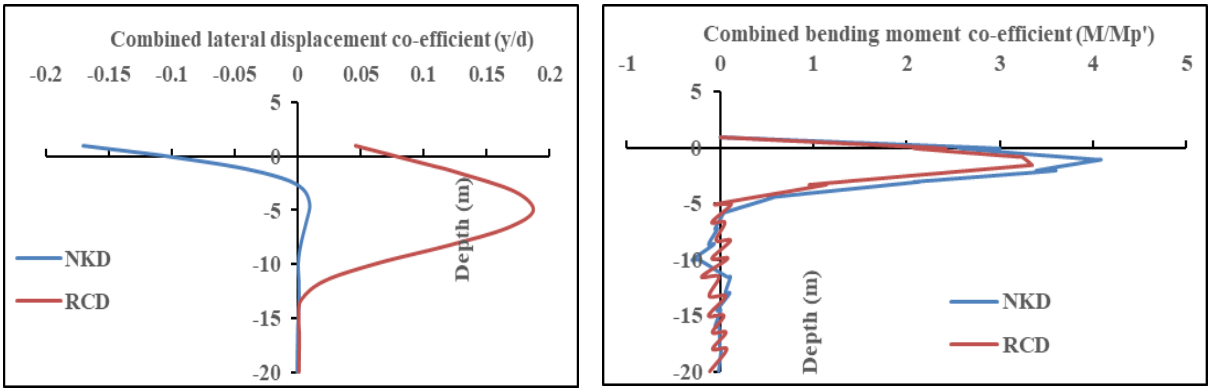

(a) **(b)**

Fig. 6.12 Variation of combined **a** lateral displacement co-efficient and **b** bending moment co-efficient of pile with depth in NKD and RCD soil for 5-degree ground slope under scaled IMV motion

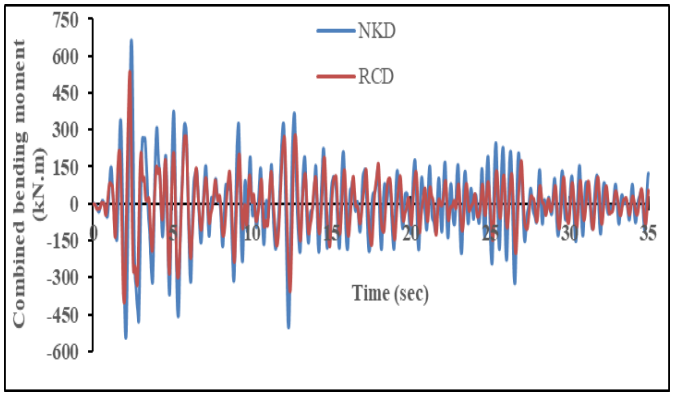

Fig. 6.13 Comparison of combined bending moment time-history at ground level between NKD and RCD soil for 5-degree ground slope under scaled IMV motion

6.5.2.3 Influence of Input Ground Motions

Figs. 6.14(a) and (b) illustrated the effect of input ground motions on lateral displacement and bending moment response of 0.5 m diameter pile in RCD soil for 5-degree ground slope under combined loading condition. The peak lateral displacement co-efficient are 0.080, 0.19, 0.37 and peak bending moment co-efficient are 1.42, 3.35, 4.94 under BHJ, scaled IMV and IMV input motion respectively. Hence, amplitude of input motion has significant effect on pile response. The comparison of pile lateral displacement co-efficient and bending moment co-

efficient for level and 5-degree sloping ground are shown in Fig. 6.15(a) and (b) respectively. The combined peak lateral displacement response is 2.5 times more in level ground and 4.6 times more in sloping ground when ground motion changes from BHJ to IMV. Similarly, the combined peak bending moment response is 3.1 times more in level ground and 3.45 times more in sloping ground when ground motion changes from BHJ to IMV.

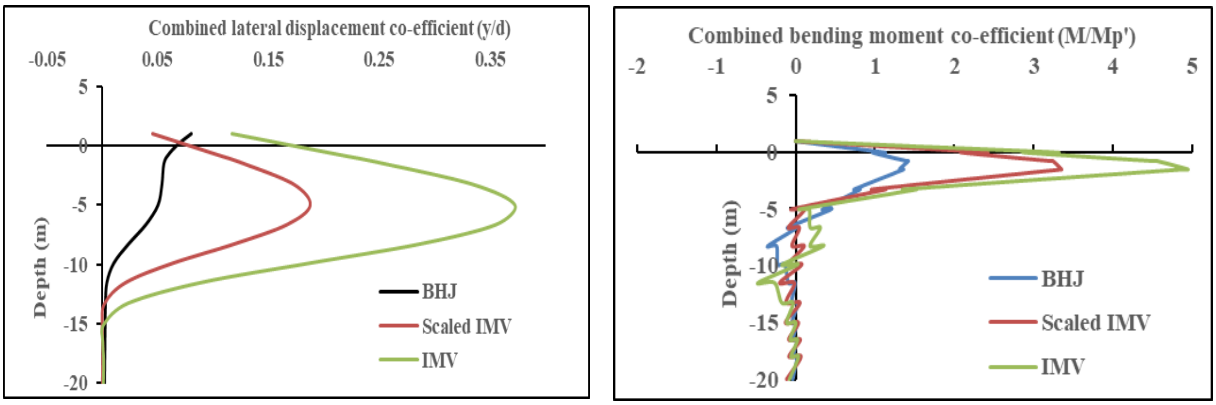

(a) **(b)**

Fig. 6.14 Variation of combined **a** lateral displacement co-efficient and **b** bending moment co-efficient of pile with depth in RCD soil for 5-degree ground slope under various ground motions

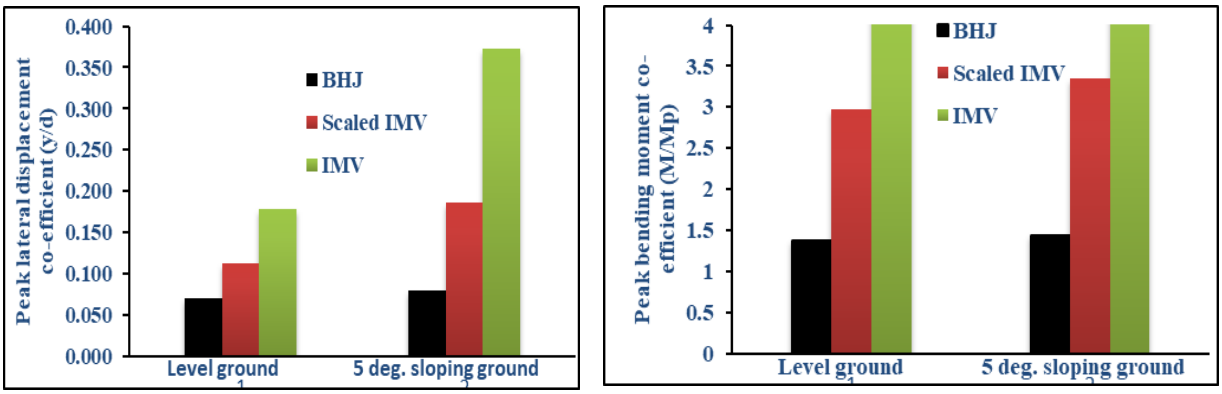

(a) **(b)**

Fig. 6.15 Combined peak **a** lateral displacement co-efficient and **b** bending moment co-efficient in RCD soil for different ground slopes under scaled IMV motion

6.5.2.4 Influence of *L/d* Ratio of Pile

The effect of *L/d* ratio on combined response of piles in RCD soil for 5-degree ground slope under scaled IMV motion is evaluated in the present study considering 21.0 m length (*L*) with diameters (*d*) of 0.5, 0.75 and 1.0 m and presented in Figs 6.16(a) and (b). It is observed from Fig. 6.16(a) that the flexible pile behaviour changes to rigid behaviour due to decrease of *L/d* ratio from 42 to 28. The combined peak lateral displacement and bending moment co-efficent decreases by 46.5% and 29.5% respectively when *L/d* ratio decreases from 42 to 28. The reductions are 62.6% and 44.2% when *L/d* ratio decreases from 42 to 21. Peak lateral displacement co-efficient in 5-degree sloping ground increases by 1.67, 1.39 and 1.37 times with respect to level ground for *L/d* ratio 42, 28 and 21 respectively as shown in Fig.6.17. Fig. 6.18 shows that the peak bending moment co-efficent in 5-degree sloping ground increases by 1.14 times with respect to level ground for all *L/d* ratios. Hence, it is recommended to adopt large diameter piles in liquefiable sloping ground for avoiding bending failure due to combined loading.

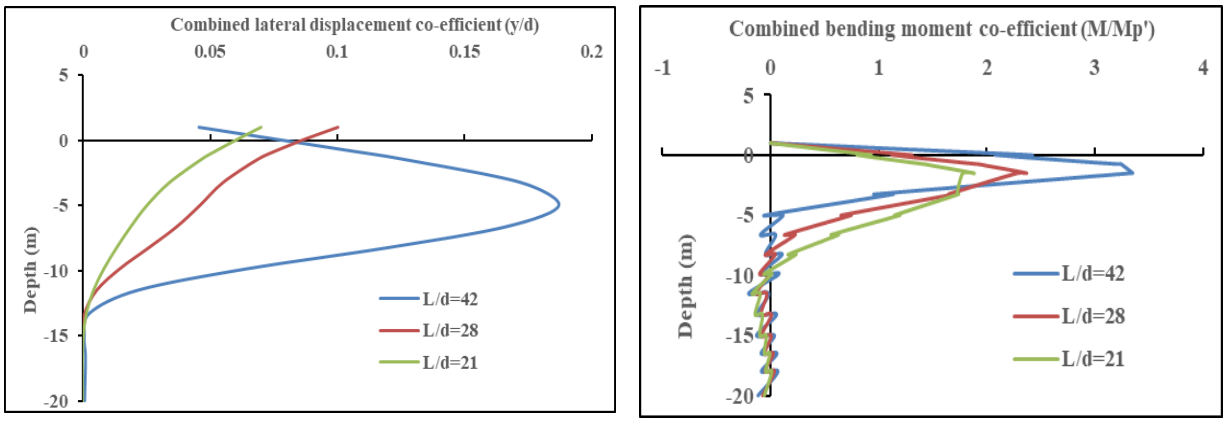

(a) **(b)**

Fig. 6.16 Variation of combined **a** lateral displacement co-efficient and **b** bending moment co-efficient profile with pile *L/d* ratio in RCD soil for 5-degree ground slope under scaled IMV motion

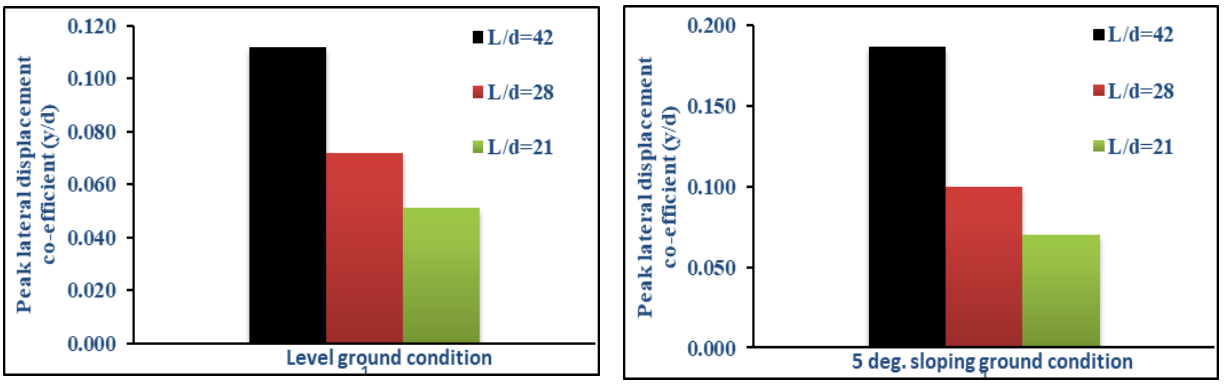

(a) **(b)**

Fig. 6.17 Combined peak lateral displacement co-efficient for **a** level and **b** 5-degree sloping ground in RCD soil for different *L/d* ratios under scaled IMV motion

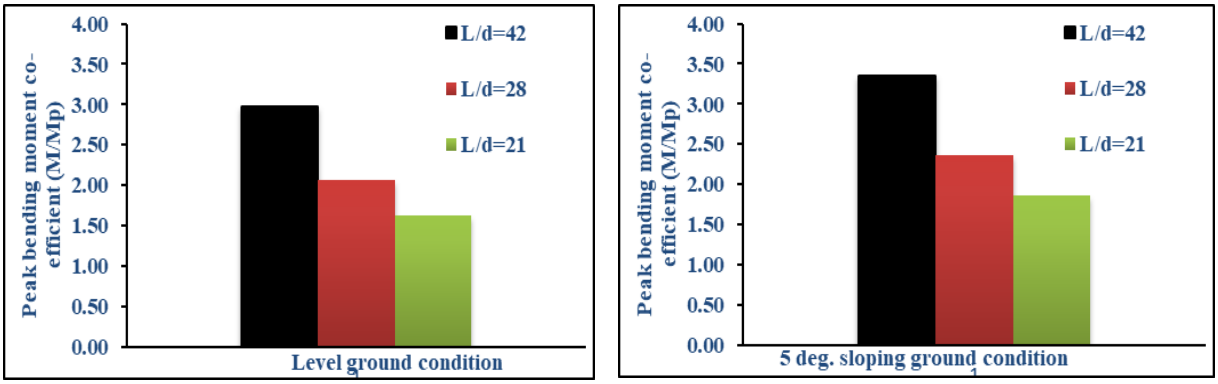

(a) **(b)**

Fig. 6.18 Combined peak bending moment co-efficient for **a** level and **b** 5-degree sloping ground in RCD soil for different *L/d* ratios under scaled IMV motion

6.5.2.5 Influence of Pile Head Fixity Conditions

The boundary condition of pile head has profound influence on pile responses in liquefiable sloping ground as shown in Figs. 6.19(a) and (b). The peak combined lateral displacement decreases by 9.1% and combined bending moment co-efficient of pile increases by 8.9% when pile head changes from free to fixed head fixity condition. The peak bending moment (751.09 kN-m) develops at the boundary between liquefiable and non-liquefiable soil in case of free head pile. However, for fixed head pile, the peak bending moment occurs both at pile head (820.40 kN-m) and boundary between liquefiable and non-liquefiable soil (206.40 kN-m). Fig.6.20 shows the comparison of combined bending moment time-history with pile head fixity conditions at ground level for 5-degree slope under scaled IMV motion. It is seen that

fixed head pile response is significantly different from free head pile at ground surface. Fixed head pile shows residual bending moment after end of the shaking. This additional bending is caused by the lateral displacement of soil in sloping ground for fixed head pile even after earthquake.

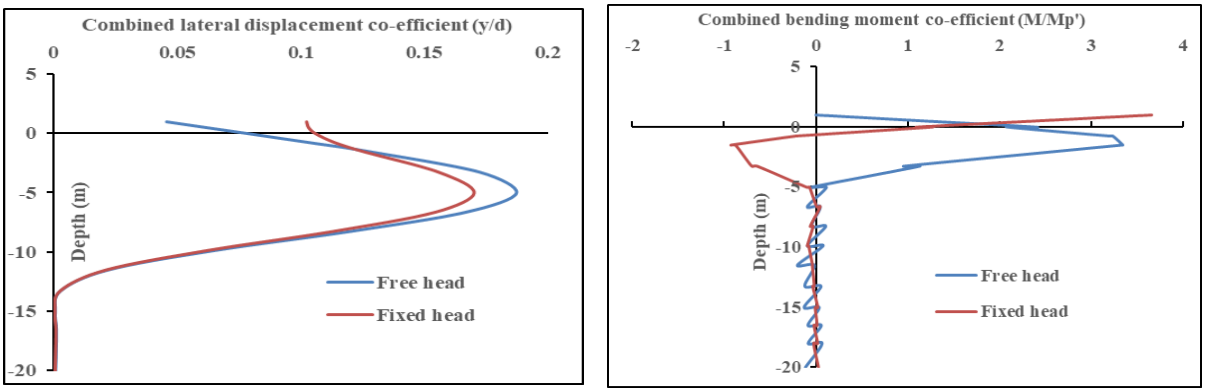

(a) **(b)**

Fig. 6.19 Variation of combined **a** lateral displacement co-efficient and **b** bending moment co-efficient profile with pile head fixity conditions in RCD soil for 5-degree ground slope under scaled IMV motion

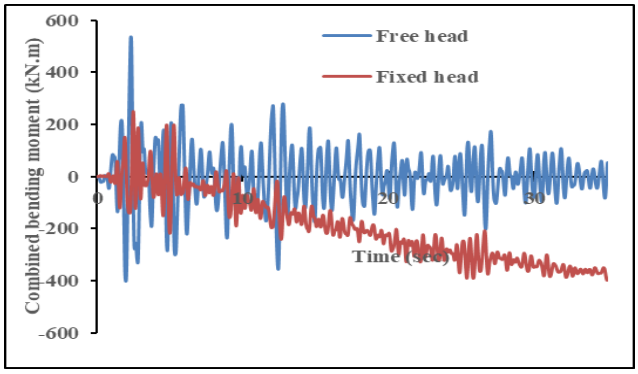

Fig. 6.20 Comparison of combined bending moment time-history with pile head fixity conditions at ground level for 5-degree ground slope under scaled IMV motion

6.5.2.6 Influence of Depth of Ground Water Table (*GWT*)

The depth of *GWT* has profound influence on pile response. The depth of *GWT* varies from 0 to 3.0 m at different locations in Kolkata city (Akhila et al. 2012; Govindaraju and Bhattacharya 2012; Chatterjee 2018). Hence, in the present study, variation of *GWT* from 0 to 5.0 m and without *GWT* has been considered for piles in RCD soil having ground slope of 5-

degree under scaled IMV motion. The lateral displacement decreases and bending moment increases with an increase of depth of *GWT* as shown in Figs. 6.21(a) and (b) respectively. The peak combined lateral displacement decreases by 48.7% and combined bending moment co-efficient of pile increases by 14.3% when soil condition changes from liquefiable (*GWT*=0 m) to non-liquefiable condition (without *GWT*).

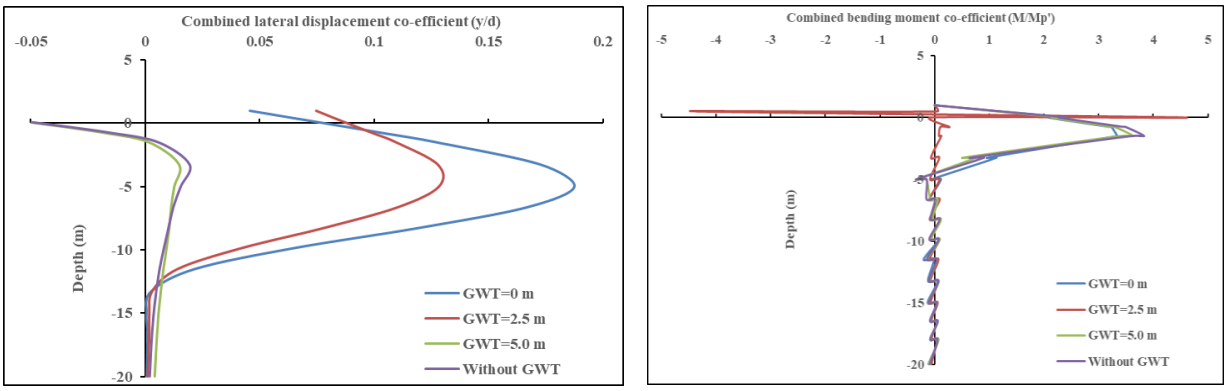

(a) **(b)**

Fig. 6.21 Variation of combined **a** lateral displacement co-efficient and **b** bending moment co-efficient profile with depth of *GWT* in RCD soil for 5-degree ground slope under scaled IMV motion

6.5.3 Bending-Buckling Interaction Diagram

Bending-buckling interaction diagram is very important for analysis of piles in liquefiable soil under combined vertical and lateral load. It is a plot of buckling co-efficient (σ/σ_f) vs bending moment co-efficient (M/M_p') for a particular combination of pile and soil configurations. Buckling failure of piles in liquefiable soil is happened when axial stress (σ) exceeds the Rankine's failure stress (σ_f). On the other hand, pile fails in bending when the bending moment in pile overcomes its available plastic moment capacity (M_p') under combined vertical and lateral loading. A pile may be considered as safe when both M/M_p' and σ/σ_f are less than 1. Bending-buckling analysis has been done for 21.0 m long M-30 grade concrete circular piles in RCD soil under various pile geometry, ground motions characteristics and ground slopes. Tables 1 and 2 examines the bending and buckling failure criteria respectively for different diameters pile in level and 5-degree sloping RCD soil profile under scaled IMV motion and Fig.6.22 is the bending-buckling interaction diagram for the same. It is observed

that 0.5 m diameter pile is unsafe for both bending and buckling. However, 0.75 m and 1.0 m diameter piles are safe in buckling but unsafe in bending for both level and 5-degree sloping ground. Both the bending and buckling co-efficient reduces significantly with an increase of pile diameter. Also, bending co-efficient is more in mildly sloping ground than level ground though buckling co-efficient does not change significantly with slopes for a particular pile diameter.

Table 6.1 Examining bending failure criteria of different diameters pile in RCD soil under scaled IMV motion

d (m)	S (^{0})	P (kN)	f_{ck} (MPa)	P_y (kN)	M_p(kN-m)	Mp'(kN-m)	M(kN-m)	M/Mp'
0.5	0	1330	30	3944.6	279	224.38	667.45	2.97
	5	1330				224.38	751.09	3.35
0.75	0	2430	30	8875.40	941	806.52	1668.76	2.07
	5	2430				806.52	1906.61	2.36
1.0	0	4280	30	15778.5	2230	1915.00	3116.88	1.63
	5	4280				1915.00	3584.10	1.87

Table 6.2 Examining buckling failure criteria of different diameters pile in RCD soil under scaled IMV motion

d (m)	S (^{0})	P (kN)	E (GPa)	D_L (m)	D_F (m)	L_0 (m)	β	L_e (m)	r_{min} (m)	λ	σ_y (Mpa)	σ_{cb} (Mpa)	σ_f (Mpa)	σ (Mpa)	σ/σ_f
0.50	0	1330	27.4	10.8	3.2	15.0	2	30.0	0.125	240.0	13.38	4.69	3.47	6.78	1.95
	5	1330		9.9	3.2	14.1	2	28.2		225.6		5.31	3.80		1.78
0.75	0	2430	27.4	10.8	4.5	16.3	2	32.6	0.187	174.3	13.38	8.89	5.34	5.50	1.03
	5	2430		9.9	4.5	15.4	2	30.8		164.7		9.96	5.71		0.96
1.0	0	4280	27.4	10.8	5.6	17.4	2	34.8	0.25	139.2	13.38	13.94	6.83	5.45	0.80
	5	4280		9.9	5.6	16.5	2	33.0		132.0		15.50	7.18		0.76

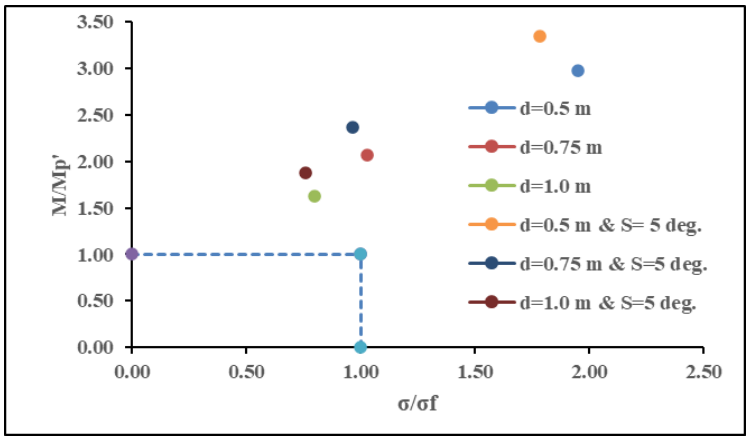

Fig. 6.22 Bending-buckling interaction diagram of different diameters pile in level and sloping RCD soil under scaled IMV motion

Tables 3 and 4 examines the bending and buckling failure criteria respectively for 0.5 m diameter pile in level and 5-degree sloping RCD soil profile under BHJ, scaled IMV and IMV input motions and Fig.6.23 is the bending-buckling interaction diagram for the same. As the liquefaction of soil is dependent on both the characteristics of soil and input motion, bending-buckling interaction is greatly influenced by PGA of input motion. Bending and buckling co-efficient increases many times due to increase of PGA for both level and 5-degree sloping ground. As all the points in the graph are outside the safe area shown with dotted line, 0.5 m diameter pile is unsafe in level and 5-degree sloping ground under considered input motions.

Table 6.3 Examining bending failure criteria of 0.5 m diameter piles in RCD soil under different ground motions

GM	S (^{0})	P (kN)	f_{ck} (MPa)	P_y (kN)	M_p(kN-m)	Mp'(kN-m)	M(kN-m)	M/Mp'
BHJ	0	1330	30	3944.6	279	224.38	307.24	1.37
	5	1330				224.38	320.11	1.43
Scaled IMV	0	1330	30	3944.6	279	224.38	667.45	2.97
	5	1330				224.38	751.09	3.35
IMV	0	1330	30	3944.6	279	224.38	953.32	4.25
	5	1330				224.38	1108.86	4.94

Table 6.4 Examining buckling failure criteria of 0.5 m diameter piles in RCD soil under different ground motions

GM	S (^{0})	P (kN)	E (GPa)	D_L (m)	D_F (m)	L_0 (m)	β	L_e (m)	r_{min} (m)	λ	σ_y (Mpa)	σ_{cb} (Mpa)	σ_f (Mpa)	σ (Mpa)	σ/σ_f
BHJ	0	1330	27.4	8.5	3.2	12.7	2	25.4	0.125	203.2	13.38	6.54	4.39	6.78	1.54
	5	1330		10.0	3.2	14.2	2	28.4		227.2		5.23	3.76		1.80
Scaled IMV	0	1330	27.4	10.8	3.2	15.0	2	30.0	0.125	240.0	13.38	4.69	3.47	6.78	1.95
	5	1330		9.9	3.2	14.1	2	28.2		225.6		5.31	3.80		1.78
IMV	0	1330	27.4	13.5	3.2	17.7	2	35.4	0.125	283.2	13.38	3.37	2.69	6.78	2.52
	5	1330		13.8	3.2	18.0	2	36.0		288.0		3.26	2.62		2.59

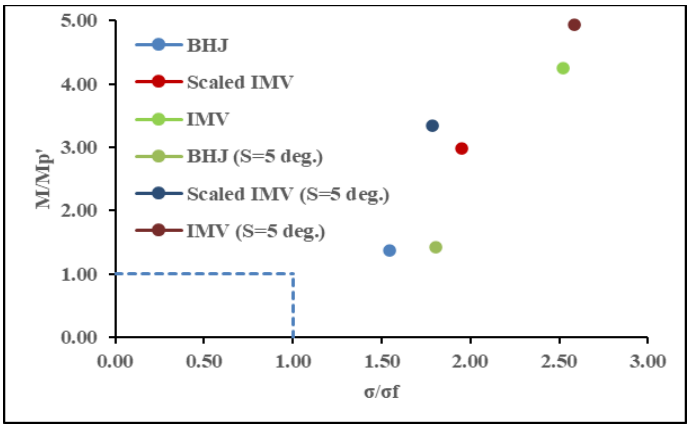

Fig. 6.23 Bending-buckling interaction diagram of 0.5 m diameter piles in level and sloping RCD soil under different ground motions

Finally, Tables 5 and 6 examines the bending and buckling failure criteria respectively for 0.5 m diameter pile in 0, 2.5, 5.0 and 10.0 degree sloping RCD soil profile under scaled IMV motion and Fig.6.24 is the bending-buckling interaction diagram for the same. It is observed that 0.5 m diameter pile is unsafe in both bending and buckling for all the ground slopes as all the point in the diagram are outside the safe area. So, for design of piles in liquefiable sloping ground proper selection of pile section and material strength is utmost important to avoid bending and buckling failure.

Table 6.5 Examining bending failure criteria of 0.5 m diameter piles in RCD soil for different ground slopes

S (^{0})	P (kN)	f_{ck} (MPa)	P_y (kN)	M_p(kN-m)	Mp'(kN-m)	M(kN-m)	M/Mp'
0	1330	30	3944.6	279	224.38	667.45	2.97
2.5	1330	30			224.38	727.57	3.24
5.0	1330	30			224.38	751.09	3.35
10.0	1330	30			224.38	785.60	3.50

Table 6.6 Examining buckling failure criteria of 0.5 m diameter piles in RCD soil for different ground slopes

S (^{0})	P (kN)	E (GPa)	D_L (m)	D_F (m)	L_0 (m)	β	L_e (m)	r_{min} (m)	λ	σ_y (Mpa)	σ_{cb} (Mpa)	σ_f (Mpa)	σ (Mpa)	σ/σ_f
0	1330	27.4	10.8	3.2	15	2	30.0	0.125	240.0	13.38	4.69	3.47	6.78	1.95
2.5	1330		10.4	3.2	14.6	2	29.2		233.6		4.95	3.61		1.88
5.0	1330	27.4	9.9	3.2	14.1	2	28.2		225.6		5.31	3.80		1.78
10.0	1330		10.2	3.2	14.4	2	28.8		230.4		5.09	3.69		1.84

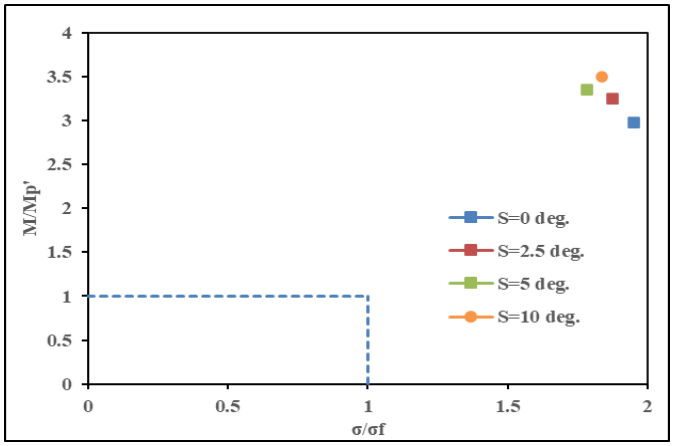

Fig. 6.24 Bending-buckling interaction diagram of 0.5 m diameter piles in RCD soil for different ground slopes under scaled IMV motion

Chapter 7

Summary and Conclusions

7.1 Summary

1D nonlinear GRA has been conducted for two typical soil profile of Kolkata city using three widely distinct strong ground motions to study the behaviour of typical Kolkata soil. Two typical soil profile of Kolkata city such as Normal Kolkata Deposit (NKD), and River Channel Deposit (RCD) have been chosen for this study. The input motions considered for present analysis are 1940 Imperial Valley, 2001 Bhuj and 2011 Sikkim earthquakes. The procedure of obtaining the required input parameters for modelling the materials of each soil layer from field and laboratory tests are presented. The main objective of the present study is how the ground response and liquefaction susceptibility would be if these considered scenario earthquake motions are experienced at bedrock level. Also, liquefaction-induced damage to building supported on pile foundation during earthquake is presented in this study using a reported case study on damages to the Kandla Port building during the 2001 Bhuj earthquake in India. The 22.0 m high six-storied RCC frame building supported on combined pile-raft foundation was tilted towards sea side after this earthquake. The effective stress-based ground response analysis (GRA) of the port site has been carried out using nonlinear finite element program Cyclic1D considering nonlinearity of soil.

A finite element based BNWF numerical model has been developed using the open-source software platform OpenSees to study the static response of single pile in homogenous cohesionless soil and seismic response of laterally load single pile in liquefiable multi-layered sloping ground of Kandla Port site considering both kinematic and inertial effects. The present model is validated with the theoretical solution and past case study. The effects of different parameters such as ground slope, *L/d* ratio of pile, pile head fixity condition, existence of liquefiable layer, depth of liquefiable soil layer and embedment depth of pile on kinematic pile response are also evaluated.

Then, three-dimensional numerical study using an advanced nonlinear finite-element based computer program OpenSeesPL has been carried out to investigate the dynamic response of soil-pile system in liquefiable layered soil of Kolkata city under the influence of axial Loading. The same soil profile such as Normal Kolkata Deposit (NKD), and River Channel Deposit (RCD) have considered to replicate typical soil layers of Kolkata metropolitan city. Two acceleration time histories, viz., Imperial Valley (1940) and Bhuj (2001), have been considered in the present analysis, and their PGA values are well within the reported range of Kolkata city. The present model is validated with the experimental results prior to carrying out parametric study. Then, a detailed systematic parametric study is performed for numerical simulation of pile failures in layered soil deposit of Kolkata city in liquefiable and non-liquefiable condition by taking into account various soil, pile parameters and ground motion characteristics.

Next, the same 3D numerical model has been used for dynamic analysis of piles in liquefiable multi-layered sloping ground considering the effect of static axial load as well as ground motions simultaneously. Parametric study has been conducted systematically to evaluate the effect of ground slope, soil type, input ground motion, pile *L/d* ratio, pile head fixity condition and depth of ground water table (*GWT*) on dynamic response of soil-pile system.

7.2 Conclusions

The major conclusions from the results of nonlinear ground response analysis are as follows:

- The study shows that the acceleration is reduced at the surface in case of IMV and SIKM motions and magnified in case of BHJ motion for NKD soil, although the IMV motion had the highest maximum bedrock level acceleration (MBRA). Thus, BHJ earthquake motions caused higher acceleration magnifications at NKD soil as compared to other motions because of its large bracketed duration and frequency contentment. The acceleration is reduced for RCD soil for all the considered earthquake motions. As stiffness of top soil of RCD is comparatively lower than NKD soil, the reduction of MBRA is more at surface of RCD soil.
- The PGA at surface level varies in a small range of 0.109g to 0.119g for NKD soil and 0.072g to 0.091g for RCD soil in spite of wide variation of the MBRA used in the analysis. Hence, the MBRA has little influence over the surface PGA.
- Peak spectral acceleration obtained in this study varies in the range of 0.51g to 0.67g for NKD soil and 0.33g to 0.46g for RCD soil which are beneficial for the

design of earthquake resistant structures. From response spectra, it is observed that IMV and BHJ motions have immense effect on long period structures resting on soft soil and SIKM motions are vulnerable for short period structure resting on soft soil, respectively.

- The PGA and PGD value at surface increases by almost 39% and 37% respectively for RCD soil for BHJ earthquake motion with variation of ground water table (*GWT*) depth from surface to 5.0m depth below surface. Large value of PGA and PGD is observed for mildly-inclined slope site even for low MBRA indicating the tendency of lateral spreading of RCD. So, the fluctuation of GWT and topography of site has significant influence on seismic ground response in addition to the input motion characteristics, local soil condition.
- The large shear strain is observed for depth 0 to 12.0 m of RCD soil. The large shear strain value gives an idea of probability of liquefaction hazard at considered site.
- As this nonlinear analysis is effective stress-based approach, it presents the variation of pore pressure with depth which is useful to predict liquefaction evaluation of soil. In present study, the excess pore pressure ratio is less than 1.0 in all the soil layers of NKD soil but the ratio is more than 1.0 at top 12.0 m of RCD soil indicating the top soil layers are prone to liquefaction.
- FOS/FOSD of RCD soil using both Simplified deterministic method and nonlinear dynamic method is less than 1 for top 12.0 m soil. So, top soil of RCD is highly liquefiable under BHJ earthquake motion.
- It is found that top 12 m soil of RCD is mainly contribute the total post-liquefaction settlement because of presence of saturated silty fine sand. Also, Post-liquefaction settlement reduces drastically due to change of location of *GWT*.

The key conclusions from the present analysis of Kandla Port case study are as follows:

- The acceleration at the ground surface does not magnify significantly with respect to MBRA for the Kandla port site under Bhuj earthquake.
- 12.0 m thick intermediate loose to medium dense saturated sand below soft clay strata is potentially liquefiable under 2001 Bhuj earthquake motion.

- The post-earthquake observed ground settlement of 0.3 m is matching well with the evaluated post-liquefaction settlement of 0.288 m obtained from present study.
- The field-observed lateral spreading of 0.8 to 1.0 m is also consistent with the present results of lateral spreading analysis.
- The pile foundation travel through non-liquefiable layer and terminated in liquefiable soil can experience undue settlement. This exercise can be avoided as far as possible in practical situation.

The key conclusions from the results of static response of single pile in homogenous cohesionless soil are as follows:

- The relative density of soil has profound influence on pile response. The maximum bending moment of free head and fixed head long pile is reduced by 41.10% and 45.60% respectively for changes of relative density from loose to dense.
- The depth of point of contra flexure from ground surface decreases with the increase of relative density of soil.
- The rigid or flexible nature of pile is extremely dependent on *L/d* ratio and pile head fixity. Pile of *L/d* less than 10 behaves like short rigid pile and more than 10 behaves like long pile.
- Pile having *L/d* ratio 10 undergoes significant negative displacement. The maximum negative displacement occurred at the base of the pile. The same is occurred in between inflection point and the base of pile for *L/d* ratio 30 in loose sand. The soil reaction is 46.80% more for pile having *L/d* ratio 10 than other *L/d* ratio of pile in loose sand.
- The lateral displacement of pile having *L/d* ratio 30 for loose and dense sand is reduced by 69.75% and 73.90% respectively when the pile head fixity changes from free to fixed head condition.

The following major conclusions are derived based on the results of pseudo-static analysis of laterally load single pile in liquefiable multi-layered sloping ground:

- The bending response at pile head is mainly governed by the inertial loading and it diminishes rapidly below pile head. The kinematic response of pile is predominant at greater depth for liquefiable sloping ground. So, proper combination of kinematic and

inertial interaction effects should be considered for seismic design of pile foundations in liquefiable sloping ground.

- The seismic response of pile is significantly influenced by the ground slope. The highest PGD value observed for 2.5-degree ground slope. The distribution of PGD profile is almost constant for top non-liquefiable crust and linearly decreases in liquefiable layer and becomes negligible at the bottom of the liquefiable layer for all the ground slopes except 8-degree. PGD is almost constant from 10 m to 30 m for slope of 8 degree is due to movement of whole liquefiable soil layer together owing to liquefaction-induced lateral spreading because of higher inclination. The peak lateral displacement and bending moment coefficient are magnified by 22 and 5 times respectively when the slope of ground changes from 0-degree to 2.5-degree. So, pile foundation in sloping ground may be damaged during earthquake due to kinematic bending arising from lateral spreading.

- The peak lateral pile displacement coefficient decreases by 52% and peak bending moment developed in the pile increases by 163% when the pile diameter increases from 0.4 m to 1.0 m. However, the peak bending moment coefficient (*M/Mp*) decreases by 83.33 % due to change of pile diameter from 0.4 m to 1.0 m. This is because of increase of load carrying capacity of pile with pile diameter. Large diameter pile can sustain a large bending moment. *M/Mp* ratio more than 1.0 for pile diameter of 0.4 m indicates the kinematic bending failure of pile of Kandla port building using Bhuj earthquake. So, use of large diameter pile is recommended to avoid kinematic bending failure in liquefiable sloping ground.

- The boundary condition of pile head has a profound influence on seismic response of pile foundation. For free head pile, the peak bending moment occurs at 6.25d above the interface of liquefiable and non-liquefiable layer due to discontinuity of shear strain of soil across the interface. However, for fixed head pile, the peak bending moment occurs at pile head as well as 6.25d above the interface of liquefiable and non-liquefiable layer. The peak bending moment at the pile head is almost one-fourth of the peak bending moment at interface.

- The lateral pile displacement coefficient is magnified at the liquefiable condition of intermediate layer and magnification factor is 3.5 considering kinematic effects only. However, the maximum kinematic bending moment at the interface at liquefiable

condition of intermediate layer is less with compared to the non-liquefiable condition. The maximum displacement coefficient in liquefied condition is increased because of reduction of soil strength and stiffness owing to liquefaction. However, the maximum kinematic bending moment is less in case of liquefiable condition because of reduction of stiffness contrast between the top non-liquefiable and intermediate liquefiable soil. So, for a particular soil profile and under same ground motion, the kinematic bending moment can be higher when the soil did not liquefy, with reference to the case when soil liquefies. The designer should be considered both extreme scenarios for safe and economical design.

- The depth of liquefiable layer and embedment of pile has a significant impact on the seismic response of soil-pile system. The bending moment developed in the pile is maximum when the depth of liquefiable layer is almost 22% and embedment depth is almost 45% of total length of pile. With subsequent increase of depth of liquefiable layer and decrease of embedment depth, the value of bending moment reduces significantly. This is because soil failed prior to pile failure during liquefaction and stresses developed in the soil exceeds shear strength of soil.
- It is observed that peak lateral displacement of pile occurs for embedment depth of five times the pile diameter and depth of liquefiable layer is almost 55% of total length of pile and reduces for further increase of embedment depth. However, the kinematic pile bending in liquefiable sloping ground increases with increasing embedment depth of pile.

The major conclusions from the results of three-dimensional dynamic study are as follows:

- The weight of the super structure on pile foundation has profound influence on depth of liquefaction. It is noteworthy that the depth of liquefaction decreases significantly adjacent to the pile with an increase of superstructure weight. Hence, it is recommended to use effective ground improvement techniques like dynamic compaction for liquefiable soil adjacent to pile foundations instead of adopting heavy pile section.
- The peak lateral displacement and bending moment decreases more in non-liquefiable condition with compared to the liquefiable condition due to decrease of axial load. So, kinematic force is predominant in liquefiable soil condition and inertial force is prevalent in non-liquefiable soil condition and mainly accountable for peak bending moment in the vicinity of pile head. Therefore, kinematic and inertial interaction

should be carefully considered for safe and reliable design of pile foundations under different soil conditions.

- The present results indicate that the laterally loaded slender end-bearing pile is prone to buckling failure mode in liquefiable soil when axial load on the pile exceeds certain percentage of P_{all} depending on the material and geometric properties of pile and input motion characteristics. Hence, it is recommended that larger diameter pile may be used in liquefiable soil to avoid buckling failure mode and thus is likely to fail because of bending also.
- Parametric studies reveal that bending and buckling failure mode can be avoided by selecting a suitable combination of material strength and pile geometry for designing of piles under combined axial and lateral load in liquefiable soil.
- It is observed that maximum kinematic bending moment is developed near the boundary between liquefiable and non-liquefiable layer due to stiffness contrast. Hence, extra care should be taken for designing of pile foundations in multi-layered soil profile as abrupt increase of bending moment may be occurred at the boundary due to change of soil stiffness.
- It is noticed that the NKD soil is non-liquefiable except top 1.0 m depth but RCD soil is liquefiable up to depth of 10.8 m for level ground condition under scaled IMV motion. However, depth of liquefaction is 10.75 m in NKD soil and 9.9 m in RCD soil for 5-degree ground slope under same input motion. Depth of liquefaction also increases from 10.0 m to 13.8 m when PGA of input motion increases from 0.106g to 0.348g in RCD soil for 5-degree ground slope. Also, depth of liquefaction decreases with an increase of depth of *GWT*. Hence, the depth of liquefaction is dependent on types of soil, ground motion characteristics, depth of *GWT* and topography of the ground.
- It is observed that the PGD value increases with an increase of ground slopes under a particular ground motion. The maximum value of PGD increases by 238.0% due to increase of ground slope from 0 degree to 10 degree under scaled IMV motion in RCD soil. The residual displacement at ground level increases from 4.55 mm to 62.2 mm when ground slope changes from 0 to 10-degree. So, mildly inclined liquefiable ground is susceptible to lateral spreading.
- The PGA amplification factor at ground surface does not change with ground slopes and the value is 1.26 for all the ground slopes in RCD soil. However, PGA is amplified

by 6.5 times in dry condition with respect to liquefiable condition under same input motion because of the higher strength of dry soil. Hence, effective stress based nonlinear ground response analysis is extremely necessary for liquefiable soil.

- It is observed from parametric studies that with slight increase of ground slope from 0 to 2.5 degree, peak bending moment co-efficient due to kinematic loading in RCD soil increases from 0.41 to 1.44. So, the pile which is safe against kinematic bending in level ground is unsafe in mildly sloping ground under same loading condition. Also, the maximum bending moment at ground surface increases significantly due to mass of the superstructure. Hence, it is necessary to consider both the kinematic and inertial interaction effect for piles in liquefiable sloping ground.
- The combined peak lateral displacement and bending moment co-efficient decreases by 62.60 % and 44.20 % respectively when *L/d* ratio decreases from 42 to 21 by increasing pile diameter from 0.5 m to 1.0 m in RCD soil. So, it is recommended to use larger diameter piles in liquefiable sloping ground for avoiding bending failure.
- The peak combined lateral displacement decreases by 48.7% and combined bending moment co-efficient of pile increases by 14.3% when soil condition changes from liquefiable to non-liquefiable condition in 5 degree sloping RCD soil. Hence, the designer should consider both liquefiable and non-liquefiable conditions for safe and economical seismic design of piles in liquefiable sloping ground.
- It is revealed that bending-buckling interaction diagram is extremely necessary for safe seismic design of piles in liquefiable sloping ground under combined action of axial and lateral load. Bending and buckling may be avoided by selecting suitable pile sections and material strength.
- The maximum kinematic bending moment develops at the boundary between liquefiable and non-liquefiable soil strata owing to stiffness contrast. Additional measures should be taken for seismic design of piles in multi-layered sloping ground. Due to abrupt change of soil stiffness at adjacent soil layer, large kinematic bending moment may develop causing failure of piles.

Hence, in absence of site-specific data, PGA and response spectrum curves obtained from present nonlinear ground response analysis are beneficial to the designers for safety assessment of the existing structures and designing of various new earthquake resistant structures in Kolkata city.

In contrast to the horizontal ground condition adopted in most of the earlier studies, it is very well understood that the laterally loaded pile responses in sloping ground is totally different due to kinematic effect. The present pseudo-static analysis methodology should be of interest to practising engineers as it provides step by step procedure for seismic design of laterally loaded piles in liquefiable and non-liquefiable level or sloping ground under kinematic and inertial loading.

The present dynamic analysis also indicates that the laterally loaded slender end-bearing pile is prone to buckling failure mode in liquefiable soil when axial load on the pile exceeds certain percentage of allowable load depending on the material and geometric properties of pile and input motion characteristics. Hence, bending-buckling interaction diagrams presented in this study are useful to the designers for safe and economical design of piles in liquefiable level and sloping ground of Kolkata city under combined loading scenario.

7.3 Limitations of the Present Study

The limitations of this study are as follow:

- In this study shear wave (V_s) of each layer is calculated using site specific co-relation between SPT-N and V_s for ground response analysis. However, in-situ testing may be conducted for predicting more reliable data of V_s. Also, field and laboratory test may be conducted for each soil layer to determine friction angles (φ) for cohesionless soils and undrained shear strength (C_u) for cohesive soil instead of empirical co-relation.
- Due to absence of site-specific strong motions data, 1940 Imperial valley, 2001 Bhuj and 2011 Sikkim earthquake motion whose PGA values are well within the reported range of the Kolkata City have been considered in this study for ground response analysis. It would be more realistic to perform ground response analysis using more numbers of ground motion including the low-frequency long duration earthquakes and recorded actual acceleration time-history in case of occurrence of earthquake in Kolkata City.
- Limitation of the present pseudo-static study is that only lateral soil-pile interaction has been considered without considering axial soil-pile interaction. Also, ultimate lateral resistance of soil is influenced by ground slope. However, this effect has not been considered in the present study. The whole study in this work is done by using the 2001 Bhuj earthquake motion only. As the soil response and thereby pile response

would depend on the base shaking being applied, further investigation deemed necessary with consideration of various other earthquake ground motions as input loading.

7.4 Scope of Future Work

The following suggestions are given as future scope of research in this area:

- The present study may be extended for seismic response of group of piles with various configurations.
- The behaviour of raker pile may be investigated using present methodology.
- Separate dynamic centrifuge testing may be performed to compare the results obtained from present numerical model for better validation.
- The acceleration time-history is applied in only one direction horizontal direction for dynamic analysis neglecting vertical accelerations as vertical load provides adequate factor of safety against vertical forces. However, combined effects may be studied as future scope.
- It is worthy to consider various end conditions of pile, dynamic effects of superstructure on axial force, more ground motion records and performing cyclic simple shear or cyclic triaxial shear test to carefully calibrate the model instead of SPT correlation for future scope.
- In this study, superstructure is modelled as lumped mass at pile head. However, response of piles with superstructure on it in liquefiable layered soil may be considered as future scope.

References

- Bhattacharya S (2003) Pile instability during earthquake liquefaction. Ph.D. Thesis, University of Cambridge, UK
- Kramer SL (2005) Geotechnical earthquake engineering. Pearson Education, London
- Elgamal A, Yan L, Yang Z, Conte JP (2008) Three-Dimensional Seismic Response of Humboldt Bay Bridge-Foundation-Ground System. J. Struct. Eng., 134(7), 1165
- Bao Y, Ye G, Ye B, Zhang F (2012) Seismic evaluation of soil–foundation–superstructure system considering geometry and material nonlinearities of both soils and structures. Soils and Foundations, 52(2): 257-278
- Mylonakis G, Nikolaou A, Gazetas G (1997) Soil–pile–bridge seismic interaction: kinematic and inertial effects. Part I: soft soil. Earthquake Engineering & Structural Dynamics, 26(3): 337-359
- Stewart JP, Fenves GL (1998) System identification for evaluating soil–structure interaction effects in buildings from strong motion recordings. Earthquake Engineering & Structural Dynamics, 27(8): 869-885
- Dash SR, Bhattacharya S (2012) Mechanism of failure of three pile-supported structures structure's failure of during three different earthquakes. In: Proceedings of 15 WCEE, LISBOA
- Choudhury D, Chatterjee K, Kumar A, Phule RR (2014) Pile foundations during earthquakes in liquefiable soils – theory to practice, In: Proceedings of 15th Symposium on Earthquake Engineering, IIT Roorkee, India, 327-342
- Dash SR, Govindaraju L, Bhattacharya S (2009) A case study of damages of the Kandla Port and Customs Office tower supported on a mat–pile foundation in liquefied soils under the 2001 Bhuj earthquake. Soil dynamics and Earthquake Engineering, 29(2): 333–346
- Bhattacharya S, Sarkar R, Huang Y (2012) Seismic Design of Piles in Liquefiable Soils. New Frontiers in Engineering Geology and the Environment, DOI: 10.1007/978-3-642-31671-5_3

- Rai DC, Mondal G, Singhal V, Parool N, Pradhan T (2012) 2011 Sikkim Earthquake: Effects on Building Stocks and Perspective on Growing Seismic Risk. In: Proceedings of 15 WCEE, LISBOA
- GovindaRaju L, Gunturi R, Hanumantharao C, Sitharam T (2004) Site-specific ground response analysis. Current science, 87: 1354-136
- Hanumantharao C, Ramana GV (2008) Dynamics soil properties for micro zonation of Delhi, India. J Earth Syst. Sci 117(S2):719–730
- Phanikanth VS, Choudhury D, Reddy GR (2011) Equivalent linear seismic ground response analysis of some typical sites in Mumbai. Journal of Geotechnical Geological Engineering 29(6): 1109-1126
- Desai SS, Choudhury D (2015) Site-specific seismic ground response study for nuclear power plants and ports in Mumbai. Natural Hazards Review 16(4): 04015002
- Sitharam TG, Anbazhagan P (2007) Seismic hazard analysis for the Bangalore region. Natural Hazards 40: 261-278
- Puri N, Jain A, Mohanty P, Bhattacharya S (2018) Earthquake Response Analysis of Sites in State of Haryana using DEEPSOIL Software. Procedia Computer Science 125 :357-366
- Satyam N, Towhata I (2016) Site-specific ground response analysis and liquefaction assessment of Vijayawada city (India). Natural Hazards. DOI: 10.1007/s11069-016-2166-7
- Shylamoni P, Choudhury D, Ghosh S, Ghosh AK, Basu PC (2014) Seismic ground response analysis of KK-NPP site in the event of NCO earthquake using DEEPSOIL. In: Geo-Congress 2014: geotechnical special publication no. GSP 234. ASCE, pp 840–849. doi:10.1061/9780784413272.082
- Boominathan A, Dodagoudar GR, Suganthi A, Maheswari RU (2008) Seismic hazard assessment of Chennai city considering local site effects. Journal of Earth System Science 117(S2):853-863
- Jishnu RB, Naik SP, Patra NR, Malik JN (2013) Ground response analysis of Kanpur soil along Indo-Gangetic Plains. Soil Dynamics and Earthquake Engineering 51: 47–57
- Naik NP, Choudhury D (2014) Comparative study of seismic ground responses using DEEPSOIL, SHAKE and D-MOD for soils of Goa, India. In: Geo-Congress 2014:

geotechnical special publication no. GSP 234. ASCE, pp 1101–1110. doi: 10.1061/9780784413272.107

- Vivek BS, Mohanty S (2016) 1D Ground Response Analysis of Bhubaneswar Soil in India. In: Sixth International Conference on Recent Advances in Geotechnical Earthquake Engineering and Soil Dynamics, IIT Roorkee Extension Centre, 20 Knowledge Park II, Greater Noida, India
- Kumar SS, Krishna AM (2013) Seismic ground response analysis of some typical sites of Guwahati city. International Journal of Geotechnical Earthquake Engineering 4(1):83-101
- Kumar SS, Dey A, Krishna AM (2014) Equivalent linear and nonlinear ground response analysis of two typical sites at Guwahati city. In: Proceedings of Indian Geotechnical Conference IGC-2014, Kakinada, India
- Ajom BE, Bhattacharjee (2017) Advanced Non-Linear Finite-Element Model for Site Response Analysis of a Saturated Layered Soil Profile. In: Indian Geotechnical Conference 2017 GeoNEst, IIT Guwahati, India
- Shukla J, Choudhury D (2012) Seismic hazard and site-specific ground motion for typical ports of Gujarat. Natural hazards 60(2): 541-565
- Rao VD, Choudhury D (2020) Estimation of Shear Wave Velocity and Seismic Site Characterization for New Nuclear Power Plant Region, India. Natural Hazards Review 21(4): 06020004
- Rao VD, Choudhury D (2020) Probabilistic modelling for earthquake forecasting in the northwestern part of Haryana state, India. Pure and Applied Geophysics 177(7): 3073-3087
- Rao VD, Choudhury D (2021) Deterministic Seismic Hazard Analysis for the Northwestern Part of Haryana State, India, Considering Various Seismicity Levels. Pure and Applied Geophysics 178(2): 449-464
- Desai SS, Choudhury D (2014) Spatial variation of probabilistic seismic hazard for Mumbai and surrounding region. Natural hazards 71(3): 1873-1898
- Akhila M, Ghosh C, Satyam N (2012) Detailed Ground Response Analysis at Park Hotel in Kolkata City, India. In: 15th World conference on Earthquake Engineering (15 WCEE), Lisbon, Portugal, Paper No:5158
- Govindaraju L, Bhattacharya S (2012) Site-specific earthquake response study for hazard assessment in Kolkata city, India. Nat Hazards 61:943–965

- Roy N, Sahu RB (2012) Site specific ground motion simulation and seismic response analysis for microzonation of Kolkata. Geomechanics and Engineering 4(1):1-18
- Chatterjee K, Choudhury D (2016) Influences of Local Soil Conditions for Ground Response in Kolkata City During Earthquakes. Proceedings of the National Academy of Sciences, India Section A: Physical Sciences 88: 515–528
- Chatterjee K (2018) Impact of Ground Response Analysis on Seismic Behavior and Design of Piles in Kolkata City. Indian Geotech Journal 48(3):459–473
- Shiuly A, Sahu,RB , Mandal S (2015) Seismic Microzonation of Kolkata. Geomechanics and Engineering 9(2):125-144
- Seed B, Idriss IM (1971) Simplified procedure for evaluating soil liquefaction potential. Journal of Geotechnical Engg, Division, ASCE 97(9):1249-1273
- Seed HB, Tokimatsu K, Harder LF, Chung RM (1985) The influence of SPT procedures in soil liquefaction resistance evaluations. J Geotech Eng 111(12):1425–1445
- Boulanger RW, Idriss IM (2014) CPT and SPT based liquefaction triggering procedures. Report No. UCD/CGM-14/01, Center for Geotechnical Modeling, University of California, Davis
- Filali K, Sbartai B (2017) A comparative study between simplified and nonlinear dynamic methods for estimating liquefaction potential. Journal of Rock Mechanics and Geotechnical Engineering 9 :955-966
- McVay M, Casper R, Shang TI (1995) Lateral Response of Three-Row Groups in Loose to Dense Sands at 3D and 5D Pile Spacing. Journal of Geotechnical Engineering, 121(5): 436-441
- McVay M, Zhang LM, Molnit T, Lai P (1998) Centrifuge testing of large laterally loaded pile groups in sands. Journal of Geotechnical and Geoenvironmental Engineering, 124(10): 1016-1026.
- Brown DA, Morrison C, Reese LC (1988) Lateral load behavior of pile group in sand. J. Geotech. Engng., Am. Soc. Civ. Engrs. 114(11): 1261-1276
- Rollins KM, Peterson KT, Weaver TJ (1998) Lateral load behavior of fullscale pile group in clay. Journal of Geotechnical and Geoenvironmental Engineering, 124(6): 468-478

- Rollins KM, Olsen RJ, Egbert JJ, Jensen DH, Olsen KG, Garrett BH (2006) Pile Spacing Effects on Lateral Pile Group Behavior: Load Tests. Journal of Geotechnical and Geoenvironmental Engineering, 132(10): 1262-1271
- Matlock H, Reese LC (1960) Generalized solutions for laterally loaded piles. J. of Soil Mechanics and Foundation Div., ASCE 86(5): 63-91
- Hansen JB (1961) Ultimate resistance of rigid piles against transversal forces. Geoteknisk Institut -- Bulletin (Danish Geotechnical Institute -- Bulletin), 12 (59)
- Broms BB (1964a) Lateral Resistance of Piles in Cohesive Soils. Journal of Soil Mechanics and Foundation Engineering Division, ASCE 90 (2):27–64
- Broms BB (1964b) Lateral Resistance of Piles in Cohesionless Soils. Journal of Soil Mechanics and Foundation Engineering Division, ASCE 90 (3): 123–158
- Reese LC, Welch RC (1975) Lateral loading of deep foundations in stiff clay. Journal of the Geotechnical Engineering Division, 101(7): 633-649
- Randolph MF (1977) A theoretical study of the performance of piles. PhD, University of Cambridge
- Poulos HG (1971a) Behavior of laterally loaded piles: I – single piles. J. Soil Mech. Fdn Div., Am. Soc. Civ. Engrs. 97(5): 711-731
- Poulos HG (1971b) Behavior of laterally loaded piles: II – pile groups. J. Soil Mech. Fdn Div., Am. Soc. Civ. Engrs. 97(5): 733-751
- Banerjee PK, Davies TG (1978) The behavior of axially and laterally loaded single piles embedded in nonhomogeneous soils. Geotechnique 28(3): 309-326
- Poulos HG, Davis EH (1980) Pile Foundation Analysis and Design. John Wiley & Sons, New York.
- Allotey N, El Naggar MH (2008) A numerical study into lateral cyclic nonlinear soil-pile response. Canadian Geotechnical Journal, 45(9): 1268-1281
- Zhang L (2009) Nonlinear analysis of laterally loaded rigid piles in cohesionless soil. Computers and Geotechnics, 36(5): 718-724
- Reese LC, Cooley LA, Radhakrishnan N (1984) Laterally loaded piles and computer program COM624G. Tech. Rep. K-84-2, U.S. Army Engineer Waterways Experiment Station, Vicksburg, Miss
- Davisson MT (1970) Lateral load capacity of piles. Highway Res. Rec. 333: 104-112
- Reese LC, Matlock H (1956) Non-dimensional Solutions for Laterally Loaded Piles with Soil Modulus Assumed Proportional to Depth, Proceedings Eighth Texas

Conference on Soil Mechanics and Foundation Engineering, Special Publication No. 29, Bureau of Engineering Research, University of Texas, Austin, TX.

- Matlock H (1970) Correlations for design of laterally loaded piles in soft clay. In: Proc. 2nd Offshore Tech. Conf., Houston, Texas, 1, 577-594
- Reese LC, Cox WR, Koop FD (1974) Analysis of laterally loaded piles in sand. In: Proc. 6th Offshore Tech. Conf., Houston, Texas, 2, 473-483
- Reese LC, Welch RC (1975) Lateral loading of deep foundations in stiff clay. Journal of the Geotechnical Engineering Division, 101(7): 633-649
- Reese LC, Wang ST (1986) Method of Analysis of Piles under Lateral Loading. ASTM, Shanghai, China, 199-211
- Brown DA, Shie CF (1991) Modification of p-y curves to account for group effects on laterally loaded piles. In: Proc. Congress Geotech. Engng. Div. 1, Am. Soc. Civ. Engrs., 479-489
- McVay M, Zhang L, Molnit T, Lai P (1998) Centrifuge testing of large laterally loaded pile groups in sands. J. Geotech. Geoenv. Engng., Am. Soc. Civ. Engrs. 124(10): 1016-1026
- Reese LC, Isenhower WM, Wang ST (2006) Analysis and design of shallow and deep foundations. John Wiley & Sons, Inc
- Randolph MF (1981) Response of flexible piles to lateral loading. Geotechnique, 31(2): 247-259
- Kooijman AP, Vermeer PA (1988) Elastoplastic analysis of laterally loaded piles. In: Proc. 6th Int. Conf. Num. Meth. Geomech., Innsbruck, Austria. 2, 1033-1042
- Bhowmik SK, Long JH (1991) An analytical investigation of the behavior of laterally loaded piles. In: Proc. Congress Geotech. Engng. Div. 2, Am. Soc. Civ. Engrs, 1307-1318
- Bezgin O, Najm H, Nassif H (2004) Modeling of Laterally Loaded Shaft Foundations Using Continuous Soil Medium. In: Proceedings of Proc., Structures Congress 2004, ASCE, Nashville, Tennessee, USA, 137
- Muqtadir A, Desai CS (1986) Three-dimensional analysis of a pile-group foundation. International Journal for Numerical and Analytical Methods in Geomechanics, 10(1): 41-58
- Brown DA, Shie CF (1990) Numerical experiments into group effects on the response of piles to lateral loading. Computers and Geotechnics, 10(3): 211-230

- Zhang L, McVay MC, Lai P (1999) Numerical analysis of laterally loaded 3×3 to 7×3 pile groups in sands. J. Geotech. Geoenv. Engng., Am. Soc. Civ. Engrs. 125(11): 936-946
- Karasev OV, Talanov GP, Benda SF (1977) Investigation of the work of single situ-cast piles under different load combinations, Journal of Soil Mechanics and Foundation Engineering, 14(3): 173-177
- Trochanis AM, Bielak j, Christiano P (1991) Three-dimensional nonlinear study of piles. Journal of Geotechnical Engg, 117(3): 429-447
- Anagnostopoulos C, Georgiadis M (1993) Interaction of axial and lateral pile responses. J. Geotech. Engg: ASCE 119 (4): 793–798
- Karthigeyan S, Ramakrishna VVGST, Rajagopal K (2006) Influence of vertical load on the lateral response of piles in sand, Computer and Geotechnics, 33: 121-131
- Karthigeyan S, Ramakrishna VVGST, Rajagopal K (2007) Numerical investigation of the effect of vertical load on the lateral response of piles. J. Geotech. Geoenviron. Eng.: ASCE 133 (5): 512–521
- Achmus M, Thieken K (2010) On the behaviour of piles in non-cohesive soil under combined horizontal and vertical loading. Acta Geotechnica, 5(3):199-210
- Hussien MN, Tobita T, Iai S, Rollins KM (2011) Vertical load effect on the lateral pile group resistance in sand response. Geomechanics and Geoengineering, 7(4):263-82
- Hussien MN, Tobita T, Iai S, Karray M (2014) On the influence of vertical loads on lateral response of pile foundation. Computers and Geotechnics, 55:392-403
- Chatterjee K, Choudhury D (2015) Analytical and numerical approaches to compute the influence of vertical load on lateral response of single pile. Japanese Geotechnical Society Special Publication, In: 15th Asian Regional Conference on Soil Mechanics and Geotechnical Engineering
- Chatterjee K, Choudhury D, Rao VD, Mukherjee SP (2015a) Dynamic analyses and field observations on piles in Kolkata city. Geomechanics and Engineering, 8(3): 415-440
- Chatterjee K, Choudhury D, Poulos HG (2015b) Seismic analysis of laterally loaded pile under influence of vertical loading using finite element method. Computers and Geotechnics 67:172-186

- Hazzar L, Hussien MN, Karray M (2017) Investigation of the influence of vertical load on lateral response of pile foundations in sands and clays. Journal of Rock Mechanics and Geotechnical Engineering, 9: 291-304
- EN1998-5 (2004). Eurocode 8 - Design provisions for earthquake resistance of structures- Foundations, retaining structures and geotechnical aspects
- JRA (2019). Specifications for highway bridges. Japan Road Association, Preliminary English Version, prepared by Public Works Research Institute (PWRI) and Civil Engineering Research Laboratory (CRL), Japan, November
- ASCE 7 (2022) Minimum Design Loads for Buildings and Other Structures
- AASHTO LRFD (2020) Bridge Design Specifications
- ISO 23469 (2005) Bases for design of structures — Seismic actions for designing geotechnical works
- IS: 1893-Part 1 (2016) Criteria for earthquake resistant design of structure. Bureau of Indian Standards, New Delhi, India
- NEHRP (2020) Recommended Seismic Provisions for New Buildings and Other Structures
- Caltrans (2011) Guidelines on Foundation Loading Due to Liquefaction Induced Lateral Spreading
- Feng S, Wang J (2006) Research on lateral resistance on pile in saturated sand under shake loading. In: GeoShanghai International Conference, 6–8 June
- Cubrinovski M, Kokusho T, Ishihara K (2006) Interpretation from large scale shake table test on piles undergoing lateral spreading in liquefied soil. Soil Dynamics and Earthquake Engineering, 26 (2–4): 275–286. doi:10.1016/j.soildyn.2005.02.018
- Su D, Li XS (2006) Effect of shaking intensity on seismic response of single-pile foundation in liquefiable soil. Ground modification and seismic mitigation. ASCE, 379–386
- Dungca JR et al. (2006) Shaking table tests on the lateral response of a pile buried in liquefied sand. Soil Dynamics and Earthquake Engineering, 26 (2–4): 287–295 doi:10.1016/j.soildyn.2005.02.021Ebeido
- Li P, Lu X, Chen Y (2006) Study and analysis on shaking table tests of dynamic interaction of soil-structure considering soil liquefaction. In: 4th international conference on earthquake engineering, Taipei, Taiwan

- Elgamal A et al. (2006) Liquefaction-induced lateral load on piles. In: 4th International conference om Earthquake Engineering, Taipei, Taiwan 145
- He L et al. (2008) Shadowing and group effects for piles during earthquake-induced lateral spreading, In: Proceedings of the 14th world conference on earthquake engineering, Beijing, China
- Tang L et al. (2009) Case studies on shaking table test of Soil- pile Groups-bridge Structure Interaction in Liquefiable Ground, Critical issues in transportation system planning development and management. ASCE, 934–941
- Motamed R, Towhata I (2010) Shaking table model test on pile groups behind quay walls subjected to lateral spreading. Journal of Geotechnical and Geoenvironmental Engineering, 136 (3): 477–498. doi:10.1061/(ASCE) GT.1943-5606.0000115
- Haeri SM et al. (2012) Response of group of piles to liquefaction induced lateral spreading by large scale shake table testing. Soil Dynamics and Earthquake Engineering, 38: 25–45. doi:10.1016/j.soildyn.2012.02.002
- Chen CH, Sueng T, Chen CH (2012) Shaking table tests on model pile in saturated sloping ground. In: The 15th World Conference on Earthquake Engineering, LISBOA, 24–28
- Motamed R et al. (2013) Pile group response to liquefaction-induced lateral spreading: e-Defence large shake table test. Soil Dynamics and Earthquake Engineering, 51: 35–46 doi:10.1016/j. soildyn.2013.04.007
- Ling XZ, Gao X, Su L (2014) Effect of shaking intensity on interactive behavior of soil-pile group foundation in liquefiable soil during shaking table test. International efforts in lifeline earthquake engineering. In: Proceedings of the sixth China-Japan-US Trilateral Symposium on lifeline earthquake engineering, ASCE, 616–623
- Hall FE, Lombardi D, Bhattacharya S (2018) Identification of transient vibration characteristics of pile-group models during liquefaction using wavelet transform. Engineering Structures, 171, 712–729. doi:10.1016/j.engstruct.2018.06.028
- Zhanfang H et al. (2020) Vertical bearing capacity of a pile-liquefiable sandy soil foundation under horizontal seismic force. PloS one, 15 (3). doi:10.1371/journal. pone.0229532
- Wilson DW (1998) Soil-pile-superstructure interaction in liquefying sand and soft clay, Ph.D. Dissertation, University of California at Davis

- Haigh SK, Madabhushi SPG (2002) Centrifuge Modelling of Lateral Spreading past Pile Foundations. In: International Conference on Physical Modelling in Geotechnics, St John's, Newfoundland, Canada
- Boulanger RW et al. (2003) Pile foundations in liquefied and laterally spreading ground during earthquakes: centrifuge experiments and analysis. California: University of California, Davis and California Department of Transportation
- Abdoun T et al. (2003) Pile response to lateral spreads: centrifuge modelling. Journal of Geotechnical and Geoenvironmental Engineering, 129 (10): 869–878. doi:10.1061/(ASCE)1090-0241(2003)129:10(869)
- Iai S, Tobita T (2004) Centrifuge model tests on group piles in liquefiable and nonliquefiable ground. In: 13th world conference, Vancouver, B.C., Canada
- Hung WY et al. (2014) Seismic behavior of pile in liquefiable soil ground by centrifuge shaking table tests. Journal of Vibro engineering, 16 (6): 2712–2721.
- Zhang X et al. (2020a) Critical buckling load of pile in liquefied soil. Soil Dynamics and Earthquake Engineering, 135, 106–197. doi:10.1016/j.soildyn.2020.106197
- Chatterjee K, Choudhury D (2017) Influence of seismic motions on behaviour of piles in liquefied soils. Int J Number Anal Methods Geomech 1-26. DOI: https:/doi.org/10.1002/nag.2753
- Mylonakis G (2001) Simplified model for seismic pile bending at soil layer interfaces. Soils and Foundations 41(4):47–58
- Flores-Berrones R, Whitman RV (1982) Seismic response of end-bearing piles. Journal of Geotech. Engg. Div., ASCE 108(4): 554-569
- Dobry R, O'Rourke MJ (1983) Discussion on "Seismic response of end-bearing piles' by Flores-Berrones R., Whitman RV." J. Geotech. Engng Div., ASCE 109: 778-781
- Kavvadas M, Gazetas G (1993) Kinematic seismic response and bending of free-head piles in layered soil. Géotechnique 43(2): 207-222
- Poulos HG, Tabesh A (1996) Seismic response of pile foundations – Some important factors. In: Proceedings of 11th WCEE, Acapulco, paper No. 2085
- Nikolaou AS, Mylonakis G, Gazetas G, Tazoh T (2001) Kinematic pile bending during earthquakes analysis and field measurements. Geotechnique 51(5):425–440
- Dobry R, Abdoun T, O'Rourke TD, Goh SH (2003) Single piles in lateral spreads: field bending moment evaluation. Journal of Geotech Geoenviron Engg ASCE 129: 879-889

- Maiorano RMS, de Sanctis L, Aversa S, Mandolini A (2009) Kinematic response analysis of piled foundations under seismic excitations. Canadian Geotech Journal 46(5):571–584
- Sica S, Mylonakis G, Simonelli AL (2011) Transient kinematic pile bending in two-layer soil. Soil Dynamics and Earthquake Engineering 31(7):891–905
- Di Laora R, Mandolini A, Mylonakis G (2011) Kinematic bending moments at pile head in layered soil. In: Proceedings of 5th International Conference on Earthquake Geotechnical Engineering, Santiago, Chile
- Margason E, Halloway DM (1977) Pile design during earthquakes. In: Proceedings of 6th World Conf. Earthq. Engng, New Delhi, pp. 237-243
- Wu G, Finn WDL (1997) Dynamic nonlinear analysis of pile foundations using finite element method in the time domain. Canadian Geotechnical Journal 34: 44-52
- Bentley KJ, El Naggar MH (2000) Numerical analysis of kinematic response of single piles. Canadian Geotechnical Journal 37: 1368–1382
- Cai YX, Gould PL, Desai CS (2000) Nonlinear analysis of 3D seismic interaction of soil–pile–structure system and application. Engineering Structures 22(2): 191–199
- Mahesshwari BK, Truman KZ, Gould PL, El Naggar MH (2005) Three-dimensional nonlinear seismic analysis of single piles using finite element model: effect of plasticity of soil. International Journal of Geomechanics, ASCE 5(1): 35-44
- Cubrinovski M et al. (2004) 3-D Numerical simulation of shake-table tests on piles subjected to lateral spreading. In: TC4 Geotechnical earthquake engineering satellite conference, Osaka, Japan, pp. 199–206
- Kerciku AA et al. (2008) Fixity of pile foundations in seismically liquefied soils for buckling calculations- An eigenvalue analysis. In: Proceedings of 14th world conference on Earthquake, Engineering, Beijing, China
- Dash SR et al. (2008) p-y curve to model lateral response of pile foundations in liquefied soils. In: 14th World Conference on Earthquake Engineering, Beijing, China, 12–17
- Ren H, Lu X, Li P (2008) Computer simulation on dynamic soil-pile-structure interaction system considering liquefiable foundation. In:14th World Conference on Earthquake Engineering, Beijing, China

- Cheng Z, Jeremic B (2009) Numerical modeling and simulation of pile in liquefiable soil. Soil Dynamics and Earthquake Engineering, 29 (11–12): 1405–1416 doi:10.1016/j.soildyn.2009.02.008
- McGann CR, Arduino P, Mackenzie-Helnwein P (2011) Applicability of conventional py relations to the analysis of piles in laterally spreading soil. Journal of geotechnical and geoenvironmental engineering. 137(6): 557-567
- Maheshwari B, Sarkar R (2011) Seismic behavior of soil-pile structure interaction in liquefiable soils: parametric Study. International Journal of Geotechnical Engineering, 11 (4). doi:10.1061/(ASCE)GM.1943-5622.0000087
- Rahmani A, Pak A (2012) Dynamic behavior of pile foundations under cyclic loading in liquefiable soils. Computers and Geotechnics 40:114-126
- Phanikanth VS, Choudhury D, Reddy GR (2013) Behavior of single pile in liquefied deposits during earthquakes. International Journal of Geomechanics, 13 (4): 454–462 doi:10.1061/(ASCE)GM.1943- 5622.0000224
- Wang S, Orense RP (2014) Modelling of raked pile foundations in liquefiable ground. Soil Dynamics and Earthquake Engineering 64: 11-23
- Finn WL (2015) 1st Ishihara Lecture: An overview of the behavior of pile foundations in liquefiable and non-liquefiable soils during earthquake excitation. Soil Dynamics and Earthquake Engineering 68: 69-77
- Janalizadeh A, Zahmatkesh A (2015) Lateral response of pile foundations in liquefiable soils, Journal of Rock Mechanics and Geotechnical Engineering 7: 532-539
- Lombardi D, Bhattacharya S (2016) Evaluation of seismic performance of pile-supported models in liquefiable soils. Earthquake Engineering & Structural Dynamics, 45 (6): 1019–1038. doi:10.1002/eqe.2716
- Wang R, Liu X, Zhang JM (2016) Numerical analysis of the seismic inertial and kinematic effects on pile bending moment in liquefiable soils. Acta Geotechnica, 12 (4): 773–791 doi:10.1007/s11440-016-0487-z
- Oliaei M, Ghotbi Siabil SMA (2017) Dynamic behavior of large-diameter piles considering liquefaction under clay layer. Scientia Iranica A 24(6): 2665-2683
- Saeedi M et al. (2018) Numerical analysis of pile-soil system under seismic liquefaction. Engineering Failure Analysis, 94: 96–108. doi:10.1016/j.engfailanal.2018.07.031

- Zhang X. et al. (2018) Using peak ground velocity to characterize the response of soil-pile system in liquefying ground. Engineering Geology, 240: 62–73. doi:10.1016/j. enggeo.2018.04.011
- Ali Z (2019) Numerical analysis of pile foundation in liquefiable soils: parametric study. International Journal of Geotechnical Engineering. doi:10.1080/19386362.2019.1684655
- Chatterjee K, Choudhury D, Rao VD, Poulos HG (2019) Seismic response of single piles in liquefiable soil considering P-delta effect. Bulletin of Earthquake Engineering. DOI: https://doi.org/10.1007/s10518-019-00588-2
- Jimenez GAL, Dias D, Jenck O (2019) Effect of layered liquefiable deposits on the seismic response of soil-foundations-structure systems. Soil Dynamics and Earthquake Engineering 124: 1-15
- Li W et al. (2019) Response of pile groups with X and circular cross-sections subject to lateral spreading: 3D numerical simulations. Soil Dynamics and Earthquake Engineering, 126: 105774. doi:10.1016/j.soildyn.2019.105774
- Fiky EL, Metwally KG, Akl AY (2020) Effect of topsoil liquefaction potential on the seismic response of the embedded piles. Ain Shams Engineering Journal. doi:10.1016/j.asej.2020.03.002S
- Zhang X et al. (2020b) Effect of the combined action of lateral load and axial load on the pile instability in liquefiable soils. Engineering Structures, 205: 110074. doi:10.1016/j.engstruct.2019.110074
- Rajeswari JS, Sarkar R (2020) Estimation of transient forces in single pile embedded in liquefiable soil. International Journal of Geomechanics, 20 (9): 06020023 doi:10.1061/(ASCE)GM.1943-5622.0001788
- Sinha R, Sarkar R, Rajeswari JS (2020) Flexural Response of Pile Foundation in Liquefiable Soil Using Finite-Difference Formulation Following Pseudostatic Approach, Indian Geotechnical Journal 50(6):880-906
- Kwon SY, Yoo M (2020) Study on the Dynamic Soil-Pile-Structure Interactive Behavior in Liquefiable Sand by 3D Numerical Simulation. Appl. Sci. 10, 2723
- Mehdi E, Amir H, Kontoni DN, Maedeh S (2021) Numerical FEM assessment of soil-pile system in liquefiable soil under earthquake loading including soil-pile interaction. Geomechanics and Engineering 27(5): 465-479

- M K Pradhan, Praveen Kumar, V. S. Phanikanth, Deepankar Choudhury & K. Srinivas (2022) A review on design aspects and behavioral studies of pile foundations in liquefiable soil. Journal of Geomechanics and Geoengineering, https://doi.org/10.1080/17486025.2022.2052193
- Knappett JA, Madabhushi SPG (2005) Modelling of liquefaction-induced instability in pile groups. In: ASCE Geotechnical Special Publication No 145 on Seismic Performance and Simulation of Pile Foundations in Liquefied and Laterally Spreading Ground, University of California, Davis, California, United States, pp 255–267
- Kimura Y, Tokimatsu K (2007) Buckling stress of slender pile with lateral displacement at the pile head in liquefied soils. Journal of Structure and Construction Engineering 617:169–175
- Bhattacharya S, Madabhushi SPG, Bolton MD (2004) An Alternative Mechanism of Pile Failure in Liquefiable Deposits during Earthquakes, Géotechnique 54(3): 203-213
- Dash SR, Bhattacharya S and Blakeborough A (2010) Bending-buckling interaction as a failure mechanism of piles in liquefiable soils. Soil Dynamics and Earthquake Engineering 30(1-2): 32-39
- Knappett JA, Madabhushi SPG (2012) Effects of axial load and slope arrangement on pile group response in laterally spreading soils. Journal of Geotechnical and Geoenvironmental Engineering, ASCE 138: 799 – 809
- Bhattacharya S, Bolton MD, Madabhushi SPG (2005) A reconsideration of the safety of the piled bridge foundations in liquefiable soils. Soils and Foundation 45(4):13–26
- Bhattacharya S, Goda K (2013) Probabilistic buckling analysis of axially loaded piles in liquefiable soils. Soil Dynamics and Earthquake Engineering 45(2):13–24
- Mezazigh S, Levacher D (1998) Laterally loaded piles in sand: slope effect on p-y reaction curves. Can. Geotech. J. 35(3): 433–441
- Yasuda S, Ishihara K, Morimoto I, Orense R, Ikeda M, Tamura S (2000) Large Scale shake table tests on pile foundations in liquefied ground. In: Proc., 12th World Conference on Earthquake Engineering, Auckland, New Zealand
- Boominathan A, Ayothiraman R (2007) An experimental study on static and dynamic bending behavior of piles in soft clay. Geotech.Geologic. Eng. 25: 177–189
- Muthukkumaran K, Sundaravadivelu R, Gandhi SR (2008) Effect of slope on P-Y curves due to surcharge load. Soils and Foundations 48(3): 353 -361

- Georgiadis K, Georgiadis M (2010) Undrained Lateral Pile Response in Sloping Ground. Journal of Geotechnical and Geoenvironmental Engineering, ASCE 136 (11): 1489–1500
- Liyanapathirana DS, Poulos HG (2010) Analysis of pile behaviour in liquefying sloping ground. Computers and Geotechnics 37: 115–124
- Sawant VA, Shukla SK (2014) Effect of Edge Distance from the Slope Crest on the Response of a Laterally Loaded Pile in Sloping Ground. Geotechnical and Geology Engineering 32 (1): 197–204
- Muthukkumaran K (2014) Effect of Slope and Loading Direction on Laterally Loaded Piles in Cohesionless Soil. International Journal of Geomechanics, ASCE 14 (1): 1–7
- Muthukkumaran K, Almas Begum N (2015) Experimental Investigation of Single Model Pile Subjected to Lateral Load in Sloping Ground. Geotechnical and Geological Engineering Journal 33(4): 935–946
- Deendayal R, Muthukkumaran K, Sitharam TG (2016) Response of laterally loaded pile in soft clay on sloping ground. International Journal of Geotechnical Engineering 10 (1): 10–22
- Jegatheeswaran B, Muthukkumaran K (2016) Behavior of pile due to combined loading with lateral soil movement. International Journal of Geo-Engineering 7 (1): 1-10
- Deendayal R, Muthukkumaran K, Sitharam TG (2017) Development of Non-dimension p–y Curves for Laterally Loaded Piles in Sloping Ground. Indian Geotechnical Journal 47 (1): 47–56
- Deendayal R, Muthukkumaran K, Sitharam TG (2018) Analysis of laterally loaded group of piles located on sloping ground. International Journal of Geotechnical Engineering 14(2):1-9
- Peng W, Zhao M, Xiao Y, Yang C, Zhao H (2019) Analysis of laterally loaded piles in sloping ground using a modified strain wedge model. Computers and Geotechnics 107: 163–175
- Elgamal A, Yang Z, Lu J (2006) Cyclic1D: A Computer Program for Seismic Ground Response. Report No. SSRP-06/05, Department of Structural Engineering, University of California, San Diego, La Jolla, CA
- Yang Z, Lu J, Elgamal A (2004) A web-based platform for computer simulation of seismic ground response Advances in Engg. Software 35(5): 249-259

- Roy N, Shiuly A, Sahu RB, Jakka RS (2018) Effect of uncertainty in Vs-N correlations on seismic site response analysis. Journal of Earth System Science 127: 103
- Chatterjee K, Choudhury D (2013) Variations in shear wave velocity and soil site class in Kolkata city using regression and sensitivity analysis. Nat Hazards 69: 2057-2082
- Das BM (1983) Advanced Soil Mechanics. Taylor and Francis Publisher
- Seismosoft (2012) Seismosignal, version 5.00. *www.seismosoft.com*
- Elgamal A, Yang Z, Lu J (2015) Cyclic1D: Seismic Ground Response, Version 1.4, User's Manual, Department of Structural Engineering, University of California, San Diego, La Jolla, CA
- McKenna F, Fenves G (2001) The OpenSees Command Language Manual: version 1.2, Pacific Earthquake Engineering Research Center (PEER), University of California, Berkeley
- Newmark, NM (1959) A method of computation for structural dynamics. J. Engg. Mech. Div., ASCE 85(3): 67-95
- Parra E (1996) Numerical Modeling of Liquefaction and lateral Ground Deformation including Cyclic Mobility and Dilative Behavior is Soil Systems, PhD Dissertation, Department of Civil Engineering, Rensselaer polytechnic Institute, Try, NY
- Yang Z (2000) Numerical Modeling of Earthquake Site Response Including Dilation and Liquefaction, Ph.D. Dissertation, Dept. of Civil Engineering and Engineering Mechanics, Columbia University, New York
- Prevost JH (1985) A Simple Plasticity Theory for Frictional Cohesionless Soils. Soil Dynamics and Earthquake Engineering 4(1): 9-17
- Elgamal A, Yang Z, Parra E, Ragheb A (2003) Modeling of Cyclic Mobility in Saturated Cohesionless Soils. Int. J. Plasticity 19(6): 883-905
- Dash SR, Govindaraju L, Bhattacharya S (2009) A case study of damages of the Kandla Port and Customs Office tower supported on a mat–pile foundation in liquefied soils under the 2001 Bhuj earth-quake. Soil dynamics and Earthquake Engineering 29(2): 333–346
- Rajaram C, Kumar RP (2014) Vulnerability Assessment of Coastal Structure: A Study on Port Buildings, International Journal of Education and Applied Research, 4(2)

- Kramer SL, Smith MW (1997) Modified Newmark model for seismic displacements of complaint slopes. Journal of Geotechnical and Geoenvironmental Engineering 123(7): 635-644
- Bray JD, Rathje EM, Augello AJ, Merry SM (1998) Simplified seismic design procedures for geosynthetic-lined, solid waste land-fills. Geosynth Int 5(1-2): 203-235
- Bray JD, Travasarou T (2007) Simplified procedure for estimating earthquake-induced deviatoric slope displacements. Journal of Geotechnical and Geoenvironmental Engineering 133(4): 381-392
- Escudero JLM (2017) Simplified Procedures for Estimating Earthquake-Induced Displacements. Ph.D. Thesis, University of California, Berkeley
- Murthy VNS (2018) Text Book of Soil Mechanics and Foundation Engineering, Geotechnical Engineering Series, CBS Publishers and Distributors
- IS 2911- Part1 Section 4 (1984) Indian standard code of practice for design and construction of pile foundations, Bureau of Indian Standards, New Delhi
- API (2007) American Petroleum Institute Recommended practice for planning, design and constructing fixed offshore platforms. RP 2A-WSD, Washington, DC
- Boulanger RW, Curras CJ, Kutter BL, Wilson DW, Abghari A (1999) Seismic soil-pile-structure interaction experiments and analyses. ASCE Journal of Geotechnical and Geoenvironmental Engineering, Vol. 125(9): 750-759
- Boulanger RW (2000) The PySimple1, TzSimple1 and QzSimple1 Material Models. Documentation for the OpenSees platform. URL: http: //opensees.berkeley.edu
- IS 456 (200) Indian standard on plain and reinforced concrete-code of practice, Bureau of Indian Standards, New Delhi
- Finn WDL, Fujita N (2002) Piles in liquefiable soils: seismic analysis and design issues. Soil Dynamics and Earthquake Engineering 22(9-12):731-42
- Nikolaou A, Gazetas G (1997) Seismic design procedure for kinematically stressed piles, Seismic behaviour of ground and geotechnical structures. Pedro S. Seco e Pinto, Editor. In: Proceedings of the Fifteenth International Conference on Soil Mechanics & Geotechnical Engineering, Hamburg, pp. 253-260
- Miura F, Stewart HE, O'Rourke TD (1989) Nonlinear analysis of piles subjected to liquefaction induced large ground deformation. In: Proceedings of the 2nd US-Japan Workshop on Liquefaction, Large Ground Deformations and Their Effect on Lifelines. MCEER

- Liu L, Dobry R (1995) Effect of liquefaction on lateral response of piles by centrifuge model tests. NCEER Bulletin 9(1):7-11
- Architectural Institutive of Japan (AIJ) (1998) Recommendation for design of building foundations
- Liyanapathirana DS, Poulos HG (2005a) Seismic lateral response of piles in liquefying soil. Journal of Geotechnical and Geoenvironmental Engineering, ASCE 131: 1466-1479
- Liyanapathirana DS, Poulos HG (2005b) Pseudo-static approach for seismic analysis of piles in liquefying soil. Journal of Geotechnical and Geoenvironmental Engineering, ASCE 131: 1480-1487
- Elahi H, Moradi M, Poulos HG, Ghalandarzadeh A (2010) Pseudostatic approach for seismic analysis of pile group. Computers and Geotechnics 37(1-2): 25-39
- Matlock H (1970) Correlations for design of laterally loaded piles in soft clay. In: Proceedings of the II Annual Offshore Technology Conference, Houston, Texas, (OTC 1204), pp. 577-594
- Boulanger RW, Kutter BL, Brandenberg SJ, Singh P, Chang D (2003) Pile Foundations in liquefied and laterally spreading ground during earthquakes: Centrifuge experiments and analyses. Center for Geotechnical Modeling, University of California at Davis, Davis, CA. Rep. UCD/CGM-03/01
- Brandenberg J, Boulanger RW, Kutter BL, Chang D (2007) Static pushover analyses of pile groups in liquefied and laterally spreading ground in centrifuge tests. Journal of Geotechnical and Geoenvironmental Engineering 133(9):1055-66
- Tokimatsu K, Oh-oka H, Satake K, Shamoto Y, Asaka Y (1998) Effects of lateral ground movements on failure patterns of piles in the 1995 Hyogoken-Nambu earthquake. In: Proceedings of Geotechnical Earthquake Engineering and Soil Dynamics III, Reston, pp. 1175-1186
- O'Rourke TD, Meyersohn WD, Shiba Y, Chaudhuri D (1992) Evaluation of pile response to liquefaction induced lateral spread. Technical Rep. NCEER-94-0026, National Center for Earthquake Engineering Research (NCEER), Buffalo, NY: 457–479
- Phanikanth VS, Choudhury D, Reddy GR (2013) Behavior of Single Pile in Liquefied Deposits during Earthquakes. Int. J. Geomech. 13:454-462.

- Meera RS, Shanker K, Basudhar PK (2007) Flexural response of piles under liquefied soil conditions. Geotech. Geol. Eng. 25(4): 409–422
- Haldar S, Babu GLS (2010) Failure mechanisms of pile foundations in liquefiable soil: Parametric study. Int. J. Geomech. 10(2): 74–84.
- Davisson MT, Robinson KE (1965) Bending and Buckling of Partially Embedded Piles. In: Proceedings of the Sixth International Conference on Soil Mechanics and Foundation Engineering, Montreal, Canada, Vol. 2, pp. 243-246
- Chatterjee K, Choudhury D, Poulos HG (2015) Seismic analysis of laterally loaded pile under influence of vertical loading using finite element method. Comput Geotech 67:172–186
- McGann CR, Arduino P, Mackenzie Helnwein P (2011) Simplified procedure to account for a weaker soil layer in lateral load analysis of single piles. Journal of Geotechnical and Geoenvironmental Engineering 138(9): 1129-1137
- Lombardi D, Dash SR, Bhattacharya S, Ibraim, E, Muir Wood D, Taylor CA (2017) Construction of simplified design p-y curves for liquefied soils. Geotechnique 67(3): 216-227
- Dobry R, Abdoun T, O'Rourke TD, Goh SH (2003) Single piles in lateral spreads: field bending moment evaluation. Journal of Geotech Geoenviron Engg ASCE 129: 879-889
- Abdoun T, Dobry R, O'Rouke TD, Goh SH (2003) Pile foundation response to lateral spreads: Centrifuge modelling. Journal of Geotechnical and Geoenvironmental Engineering, ASCE 129(10): 869-878
- Dash SR, Bhattacharya S and Blakeborough A (2010) Bending-buckling interaction as a failure mechanism of piles in liquefiable soils. Soil Dynamics and Earthquake Engineering 30(1-2): 32-39
- Elgamal A, Lu J, Yang Zh, Shantz T (2010) A 3D soil-structure interaction computational framework. In: 5th International Conference on Earthquake Engineering, Tokyo, Japan
- Lu J, Elgamal A, Yang Zh (2011) OpenSeesPL: 3D lateral pile–ground interaction user manual (Beta 1.0). Dept. of Structural Engineering, Univ. of California, San Diego

- Yang Z, Elgamal A, Parra E (2003) A computational model for cyclic mobility and associated shear deformation. Journal of Geotechnical and Geoenvironmental Engineering 129(12): 1119-1127
- Mazzoni S, McKenna F, Fenves G L (2006) Open system for earthquake engineering simulation user manual, Pacific Earthquake Engineering Research Center, University of California, Berkeley
- Davisson MT, Robinson KE (1965) Bending and Buckling of Partially Embedded Piles. In: Proceedings of the Sixth International Conference on Soil Mechanics and Foundation Engineering, Montreal, Canada, 1965, Vol. 2, pp 243-246
- Bhattacharya S (2006) Safety assessment of existing piled foundations in liquefiable soils against buckling instability. ISET Journal of Earthquake Technology, Technical Note 43(4): 133-147
- Thomson WT (1996) Theory of Vibration with applications. Taylor and Francis Ltd
- Murty CVR, Rai DC, Jain SK, Kaushik HB, Mondal G, Dash SR (2006) Performance of Structures in the Andaman and Nicobar Islands (India) during the December 2004 Great Sumatra Earthquake and Indian Ocean Tsunami. Earthquake Spectra, Vol. 22 (S3): S321–S354
- Mohanty WK, Walling MY (2008) Seismic hazard in mega city Kolkata, India. Nat Hazards 47: 39–54. DOI 10.1007/s11069-007-9195-1
- Nath SK, Adhikari MD, Maiti SK, Devaraj N, Srivastava N, Mohapatra LD (2014) Earthquake scenario in West Bengal with emphasis on seismic hazard microzonation of the city of Kolkata, India. Nat. Hazards Earth Syst. Sci., 14: 2549–2575. doi:10.5194/nhess-14-2549-2014
- Giardini D, Grunthal G, Shedlock KM, Zhang P (1999) The global seismic hazard assessment program (GSHAP). Ann Geofis 42:1225–1228

Monirul Mallick
05/04/2023